Engineering artificial biomolecular condensates to study the aggregation of α-Synuclein

Marian-Leonard Piroska

Sorbonne Université

Ecole doctorale 388

Chimie Physique et Chimie Analytique de Paris Centre

Département de Chimie

École Normale Supérieure

Engineering artificial biomolecular condensates to study the aggregation of α-Synuclein

Par Marian-Leonard Piroska

Thèse de doctorat de Chimie Physique

Dirigée par Zoher Gueroui

Présentée et soutenue publiquement le 15/12/2023

Devant un jury composé de :

M. Franck Artzner	Directeur de recherche	Rapporteur
M^{me} Céline Galvagnion-Büll	Associate Professor	Rapportrice
M. Gueroui Zoher	Directeur de recherche	Directeur de thèse
M. Laferrière Florent	Chargé de recherche	Examinateur
M^{me} Sykes Cécile	Directrice de recherche	Examinatrice

ACKNOWLEDGEMENTS

Dans le travail de recherche, on est toujours amené à citer d'autres personnes pour leur travail, pour leurs hypothèses, leurs expériences scientifiques et leurs résultats. Je suis très heureux de pouvoir, pour une fois, mentionner des gens juste pour ce qui ils sont pour moi, pour les qualités que je vois en eux, pour ce qu'ils m'ont appris et pour les bons moments qu'on a passés ensemble. Je tiens donc à consacrer cet espace pour exprimer ma profonde reconnaissance envers toutes les personnes exceptionnelles qui ont rendu possible la réalisation de cette thèse.

Je voudrais débuter en exprimant ma gratitude envers mes rapporteurs, Franck Artzner et Céline Galvagnion, pour avoir accepté de lire et évaluer mon manuscrit de thèse. Un grand merci aux examinateurs, Florent Laferrière et Cécile Sykes, pour avoir accepté de participer à ma soutenance.

Un énorme merci à Zoher, pour l'accueil dans le laboratoire, ton investissement constant dans mes projets, toutes nos discussions toujours très enrichissantes, la confiance que tu as eue en moi, ton enthousiasme qui m'a aidé à rester motivé et pour ces presque quatre années (en comptant le stage) où je trouve qu'on a toujours si bien collaboré. Je trouve que tu as construit une très belle équipe, avec une atmosphère toujours très positive, et je me considère très chanceux d'en avoir fait partie.

Aux membres de l'équipe de Zoher (les #cool-kids-sous-sol):

A tous en même temps : merci pour cette incroyable atmosphère qu'on a toujours eue, pour les tous les fous rires, les fat Fridays (qui finalement étaient n'importe quel jour), pour les pauses café dans le jardin, les gossips (ah, les gossips), les bruits bizzares quand la fatigue s'installait après 17h. Vous allez me manquer énormément !

Je tiens à remercier Scott, pour ton investissement dans mes projets. Cela a été un grand soulagement, mais aussi très agréable, d'avoir un binôme pendant ma dernière année de thèse (je pense à ces western blots qui m'auraient rendu fou si j'était tout seul). Merci aussi pour l'ambiance joyeuse que tu as apporté sur la mezzanine. Un jour peut-être je comprendrai tes refs de publicités.

Pauline, je ne pense pas qu'un paragraphe suffirait pour que j'exprime ce que notre amitié vaut pour moi (mais bon je me restreint, j'ai déjà fait le devis d'impression de la thèse en déclarant 140 pages). Merci pour tout ce temps qu'on a passé ensemble, au labo et en dehors, et pour tous ces bons souvenirs, que je n'essaye même pas de lister car je risquerais de doubler la taille de la thèse si je le fais. Cela va me manquer de passer venir te chercher le matin devant l'immeuble pour faire le trajet vers l'ens ensemble. Merci pour ta contribution au maintien de l'ordre et de la propreté dans le labo (fameuse GestaPauline). Semaine bleu zzz

Laura, pour toi aussi un paragraphe me semble beaucoup trop court. Je pense que je n'ai jamais développé une si forte amitié avec quelqu'un aussi vite qu'avec toi. Merci pour toutes ces petites pauses l'après-midi, pour les sessions de natation sur la ligne des vacanciers les lundi, pour ces incroyables repas de dimanche à Suresnes et pour les innombrables fois où on a rigolé ensemble en faisant autant de bruit qu'un avion de chasse (attesté par le décibel mètre du Baker). On a tous apprécié l'effort esthétique que tu as fait pour la mezzanine en apportant des plantes, même si bon ça a pas tenu faute de conditions propices à la vie.

Marie-Aude (a.k.a directrice de l'ENS d'après moi), merci d'avoir maintenu le labo fonctionnel pendant ces années. Je ne sais pas comment on s'en sortirait si on pouvait pas dire « demande à Marie-Aude ». Nos petites pauses café vont beaucoup me manquer, mais aussi le « carton basketball », et les bons gâteaux que tu nous faisais.

Chems, un grand merci pour ton inépuisable patience, surtout quand il s'agit d'expliquer ce qui ne marche pas dans les codes Python. Il y a une partie de ces résultats que je n'aurais pas pu exploiter comme je l'ai fait sans ton aide. Merci aussi de nous avoir fait découvrir les endroits les plus inédits et palpitants, que ce soit dans les profondeurs de la terre ou bien en hauteur.

Audrey, merci pour tout ce que tu m'as appris pendant mon stage. J'ai démarré la thèse en étant en confiance, et cela est grâce à toi. Merci aussi pour ta patience et ta bonne humeur. Je suis content qu'on arrive à s'envoyer toujours des messages de temps en temps, malgré le décalage horaire.

Théodore, cela a été très sympathique de t'encadrer pendant 6 mois, et même si tu n'es pas resté chez nous en thèse, sache que tu es toujours resté un membre honorifique de l'équipe pour moi. Damien, merci pour ta bonne humeur, et tu as vu je me suis amélioré au lance-papier-dans-la-poubelle. Emma, même si tu viens d'arriver au moment où je pars (ah, le grand remplacement) on a déjà eu l'occasion de passer des moments très agréables ensemble. Bon courage pour ta thèse, qui s'annonce pleine de succès.

Merci à la mezzanine d'avoir soutenu (littéralement) le poids de l'équipe sans s'écrouler. C'était pas donné.

Merci aussi à tous les membres du pôle CPBMV : Hélène, Aliénor, Fayrouz, Valentine, Damien, Anamaria, Marc, Emma, Thomas, Isabelle, Emmanuelle, Hessam, Alina, Ludovic, Yoan, Mrinal, Yuriy (désolé si j'ai oublié des gens). Mention spéciale pour Ian, qui m'a aidé à rester motivé à faire aussi du sport ces années (tu as vu je t'écris en français parce que tu as bien appris la langue à mon avis). Merci à Pierre-Louis, pour les nombreuses pauses midi ensemble et pour le fait qu'à son arrivé je n'étais plus le seul du coin à être addict à la caféine (d'ailleurs merci à Nespresso aussi).

Merci à Monsieur Ronald Melki d'avoir accepté de collaborer avec nous, pour toutes vos contributions à ce travail, pour les discussions toujours enrichissantes. Merci aussi aux membres de votre équipe : Alexis, Virginie, Nolwenn, Tracy, qui se sont mobilisés quand il y avait besoin et qui m'ont si bien accueilli dans votre laboratoire quand je vous ai rendu visite.

Merci aux membres de l'admistration Elza, Delphine, Pauline, Cécile, pour votre aide dans les dénmarches pas toujours faciles. Merci à Nathalie et Khan pour leur aide dans l'organisation des séminaires jeunes chercheurs.

Merci aussi à mes amis, avec une première mention spéciale pour Alina, qui a accepté de faire une relecture de cette thèse, et grâce à qui le nombre de coquilles et phrases tournées bizarrement s'est diminué significativement. Aussi pour les appels réguliers, et pour les voyages à Frankfort. Merci aussi à Yvan (même si bon les karaages c'est toujours pas fait), à tous mes amis de Paris, de Nice et de Roumanie. Merci à Cristian de m'avoir supporté au quotidien, et pour les discussions toujours stimulantes intellectuellement. À Marina et Yuliya, pour tous ces bons moments depuis la licence, et parce qu'elles se sont déplacées de si loin pour venir à ma thèse. À Denisa, Mara et Alina, parce que même si on est très loin nos conversations whatsapp me font toujours plaisir.

Et enfin un énorme merci à ma famille, mes parents et mon frère, qui se sont toujours si bien amusé sur le fait que je « lave des cellules », pour le support, l'amour et la confiance au quotidien! Merci de ne vous être jamais douté de moi, d'avoir répondu toujours à mes appels vidéo quand je cuisinais et j'avais envie de parler de ma journée, pour les séjours à Nice toujours si reposants, pour vos voyages à Paris à chaque occasion.

J'espère n'avoir oublié personne.

LIST OF ABBREVIATIONS

α-Syn: α-Synuclein

Aβ: Amyloid Beta

AD: Alzheimer's Disease

AFM: Atomic Force Microscopy

ALS: Amyotrophic Lateral Sclerosis

BFP: Blue Fluorescent Protein

BSA: Bovine Serum Albumin

bvFTD: behavioural variant of FTD

C. elegans: Caenorhabditis elegans

CaMKII: calcium/calmodulin-dependent protein kinase II

Cry2: cryptochrome circadian regulator 2

C_{sat}: saturation concentration

DDB: dynein-dynactin-BicD2N

DDR: DNA damage repair

DIC: Differential interference contrast

DLB: Dementia with Lewy Bodies

DOPA: L-3,4-dihydroxyphenylalanine

DOPE-Cy5; 1,2-dioleoyl-sn-glycero-3-phosphoethanolamine-N-[amino (polyethylene glycol)-2000]-N- (Cyanine 5)

EBFP2: Enhanced blue variant of the Green Fluorescent Protein

EGFP: Enhanced Green Fluorescent Protein

emGFP: emerald Green Fluorescent Protein

EndoA1: Endophilin A1

FBS: Foetal bovine serum

FKBP: FK506 binding protein

FlAsH-EDT2: fluorescein arsenical hairpin binder-ethanedithiol

FLIM: fluorescence lifetime imaging

Fm: F36M-FKBP12

FRB: FKBP–rapamycin binding protein

FRAP: Fluorescence Recovery After Photobleaching

FRET: Förster resonance energy transfer

FTD: Frontotemporal Dementia

FUS: Fused in Sarcoma

HD: Huntington Disease

HEK293: Human Embryonic Kidney 293

HeLa: Henrietta Lacks (name of the person from whom the cells were harvested)

hnRNPA1: heterogeneous nuclear ribonucleoprotein A1

hnRNPA2: heterogeneous nuclear ribonucleoprotein A2

IDP: Intrinsically Disordered Protein

iPOLYMER: intracellular production of ligand-yielded multivalent enhancers

kDa: KiloDalton

LB: Lewy Body

LLPS: Liquid-Liquid Phase Separation

MT: Microtubule

MTT: 3- (4,5-dimethylthiazol-2-yl)-2,5-diphenyltetrazolium bromide

MSA: Multiple System Atrophy

NAC: non-amyloid-beta component

NCID: Nefrin Intracellular Domain

nfvPPA: non-fluent variant primary progressive aphasia

PABP1: poly- (A) Binding Protein

PARP: Poly (ADP-ribose) polymerase

PBS: Phosphate Buffer Saline

PD: Parkinson's Disease

PEG: Poly-Ethylene Glycol

pLK: poly-L-lysin

POI: Protein of interest

PRM: Proline-rich domain

PrP: Major Prion Protein

PTM: Post-Translational Modification

RBP: RNA-binding protein

RIM: Rab3 Interacting Molecule

RIM-BP: RIM-binding protein

RRM: RNA-recognition motif

SDS: Sodium Dodecyl Sulfate

sfGFP: superfolder Green Fluorescent Protein

SH3: SRC homology 3

SG: Stress Granule

SIM: SUMO Interacting Motifs

SNARE: soluble NSF attachment protein receptor

SUMO: Small Ubiquitin-like Modifier

SV: synapsin vesicle

svPPA: semantic variant primary progressive aphasia

TDP43: TAR DNA-binding protein 43

TEM: Transmission Electron Microscopy

TH: Tyrosine Hydroxylase

ThioS: Thioflavin S

ThT: Thioflavin T

TIA-1: Tia 1 cytotoxic granule-associated rna binding protein

UBQLN2: Ubiquilin 2

VCP: Valosin Containing Protein

WGA: wheat germ agglutinin

XL–MS: cross-linking mass spectrometry

YFP: Yellow Florescent Protein

CONTENTS

CHAPTER I: THE STUDY OF BIOMOLECULAR CONDENSATES TO UNDERSTAND THE AGGREGATION OF PROTEINS IN NEURODEGENERATIVE DISEASES

I.1 Brief presentation of neurodegenerative diseases

I.1.1 Definition and socio-economic impact of neurodegenerative diseases

Neurodegenerative diseases are incurable medical conditions caused by progressive and irreversible neuronal death. Loss of nerve cells can happen in various parts of the brain, engendering a diverse set of pathologies, with symptoms ranging from speech problems, impaired movement, cognitive deteriorations, etc. The societal impact of these illnesses is substantial. The two most prevalent neurodegenerative conditions (Alzheimer's and Parkinson's) alone are estimated to affect more than 30 million people worldwide, with associated annual costs reaching hundreds of billions of euros (*1*). Age is the main risk factor for the development of these diseases, and the predicted increase in geriatric population over the next decades is expected to drive an increase in both their victim toll and socio-economic burden (*2*, *3*).

Despite being subject to widespread research, no definite cure for neurodegenerative illnesses has been discovered yet. This is due to our incomplete understanding of the biological and environmental factors underlying their occurrence. This thesis will provide an overview of the past and current understanding of neurodegenerative diseases, particularly focusing on protein aggregation. Additionally, it will mention some unanswered questions from the field, and it will illustrate some novel approaches to tackle these inquiries.

I.1.2 Historical context of research in neurodegenerative diseases

Throughout the history of medicine, there have been numerous accounts that align with what we currently define as neurodegenerative diseases. Writings about age-dependent symptoms such as tremors, memory loss, and cognitive impairment (dementia) can be traced back to the ancient Egyptians and the Greco-Roman period (*4–6*). In more modern times, doctors have begun to define the multifaceted profiles of neurological conditions, and not just isolated symptoms. One of the pioneers of this progress was P. Pinel, who, in 1809, provided a rich description of dementia, highlighting its chronic nature and classifying it separately it from acute mental disorders, such as mania (*7*). Another early text documenting a pattern of symptoms of neurodegenerative nature was the description of the "Shaking Palsy" (today

known as Parkinson's disease), by J. Parkinson in 1817 (*8*). In this essay, Parkinson uses six cases to illustrate a disease that manifests through "involuntary tremulous motion, with lessened muscular power" and "a propensity to bend the trunk forwards", and describes the effects of its irreversible time-dependent aggravation (*8*).

During the same period, details started to resurface about the physio-pathological substrates of these diseases. Parkinson described in his essay a "disordered" state of *the medulla oblongata* (*8*), a part of the brain that has been demonstrated much later to be touched by Parkinson's Disease from its earliest phases (*9*). He even intuited a link between the digestive system and the disease, a hypothesis that has been initially largely ignored, and regained attention nearly two centuries later (*10*). G. Huntington also hypothesized in his 1872 paper that the disease which now bears his name would be caused by a "functional derangement in the cerebellum" (*11*). At this point, details about the nature of these "derangements" remained quite vague.

A significant leap forward in the description of neurodegenerative diseases happened at the beginning of the 20th century, with the development of staining techniques, that afforded fine-detail structural observations of nervous tissue (*12*). These techniques were particularly applied to tissues from diseased patients, in attempts to better understand the pathological phenomena underlying their illnesses. Such an analysis allowed A. Alzheimer to identify the "deposition of a pathological metabolic substance" within the damaged cortical tissue from one of his presenile dementia patients (*13*). At that time, little was known about the composition of these deposits, and, even to this day, no conclusive causal link with illness was demonstrated. Nonetheless, the assumption that they could be pathological gained momentum in the following decades because numerous other neurodegenerative diseases, such as Parkinson's disease (PD), Huntington Disease (HD) and Amyotrophic Lateral Sclerosis (ALS) were shown to develop synchronously with the formation of some type of inclusion within the affected nervous tissues (**Figure I.1**) (*14–16*).

Another major milestone in neurodegenerative disease research was reached at the end of the 20th century when details about the composition of these potentially pathological brain deposits started to resurface. First, it was revealed that Alzheimer's plaques were composed mostly of a protein called amyloid beta (Aβ), in aggregated form (*17*, *18*). This was followed by the discovery of aggregates of the protein Huntingtin in the brains of HD patients (*15*, *19*). Within the same period, α-Synuclein (α-Syn) was identified as the main protein component of inclusions called Lewy Bodies (LB), that populate degenerated tissues in PD and Dementia with Lewy Bodies (DLB) (**Figure I.2**) (*20*). A train of similar discoveries has followed, such that by the early 21st century, virtually all neurodegenerative diseases had been associated with some form of protein aggregates. This common characteristic has kindled the hypothetical idea that protein aggregation could be a part of a unified model for the initiation of neurodegenerative pathology (*21*). To this day, this phenomenon remains one of the most intensely researched subjects in relation to neurodegenerative diseases.

Disease	Etiology	Regions most affected	Characteristic pathology	Disease proteins deposited
Huntington's disease	Huntingtin (dominant)	Striatum, other basal ganglia, cortex, other regions	Intranuclear inclusions and cytoplasmic aggregates	Huntingtin with polyglutamine expansion
Other polyglutamine diseases (DRPLA, SCA1–3, etc., SBMA)	Atrophin-1, ataxin-1–3, etc.; androgen receptor (AR) (dominant)	Basal ganglia, brain stem cerebellum, and spinal cord	Intranuclear inclusions	Atrophin-1, ataxins or AR
Alzheimer's disease (AD)	Sporadic (ApoE risk factor)	Cortex, hippocampus, basal forebrain, brain stem	Neuritic plaques and neurofibrillary tangles	Aβ peptide (from APP) and hyperphosphorylated tau
	Amyloid precursor protein (APP) (dominant)	Same as sporadic	Same as sporadic	Same as sporadic
	Presenilin 1, 2 (dominant)	Same as sporadic	Same as sporadic	Same as sporadic
Fronto-temporal dementia with Parkinsonism	Tau mutations (dominant)	Frontal and temporal cortex, hippocampus	Pick bodies	Hyperphosphorylated tau protein
Parkinson's disease (PD)	Sporadic	Substantia nigra, cortex, locus ceruleus, raphe, etc.	Lewy bodies and Lewy neurites	α-Synuclein
	α-Synuclein (dominant)	Similar to sporadic, but more widespread	Similar to sporadic	α-Synuclein
	Parkin (also DJ-1, PINK1) recessive (some dominant)	Substantia nigra	Lewy bodies absent (or much less frequent)	α-Synuclein (when present)
Amyotrophic lateral sclerosis (ALS)	Sporadic	Spinal motor neurons and motor cortex	Bonina bodies and axonal spheroids	Unknown (neurofilaments)
	Superoxide dismutase-1 (dominant)	Same as sporadic	Same	Unknown
Prion diseases (kuru, CJD, GSS disease, fatal familial insomnia, new variant CJD)	Sporadic, genetic and infectious	Cortex, thalamus, brain stem, cerebellum, other areas	Spongiform degeneration, amyloid, other aggregates	Prion protein

ApoE, apolipoprotein E; APP, amyloid precursor protein; CJD, Creutzfeldt–Jakob disease; DRPLA, dentato-rubral and pallido-Luysian atrophy; GSS, Gerstmann–Straussler–Scheinker; SBMA, spinal and bulbar muscular atrophy; SCA, spino-cerebellar ataxia.

Figure I.1 Different neurodegenerative diseases and their corresponding neural inclusions enriched in aggregated proteins. *Adapted from (21).*

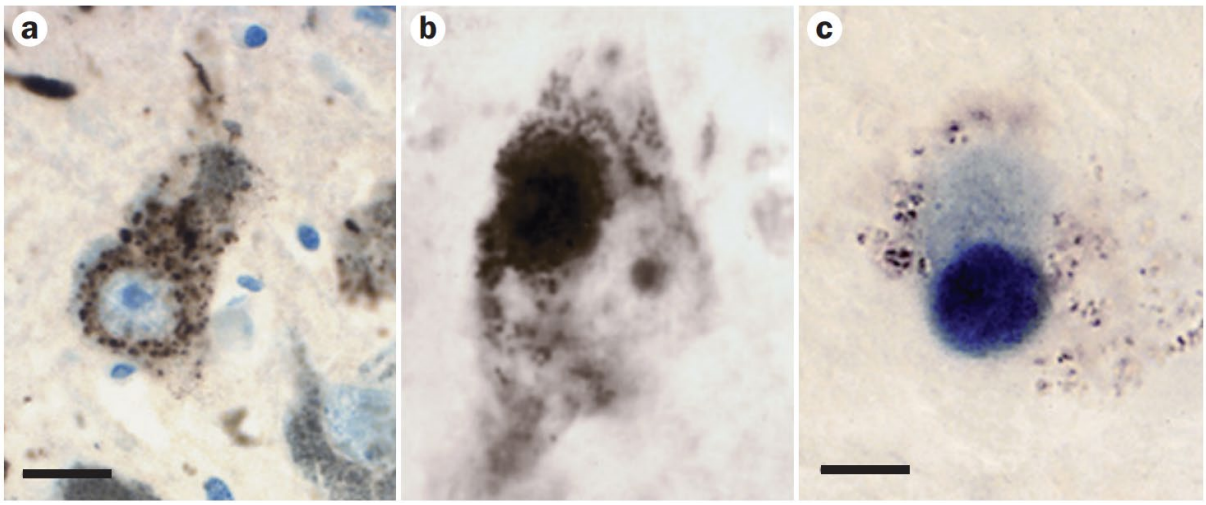

Figure I.2 Images of LBs obtained through anti- α-Syn immunostaining on neurons. *Scale bars, 20 µm. Adapted from (14).*

Since the late 20th century, the research on neurodegenerative diseases has significantly diverged, and the subject has also been approached from different angles, such as the digestive system (*22*). The current work fits best within the category of research that focuses on the protein aggregation aspect of neurodegenerative diseases. Therefore, this branch will be preferentially developed in the following chapters.

I.2 Protein aggregation: a driver for neurodegenerative diseases?

I.2.1 What are protein aggregates? Structural elements.

In the context of proteins, the term 'aggregate' can be ambiguous, as there is no precise list of criteria for a protein species to fit into this category. Assemblies described as aggregates in the literature range widely in size (from less than 100 nm to almost macroscopic scales), composition and morphology (*23–26*). Although the term is most often employed in the context of pathologies, some broad descriptions include physiological species, such as certain protein complexes, oligomers and biological polymers (*21*, *23*, *27*). In the absence of an established consensus, a clarified stance seems appropriate, if not necessary. Herein, the term protein aggregate designates insoluble supramolecular assemblies of monomers issued from aberrant cellular processes, that have potential toxic effects and putative implications in pathology.

A particularly critical aspect of protein aggregates is their structure. Although amorphous protein aggregates exist and could be involved in pathology, the research in neurodegenerative diseases has mainly focused on structurally orderly assemblies (*28*, *29*). This is because most of the protein deposits associated with neurodegenerative diseases have been shown to be highly enriched in amyloids - fibrillar structures composed of unfolded protein monomers stacked in a greatly regular manner, approximately 4.8 Å apart (**Figure I.3**) (*30*, *31*). Cryo-EM and X-ray diffraction analyses revealed that amyloid states of different proteins share similar structural patterns: they are generally double-stranded and feature a characteristic cross-beta architecture (*32*, *33*). This structural motif is cemented by numerous hydrophobic interactions and H-bonds within strands, and steric zipper interactions between strands, which render amyloids remarkably stable and resistant to harsh conditions (*32*, *34*). This stability contributes to the tendency of amyloids to accumulate in the tissue with time, leading to the formation of the inclusions that were mentioned in the previous section.

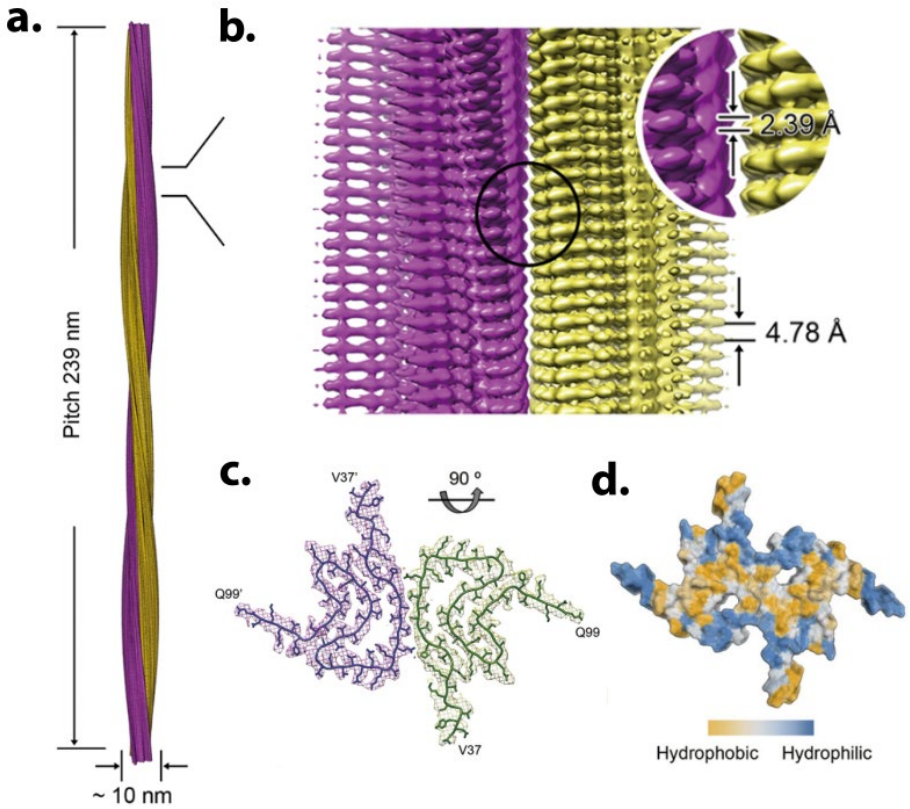

Figure I.3 Structure of α-Syn amyloid fibrils determined through cryo-electron microscopy. ***a****. Side view of the amyloid fibril. The thickness and 'pitch' (distance required for a 360° spin of the fibril) are presented.* ***b.*** *Zoom on the side view. The distance between two sheets -4,78 Å- is presented.* ***c****. Top view of the amyloid electron density map, with atomic resolution.* ***d****. Representation of the hydrophobic/hydrophilic residue distribution within the beta-sheet, displaying how hydrophobic residues are placed at the core of the amyloid fibril, whereas the hydrophilic ones are at the surface. Adapted from (30).*

Despite this highly conserved structural backbone, amyloids can also display structural diversity, even when they are composed of the same protein. Indeed, variations in the topology of amyloid fibrils can arise from differences in the monomer's conformation within the cross-beta sheets (*35*). This can in turn be due to numerous factors, such as environmental stress, but also protein truncations, post-translational modifications (PTM), mutations, etc (*36–38*). Beyond the structural dimension, some of these amyloid fibril polymorphisms could have pathological relevance, because they could help explain why the aggregates of the same protein can trigger different pathologies. Indeed, various strains of tau and α-Syn fibrils have been shown to be specific to different tauopathies/synucleinopathies respectively (*39–42*). This structure-pathology relationship highlights the importance of understanding the mechanisms underlying protein aggregation, and the factors that dictate the architecture of aggregates.

I.2.2 Mechanisms of protein aggregation. Protein unfolding in neurodegenerative diseases.

Although multiple mechanisms for aggregation were described, one in particular stands out in the context of neurodegenerative diseases: the unfolding-to-aggregation pathway (*43*, *44*). For this reason, neurodegenerative illnesses are also commonly referred to as 'conformational diseases' in the specialized literature. A compelling argument in favour of such a mechanism is that amyloids contain proteins in non-physiological conformations, suggesting that unfolding was involved somewhere in the process of their formation (*32*). Moreover, numerous factors associated with aging and neurodegeneration, such as oxidative stress, changes in pH, disturbances in proteostasis and impaired chaperone function were also associated with the misfolding of proteins. (*44–47*).

The link between unfolding and aggregation can be described using a mix of thermodynamics and kinetics. From a thermodynamic standpoint, the stability of proteins - and implicitly their capacity to stay soluble/non-aggregated - depends on their conformational energy state. In physiological conditions, most proteins predominantly populate a specific folding pattern called the native state, which corresponds to a local minimum of free energy which provides them with solubility and operativity (*48*). With very few exceptions, this state in non-aggregative (*49*). However, most proteins that form amyloids (α-Syn, tau, Fused in Sarcoma (FUS) etc.), do not fit into this description, because they feature highly flexible polypeptide chains which do not form permanent secondary structures and, thus, have no native state (*50*). In the absence of a thermodynamically favourable fold, they tend to sample thousands of different conformations in solution, hence the name Intrinsically Disordered Protein (IDP). Some of these conformations are partially unfolded and, hence, more prone to participate in aggregation initiation (*51*).

Why are unfolded states more prone to aggregate? The main reason is that they are less energy-optimised than a native state; the increased rotational and translational freedom of their peptide chains allows the exposure of non-polar and hydrophobic residues to the solvent, creating chemically frustrated surfaces (*43*). To counter this frustration, they acquire the tendency to self-assemble in supramolecular species, such that hydrophobic-hydrophilic interfaces are minimised (*52*). However, self-assembly does not necessarily lead to aggregation. In absence of an aggregation-inducing stimulus, the entropic effect prevents these assemblies from surpassing oligomeric sizes. In aggregation-inducing conditions, on the contrary, assemblies can reach a size where the monomer-monomer interactions are numerous enough to

overcompensate for entropy loss and solvent interface energy (*53*). At this point, the assembly becomes stable enough to recruit monomers at much higher rates than it dissociates, becoming the germinal species that triggers an unsuppressible aggregation cascade.

This picture is supported by kinetic models, which describe the initiation of aggregation as nucleation-dependent, meaning that the rate-limiting step is the initial binding of monomers and that once the oligomeric 'seed' is formed the aggregate grows rapidly *(*43*)*. Following the trajectory of primary nucleation-dependent polymerization, aggregates were shown to grow through monomer addition from the soluble pool or through aggregate-aggregate condensation *(*29, 54*)*. However, experimental data suggests that the growth curve of amyloids is often too abrupt to be accounted for solely by primary events, and that secondary nucleation is likely also involved *(*55*)*. This is a phenomenon where the surface of existing aggregates catalyses the formation of de novo (or secondary) nuclei, leading to an exponential propagation of the aggregation (**Figure I.4**).

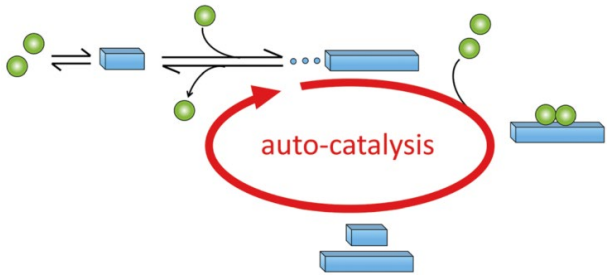

Figure I.4 Widely proposed mechanism for protein aggregation. *The initiating step is the primary nucleation starting from soluble monomers (green balls). Once formed, the aggregate (blue bar) catalyses the de novo formation of aggregates through secondary nucleation, triggering a fast spreading of aggregation. Adapted from (*53*).*

Indeed, *in vitro,* and *in vivo* studies show that, in some cases, the inoculation with a preformed aggregate 'seed' can single-handedly trigger aggregation, bypassing the initial nucleation event (*56–58*). Moreover, the *de novo* created species will, in some cases, reproduce the strain topology of the aggregate 'seed', suggesting that aggregates imprint their misfolded conformation into soluble monomers from the native-state pool (*58*, *59*). This behaviour was first discovered in the prion protein (condensed from "proteinaceous infectious particle"), but was subsequently reported for various other 'prion-like' proteins such as α-Syn, tau, TDP43 etc. (*60–63*). This mode of aggregation propagation has been proposed to be supported by different pathways that allow a cell-to-cell transmission of aggregates (*64*), as illustrated in **Figure I.5**.

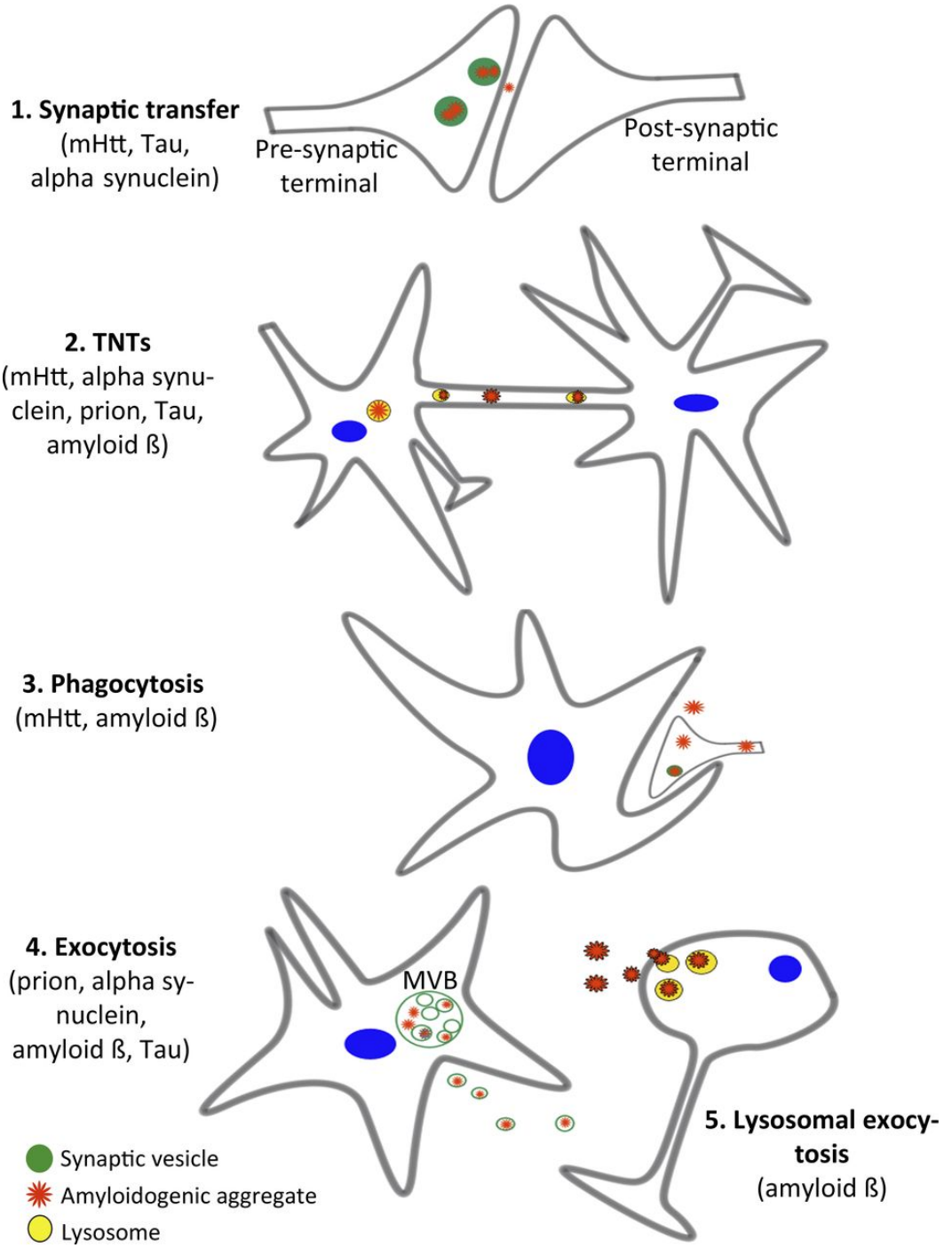

Figure I.5 Some proposed pathways for prion-like propagation of amyloid fibrils. ***1.*** *Certain aggregated proteins can bind to synaptic vesicles, which can fuse with the membrane at the presynapse, releasing aggregates into the synaptic cleft. Therein, they can be incorporated by the post-synaptic neuron.* ***2.*** *Prion-like aggregates can be transferred from cell to cell through micrometric conduits that link cells to each other, called tunnelling nanotubes (TNT).* ***3.*** *Some prion-like aggregates could be spread through engulfment of cellular debris by glial cells.* ***4.*** *and* ***5.*** *Aggregates could be realeased into the extracellular space through exocytosis of either exosomes (****4.****) or lysosomes (****5.****) Adapted from (64).*

I.2.3 The pathogenicity of aggregates: grey areas and conflicting results

Alongside the massive amounts of insight that we have gained in the last decades about the mechanisms of protein aggregation in neurodegenerative diseases, a lot of open questions have also resurfaced: Is the aggregation of proteins - and subsequent deposition of aggregates - a causal element in the development of pathology, or could it be an effect? Could protein aggregates be the by-product of other processes that inflict toxicity within neurons, or the response of the tissue against other toxic factors?

We could suppose that a straightforward way to approach these inquiries would be to inject aggregates in healthy model organisms, and to assess their pathogenic potency based on the observed symptoms, or the absence thereof. However, observations of toxicity in animal models cannot constitute direct evidence of identical phenomena in humans. Even aside from that shortcoming, such studies are far from having settled the debate, because they yielded extremely varied and even contradictory responses. Whilst some studies reported that the exposure of mice to α-Syn amyloid fibrils caused pathological symptoms (*65*), others noted only an acceleration of the diseased state with no direct causality (*66*). In contrast, some studies reported an absence of symptoms such as motor or cognitive impairment (*67*). Similarly, other aggregates such as tau and Aβ fibrils also yielded different pathological responses from one study to the other (*68–70*).

The lack of convergence in the results of these studies is perhaps not surprising, given that there is some methodological variability; multiple different model organisms are currently used, and the aggregates can originate either from diseased brain tissues or from *in vitro* polymerization of protein monomers. In the absence of an ideal model, it is essential to consider both perspectives. In the next sections, I will discuss the current arguments supporting and opposing a potential causal relationship between aggregation and disease.

I.2.4 Aggregation hypothesis in neurodegenerative diseases. Pro arguments

During the last two decades, considerable pieces of scientific evidence have amounted in favour of the amyloid hypothesis. A compelling argument that gives aggregates visibility in this context is that they appear to be specific to the regions in the nervous system that are impacted by neurodegeneration. For example, LB pathology has been reported to emerge in the olfactory bulb, and to progress towards the brainstem, the limbic system, and finally, the

neocortex (*71*). These correspond to the areas of the brain that are affected by neuronal death in synucleinopathies. (*72*) Moreover, an association between the density of LB and neuronal death was reported, which lead to the classification of the disease progression stage according to their degree of progression within the tissues (*71*, *73*). In AD patient's brains, detection methods such as [18F] flutemetamol amyloid positron emission tomography revealed that the progression of the disease is concomitant with the spreading and densification of Aβ deposits **(Figure I.6)** (*74*). Similarly, it was reported that in the brains of Frontotemporal Dementia (FTD) patients, neuroinflammation was strongly correlated with the presence of TDP43 and tau aggregates (*75*). These studies illustrate the fact that, along with symptomatic evaluations, aggregate-containing lesions remain among the most widely used and reliable markers of neurodegeneration severity.

Another aspect that can support this hypothesis is the genetic factor. In familial cases of neurodegenerative diseases, many of the recorded illness-inducing mutations boost the aggregating propensity of proteins, suggesting that this plays a part in disease onset. A clear example to illustrate this is HD, which is a purely hereditary neurodegenerative disease caused by the expansion of a CAG trinucleotide repeat in the huntingtin (*HTT*) gene. The mutated gene codes for an mHTT protein that features an aberrantly long polyglutamine (poly Q) repeat sequence, which directly correlates with a propensity to form amyloid fibrils (*19*, *76*). Since the mutation is an established prerequisite for the disease onset, but also for the aggregation of HTT, a strong corelation between the two can be argued. Another genetics-related observation in favour of the amyloid hypothesis is that the enhanced risk of Aβ aggregation in individuals with Down syndrome appears to make them substantially more prone to early-onset AD. Indeed, in Down syndrome, the *APP* gene has a third copy, which results in a higher expression of the Amyloid Precursor Protein, and in turn triggers the accumulation of the amyloidogenic Aβ peptide. Aggregation-inducing mutations have been reported also in diseases that are not exclusively genetic in origin. Some of the most prevalent familial PD mutations from the *SNCA* gene have been found to promote α-Syn aggregation (*77*, *78*). In the case of tau, a series of mutations were found around an amyloidogenic region of the protein, where they modify the local energetic landscape in a manner that facilitates aggregation (*79*). It is essential, however, to note that there are also numerous mutations that do not promote aggregation, or whose pathogenic mechanisms remain unknown (*80*, *81*).

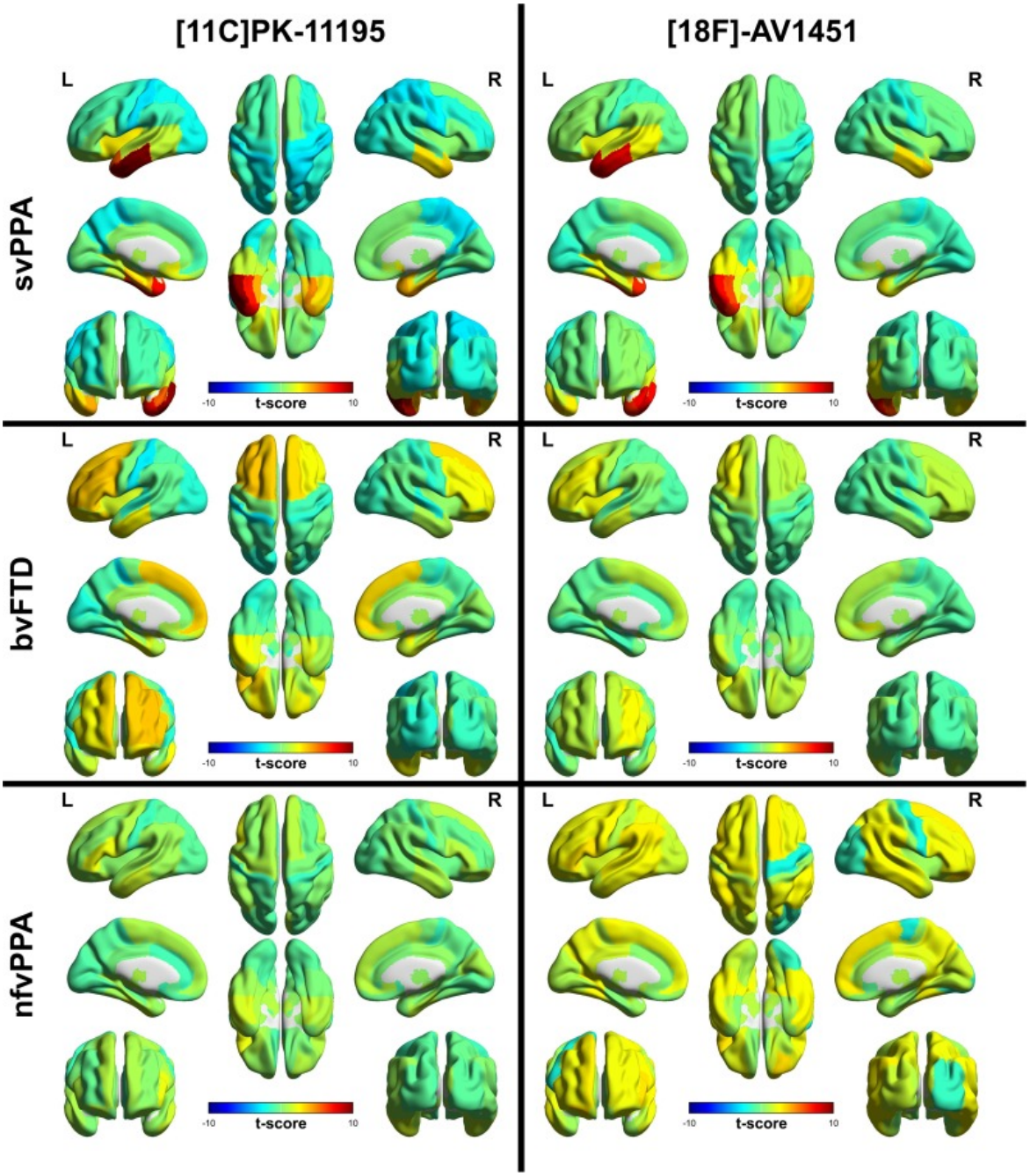

Figure I.6 Investigation of the colocalization between neuroinflammation and the presence of protein aggregates in different regions of the brain. *The image depicts positron emission tomography (PET) scans using two radioactive probes: [11C]PK-11195 indicates neuroinflammation by marking activated microglia; [18F]-AV1451 is a marker of non-amyloid-β pathological proteins from FTD. The three rows represent different variants of FTD: semantic variant primary progressive aphasia (svPPA), behavioural variant (bvFTD) and non-fluent variant primary progressive aphasia (nfvPPA). The results show an overlap between protein aggregation and neuroinflammation, suggesting a link between the two. Adapted from* (*74*).

I.2.5 Counterarguments for the amyloid hypothesis.

The observations outlined in the previous section have established the amyloid hypothesis as a prominent topic of consideration in most of the discussions related to the origins and mechanisms of neurodegenerative disease. However, caution is required, not only because this model has yet to be definitively validated, but also because an expanding body of evidence appears incompatible to it. The correlation between amyloids and cognitive or motor dysfunctions is not valid in both directions. It is true that the pathological state is associated with amyloids, however the presence of amyloids does not appear to systematically result in disease. This is illustrated in studies reporting that a substantial amount of non-demented individuals was found to have amyloid deposits in their brains after a certain age (*82*, *83*). Interpretations of this include the claims that these inclusions represent a marker of a preclinical state of the diseases (*82*, *84*), or that some individuals might naturally have a reduced sensitivity to amyloid burden (*85*). However, at this point we cannot rule out the possibility that this occurs because amyloid-like aggregates are simply not the direct cause for disease.

The prospects of research regarding the mechanisms of disease have therefore expanded to include other plausible causes. Notably, a rising hypothesis postulates that it is not the fibrillary, aggregated form of the proteins that is cytotoxic, but rather that the culprits could be smaller molecular weight species that assemble during the initial stages of aggregation. Indeed, the oligomeric species of multiple disease-related proteins, such as Aβ, α-Syn, or TDP43, were reported to be cytotoxic (**Figure I.7**) (*86–88*). A mechanistic hypothesis that is often mentioned is that they can favour the formation of membrane pores, which induces serious cellular insults and promotes the prion-like spreading of aggregates between cells (*86*, *89*, *90*). In such studies, amyloid aggregates are not presented as the initiators of pathology, but rather as the endpoint of a cytotoxic protein oligomerization process.

Some other hypotheses go as far as considering protein aggregates as protective species, that isolate aberrant cellular factors which escaped degradation. Indeed, neurodegenerative diseases have been linked to dysregulations in protein degradation cellular machineries, such as the ubiquitin-proteasome pathway (*91*), which poses serious threats to the fate of the cell by preventing malfunctioning proteins from being cleared out. Intriguingly, in neurodegenerative diseases, this dysregulation does not appear to be caused by the formation of protein aggregates, but to occur well sooner (*92*). Therefore, it was proposed that protein aggregation could be a

cellular response to faulty degradation machinery, as an attempt to trap and deactivate unwanted factors by isolating them in highly stable structures such as amyloids (*93*).

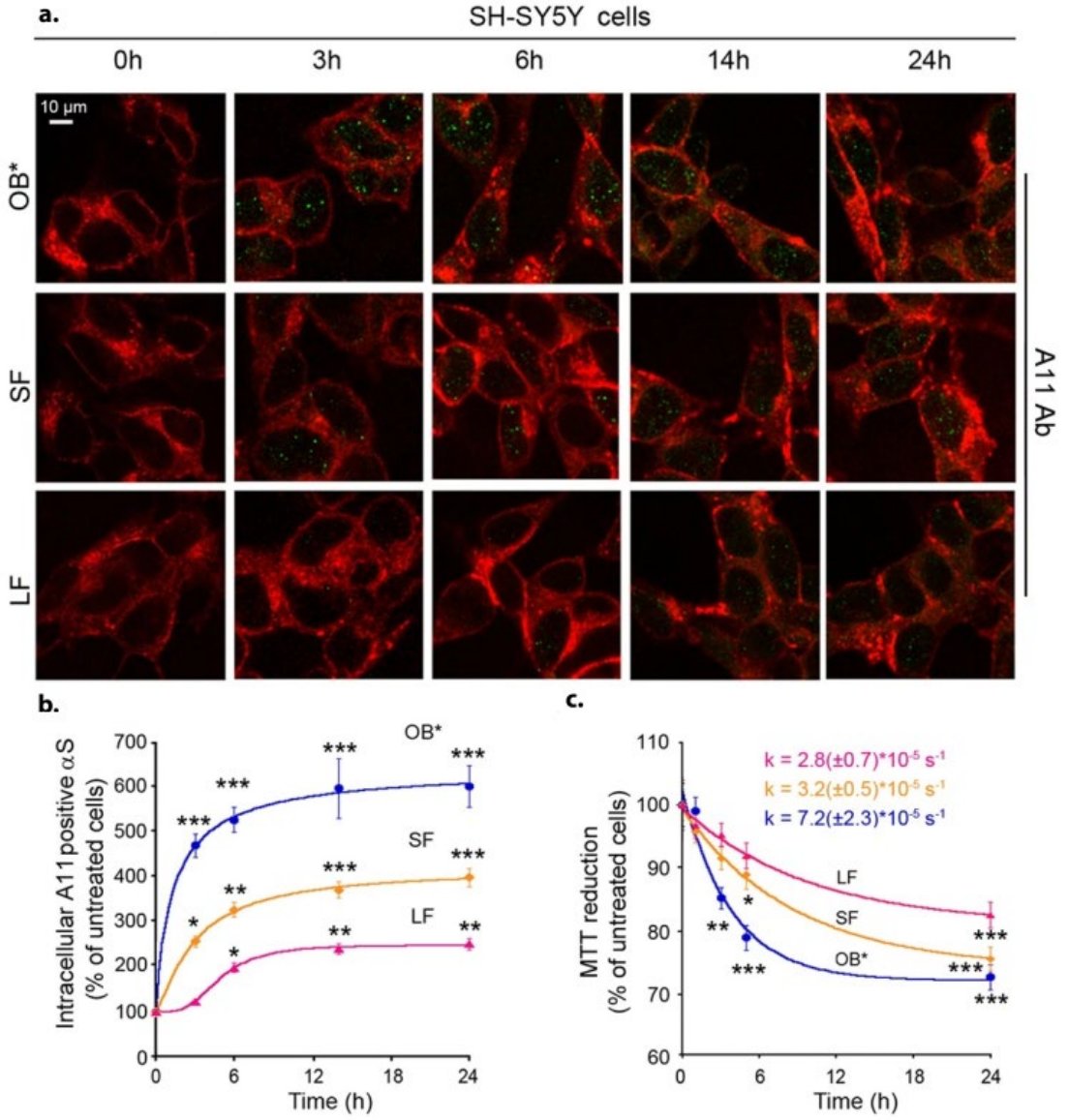

Figure I.7 *Toxicity of α-Syn oligomers in SY-SY5Y cells.* ***a.*** *Microscopy images displaying SH-SY5Y cells exposed to 0.3 µM prefibrillar α-Syn oligomers (OB*), short fibrils (SF) or long fibrils (LF) for the time periods indicated. The cell membrane marker wheat germ agglutinin (WGA) is in red and the anti-oligomeric α-Syn antibody A11 in green.* ***b.*** *Plot following the time-dependent evolution of A11 signal-positive cells (which contain oligomeric α-Syn). For cells exposed to OB*, the increase in positive cells indicates a good internalization of preformed oligomers. For cells exposed to SF and LF, the increase in A11 positive cells indicates a release of oligomers that was subsequent to the addition of SF and LF to cells.* ***c.*** *MTT-based viability assay on cells exposed to OB*, SF and LF as a function of time. OB* appear to be the most toxic, whereas toxicity for SF and LF exposed cells seems to be concomitant to the increase in A-11 positive cells. Adapted from* (*86*).

Overall, the current section illustrated how the presence of aggregates does not constitute the full picture of the neurodegenerative diseases; instead, it seems to only be an easily detectable remnant from an intricate and incompletely understood array of neurotoxic phenomena. To better grasp the disease process, more insight is required related to the preliminary phases of inclusion formation, rather than focusing on the endpoint. The next sections will be dedicated to a new research direction that could help better understand the behaviour of neurodegeneration-related proteins in relation to the early events underlying aggregation and other disease-related processes.

I.3 Phase Separation of neurodegeneration-related proteins – a fresh axis in research

I.3.1 Emergence of Phase Separation as a vantage point to study protein aggregation

During the last decade, it was progressively demonstrated that an increasing number of neurodegeneration-related proteins (such as FUS (*94*), Tau (*95*), TDP43 (*96*) and hnRNPA1 (*97*)) can undergo a physical process called Phase Separation (PS) *in vitro* (**Figure I.8.a.**). PS is a term borrowed from polymer physics, which designates the separation of macromolecules from their soluble state in favour of a highly concentrated phase that is distinct from the solvent. It has been initially associated with proteins in the 1990's, as a putative intermediate step in the process of crystallization (*98*). *In vitro* experiments showed, subsequently, that this process occurs spontaneously when certain proteins are incubated at high concentration and/or with crowding agents. In most cases, biophysical characterizations indicate that the separated phases exhibit characteristics of a "liquid in a liquid", such as the presence of surface tension as well as high mobility of their component molecules (as illustrated for Tau in **Figure I.8.b,c**) (*95*). Liquid-like properties explain the more widespread use of the derivate term Liquid-Liquid Phase Separation (LLPS), and also differentiate separated phases from other protein-based supramolecular structures such as aggregates.

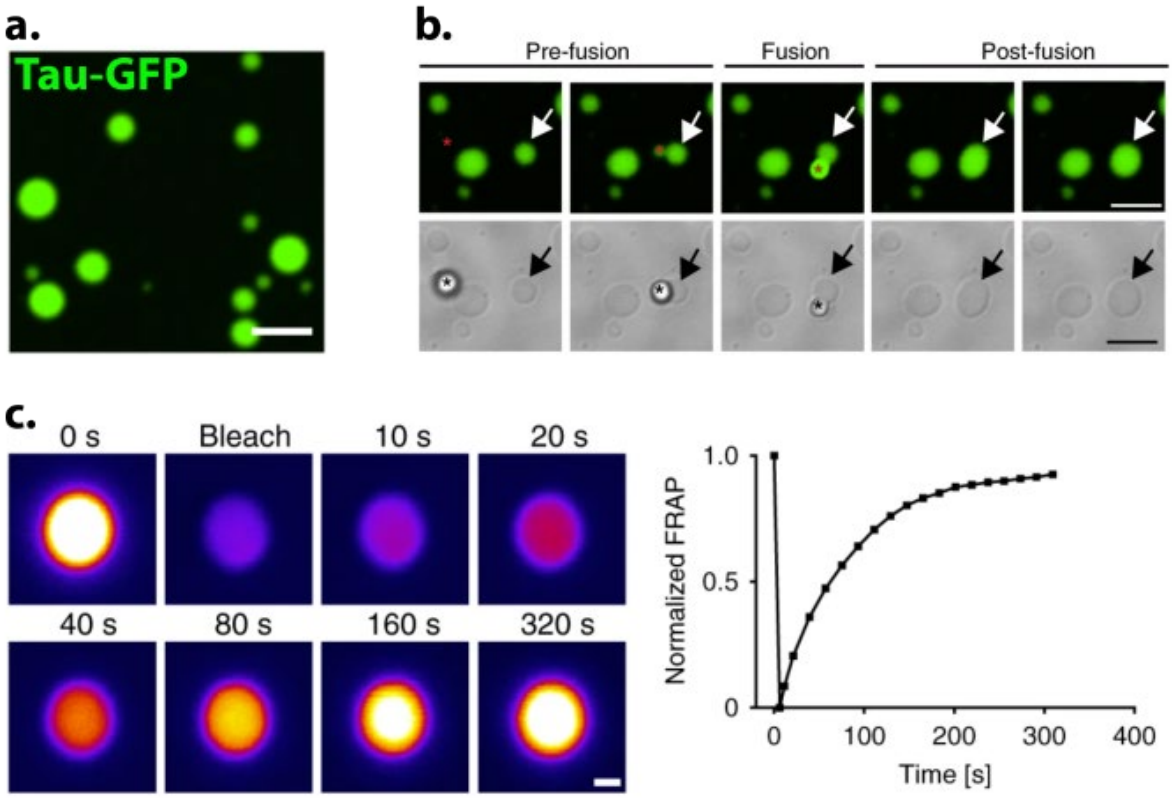

Figure I.8 Phase Separation of the protein Tau in vitro a. *Microscopy image of Tau-GFP PS-derived droplets. Scale Bar, 5 µm.* ***b.*** *Live microscopy frames illustrating the fusion and relaxation of Tau-GFP droplets into spherical shapes. This type of behaviour is associated with forces of surface tension, which are characteristic of liquids* ***c.*** *Fluorescence Recovery After Photobleaching (FRAP) of a Tau-GFP separated phase. The intensity of the fluorescence is quickly recovered after the irreversible bleaching of the its fluorescent components using a high-intensity laser beam. This is indicative of highly dynamic rearrangement of molecules within the droplet, allowing unbleached molecules to diffuse inside. Adapted from (95).*

Since *in vitro* PS-propensity appears to be a common trait of multiple neurodegeneration-related proteins, this model emerges as a novel dimension in the investigation of their relation to aggregation and disease. To better understand the relevance of PS in this context, three points need to be mentioned: I. PS is not restricted to test tubes – it is also believed to intervene in the organization of various cellular bodies. II. neurodegeneration-related proteins potentially undergo intracellular PS as part of their physiological functions. III. PS could have implications in the mechanisms of disease.

I.3.2 Intracellular Phase Separation produces biomolecular condensates

Phase separation can also occur in cells. When applied to cellular contexts, the PS model illustrates how specific biomacromolecules (proteins and sometimes nucleic acids) can assemble together in highly concentrated liquid-like droplets which are separated from the cytosol or the nucleosol. Cellular condensed phases are compositionally complex (featuring up to hundreds of different biomolecules) (*99*, *100*). This arises from the fact that proteins and nucleic acids involved in cellular phase separation interact with various other biomolecules during their functional processes, and some of these additional biomolecules can also join and become part of the separated phases. Thus, cellular PS allows the self-assembly of intricate cellular compartments without the need to enclose their contents with a membrane (*101*). A great variety of such membrane-less compartments exists, each possessing its own functionalities for the cell (**Figure I.9**). To underline their complex biochemistry, but also their condensed phase nature, scientists have coined the term 'biomolecular condensates' (or short biocondensates).

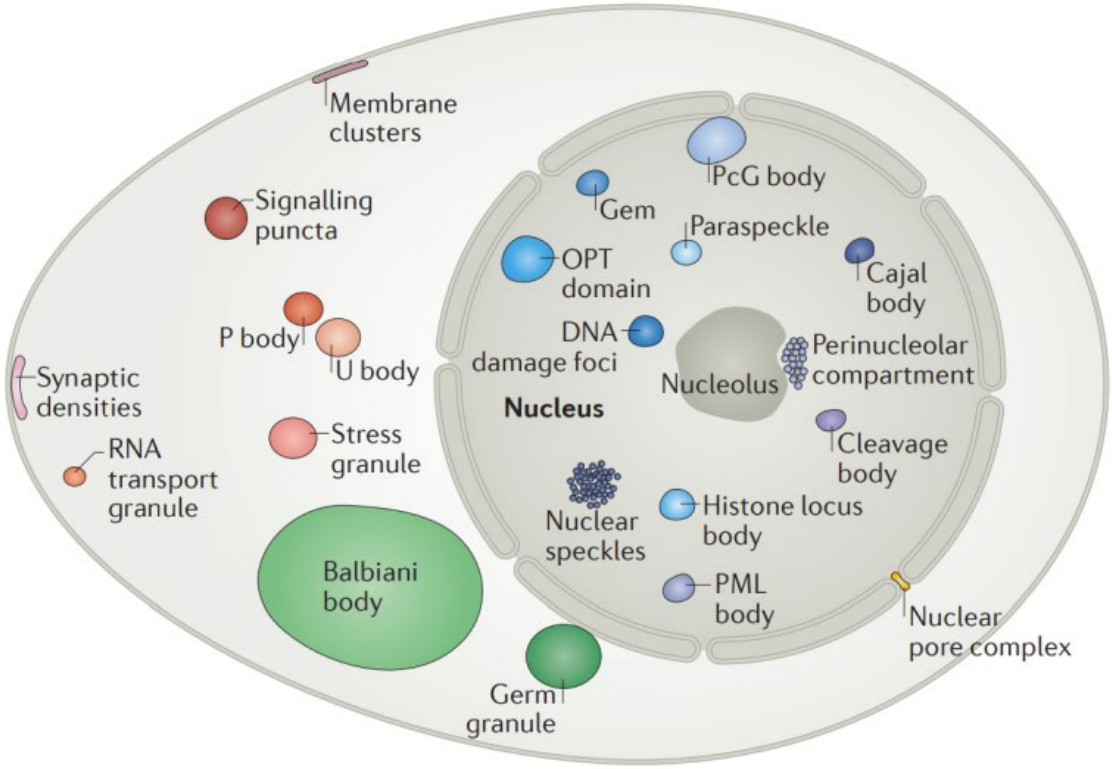

Figure I.9 Different examples of biomolecular condensates in a eukaryotic cell. *Their different localizations (nucleus, cytoplasm, membrane) are depicted. Some condensates are cell specific (such as Germ granules and Synaptic densities), others are ubiquitous (such as the nucleolus), and some are dependent on certain cellular events (such as DNA damage foci and Stress granules). Adapted from* (*101*).

The knowledge of biomolecular condensates precedes that of intracellular PS, with the first discovery of a membrane-less organelle - the nucleolus - dating back as far as the 1830's (*102*). However, until relatively recently, very little was known about their material properties, or about their mechanism of formation. The emergence of PS as a likely mechanism for the assembly of biomolecular condensates started in 2009, when Brangwynne et al. published a biophysical description of germline P granules of *C. elegans,* a type of cellular structure that is responsible for orchestrating the somatic differentiation in embryos (*103*). In this seminal paper, the authors described how the response of these P granules to shear stress (i.e., dripping, flowing, and fusing with each other and relaxing into spherical shapes) was indicative of liquid-like properties (**Figure I.10**) (*103*). They later proposed that the formation of these cellular structures involved physical phenomena that could be explained using the PS mechanism (*104*). Since then, PS has become a key model to describe the spatiotemporal organization of the cell. Indeed, numerous membrane-less cellular structures, such as nucleoli (*102*), stress granules (*105*) and Cajal bodies (*106*) have been reconceptualized as potentially originating from phase separation processes. The main argument to back this new framework is that they exhibit liquid characteristics: dynamic properties and elevated rates of component exchange with the surrounding medium. However, exceptions from this exist, including Balbiani bodies which are membraneless organelles with solid matter properties (*107*).

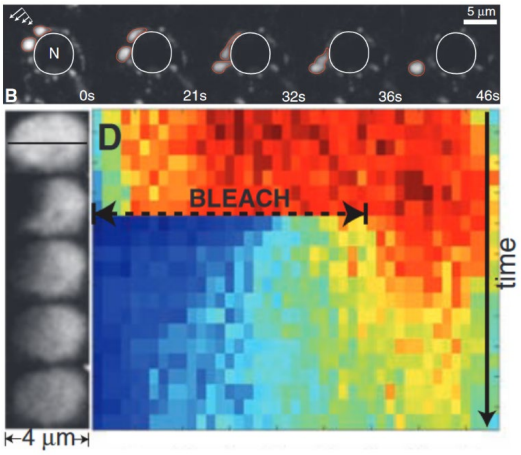

Figure I.10 The liquid nature of C elegans P granules Upper panel: *Exposure of P granules to shear stress reveals a liquid-like behaviour: granules drip and coalesce.* ***Lower panel:*** *Kymograph following the time-dependent evolution of the fluorescence intensity of P granules upon photobleaching. The graph displays a recovery of fluorescence in the bleached part and a decrease in fluorescence in the unbleached section, suggesting that a micrometric-scale rearrangement of molecules takes place within P granules. This is specific of liquid-like objects. Adapted from* (*103*).

I.3.4 PS of neurodegenerative disease-related proteins in cellular systems likely yields biomolecular condensates

A question that arises is whether neurodegenerative disease-related proteins conserve their phase-separating properties *in vivo*. In the brain, this currently remains extremely difficult to assess, because contrary to aggregates, which are accessible for isolation from brain samples due to their stability, phase separated bodies are difficult to extract directly from tissues. The relevance of PS with regards to these proteins is, however, validated by overexpression studies *in cellulo*, which underline their PS propensity in a physiological environment. For example, the U2OS or SH-SY5Y cells stably expressing TDP-43, tagged with mRuby2 or Enhanced Yellow Fluorescent Protein (EYFP) respectively, displayed nuclear condensates with liquid-like material properties (*108*).

Interestingly, some neurodegeneration-related proteins have been proposed to conserve their physiological functions within phase separated compartments *in cellula*. For example, the overexpressed ALS-related protein FUS forms nuclear liquid-like compartments in HeLa and Mouse Embryonic Stem Cells, that localize to DNA damage sites (*94*). Additionally, in conditions of heat shock, FUS condensates can also shuttle to the cytoplasm to participate in the formation of stress granules (SG), which are biomolecular condensates that may protect mRNAs during periods of interrupted translation caused by cellular stress (*94*).

Furthermore, the AD-related protein tau forms small puncta at the surface of microtubules in hippocampal neurons (*109*). Reconstitution with taxol-stabilized microtubules revealed that these were tau condensates that acted as selective barriers permitting the differential passage of different factors along the microtubules (*109*). Indeed, whilst processive movement mediated by dyneins was permitted, tau condensates remained impassable for dynactin-mediated diffusion. The study illustrates how PS allows tau to regulate molecular motor-mediated cargo transport along microtubules (**Figure I.11**).

Protein liquid droplet phases can also help with the transient storage of cellular components that need to undergo controlled trafficking. This is the case, for example, for synaptic vesicles, which are small membrane-bound compartments that contain neurotransmitters. A recent study suggests that these vesicles could be stored in presynaptic neurons in condensed phases of α-Syn and Synapsin I (*110*). This hypothesis results from the observation that the reconstitution of α-Syn/Synapsin I condensates *in vitro* was facilitated by the recruitment of synaptic vesicles (*110*). Such dynamic liquid phases reconcile the need to

cluster these SVs together with the requirement to readily release them into the synaptic space upon stimulation. The synapsin I/ α-Syn condensate is presented in more detail in chapter III.

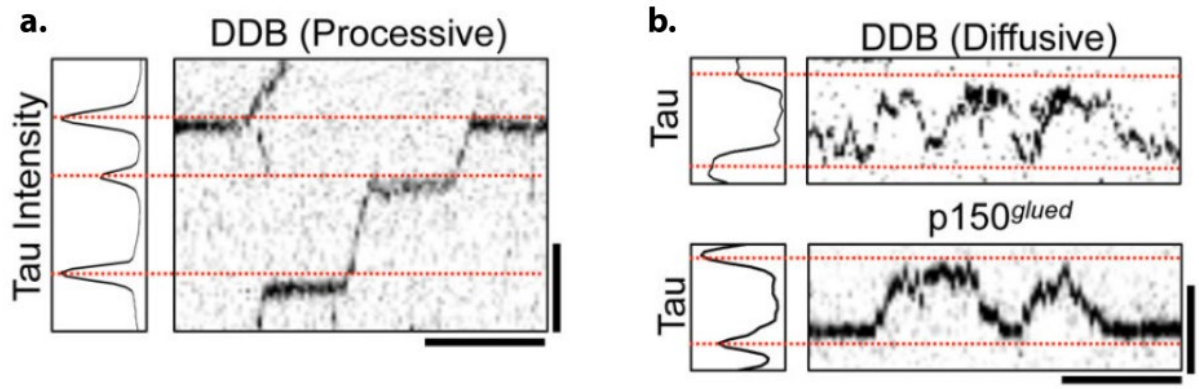

Figure I.11 Selective passage of different types of molecular motors along microtubules upon encountering tau condensates. *Left panels: Plot of the fluorescence intensity of tau- sfGFP along a microtubule. The horizontal pics indicate condensates adjacent to the microtubule. Right panels: Kymographs representing the movement of a molecular motor along the microtubule.* ***a.*** *When encountering a tau condensate, a processive dynein-dynactin-BicD2N (DDB) motor complex may pause, but can pass through the condensate and move on along the microtubule in its initial direction.* ***b.*** *On the contrary, a diffusible DDB or the p150^{Glued} component of the dynactin complex cannot pass through tau condensates. Thus, they engage in a bi-directional movement along the microtubule between two consecutive condensates Adapted from (109).*

Overall, these examples illustrate that some neurodegeneration-related proteins undergo PS upon overexpression in cells, and that some PS-generated condensates seem compatible with the physiological functions of the proteins that compose them. This aspect lends credence to the hypothesis that naturally occurring condensates of these proteins could exist as part of their physiology.

I.3.5 Phase-separated condensates of neurodegeneration-related proteins may be intermediates in aggregation

Biomolecular condensates provide numerous advantages for the regulation and the spatiotemporal control of biochemical processes. However, increasing evidence points at the possibility that they could be intermediates in protein aggregation. A pioneering study in this direction reported how FUS droplets convert from a liquid state to solid fibrillar assemblies *in vitro* - a transition that was favoured by disease-inducing mutants (**Figure I.12**) (*94*). Later, the same group reported that a liquid-to-solid transition also occurs in cells in specific conditions such as an RNA-depleted environment (*111*). Similarly, the AD-related protein tau was reported to undergo LLPS followed by a liquid-to-solid transition in a GFP-tau441 overexpression assay in primary cortical mouse neurons (*112*). Additionally, a study in *C. elegans* PD models indicate that overexpression of α-Syn in its muscle wall cells lead to the time-dependent formation of α-Syn assemblies that progress with the aging of the worm into insoluble, ubiquitin-positive assemblies likely to contain amyloid-like aggregates (*113*). The collection of observations of liquid protein states evolving into protein aggregates keeps expanding. This pattern has inspired the development of a hypothesis stating that the liquid-like droplet state could be an intermediate phase in the formation of protein aggregates. If validated, such a mechanism could represent a possible path describing the origins of pathology-related protein inclusions in the nervous system. Thus, the understanding of the mechanisms of PS and their relationship to protein aggregation have become promising axes of research in the field. In recent years, investigations in this field have laid a groundwork for our understanding of the molecular mechanisms underlying phase separation, but also of the distinct factors that could favour or trigger the transition of these phase-separated condensates towards aggregated states.

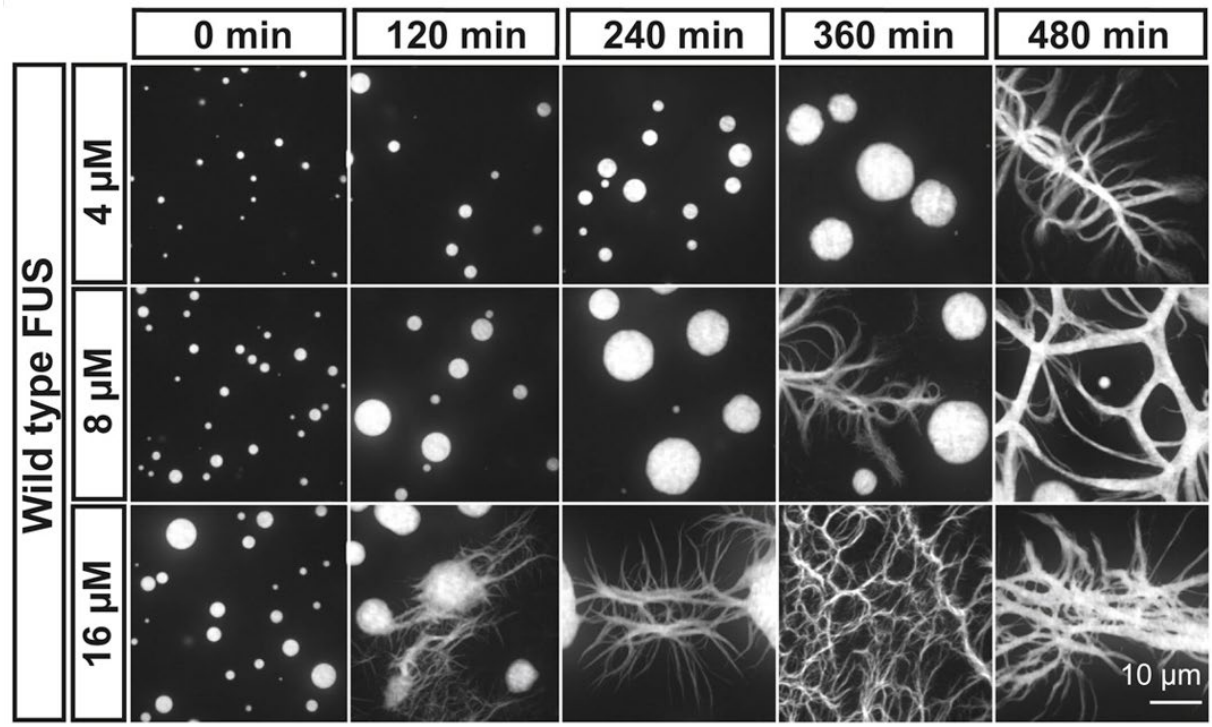

Figure I.12 In vitro liquid-to-solid transitions of the protein FUS. *The protein forms condensed phases with initially liquid properties, but spontaneously transition towards fibrillar solid-like entities within hours. Adapted from* (*94*).

I.3.6 Physico-chemical basis of PS and the formation of biocondensates

PS is a phenomenon that can be described in its simplest form for a system containing a polymer and a solvent, where there are only three types of interactions to consider: solvent-peptide, peptide-peptide and solvent-solvent. In this context, the Flory-Huggins parameter (χ) is a variable that quantifies the energetic cost of having a solvent molecule adjacent to a monomer moiety from the polymer (*114*). When χ is <0 (good solvation), solvent-polymer interactions are favoured and the polymer tends to remain soluble (**Figure I.11.a.** upper panel). On the contrary, in conditions of suboptimal solubilization (χ >0), polymer-polymer bonds become favourable and promote self-assembly (**Figure I.11.a.** lower panel). However, in this case, entropy fights against the formation of a separated phase, because solubilized polymers represent a more disordered state. Thus, phase separation can only occur above a certain saturation concentration (C_{sat}), which corresponds to enough polymer-polymer bonds to compensate for the entropic cost of assembling polymers together (*114*, *115*). A phase diagram

representation illustrates how above this concentration limit the solution separates into two different phases: a dilute one and a dense one (**Figure I.13**).

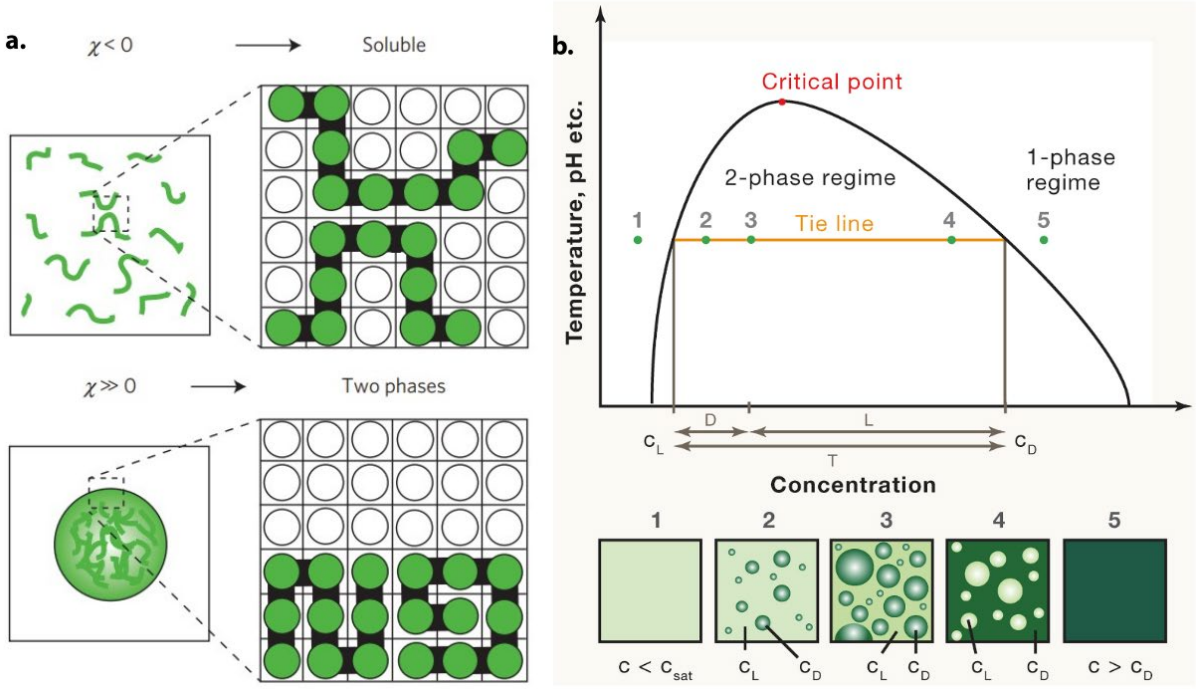

Figure I.13 Phase separation of linear polymers. a. *Illustration of LLPS tendency with Flory-Huggins parameter (χ). At χ < 0, the polymer remains soluble. At χ >> 0, polymer-solvent interactions are less favoured, and the polymer phase separates above a critical concentration. Adapted from* (*114*). ***b.*** *Phase diagram describing the concentration-dependence of PS.* C_{sat} *= saturation concentration;* C_L *= concentration of the light (dilute) phase;* C_D *= concentration of the dense phase. Phase separation occurs when the polymer concentration is higher than* C_{sat} *and lower than* C_D*. Within this regime (tie line), the solution separates in two distinct phases: one at* C_L *(dilute phase) and one at* C_D *(dense phase). Adapted from* (*115*)*.*

This model can be applied to biological macromolecules, the difference being that proteins and RNAs are heteropolymers, and that they reside in complex media with hundreds of other molecules. Since amino-acids from different proteins can interact with each other through all sorts of bonds (electrostatic, H-bonds, hydrophobic) phase separation is in theory possible for all proteins at very high concentrations (*101*). However, in physiological conditions, most proteins find themselves in what Flory would qualify as “good solvent conditions”, and thus have characteristic C_{sat} that are too high for LLPS to occur in cells. In this case, what are the factors that render a specific subset of proteins LLPS-prone? It appears that

phase transition could be sequence-determined. LLPS-prone proteins often contain Low Complexity Domains (LCD) which are segments depleted in hydrophobic residues and enriched in repetitive sequences of charged or polar residues. Their low hydrophobic content means that they do not require secondary structure to be solubilized, thus they expose 'sticky' residue repeats to the solvent. This allows the protein to engage in multiple simultaneous interactions, whose additive enthalpic effects help cross the entropic barrier of PS.

The knowledge about the sequence determinants of PS has afforded the exploration of the different chemical bonds that underlie this process. Notably, for FUS, PS is hypothesized to be driven by Tyr residues within the [Ser/Gly]Tyr[Ser/Gly] motif that is found at 24 homogenously distanced sites within the LC N-ter of the protein (*116*). The same motif was equally found to be important for the PS of TDP43 (*117*). Additionally, the authors of this study report that hydrophobic residues also contribute to phase-separation of the protein, and that an increase in its positive charge creates electrostatic repulsion with an PS-inhibitory effect. Another mechanistic description of phase separation has been made for the Nefrin Intracellular Domain (NCID). In this case, PS is driven by electrostatic interactions between 'blocks' of negatively charged residues (Asp/Glu) and a positively charged partner (here the supercharged GFP), and further stabilization of the droplets is provided by interactions involving aromatic and even some hydrophobic residues (*118*). These observations are in phase with the prediction that multivalent interactions are drivers of phase separation, and underline how the distribution of the interacting sites within the protein sequence is also essential.

Recently, a unified model for the mechanism of intracellular protein phase separation was proposed (*119*). It describes how the percolation of biomolecular macromolecules into droplets is driven by specific sequence patterns that involve short regions with high homotypic or heterotypic association propensities (called 'stickers'), which are separated by non-interacting fragments called 'spacers' (*119*). This model also allowed a binary classification of the biomolecules that participate in intracellular phase separations, proposed by Banani et al. in 2016 (*120*). On one side, they define as 'scaffolds' the macromolecules that contain enough 'sticker' regions to drive phase separation by themselves, and whose presence is mandatory to hold the condensates together. On the other side, they describe a second class of molecules – the clients – that have lower 'sticker' valences, and that can partition within condensates by interacting with scaffolds, but that lack the capacity to undergo LLPS by themselves (*120*) (**Figure I.14**).

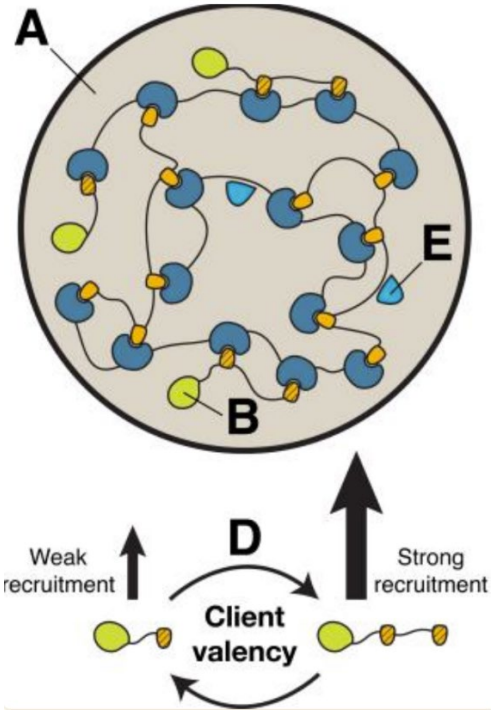

Figure I.14 Representation of the main component types in biomolecular condensates. *Scaffolds are molecules with high valency. They are represented here as long chains of blue and orange interacting domains (A). In this case, each blue "sticker" binds to a yellow one, and these bonds drive the formation of the biomolecular condensate. Clients are molecules with low valency. They are represented here as short chains containing hatched orange interacting domains (B). Clients partition into the condensates with an affinity that is proportional to their valency (D), but do not drive LLPS by themselves. Some biomolecules can also partition into the condensates through binding to regions of the scaffold other than the multivalent domains (E). Adapted from* (*120*).

I.3.7 Factors influencing liquid-to-solid transitions

Both protein aggregation and PS appear to share mechanistic common grounds: they can occur due to a multitude of interactions favoured by conformationally flexible chains of IDPs. Thus, a link between the two phenomena has been naturally postulated (*97*, *116*). Indeed, for some proteins, such as hnRNPA2, is was reported that the interactions that drive phase separation are the same as those that are found within hydrogels (*121*). Despite these similarities, however, biomolecular condensates and aggregates present drastically different material properties and cellular impacts. Thus, one question arises: what could be the difference between conditions in which proteins aggregate versus conditions in which they undergo PS? Although the exact mechanisms are not completely understood, some factors favouring liquid-to-solid transitions have been nevertheless proposed.

A notable aggregenic factor for condensates is the increased protein concentration. It seems indeed intuitive that the crowding of proteins in condensates promotes more protein-protein interactions, and that this can increase the chances for a stochastic event of aggregation nucleation. Indeed, the kinetic models of nucleation-dependent polymerization predict that the lag time for the formation of the aggregate nucleus is dependent on concentration (*122*). The conformational adaptability of IDP could also play a role in the liquid-to-solid transition. For example, tau and α-Syn were reported to undergo similar aggregation-inducing conformation alterations upon LLPS (*123*, *124*). Both proteins were proposed to adopt 'elongated' conformations within droplets, that the authors hypothesized to favour aggregation-inducing intermolecular interactions, at the expense of intramolecular bonds between their oppositely charged termini (*123*, *124*).

Liquid-to-solid transitions can also occur when PS is driven by molecules bearing disease-inducing mutations, because changes in amino acid sequences can lead to altered interactions between the components of condensates. A notable illustration for this process was presented in 2015 with the study of the condensate-mediated aggregation of the protein FUS, which was shown to be substantially accelerated by the previously known pathogenic mutations G156E and R244C (*94*, *125*). In the case of TDP43, mutations that disrupt the phase separation behaviour of a protein appear to promote accelerated aggregation, thus suggesting a protective role of PS against pathology (**Figure I.15**) (*96*). Interestingly, there are also mutations in non-PS proteins that can influence the fate of condensates. For example, Ubiquilin 2 (UBQLN2) positively regulates the liquid properties of FUS-RNA granules, and mutant versions of this protein can lead to a loss of dynamic properties of the molecules within these droplets. Similarly, mutations in the valosin-containing protein (VCP) have been shown to inhibit SG clearance (*126*). This can have pathological effects, as prolonged residence of SGs in the cytosol is hypothesized to seed pathologic inclusions related to ALS and FTD (*126*).

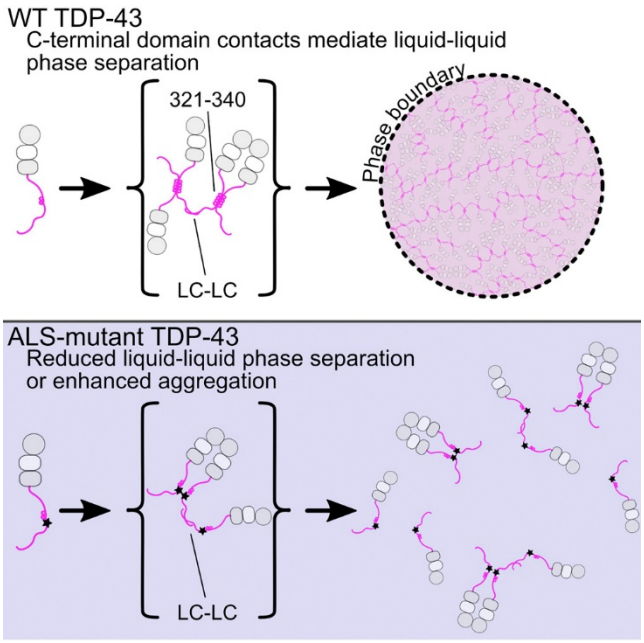

Figure I.15 Mutations in TDP43 C-terminal domain promote aggregation by preventing the protein from undergoing LLPS. *Adapted from* (*96*).

Another important factor in the regulation of the properties of droplets is RNA. Indeed, RNA is a common component of biomolecular condensates and can even act as a 'scaffold' molecule to drive phase separation in collaboration with RNA-binding proteins (RBPs) (*127*, *128*). Recent results from our team highlight the importance of RNA molecules for the modulation of some condensate properties, such as their size and number (*129*, *130*). For some proteins, such as FUS, TDP43 and hnRNPA1, the delocalization of condensates from to nucleus to the cytoplasm is strongly correlated with aggregation (*131*). A study from 2018 postulated that the persistence of the liquid-like state in the nucleus could be related to the binding of these proteins to their RNA partners (*111*). Indeed, they report that RNA binding to these RBPs modulates the properties of their corresponding condensates as follows: at physiological nuclear RNA concentration phase separation is inhibited, however some specific RNAs can nucleate LLPS and keep the resulting condensates liquid. However, absence or digestion of RNA readily triggered the liquid-to solid transition, suggesting that RNAs could act as buffers that control the formation and the properties of intracellular droplets (*111*).

I.4. Reconstitution of LLPS *in vitro* and in cells

A striking difficulty in the study of condensates *in vivo* is their compositional complexity, as they feature tens to hundreds of different factors (*100*). Following the interactions and activities of so many biomolecules simultaneously is far from achievable with current tools. Therefore, many teams seek to recreate compositionally simplified versions of condensates, whose properties and activities can be more easily traced back to a certain component.

A simple way to approach this challenge is the reconstitution of *in vitro* condensates. Based on the principles of PS, scientists have been able to recreate protein and/or RNA scaffolds that can lead to the controlled formation of assemblies that recapitulate the liquid-like properties of biomolecular condensates. An early study in this field came from Li et al., who recreated *in vitro* protein condensates using purified tandems of the SRC homology 3 (SH3) domain and of a Prolie-rich domain (PRM) (**Figure I.16**) (*132*). Repetitions of these domains occur naturally in signalling proteins and interact with each other in physiological processes. The creation of valency variations of these scaffold (containing different numbers of SH3 or PRM domains) allowed them to draw some important conclusions related to the assembly of condensates. First, they noticed that multivalence was essential for LLPS, as lower valency scaffolds were unable to yield droplets. Additionally, they also realized that the binding of high affinity monovalent ligands can disrupt LLPS, because it disrupts multivalent interactions. Thirdly, their Fluorescence Recovery After Photobleaching (FRAP) data suggested that the valency number of the scaffolds was inversely proportional with the micrometric reorganization of the scaffolds within the droplets. This suggests that the formation of liquid-like droplets relies on a specific multivalence range: too little tandem domains do not undergo LLPS, whereas too many lead to the formation of gels or even solids (*132*).

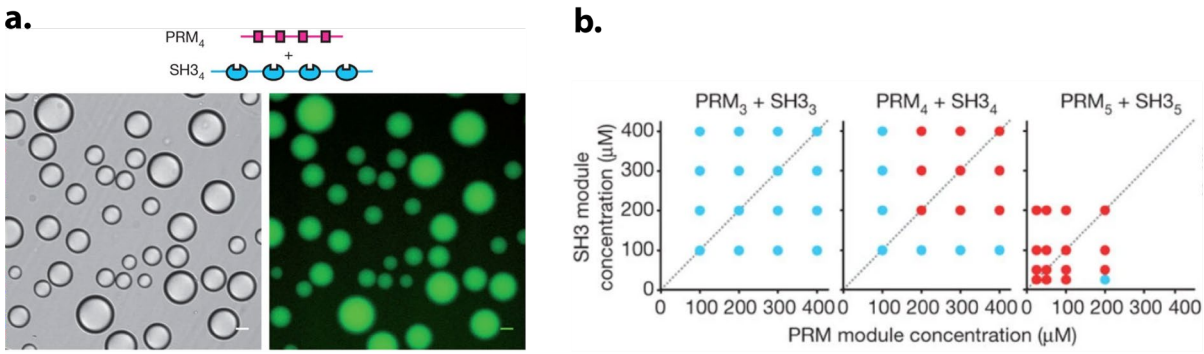

Figure I.16 Artificial condensates made from repeats of PRM and SH3. a. *Schematic representation of multivalent scaffolds containing 4 PRM repeats and 4 SH3 repeats respectively. Differential interference microscopy (left) and fluorescence microscopy (right) images of the droplets formed through incubation of 300 μM of each.* ***b.*** *Phase diagram displaying the outcomes of mixing different concentrations of PRM/SH3 trimer and tetramer tandems respectively. Blue dots = no PS, whereas red dots = PS. The importance of multivalence is highlighted here. Adapted from* (*132*).

Another bottom-up system for the reconstitution of condensates was based on repeats of the Small Ubiquitin-like Modifier (SUMO) coupled with a tandem of SUMO Interacting Motifs (SIM). This system has allowed the authors to probe how 'client' molecules (here represented by monomeric SUMO or SIM) partition into condensates (*120*). When one of the scaffolds is in stoichiometric excess, some of its interacting motifs will remain free, thus its corresponding ligand can readily partition within the condensate. On the contrary, the 'client' that binds a limiting scaffold partition a lot less, because the binding domains of its scaffold are mostly 'occupied' by interactions with other scaffold molecules. This study illustrates how the composition of artificial condensates can be modulated by designing the PS-driving scaffolds and their stoichiometric proportions, such that resulting droplets can specifically accommodate certain molecules (*120*).

Although very enriching, it is difficult to say whether observations related to *in vitro* experiments can be extrapolated to bona fide protein condensates or aggregates. Indeed, droplets of purified proteins cannot serve as accurate mimics of a biomolecular condensate's natural behaviour because they are missing the biophysical and biochemical environment of the cell. It is therefore of great utility to develop tools that would enable the study of phase-separated condensates directly in cells. A notable alternative to *in vitro* studies is the cellular overexpression of proteins of interest fused to fluorescent reporters. However this method can

yield incongruent results: for example, overexpression of α-Syn was independently reported both to form and to not form condensates *in cellula* (*110*, *133*). This matter will be developed in more detailed in section II.1.2.

To circumvent the aforementioned limitations, bottom-up strategies for the reconstitution of condensates in cells have recently been proposed. In this context, one study adopted an optogenetic approach, which involved the photolyase homology region (PHR) of *Arabidopsis thaliana* Cry2 – a protein that clusters into oligomers upon exposure to blue light (*134*). The technique consisted in fusing this oligomerization domain to different proteins that contain "sticky" IDRs, such as FUS, HNRNPA1 or DDX4 (*135*). They reported that the mix between the oligomerization of Cry2 and the self-association propensity of the IDRs allowed the light-dependent control over the formation and dissolution of artificial condensates (*135*).

A similar system was developed with the ALS-related protein TDP43 (**Figure I.17**) (*136*). This system allowed the spatiotemporal control of TDP43-enriched condensates, and was used to probe the aggregating behaviour of TDP43 upon prolonged or condensation periods. The authors concluded that repeated clustering of the Cry2-TDP43 fusion (optoTDP43) promoted the aggregation of the protein, and validated a previously existent hypothesis proposing that RNA binding in TDP43 condensates obstructs aberrant transitions into toxic solid inclusions (*136*).

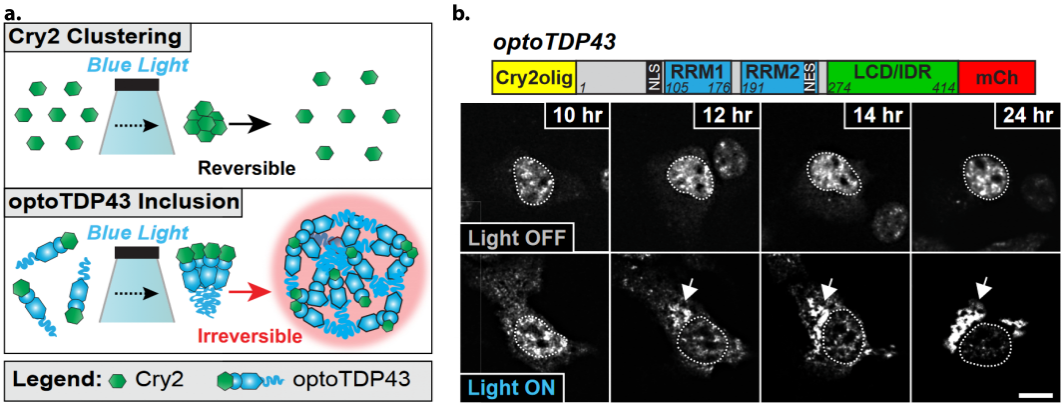

Fig I.17 The optogenetic system applied to the study of TDP43. a. *Schematic representation of the self-assembly method using the Cry2 photoreceptor (green hexagons). Fusion of this Cry2 domain with TDP43 (optoTDP43) creates light-inducible condensates.* ***b.*** *Graphic representation of the optoTDP43 fusion protein. Fluorescence microscopy images illustrating HEK293 cells expressing optoTDP43-mCherry. Upper row: no light exposure. Lower row: stimulation with blue light (~0.3 mW/cm^2, 465 nm). Scale bar, 10 µm. Continuous light stimulation yields nuclear condensates that undergo a time-dependent relocation to the cytoplasm. Adapted from (136).*

An auspicious method for controlled formation of artificial condensates was proposed by Nakamura et al (*137*). Their system, called iPOLYMER (intracellular production of ligand-yielded multivalent enhancers) is based on two multivalent scaffolds containing repeats of FK506 binding protein (FKBP) and the FKBP–rapamycin binding protein (FRB). Since these two proteins can interact only in the presence of rapamycin, the overexpression of the two scaffolds in cells allowed a stimulus-controlled nucleation of liquid-like condensates. Interestingly, the authors managed to functionalize this system, by fusing the RNA Recognition Motif (RRM) of the SG formation driver protein TIA-1 to one of the scaffolds. They used immunofluorescence to conclude that condensates recruited a poly- (A) Binding Protein (PABP1), which indicated that they reproduced the mRNA-accumulating behaviour of SGs (*137*).

Artificial intracellular condensate systems have proved to be very useful: they afforded a better understanding of the principles that underlie the biophysical properties of natural condensates, they contributed to the validation of the PS models based on weak interaction multivalence, they have proven to be functionalizable, allowing the design of simplified version of *bona fide* condensates such as SG, and proved to be useful in the understanding of the aggregation mechanisms behind proteinopathies. Thus, such methods emerge as extremely promising for tackling biological inquiries involving complex condensates which are not straightforward to investigate in their natural form.

I.5. Motivations of the thesis.

The central aim of my thesis is to **reconstitute condensates enriched in the protein α-Syn in cells**. α-Syn's amyloid transition has been linked with various neurodegenerative illnesses (Chapter I). *In vitro* evidence suggests a connection between the condensed phase of α-Syn and aggregation. However, the protein's ability to undergo intracellular PS in cells remains a subject of ongoing debate. Moreover, whether endogenously expressed α-Syn can undergo PS is still unknown as no report of such condensates was published to date.

To build α-Syn reconstituted condensates, we used **a protein scaffold, specifically designed to undergo phase separation upon expression in cellular systems**. The scaffold alone yields concentration-dependent condensates with liquid-like properties, that can be dissolved in a controlled manner. Our strategy was to attach α-Syn to this protein scaffold to obtain α-Syn condensates.

What are the biophysical characteristics of reconstituted α-Syn condensates? Specifically, we wanted to determine if the distinct micro-environment provided by the condensate modulated α-Syn's propensity to aggregate.

What is the effect of exposure of α-Syn condensates to α-Syn amyloid fibrils? α-Syn exhibits prion-like behaviour, implying that its aggregates can migrate from regions affected by disease to neighbouring healthy cells, where they promote the aggregation of native α-Syn monomers. We hypothesize that, within "healthy" cells, the assembly in a condensed liquid phase could influence the response to prion-like aggregation propagation. To test this hypothesis, we aimed to **study the incorporation of fibrils within cells expressing α-Syn-enriched condensates**. Specifically, we had the following inquiry: **does α-Syn within condensates exhibit a different response to fibrils, as compared to its diffuse state?**

In the second part of this study, we aimed at **building and studying more compositionally complex condensates, featuring heterotypic interactions involving α-syn**. We focused on the protein synapsin I, which is a natural interactor of α-Syn at the presynaptic termini of neurons. Synapsin I and α-Syn were recently shown to undergo phase separation together both *in vitro* and in cells (*110*). Thus, an objective of the thesis consisted in using our condensate reconstitution toolbox to create intracellular separated phases enriched in both proteins (Chapter III).

What is the influence of α-Syn amyloid fibrils on the α-Syn/synapsin I condensates?

We aimed to establish whether the exposure of the mixed α-Syn/synapsin I condensate to preformed α-Syn fibrils could trigger the transition from a liquid-like state to a solid fibrillar aggregate.

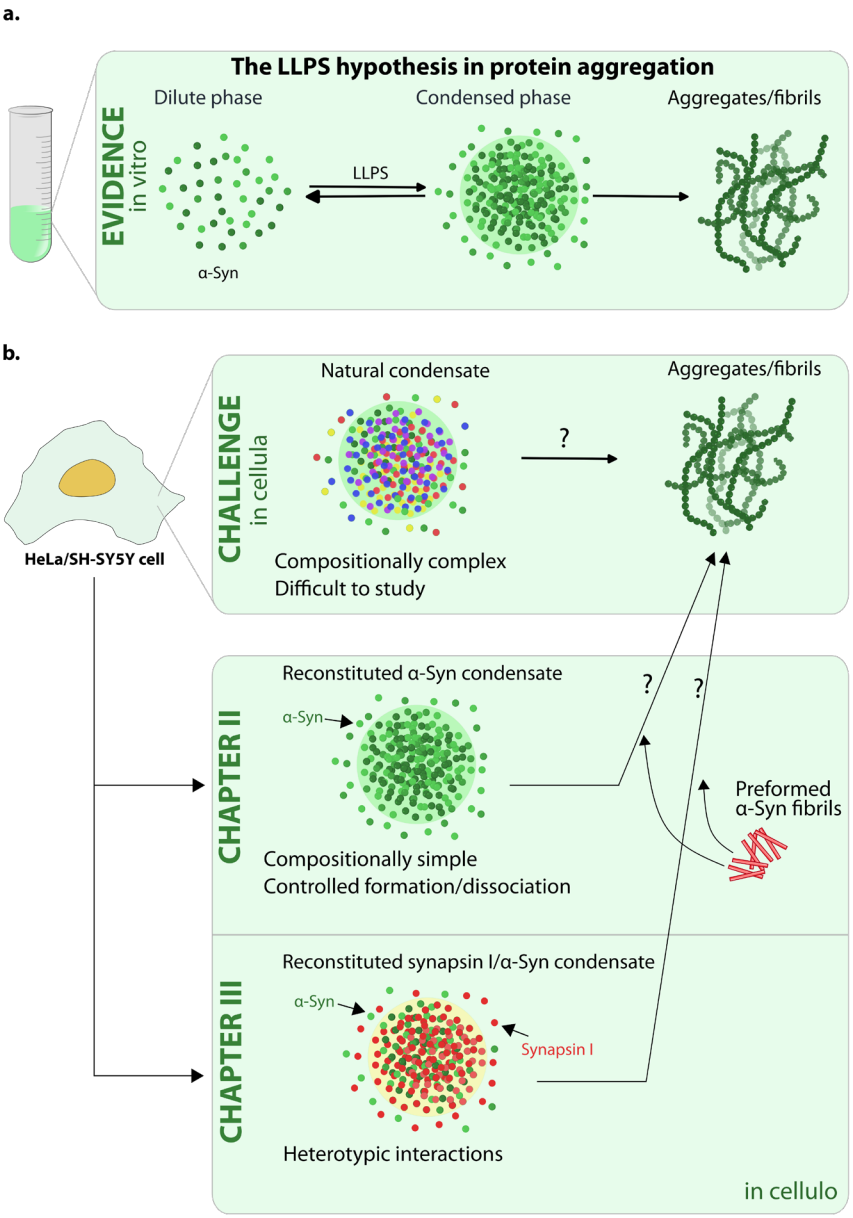

Figure I.18 Motivations of the thesis. a. *Schematic of the PS hypothesis in neurodegenerative diseases, supported by in vitro evidence.* ***b.*** *Upper Section: The study of phase separated biomolecular condensates is difficult in cellulo, due to their elevated complexity. Middle section: Chapter II will describe the reconstitution of α-Syn condensates, and their relation to preformed α-Syn fibrils. Lower section: Chapter III will describe the reconstitution and study of α-Syn/Synapsin I condensates.*

CHAPTER II: α-SYNUCLEIN LIQUID CONDENSATES FUEL α-SYNUCLEIN FIBRILLAR GROWTH

II.1 Physiopathology of α-Synuclein

II.1.1 General remarks on the physiology and pathology of α-Syn

α-Syn is a highly conserved 14 kDa protein encoded by the *SNCA* gene. The protein is expressed in various tissue types (*138*), however most of it can be found in nerve cells, notably at the pre-synaptic termini of neurons (*139*). Its 140 amino-acid residues span over 3 different domains: an amphipathic, lipid-binding N-terminus, a hydrophobic non-amyloid-beta component (NAC), and an acidic and highly disordered C-terminal domain (**Figure II.1.a.**). The protein is highly disordered in solution, however readily adopts an amphipathic helix conformation in its N-terminal and central regions upon lipid binding (**Figure II.1.b.**) (*140*, *141*). It was initially discovered in the electric organ of the *Torpedo californica,* however only gained widespread attention when its NAC domain was found in the senile plaques from Alzheimer's disease patients, hence the name non-amyloid-beta component (NAC). Since then, multiple other neurodegenerative diseases, such as PD, FTD and MSA, were linked to α-Syn aggregation, and have been classified under the umbrella term synucleinopathies.

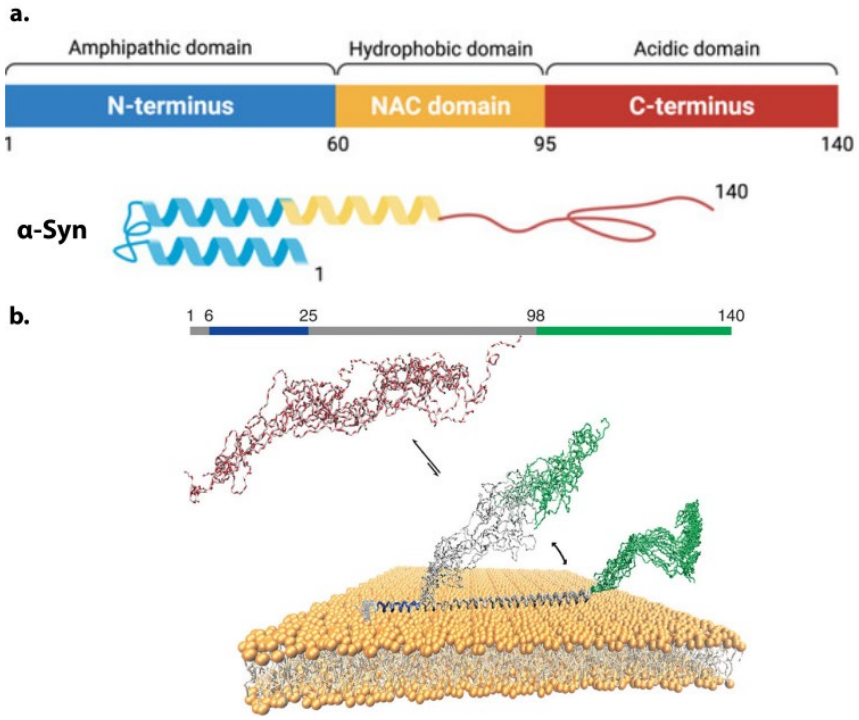

Figure II.1 Structure of α-Syn a. *Representation of the three structural domains of α-Syn. Adapted from* (*142*). ***b.*** *Structural change of α-Syn in presence of membranes: the protein is entirely disordered in solution (red), but adopts two helical structures upon binding to lipids. The N-terminal helix (blue) binds tightly to membranes, whereas the central helix (grey) has a more moderate affinity for lipids. The acidic C-terminal domain (green) remains always disordered and does not bind membranes. Adapted from* (*141*).

Physiologically, α-Syn is believed to have a variety of distinct roles, most of which are related to its capacity to interact with lipids and membranes (*143*). It is hypothesized that the protein is involved in lipid trafficking, because its lipid binding-induced amphipathic helix conformation (**Figure II.1**) is structurally reminiscent of the lipid transporter family of apolipoproteins (*140*, *144*). Moreover, the protein was also reported to be an inhibitor of phospholipases D1 and D2, suggesting that it has a regulatory role in membrane cleavage and processing (*145*). α-Syn is also an inhibitor of dopamine synthesis, by decreasing the expression levels of the enzyme Tyrosine Hydroxylase (TH), which is crucial for the creation of the dopamine precursor L-3,4-dihydroxyphenylalanine (DOPA) (*146*). Indeed, a possible function of α-Syn in dopamine-related processes could be intuited from the fact that some wide-spread synucleionpathies such as PD are particularly damaging to dopaminergic neurons.

Perhaps the most documented physiological role of α-Syn is the regulation of the synaptic vesicle (SV) cycle. SVs are membrane-enclosed compartments that store neurotransmitters at the pre-synaptic neurons. The control of the neurotransmitter-mediated

synaptic signalling is done through a cycle that involves SV exocytosis with neurotransmitter release, followed by vesicle regeneration (**Figure II.2**). α-Syn was proposed to intervene at multiple steps in this cycle. It was reported that the protein promotes the assembly of the soluble NSF attachment protein receptor (SNARE) protein complex, which mediates SV exocytosis by promoting vesicle fusion to the cellular membrane (*147*). A more recent study provided an additional layer to the α-Syn-SNARE interplay, proposing that α-Syn helps increase the size of the membrane pores created through SNARE activity (*148*). α-Syn was also reported to contribute to the clustering of synaptic vesicles by binding two different vesicles at a time (*149*). This α-Syn-mediated clustering maintains SV homeostasis by decreasing the mobility of SVs and diminishing their trafficking between different synaptic boutons (*150*).

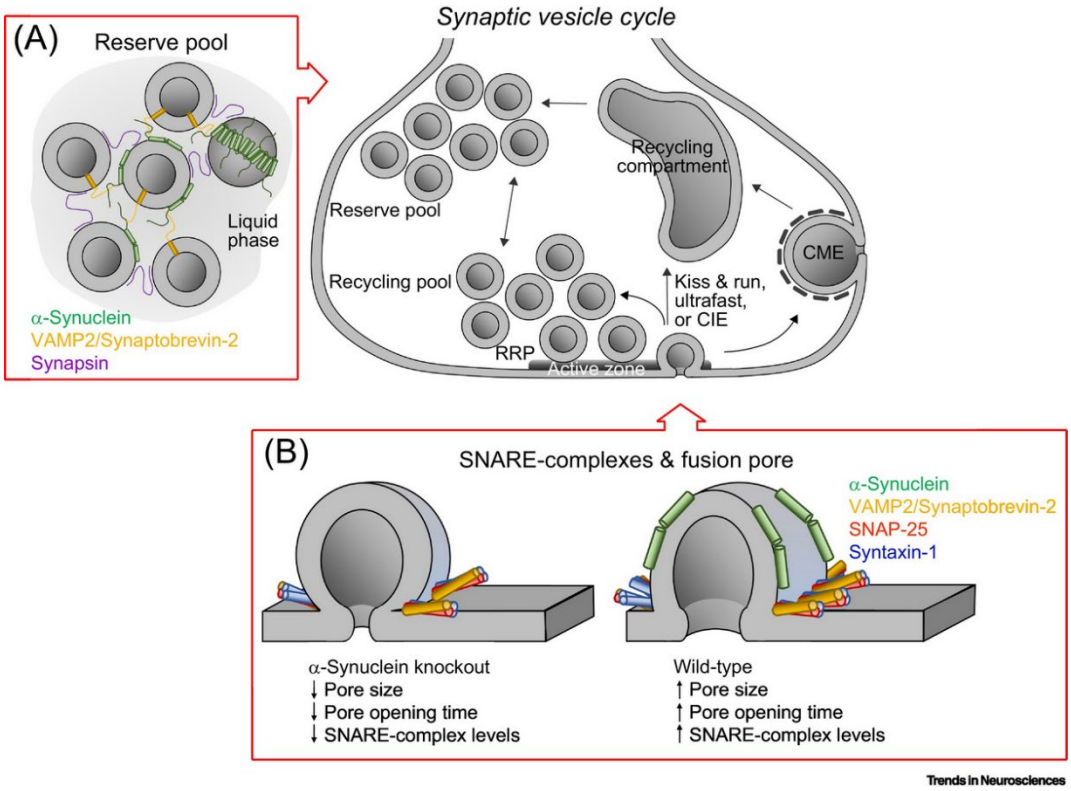

Figure II.2. Roles of α-Syn at the synapse. *Graphical representation of the different forms of SV storage: the Readily Releasable Pool (RRP), which is available for immediate neurotransmitter release into the synaptic cleft upon light stimulation, the recycling pool which releases neurotransmitters during higher stimulation, and the reserve pool, which only release neurotransmitters upon very strong stimulation. Once the neurotransmitters are released, several mechanisms lead to the recycling of SVs into the reserve pool. α-Syn contributes to the clustering of SVs within these pools (A), and to the assembly of the SNARE complex, which results in larger pore openings and better neurotransmitter release. Reproduced from (151).*

Most of the research surrounding α-Syn revolves around its aggregation and subsequent deposition in neurons affected by synucleinopathies, in the form of compositionally complex inclusions called Lewy bodies (LB). The first link between α-Syn and disease was made with the discovery of a point mutation in the *SNCA* gene, that directly causes a form of autosomal PD (*152*). Since then, a varied array of disease-promoting mutations have been found, most of them in the physiologically-relevant N-terminal domain (*153*), suggesting deleterious effects related to protein loss of function. However, it has also become evident that only a small percentage of synucleinopathies are genetic, and that the wild-type protein can also be involved in processes that lead to sporadic events of aggregation and pathogenicity.

How do aggregates relate to synucleinopathies? As seen in section I.2, the causal link between aggregation and neurodegeneration is still being disputed. However, valuable information related to potential cytotoxic mechanisms of synucleinopathies lies in the composition of LBs. While fibrillar α-Syn remains the main component of these inclusions, hundreds of other proteins, along with lipids, membrane fragments and even bits of cellular organelles were found in their composition (*24*, *154*). The entanglement of these factors in fibrous meshes of α-Syn aggregates deviates them from their physiological processes, resulting in dysfunctions related to various cellular processes such as mitochondrial activity, calcium homeostasis, protein degradation pathways and synaptic function (reviewed in (*155*); **Figure II.3**). Thus, the cytotoxicity associated with synucleinopathies is increasingly believed to be the result of multi-level interference with cellular processes, which occurs throughout all the stages of LB formation, not just at when they attain a mature state (*156*). Accordingly, the investigation of the early mechanisms of α-Syn aggregation and LB formation is an essential step in developing therapies to target synucleinopathies.

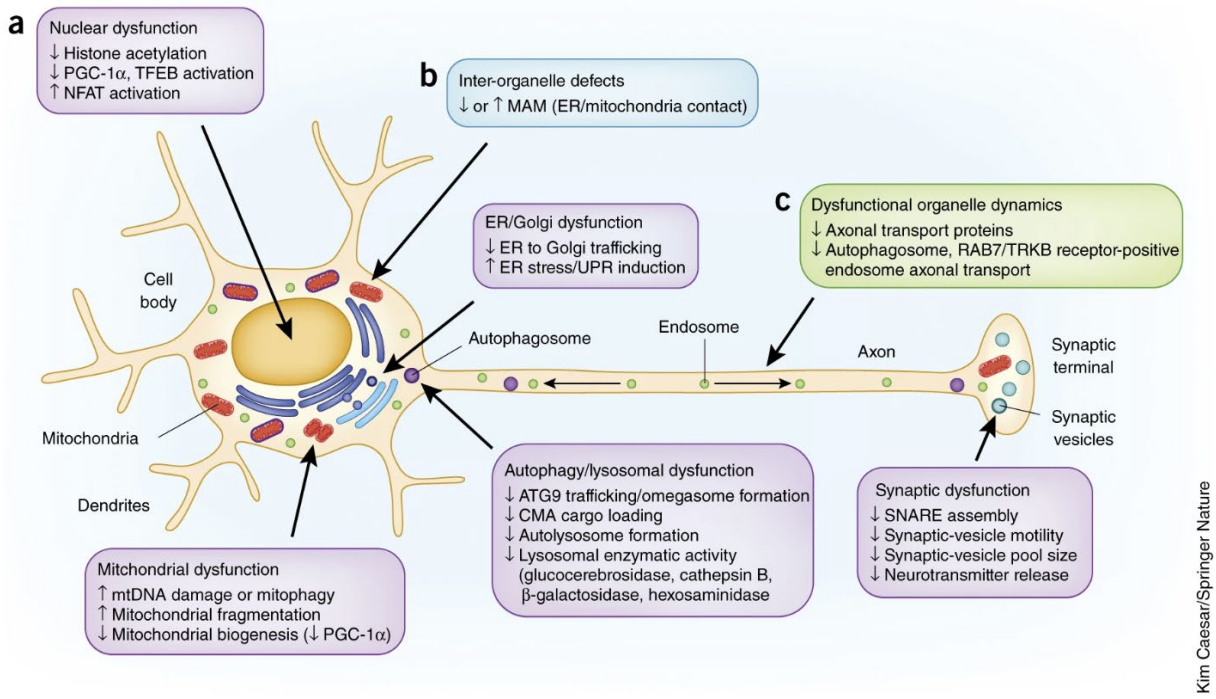

Figure II.3 Cellular processes affected by pathological forms of α-Syn. *Reproduced from (155).*

With respect to aggregate triggering factors, multiple hypothesis have been made. Firstly, the increase in the α-Syn cellular concentration has been proposed to be deleterious. This is consistent with the finding that *SNCA* gene locus multiplication, which leads to elevated α-Syn expression rates, also increases risks of PD (*157*). Moreover, *in vivo* models of α-Syn overexpression also seem to support an aggregation pathway passing through increased concentrations. For example when human α-Syn is overexpressed in primary neurons from $SNCA^{-/-}$ mice, it induces the formation of inclusions that reflect the biochemical composition of LB (*158*). The authors of this study report, however, that the structural arrangement of α-Syn fibrils within the inclusions is different from bona fide LB. Secondly, a vast array of PTMs have been observed to preferentially occur in aggregated forms of α-Syn (*159*). For example, phosphorylation, ubiquitination and truncation within the C-terminal domain are established markers of α-Syn pathology, due to their widespread occurrence in LBs (*24*). The phosphorylation of the Serine 129 (pS129) establishes a strong correlation with aggregation and pathology (**Figure II.4**), as it was found in 90% of α-Syn in human DLB brains, as opposed to less than 5% in healthy brains (*160*, *161*). It is, however, too early to conclude on the links between α-Syn phosphorylation and aggregation, as existing studies fail to find consensus on the topic (*162*). Thirdly, it was hypothesized that free cytosolic α-Syn could be inherently

aggregation-prone, and that inclusion formation is avoided in healthy cells because the protein favours a helically folded tetrameric state that is more resistant to aggregation (*163*). Multimerization of α-Syn could be an effect of membrane binding, and the inhibition of this interaction could be forcing the protein into a monomeric state that ends up aggregating (*164*).

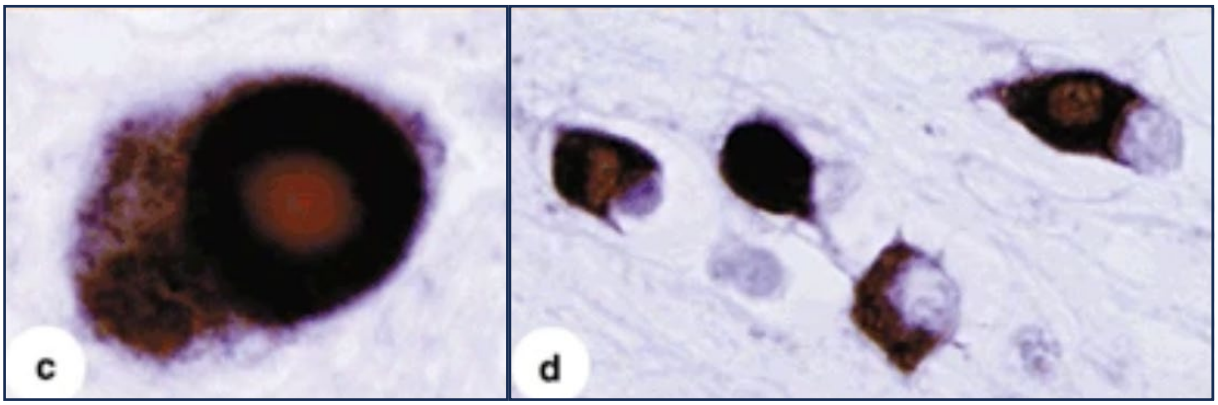

Figure II.4 Ser-129 phosphorylation is a major marker of α-Syn pathology. *The images represent paraffin-embedded brain sections immuno-stained for pSer-129. On the left: Lewy Body in the substantia nigra from a brain affected by PD. On the right: inclusions in glial cells within the basis points from a brain affected by MSA. Adapted from* (*160*).

II.2 General aspects about the phase separation of α-Syn

Like for other neurodegeneration-related proteins, an emerging hypothesis is that LLPS-derived droplet phases could be intermediates in the formation of α-Syn aggregates. The strength and weaknesses of this hypothesis, as well as novel tools to explore it, will be discussed in the next sections.

II.2.1 α-Syn is predicted to have a limited propensity to phase separate

The exploration of the α-Syn droplet state is warranted by current knowledge about the structure and sequence of the protein. Indeed, α-Syn is an IDP, which - as discussed previously - can indicate an intrinsic propensity towards phase separation (*133*). Moreover, α-Syn was predicted to be a potential phase-separating protein by FuzDrop, a machine learning tool that analyses the sequences of proteins in search for residue patterns that are compatible with PS (*165*). It is important to note, however, that α-Syn's predicted probability for PS (pLLPS) was only very slightly above the threshold for spontaneous phase separation in physiological conditions (α-Syn pLLPS =0.62 on a scale of 0 to 1, whereas the threshold pLLPS is 0.61). By comparison, other neurodegeneration-related proteins, which have confirmed droplet states, display substantially higher PS propensities (0.90 for TDP43, 1.00 for tau and FUS). Thus, α-Syn appears to be in a grey area with respect to phase separation.

II.2.2 *In vitro* phase separation of α-Syn requires high concentrations and is not systematic

Multiple occurrences of α-Syn PS have been reported in recent years. The first *in vitro* observation was in 2020, when Ray et al. noticed that purified WT α-Syn phase separated in test tubes (**Figure II.5**), to produce droplets with liquid-like properties (*133*). Since then, α-Syn PS was replicated *in vitro* in a handful of other studies (*166–169*). However, a common feature of these studies is that they report that PS was only achieved only at considerably higher α-Syn concentrations, when compared to the previously estimated physiological concentration of the protein, which was around 22 μM (*170*). Indeed, for Ray et al., PS was observed starting from 200 μM in the presence of 10% Poly Ethylene Glycol (PEG) 8000 and from 500 μM without PEG (**Figure II.5**) (*133*). Subsequent *in vitro* studies have also reported the production of an α-Syn droplet state at very high protein concentrations (200 μM (*166*, *167*), 100 μM (*168*)). One study reports phase separation at a lower concentration of 75 μM (*169*). In this study, the protein

is solubilized in buffer droplets, and undergoes PS close to the droplet-air interface, where the local protein concentration could be higher due to evaporation effects.

In contrast to the aforementioned data, other studies reported an absence of a droplet state in purified α-Syn solutions *in vitro*, even when the concentrations used were significantly greater than the protein's estimated physiological concentration (*171*, *172*). Thus, the borderline pLLPS score of α-Syn seems to manifest through a heterogeneity in results regarding the α-Syn droplet state, that reflects how, *in vitro,* slight variations in experimental conditions can impact the outcomes related to the protein's phase separation.

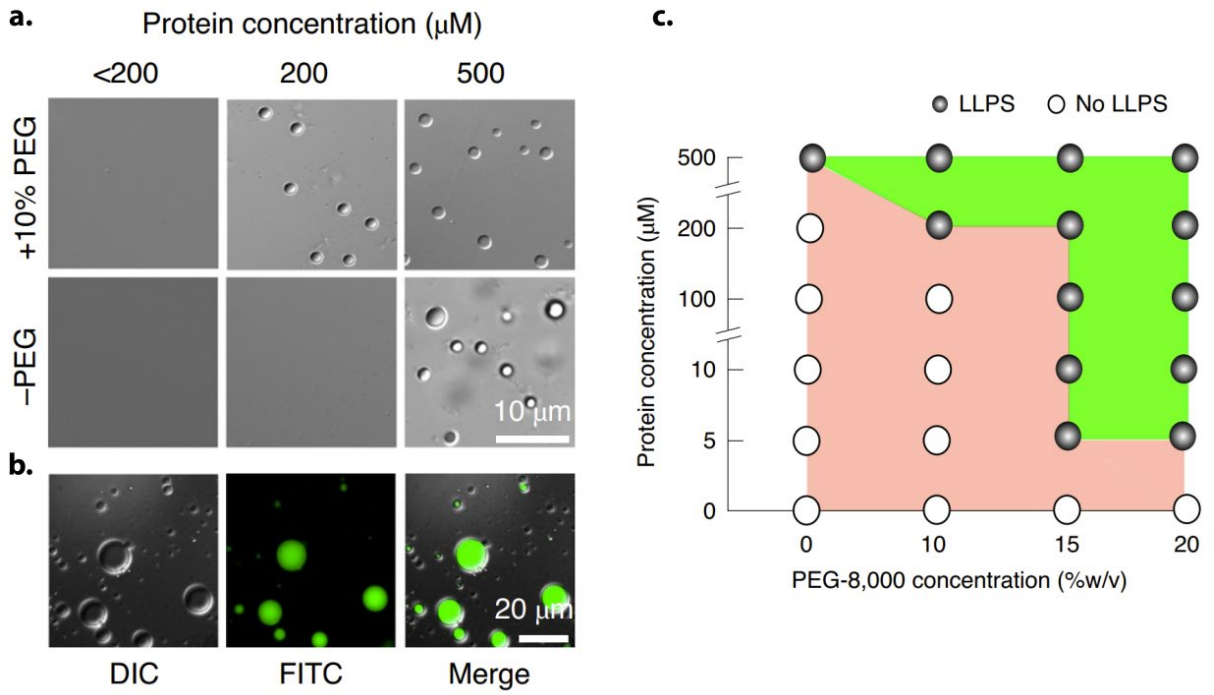

Figure II.5 In vitro liquid droplets of α-Syn. a. *Differential interference contrast (DIC) images of α-Syn droplets at different concentrations, with or without 10% Poly-Ethylene Glycol (PEG)-8000.* ***b.*** *Fluorescence microscopy images of the droplets in the condition 200 μM α-Syn + 10% PEG-8000.* ***c.*** *Diagram schematizing the different regimes where α-Syn undergoes PS. Adapted from* (133).

II.2.3 In cellula/vivo observations of α-Syn phase separation are scarce

The inconclusive *in vitro* results raise the question of whether α-Syn liquid droplets exist in cells. Indeed, the concentration regimes required for *in vitro* PS are far from the physiological environment of α-Syn, whose expression levels at the synapse are estimated to reach no more than 22 μM (*170*). Up to date, only two studies have recreated α-Syn separated phases *in cellulo*

or *in vivo.* First, a study in HeLa cells reported that overexpressed tetra cysteine-tagged α-Syn (C4-α-Syn) stained with fluorescein arsenical hairpin binder (FlAsH-EDT_2) underwent phase separation into liquid-like droplets (*133*). The apparition of α-Syn condensates was dependent on cell exposure to 10 mM ammonium ferric citrate. This could be related to findings that synucleinopathies are characterized by neuronal iron overload (*173*). However, it is important to keep in mind that the conditions used here were deviated from a natural cellular context, as the iron concentration was 4 orders of magnitude greater than its physiological levels in neurons (*174*).

Moreover, *in cellula* α-Syn LLPS does not seem systematic either. In our experimental setting, overexpressed α-Syn fused to emerald Green Fluorescent Protein (α-Syn-emGFP) did not phase separate in HeLa cells (**Figure II.6**). An absence of condensates was also reported for the overexpression of α-Syn fused to the Blue Florescent Protein (α-Syn-BFP) in HEK293 cells (*110*). However, it is relevant to mention that a possible cause for this inconsistency could be that the fluorescent protein tags used in these experiments could have exerted a more significant impact on the behaviour of α-Syn, in contrast to the smaller-sized C4 tag.

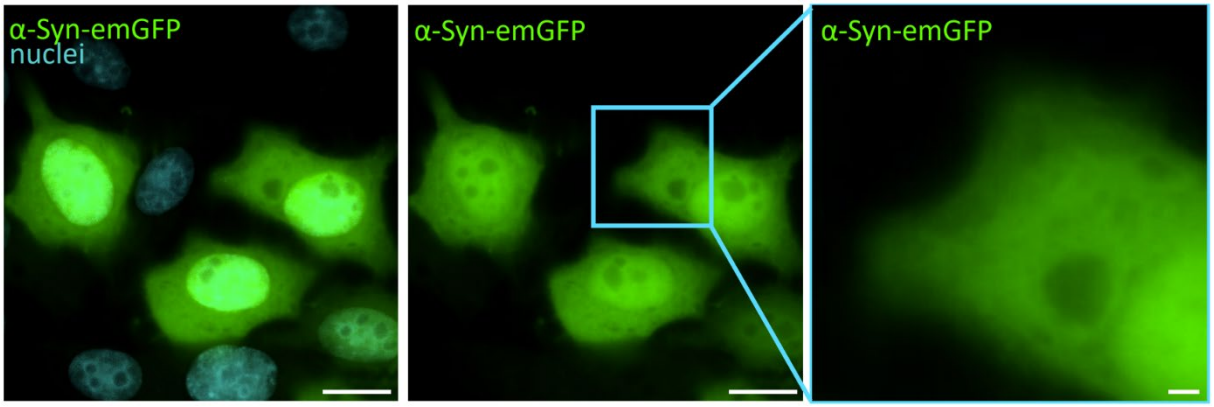

Figure II.6 Absence of α-Syn condensates in our HeLa overexpression experiment. *Epifluorescence microscopy images of HeLa cells expressing α-Syn-emGFP. No condensates were detected. Scale bar, 10 µm for whole cell images and 2 µm for the zoom-in. Included in* (*175*).

The second occurrence comes from an *in vivo* investigation, which reported the formation of liquid-like condensates upon overexpression of α-Syn fused to the Yellow Florescent Protein (α-Syn-YFP) in the muscle wall cells of *C. elegans* (**Figure II.7**) (*113*). Interestingly, a delay of 7 days starting from exposure was necessary for the condensates to occur, giving hints at the fact that, *in vivo,* the phase separation of the protein could be related to more than just the concentration of the protein, and that time-dependent cellular processes

could be involved. This result highlights that, despite current difficulties in the understanding of α-Syn phase separation, the exploration of its droplet state remains a highly relevant research direction.

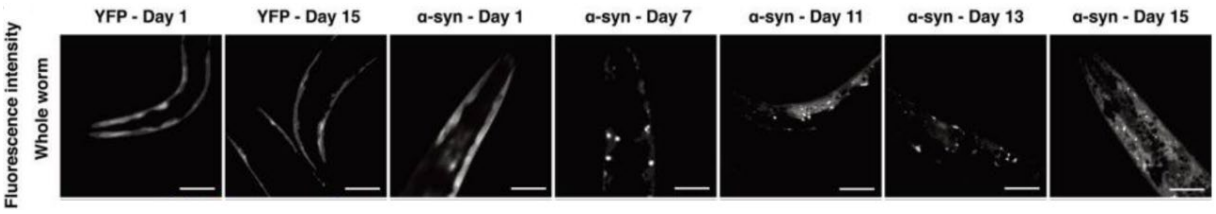

Figure II.7 In vivo α-Syn condensates. *Fluorescence microscopy images of C. elegans expressing α-Syn-YFP in muscle wall cells. By day 7, condensates become visible. Adapted from* (*113*).

II.2.4 α-Syn can also phase separate through heterotypic interactions

Whether the concentrated protein alone can or cannot form liquid droplets driven by homotypic interactions is only of moderate importance. As discussed in previous sections, naturally occurring cellular biomolecular condensates reunite plenty of cellular factors, and often require more than one macromolecule to assemble. It is therefore important to also orient our attention towards more complex condensed phases, which build on heterotypic interactions and require more than just one 'scaffold'. α-Syn has been reported to form multiple such condensates.

The first observation of an α-Syn mixed droplet was from 2021 when Hoffmann et al reported that the co-expression in primary hippocampal neurons of α-Syn and its synaptic interactor synapsin I resulted in formation of liquid-like condensed phases enriched in both proteins (*110*). While an LLPS-based model for the synapsin I-mediated clustering of SVs had previously been proposed, this was the first time that α-Syn was suggested to also participate in condensation (*176*). The authors propose that α-Syn's partition helps maintain the dynamic properties of synapsin I condensates. Thus, the study puts forth the hypothesis that a disturbance in the stoichiometric ratio between α-Syn and synapsin I could perturb SV homeostasis, as too much α-Syn impedes synapsin I's PS *in vitro,* and too little result in less dynamic, crystalline arrangements of SVs *in cellula* (*110*, *177*).

In vitro studies also suggest that heterotypic interactions could contribute to α-Syn PS, because its co-incubation with different proteins such as tau (*172*) and PrP (*171*) was reported to promote condensation in conditions where α-Syn alone stayed diffuse in solution. Tau is a

protein that can undergo PS by itself, mainly owing to its N-terminal domains (*112*). However, when Garcia et al created a ΔN_{ter}-tau incapable of PS, they noticed that its co-incubation with α-Syn resulted in a recovery of the phase-separation behaviour (*172*). This suggests that α-Syn is not just a 'client' molecule partitioning into already existing tau condensates, but rather that both proteins cooperate in the process of phase separation. In a similar manner to ΔN_{ter}-tau, PrP is a protein that does not phase separate on its own. However, its incubation with α-Syn in test tubes yielded the formation of droplets (**Figure II.8**) (*171*).

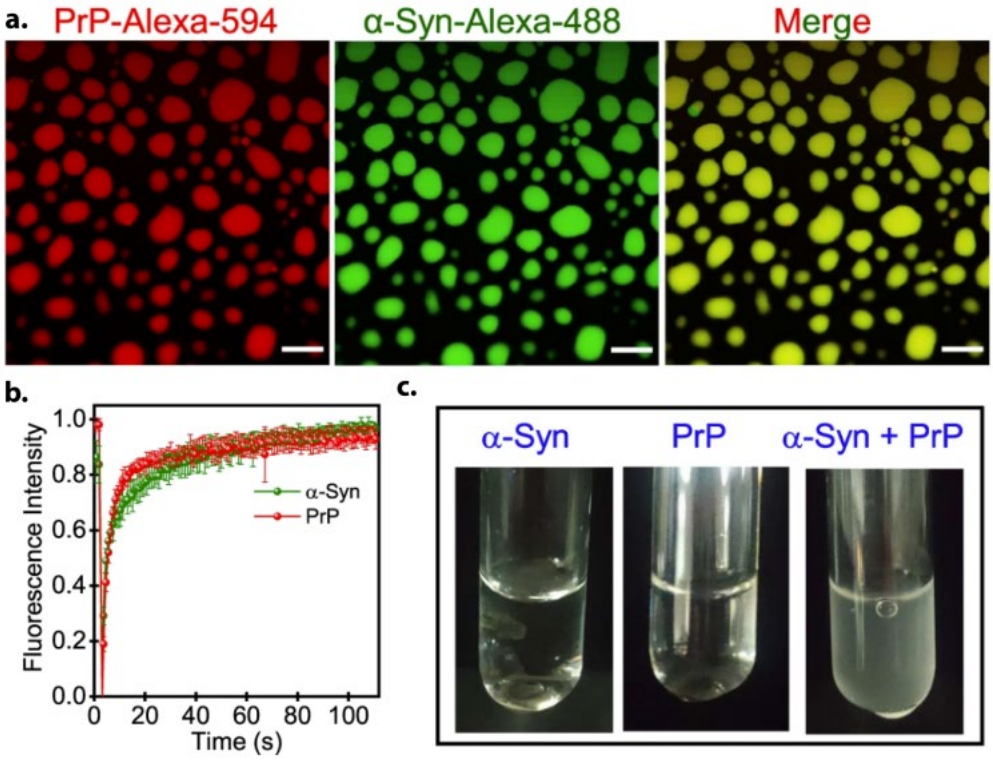

Figure II.8 Heterotypic condensates of α-Syn and PrP. a. *Mixed phase separated droplets of α-Syn-Alexa-488 (green) and PrP-Alexa-594 (red) in vitro. Scale bar, 10 µm.* ***b.*** *FRAP profiles of both α-Syn (green) and PrP (red) display fast recovery of fluorescence, indicating a liquid-like behaviour.* ***c.*** *Separately, α-Syn (45 µM) and PrP (30 µM) do not undergo LLPS in vitro. Adapted from* (*171*).

II.2.5 Proposed pathways for α-Syn PS: Coacervation and/or conformational rearrangement

In vitro studies have led to the development of hypotheses with respect to the mechanism of formation of α-Syn condensates. Different studies describe the involvement of α-Syn in phase separation events using models based on complex coacervation. This process could be described as a version of PS where the multivalent interactions represent electrostatic attractions between oppositely-charged macromolecules.

α-Syn was reported to undergo complex coacervation with positively charged polymers such as poly-L-lysin (pLK) (*172*). The authors deduced the electrostatic nature of the interactions between the two molecules from the coacervates' response to different additives. On one side, NaCl dissolved the condensates, potentially by providing stabilizing counterions for the charges of α-Syn and pLK, thereby reducing their propensity to interact with each other. On the other hand, condensates were resistant of the to 1,6-hexanediol, which is a molecule known for its ability to dissolve specific liquid condensates by disrupting hydrophobic bonds. The same study suggested that this phenomenon could also be responsible for the heterotypic condensation of α-Syn with tau, which also has a net positive charge (*172*). The propensity to partner with positively charged molecules in phase separation led to the hypothesis that complex coacervation is led by the negatively charged C_{ter} of the protein, which was substantiated by the absence of coacervation when using ΔC_{ter}- α-Syn.

Complex coacervation was also proposed for the heterotypic phase separation of α-Syn with PrP, because the two proteins were reported to only phase separate in a stoichiometric regime that allows charge neutralization of the two proteins (*171*). This behaviour is consistent with complex coacervation, because it illustrates how the condensation of the two proteins is based on a reduction of the energy associated with their net charge through the maximization of electrostatic bonds. Even though charges are neutralized within coacervates, unbound ionic units at the coacervate-solvent interface account for an accumulation of charge at the surface of the coacervate, called surface potential. One study illustrated this phenomenon by showing how α-Syn – a negatively charged protein – accumulates at the solvent interface of coacervates exhibiting a positive surface potential, in contrast to those with a negative surface potential (*178*).

Complex coacervation driven by the C-ter of the molecule was not, however, the only mechanism proposed for α-Syn phase separation. A study from Sawner et al. suggested that lower critical concentrations for α-Syn phase separation can be achieved in different conditions,

such as low pH and/or high salt concentrations (*179*). Indeed, other studies of α-Syn phase separation used buffer systems with high salt concentration to induce PS (*168*). These solution conditions would, in theory, go against complex coacervation. A decrease in pH would reduce the net negative charge of the protein by inducing the protonation of acidic residues, and an increase in the solution's ionic strength would stabilize charged residues and decrease their electrostatic attraction.

To explain PS in high salt conditions, Sawner et al. proposed a mechanistic pathway where α-Syn PS could be driven by the LCD within the N-ter and the NAC regions of the protein. Their model implies that in low salt conditions, α-Syn adopts a PS-inhibiting conformation, by folding such that the positively charged N-ter can interact electrostatically with the negatively charged C-ter. An increase in the solution's ionic strength through salt addition would stabilize these charged regions, thus enabling the protein to stretch and expose the LCD sequences that they hypothesize to be required for PS (*179*). This model is consistent with the findings from a subsequent study, that used a cross-linking mass spectrometry (XL–MS) to study the conformational state of α-Syn within a droplet state *in vitro* (*123*). The authors reported that the monomeric protein indeed appears to adopt a 'hairpin' conformation held by N_{ter} -C_{ter} electrostatic interactions, and that phase separation is synchronous with the shift towards an 'elongated' state. The aforementioned model is, however, in contradiction with the FuzDrop tool, which predicted the PS propensity of α-Syn to be driven from the intrinsically disordered C_{ter}, and not from the N_{ter} and the NAC (*165*).

II.2.6 α-Syn liquid-to-solid transitions

The liquid-to-solid model has been largely proposed for α-Syn: in virtually all studies featuring α-Syn condensates, a time-dependent maturation into solid aggregates was observed. The study of Ray et al. from 2020 reported that the physical properties of *in vitro* α-Syn condensates followed a time-dependent liquid-to-solid progression spanning on 20 days (*133*). They also determined through Transmission Electron Microscopy (TEM) and Thioflavin S (ThioS) staining that this transition was synchronous with the apparition of amyloid-like fibrillar aggregates within the condensates (**Figure II.9**) (*133*). Within the same study, the liquid droplets observed in HeLa cells in conditions of iron overload were also shown to undergo a sensible loss of dynamic properties within 48 hours, characterized by a decrease in circularity and a slight decrease in fluorescence recovery during FRAP. It remains, however, unclear whether this occurs due to an intrinsic tendency of intracellular α-Syn condensates to solidify,

or as a result of the processing of these objects by the aggresomal machinery, as the authors showed to happen (*133*).

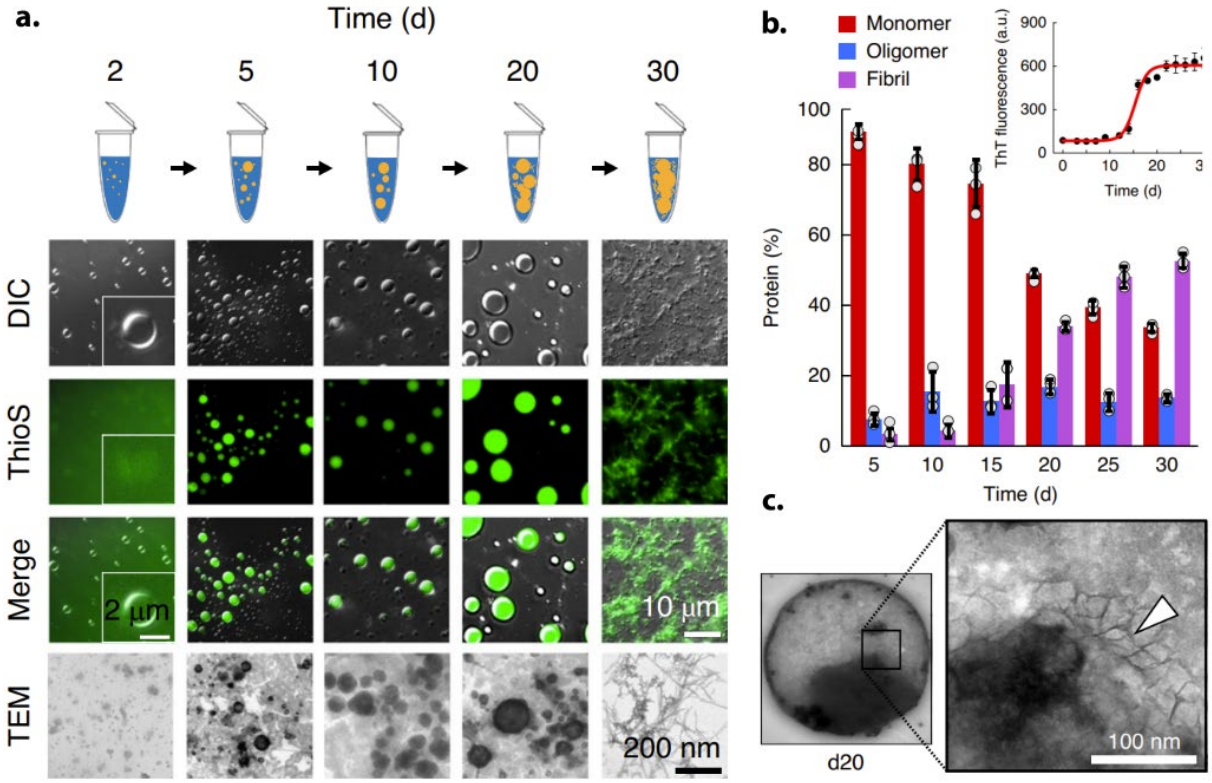

Figure II.9. Liquid-to-solid transition of α-Syn condensates a. *Observation of in vitro α-Syn droplets at different timepoints (up to 30 days), through DIC, ThioS and TEM.* ***b.*** *Evolution of the percentage of monomeric/oligomeric/fibrillar forms of α-Syn within PS conditions. The amyloid formation kinetics were also followed with Thioflavin T (ThT).* ***c.*** *Zoom-in of a TEM image of an α-Syn droplet at day 20, showcasing in detail the formation of fibrillar aggregates. Adapted from* (*133*).

Complex coacervates of α-Syn also accommodated the formation amyloids. With α-Syn/tau mixed condensates, the authors used Atomic Force Microscopy (AFM) to investigate the shape and size of the aggregates and observed that they were very small (around 15 nm) and, strikingly, globular rather than fibrillar (*172*). To probe the composition of aggregates, they have also used fluorescence correlation/cross-correlation spectroscopy, which is a technique that allows the detection of interacting fluorescent molecules diffusing through an extremely small volume (femtolitre scale), thus allowing single-molecule analysis. Interestingly, they find that the majority of aggregates contained both α-Syn and tau, suggesting that the previously observed co-aggregates of the two proteins (*180*) could form through a liquid intermediate. With α-Syn and PrP, the presence of composite aggregates issued from complex coacervation

of the two proteins was also detected, using airy-scan microscopy (*171*). Additionally, the authors detected a synergistic effect of the coacervates in the formation of amyloid aggregates, as shown with ThT assays which indicated a much faster amyloid transition within the coacervate as compared to separate α-Syn and PrP solutions (*171*).

Perhaps the most important observation of an α-Syn liquid-to-solid transition comes from Hardenberg et al. who reported this phenomenon *in vivo*, on condensates formed with α-Syn-YFP in *C. elegans* (**Figure II.10**) (*113*). The authors were able to determine that α-Syn-YFP acquired amyloid-like properties by performing fluorescence lifetime imaging (FLIM) measurements. They based their reasoning on the fact that amyloid structures contain β-sheet motifs that can act as acceptors for Förster resonance energy transfer (FRET), meaning that they can absorb some of YFP's photons shortly after emission, provided that the two are in very close proximity (of a few nm). Thus, the decrease in intra-condensate YFP fluorescence lifetime that they observed could be explained by the integration of α-Syn-YFP monomers into amyloid-containing aggregates. The amyloid nature of the inclusions was further validated by a decreased proteinase K sensitivity, loss of fluorescence recovery with FRAP and positive immunofluorescent staining with anti-Ubiquitin antibodies (*113*).

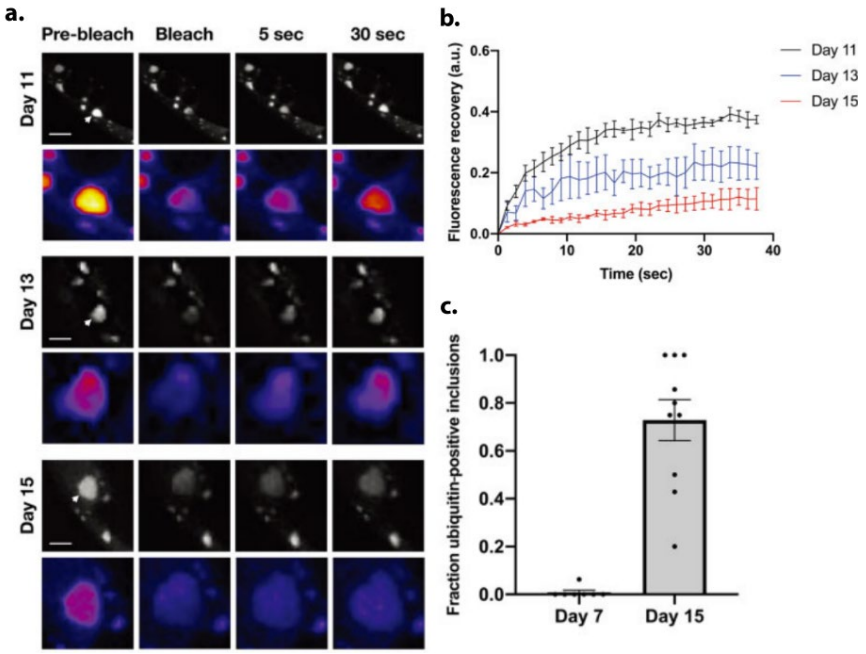

***Figure II.10. Liquid-to solid transition of α-Syn condensates in C. elegans**. **a.** and **b.** FRAP experiments on α-Syn condensates within C. elegans muscle wall at different timepoints. **c.** Fraction of condensates that appeared ubiquitin-positive upon immunostaining. Adapted from (113).*

II.3 Building intracellular artificial α-Syn condensates

II.3.1 A method for condensate reconstitution

Taking into consideration the previous sections, the study of α-Syn in the context of liquid droplets is of high importance. Multiple pieces of evidence point at the possibility that the protein can acquire a tendency for PS, and that this can play a role in its aggregation and pathogenicity. However, the conditions that underlie this process in cells remains largely unknown, because studies of cellular α-Syn PS remain extremely limited. Moreover, current methods and available data prevent us from robustly recreating a cellular α-Syn droplet, as studies on overexpressed α-Syn fail to yield convergent outcomes with respect to the phase separation of the protein. To compensate for current shortcomings, we set to recreate artificial intracellular α-Syn condensates, and to use them as a platform to study the impact of the α-Syn droplet state on protein aggregation.

A toolbox for the bottom-up creation of artificial intracellular protein condensates had already been developed in the lab (*130*). It consists on a genetically-encoded protein scaffold, in the form of the ferritin protein fused to a FKBP12 protein bearing a F36M mutation (hereafter called Fm) (*130*) (**Figure II.11.a**). The multivalence required for phase separation comes from both sides: on one side ferritin oligomerizes to form nanocages composed of 24 monomers; on the other side the F36M mutation ensures that each Fm moiety has a relatively weak homodimerizing tendency (Kd~μM). Thus, when expressed in cells, the scaffold yields nanocages decorated with 24 self-interaction modules. Upon reaching a saturation concentration, the scaffold phase separates. Condensates obtained with this method were named ArtiG (short for 'Artificial Granule'). (**Figure II.11.b**).

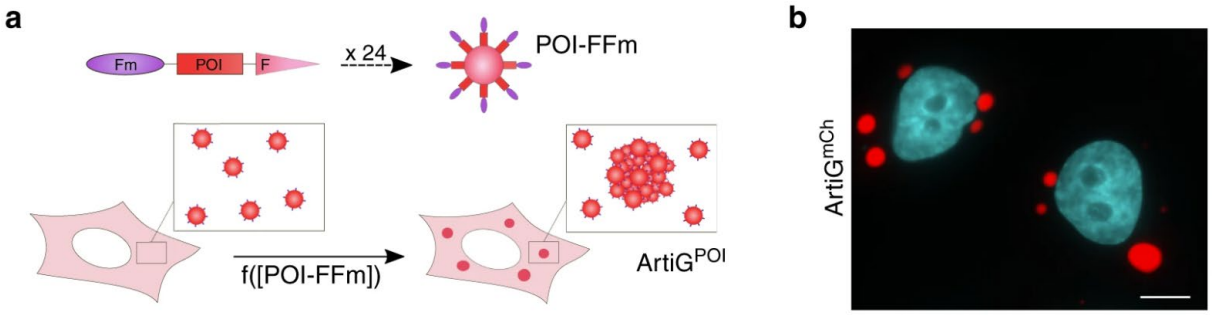

Figure II.11 A toolbox for the creation of artificial condensates. a. *Schematic of the structure of the scaffold: a protein of interest (POI) is fused on one side to ferritin, and on the other side to a Fm monomer (POI-FFm). POI-FFms self-assemble in cells and undergo phase separation.* ***b.*** *Representative confocal image of HeLa cells expressing mCherry-FFm. Scale bar, 10 µm. Adapted from* (*130*).

For the studies presented in this thesis, a variant of this method was created, consisting in a linear repetitive string of 5 Fm moieties (**Figure II.12.a**) (*181*). Similar to FFm, 5Fm scaffolds fill the main criterium for PS: they can create weak multimeric interactions between them. Indeed, live confocal microscopy revealed that upon overexpression in HeLa cells, the 5Fm bound to emGFP (emGFP-5Fm) yielded micrometric bodies that recapitulated the liquid-like biophysical profile of bona fide biomolecular condensates **(Figure II.12.b)**. For the present study, we fused WT human α-Syn in the N_{ter} extremity of the scaffold (to give α-Syn-emGFP-5Fm) such that the resulting condensates would be enriched in α-Syn (see section II.2). This novel scaffold and its corresponding condensates were used for the investigation of the behaviour of α-Syn in the context of biomolecular condensates.

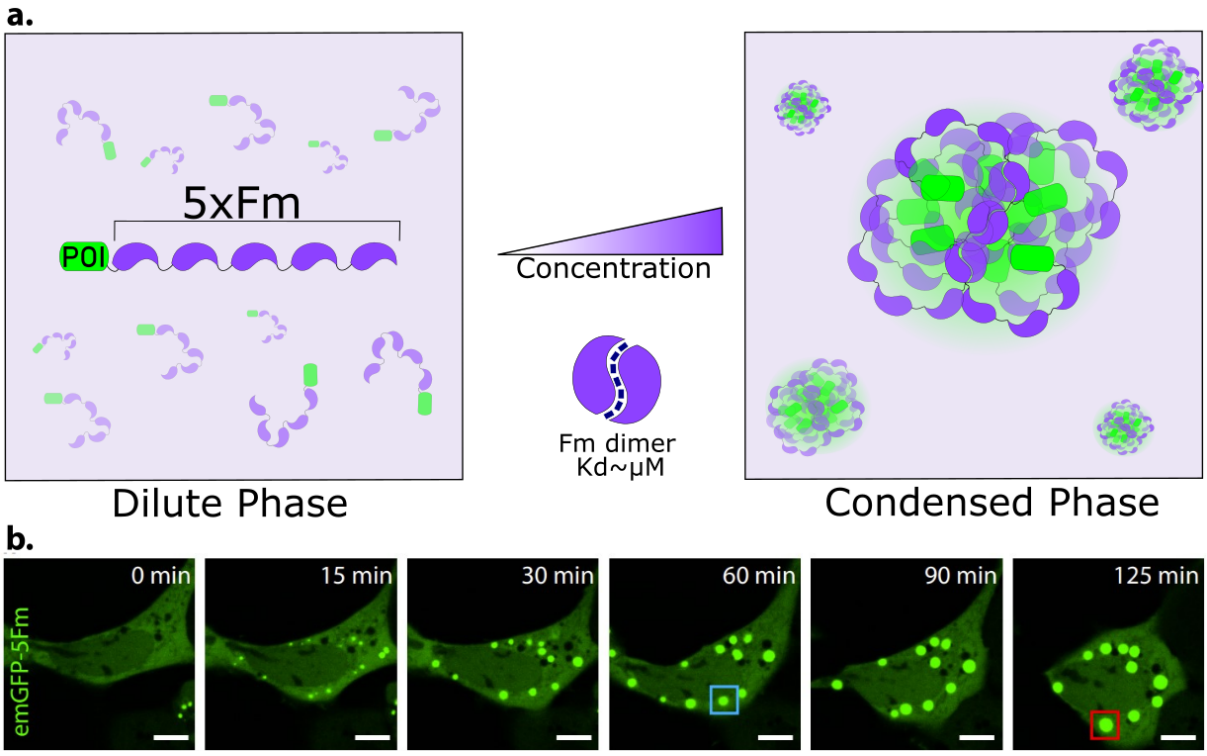

Figure II.12 The 5Fm system for artificial condensates. a. *Schematic illustration of the 5Fm scaffold attached to a Protein of Interest (POI). Above a* C_{sat}*, the homotypic interactions between Fm moieties from different scaffolds drive the formation of condensed phases, following the PS principle.* ***b.*** *Live confocal microscopy frames of HeLa cells expressing emGFP-5Fm. Scale bar, 10 µm. Section* ***b.*** *featured in* (*175*).

II.3.2 Advantages and limitations of our approach to reconstituting condensates

The use of the 5Fm scaffold presents a series of advantages for our study. Firstly, the condensates appear to be biochemically neutral. The behaviour of the 5Fm scaffold and its variants fused with fluorescent proteins (emGFP-5Fm, mCherry-5Fm, EBFP2-5Fm) was studied *in cellulo* to assess whether the expression of such an artificial protein construct could interfere with cellular processes. HeLa and SH-SY5Y cells expressing these scaffolds did not show any decrease in viability, as condensate-positive cells remained alive for at least 120h after transfection with the scaffold-encoding gene constructs (longer observations were not made). Moreover, different immunofluorescence experiments showed that condensates formed with these scaffolds did not colocalize with factors from protein degradation machinery, indicating that they are not recognized by cells as potentially toxic entities.

Secondly, the assembly of 5Fm condensates is controlled and reversible. This is because the Fm-Fm homodimer interaction that drives the formation of condensates can be disrupted using a small molecule called FK506. Thus, 5Fm condensates and their variants can be dissolved simply through exposure to this molecule (**Figure II.13**). Moreover, the addition of FK506 to cells during the expression of the scaffold, but before the PS threshold concentration is reached, impedes the formation of condensates. This is crucial for the creation of control conditions to study the scaffold in diffuse state.

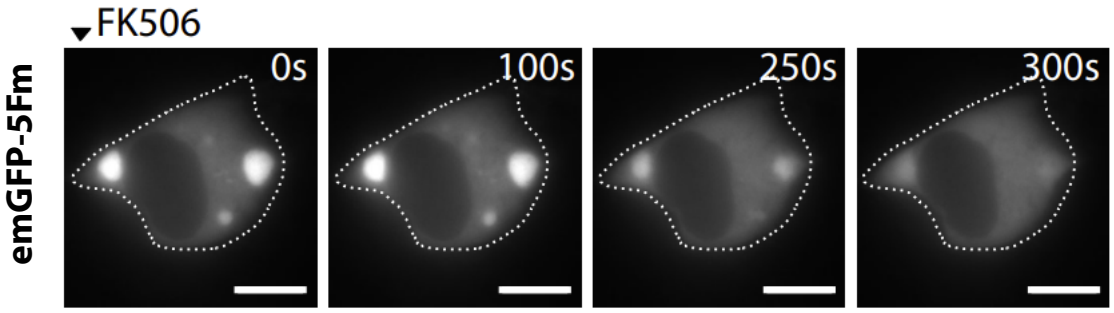

Figure II.13. Reversibility of 5Fm-based condensates. *Live epifluorescence microscopy images of HeLa cells expressing emGFP-5Fm condensates. At 0 s, cells were exposed to 2.5 µM FK506, which triggered the dissolution of the condensates within minutes. Featured in* (*175*).

With our system for the reconstitution of α-Syn condensates, some limitations also arise. Notably, the α-Syn-emGFP-5Fm scaffold is a high molecular weight fusion, where α-Syn (~14 kDa) makes up only around 15% of the molecular mass of the scaffold (~100 kDa). Indeed, we should not exclude the possibility that the covalent grafting of the emGFP-5Fm construct to α-Syn could modify its behaviour, as discussed in the article in section II.3.

II.3 Article: α-Synuclein liquid condensates fuel α-Synuclein fibrillar growth

BIOCHEMISTRY

α-Synuclein liquid condensates fuel fibrillar α-synuclein growth

Leonard Piroska[1], Alexis Fenyi[2], Scott Thomas[1], Marie-Aude Plamont[1], Virginie Redeker[2], Ronald Melki[2]*, Zoher Gueroui[1]*

α-Synuclein (α-Syn) aggregation into fibrils with prion-like features is intimately associated with Lewy pathology and various synucleinopathies. Emerging studies suggest that α-Syn could form liquid condensates through phase separation. The role of these condensates in aggregation and disease remains elusive and the interplay between α-Syn fibrils and α-Syn condensates remains unexplored, possibly due to difficulties in triggering the formation of α-Syn condensates in cells. To address this gap, we developed an assay allowing the controlled assembly/disassembly of α-Syn condensates in cells and studied them upon exposure to preformed α-Syn fibrillar polymorphs. Fibrils triggered the evolution of liquid α-Syn condensates into solid-like structures displaying growing needle-like extensions and exhibiting pathological amyloid hallmarks. No such changes were elicited on α-Syn that did not undergo phase separation. We, therefore, propose a model where α-Syn within condensates fuels exogenous fibrillar seeds growth, thus speeding up the prion-like propagation of pathogenic aggregates.

INTRODUCTION

Biomolecular condensates are subcellular compartments confining proteins and nucleic acids and organizing specific biochemistry in space and time. This particularity entails a high degree of component exchange with the surrounding medium, allowing the modulation of their composition and properties according to different cellular cues (*1*, *2*). Cells make use of these compartments for controlled spatiotemporal colocalization of various factors, whose interactions within the condensates are drivers of fundamental processes such as RNA processing (*3*), cell division (*4*), and response to cellular stress (*5*). While the function and composition are characteristics specific to each condensate or cellular context, their mechanism of formation is increasingly believed to share common principles. For instance, condensate formation is often mediated through multivalent interactions between biomolecules, which could be represented through polymer-based physical models based on phase separation (PS), including liquid-liquid PS (LLPS) (*6*, *7*).

Mounting pieces of evidence tie aberrant behaviors of biocondensates to neurodegenerative diseases (*8*–*11*). It has been hypothesized that LLPS-derived condensates might represent intermediates in the path yielding toxic protein aggregates (*12*, *13*). However, the mechanisms underlying this process associated with aging remain unclear. Rheological experiments performed with purified proteins suggest that in vitro condensates could behave as Maxwell fluids displaying glassy characteristics, implying a time-dependent change in the material properties of condensates (*14*). Alternately, elevated protein concentrations (*15*) and water molecule content reduction within condensates (*16*) were also proposed to drive their aggregation. Reconstitution experiments have revealed that numerous aggregation-prone proteins involved in neuropathological disorders, such as Tau, Fused in Sacroma (FUS), and heterogeneous nuclear RNP A1 (hnRNPA1), phase-separate through LLPS in vitro and in cellulo (*17*–*20*). In addition, in vitro, these proteins underwent a time-dependent progression into solid-like aggregates within condensates (*15*, *17*, *21*). This pattern has sparked the hypothesis that PS is involved in the pathological aggregation of proteins within cells.

In this study, we focused on α-synuclein (α-Syn), a protein whose aggregation is intimately associated with Lewy bodies formation (*22*, *23*) and the synucleinopathies Parkinson's disease, dementia with Lewy bodies, and multiple system atrophy (*24*–*26*). In vitro α-Syn droplets were generated in the presence of crowding agents or high salt concentration through LLPS and the protein was shown to acquire solid-like properties in a time-dependent manner (*27*–*31*). Besides, some data suggest that α-Syn can form nanoscale structures below the saturation concentration, playing a role in aggregation (*32*). These in vitro observations did not take into account complex biochemical phenomena that take place within cells such as promiscuous interactions, crowding within the cytosol, cellular compartmentalization, and stress (*33*–*35*). One recent study using a *Caenorhabditis elegans* model reported the formation of α-Syn condensates that initially had liquid-like properties and that progressed toward a solid state in aged animals (*36*). Yet, in cellulo work has proven to be difficult, as de novo α-Syn condensates formation could be challenging to monitor using classical optical means. As a consequence, the phase separation of α-Syn in cells and the possible evolution of condensates into pathogenic aggregates remain to be established.

To overcome this obstacle and assess the putative links between α-Syn condensates and their propensity to evolve into aggregates of amyloid nature within cells, we designed a method allowing controlled assembly and disassembly of intracellular liquid condensates enriched in α-Syn and made use of high-resolution microscopy. To drive the formation of phase-separated condensates in cells, we used a self-interacting multivalent protein scaffold based on five consecutive repeats of FKBP12-F36M (hereafter called 5Fm) that we

[1]PASTEUR, Department of Chemistry, École Normale Supérieure, PSL University, Sorbonne Université, CNRS, 75005 Paris, France. [2]Institut Francois Jacob (MIRCen), CEA, CNRS, Fontenay-aux-Roses, France.
*Corresponding author. Email: ronald.melki@cnrs.fr (R.M.); zoher.gueroui@ens.fr (Z.G.)

previously showed to undergo PS in cells (*37*). Expression of the fusion protein α-Syn-5Fm in HeLa cells and SH-SY5Y led to α-Syn condensates recapitulating bona fide liquid bodies that could be disassembled upon drug addiction. We next asked how α-Syn condensates evolve in the presence of α-Syn fibrillar assemblies of amyloid nature given that such fibrils have been shown to have prion-like properties (*38*, *39*).

Considering the ability of α-Syn fibrils to amplify through the recruitment of endogenous α-Syn and spread from cell to cell in a prion-like manner (*38*), we characterized the properties of α-Syn within condensates exposed to preformed fibrils. We show here a drastic modification in the morphology of α-Syn condensates upon interaction with preformed fibrils with the acquisition of a "spiky" aspect, reminiscent of sea urchins. We further demonstrate a transition from a liquid-like to a solid-like state. The changes we report were concomitant to the interaction of α-Syn preformed fibrils with the condensates, suggesting seeded liquid-to-solid conversion of α-Syn within the condensates. We establish that α-Syn within converted condensates resists detergents and is phosphorylated, two characteristics of Lewy bodies. We thus postulate that α-Syn condensates could act as a reservoir in the prion-like propagation of α-Syn fibrils.

RESULTS

In cellulo formation of α-Syn condensates

To generate α-Syn condensates with modular assembly/disassembly, we fused α-Syn to emerald Green Fluorescent Protein (emGFP)-5Fm, a multivalent protein scaffold designed to form micrometric and spherical condensates when expressed in cells (Fig. 1, A and B, left). Twenty-four hours after transfecting α-Syn-emGFP-5Fm in HeLa cells, we found that α-Syn condensates formed larger micrometric bodies displaying spherical shapes (Fig. 1B, right). To learn more about the α-Syn condensates' biogenesis, we monitored their formation using time-lapse confocal microscopy. Approximately 10 hours after transfection with the α-Syn-LLPS scaffold, several condensates form throughout the cytosolic space (Fig. 1C and movie S1). As also observed with control condensates (emGFP-5Fm; fig. S1, A to C, and movie S2), α-Syn condensates grew through the coalescence of nearby small condensates forming into larger spherical ones (Fig. 1D) or by addition of scaffolds from the dilute phase into the condensed phases (Fig. 1E). The 5Fm scaffold is required to drive α-Syn condensates formation, as α-Syn-emGFP expression alone yields an even fluorescence distribution (fig. S1D).

We next assessed the dynamic turnover of the α-Syn condensates' components using fluorescence recovery after photobleaching (FRAP). Typical FRAP curves of the control condensate (emGFP-5Fm) showed a mobile fraction of 40% recovering within 2 min (Fig. 1F). α-Syn condensates exhibited a larger mobile fraction (80%) with an increased dynamical turnover (minute) (Fig. 1F). Moreover, very similar patterns of recovery after photobleaching were observed for α-Syn condensates at 24 and 72 hours after transfection (fig. S1E), suggesting that the presence of α-Syn did not induce a time-dependent change of their dynamic properties within this timeframe. To assess the capacity of α-Syn condensates to disassemble, FK506, a competitive binder that disrupts Fm-Fm dimerization and impairs 5Fm capability to phase separate was added to the cells (*40*, *41*). Live epifluorescence microscopy revealed that 24-hour-old α-Syn condensates dissolved within a few minutes, in the presence of FK506 (Fig. 1G and movie S3). This fast α-Syn condensate dissolution was similarly observed for 72-hour-old α-Syn condensates (fig. S1F and movie S4), suggesting an absence of irreversible assemblies induced by putative strong α-Syn intermolecular interactions within condensates with time. Taken collectively, our data demonstrate our ability to control the assembly/disassembly of liquid α-Syn condensates.

α-Syn condensates undergo morphological changes in the presence of preformed α-Syn fibrils

Preformed α-Syn fibrils have been shown to grow by recruiting endogenous α-Syn in cellulo and in vivo. Yet, it remains unknown whether these fibrillar aggregates could affect α-Syn condensates. We therefore set an assay allowing monitoring and quantifying the spatiotemporal dynamics of α-Syn condensates in cells that have been exposed to fluorescently labeled, de novo assembled, α-Syn fibrils (fig. S2). HeLa cells were exposed to fragmented fibrillar α-Syn (0.5 nM) for 24 hours. Observation of those cells by epifluorescence microscopy revealed a notable change in the morphology of the majority of α-Syn condensates within the cells. The condensates displayed nonspherical shape and were often smaller, more anisotropic, with one or multiple bright puncta that appear as nodes for spiky or needle-shaped structures pointing outward (Fig. 2, B and C). No such abnormally shaped condensates were observed in control cells expressing emGFP-5Fm in the presence of fibrils (Fig. 2A). We quantified the incidence of this phenotype as a function of time at 24, 48, and 72 hours. We noticed that α-Syn condensates progressed steadily toward an "abnormal" morphology after fibrils addition, as their proportion rose from 72% at 24 hours to 97% at 72 hours (Fig. 2C). In contrast, cells expressing control condensates (emGFP-5Fm) displayed exclusively spherical condensates irrespective of the exposure time to the same amounts of α-Syn fibrils (Fig. 2C). This suggests that α-Syn within the condensates is responsible of the preformed fibril-mediated morphological alterations that we describe. To determine how preformed α-Syn fibrils trigger a change in condensate morphology, we first assessed whether exogenous α-Syn fibrils and the cellular condensates colocalize. Correlation-based colocalization analyses performed on several hundreds of cells revealed no colocalization between control condensates and exogenous fibrils at any time (Fig. 2D). In contrast, most α-Syn condensates colocalized with exogenous fibrils as early as 24 hours after addition of α-Syn fibrils (Fig. 2D). Furthermore, we found that the efficiency of the fibrils-triggered morphological changes we observed increased with fibrils concentration (0.01, 0.1, and 0.5 nM; fig. S3A). We found that α-Syn preformed oligomers did not trigger morphological changes of α-Syn condensates (fig. S3B), in contrast to preformed α-Syn fibrils. We conclude from these observations that α-Syn condensates somehow remodel in a time- and concentration-dependent manner in the presence of fibrils.

Abnormally shaped α-Syn condensates originate from fibril-driven maturation of regular condensates

Next, we investigated the time course of α-Syn condensate shape changes by live confocal microscopy in cells containing or not α-Syn fibrils. As indicated above, the micrometric α-Syn-emGFP-5Fm condensate shape evolved with time from spherical to anisotropic, with the formation of multiple needle-like structures

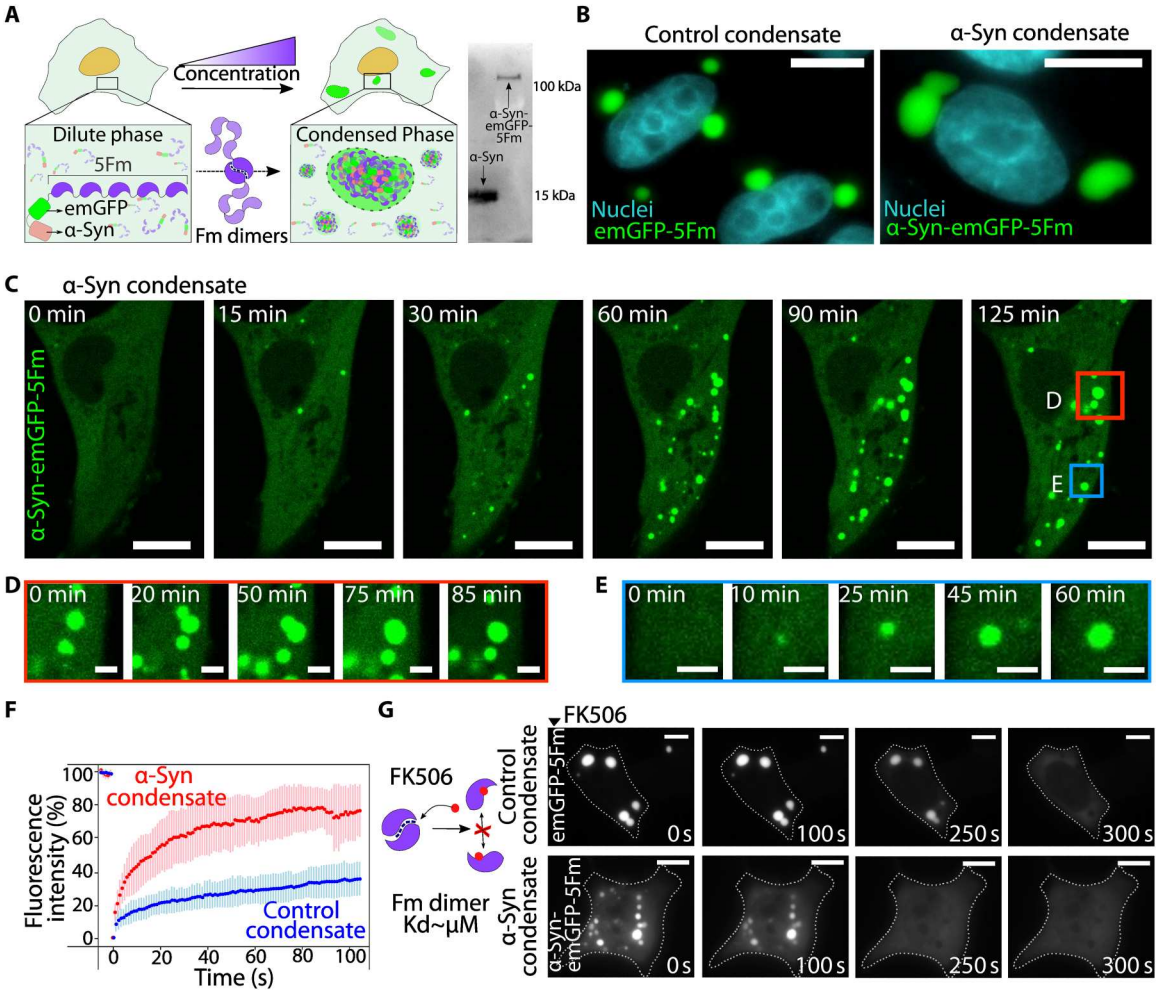

Fig. 1. Artificial α-Syn condensates with liquid-like properties. (**A**) Strategy to generate artificial condensates in cells based on a multimeric protein scaffold. Western blot displaying the molecular size of the α-Syn-emGFP-5Fm chimera compared to α-Syn alone. (**B**) Representative epifluorescence imaging of cells expressing control condensates (emGFP5-Fm scaffolds; left, green) and α-Syn condensates (α-Syn-emGFP-5Fm scaffolds, right, green). Scale bars, 10 μm. (**C**) Time-lapse confocal imaging of the formation of α-Syn condensates in HeLa cells starting 10 hours after transfection. Scale bars, 10 μm. (**D** and **E**) Enlarged regions extract from the time lapse (C) displaying growth of condensates mediated by coalescence (D) or α-Syn addition (E). Scale bars, 2 μm. (**F**) Fluorescence recovery after photobleaching performed on α-Syn condensates (red, 12 cells) and control condensates (blue, 17 cells). The dotted line in bold represents the means and the error bar represents the SD. Acquisitions were made every second. (**G**) Time-lapse imaging of the dissolution of 24-hour-old control (upper row) and α-Syn (lower row) condensates upon the addition of FK506. Dashed lines delineate cell boudaries. Scale bars, 10 μm.

sprouting from the condensate core (Fig. 2E and movie S5). This morphological transition occurred within a few hours after the addition of α-Syn fibrils, suggesting that "regular," spherical, condensates evolve into abnormal, anisotropic ones upon contact with exogenous α-Syn fibrils. Alternately, abnormally shaped condensates may form de novo in the absence of preformed condensates, e.g., upon seeding of diffuse α-Syn-emGFP-5Fm by exogenous α-Syn fibrils (*42*). To determine whether the latter scenario occurs, we exposed cells exhibiting exclusively diffuse α-Syn-emGFP-5Fm to exogenous α-Syn fibrils for 72 hours. No abnormally shaped, anisotropic condensates were observed under these experimental conditions (fig. S3C). Together, our findings suggest that the needle-like extensions we report originate from the recruitment of α-Syn-emGFP-5Fm within preformed condensates, rather than from the seeding of the cytosolic, evenly distributed form of this protein.

α-Syn fibrils-mediated abnormally shaped condensates have solid-like material properties

To examine potential modifications in the physical characteristics of abnormally shaped condensates, we performed FRAP experiments in cells exposed or not to α-Syn fibrils (24 and 72 hours). Whereas α-Syn condensates in unexposed cells displayed liquid-like properties, photobleached abnormally shaped condensates displayed no recovery of fluorescence (Fig. 3A). The lack of turnover within abnormally shaped condensates evokes a solid-like behavior that was not observed in control spherical condensates from cells exposed or not to α-Syn fibrils (fig. S3D). We conclude from these observations that α-Syn condensates interaction with α-Syn fibrils triggers a liquid-to-solid–like transition.

Next, we assessed the dissolution of α-Syn condensates in the presence of FK506. Abnormally shaped α-Syn condensates resisted prolonged FK506 treatment (over 1 hour) (Fig. 3B, fig. S3E, and

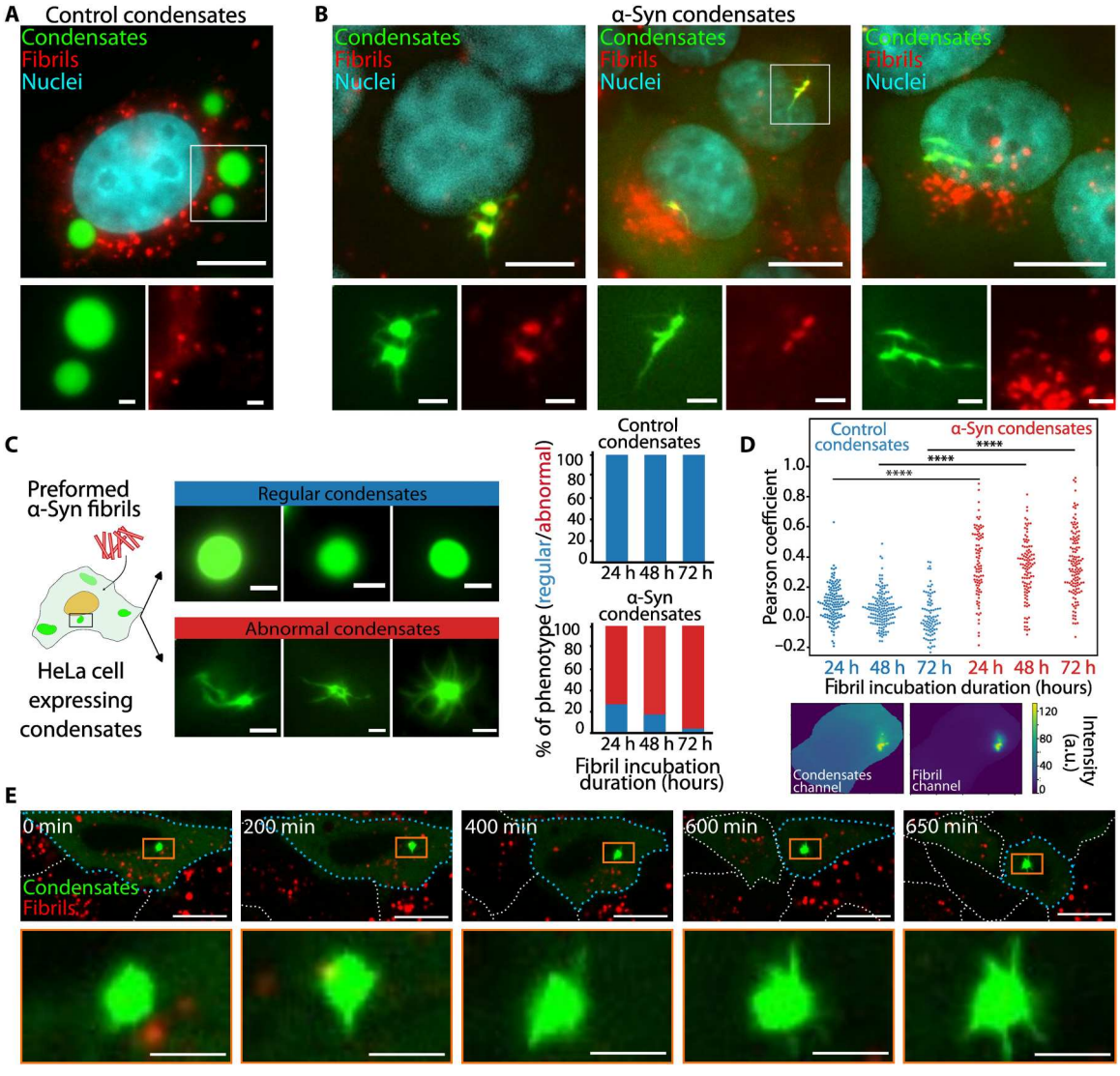

Fig. 2. α-Syn condensates are perturbed by preformed fibrils. Representative epifluorescence images of HeLa cells infected with preformed α-Syn fibrils (red) and expressing control (**A**) and α-Syn (**B**) condensates (green). Nuclei (cyan) were stained with Hoechst. Scale bars, 10 μm for full-cell images and 2 μm for zoom-ins. (**C**) Quantification of the percentage of cells with condensates expressing the two different phenotypes: regular, blue; abnormal, red. The graph is the sum of $N = 3$ experiments. (**D**) Quantification of the Pearson's coefficient calculated for the correlation between the fluorescence intensities of the fibril and condensate channels in microscopy images that were cropped to match the shape of the cell. Each point represents a cell. Differences between conditions with control and α-Syn condensates were statistically significant ($P < 10^{-7}$ using a Student's t test). a.u., arbitrary unit. (**E**) Live confocal microscopy frames depicting HeLa cells expressing α-Syn condensates (green) changing morphology upon exposure to fibrils (red). Time 0 corresponds to the time when cells expressing condensates were exposed to fibrils for approximately 48 hours. Dashed lines delineate cell boundaries. Scale bars, 10 μm.

movie S6) in sharp contrast with regular α-Syn condensates within cells unexposed to α-Syn fibrils (Fig. 1G). The resistance to dissolution was correlated with the morphological state of the condensates, as the subset of regular α-Syn condensates underwent dissolution in contrast with abnormally shaped ones within the same cells (fig. S3F). In a few cases, some condensates were found to be heterogeneous at the micrometer scale, with small abnormally shaped assemblies engulfed into a larger spherical α-Syn condensate. Consistent with the shape-reversibility relationship, we observed FK506-mediated dissolution of the spherical, not the abnormally shaped condensates (fig. S3F). An additional characteristic of the α-Syn fibril–mediated changes in condensates' properties was seen upon the fusion of two close abnormally shaped α-Syn condensates. These condensates did not yield a spherical body upon coalescence, as generally seen for liquid condensates, even after prolonged contact (hours) (Fig. 3C and movie S7). The lack of relaxation suggests an absence of internal rearrangements at the micrometer scale (Fig. 3C). Together, our findings suggest that strong bonds within condensates are sufficient to counterbalance relaxation forces and stabilize abnormally shaped condensates against micrometer-scale reorganization and dissolution.

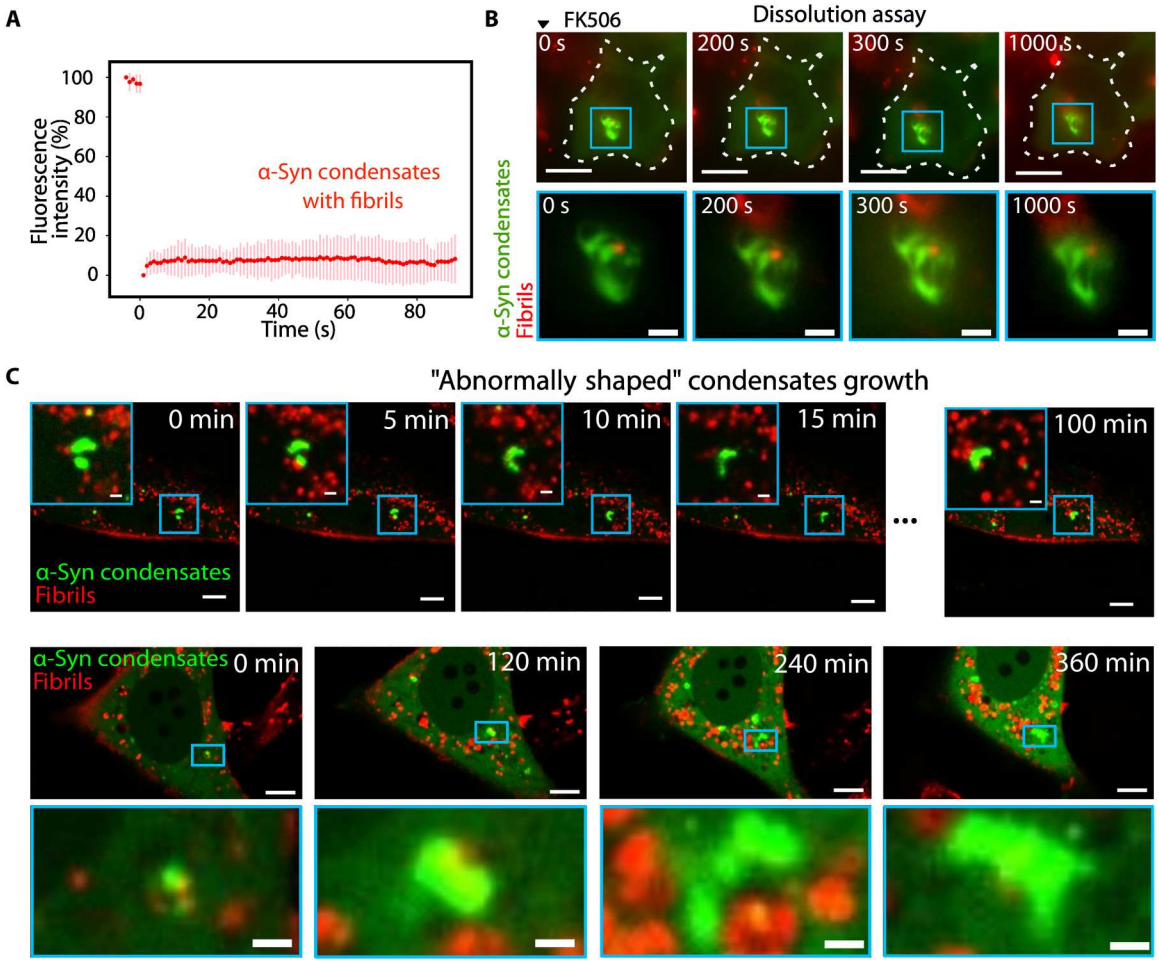

Fig. 3. Abnormally shaped α-Syn condensates have solid-like properties. (**A**) FRAP analysis of abnormally shaped condensates. The graph comprises the average of nine different experiments. The prebleaching fluorescence intensity was set at 100 and the postbleaching fluorescence was normalized at 0 for all experiments. An acquisition was made every second. Error bars correspond to the SD. (**B**) Live confocal microscopy frames depicting HeLa cells exposed to fibrils (red) and expressing α-Syn condensates (green) upon exposure to FK506 at a final concentration of 2.5 μM. Different time points are shown, with 0 s being pinpointed at the moment when FK506 was added. Scale bars,10 μm for whole-cell frames where dashed lines delineate cell bounadries and 2 μm for zoom-ins. (**C**) Confocal microscopy live images of the fusion of multiple abnormally shaped condensates (green) without coalescence. Scale bars,10 μm for whole-cell frames and 2 μm for zoom-ins.

Abnormally shaped α-Syn condensates exhibit amyloid-like properties

To further assess the biochemical properties of the abnormally shaped α-Syn condensates, we first ensured that the protein profiles and concentrations from three independent cell cultures expressing α-Syn-emGFP-5Fm or emGFP-5Fm exposed to exogenous fibrils were similar. To this end, SDS–polyacrylamide gel electrophoresis (PAGE) was performed (fig. S4A). We next demonstrated by Western blot analysis and using an anti-pS129 α-Syn antibody that α-Syn-emGFP-5Fm is phosphorylated in abnormally shaped condensates, not in control liquid counterparts (figs. S4, B and D). We also found that the quantities of preformed fibrils in cells were negligible in regard to the expressed α-Syn-emGFP-5Fm constructs (fig. S4C). We further showed using a filter retardation assay that α-Syn-emGFP-5Fm acquired resistance to detergent, upon cell exposure for 72 hours to exogenous fibrils, not in their absence (Fig. 4A). This suggests that they are of amyloid nature (Fig. 5). No such detergent-resistant aggregates were detected upon exposure of cells expressing emGFP-5Fm control condensates to exogenous α-Syn fibrils. The amyloid nature and/or content of the abnormally shaped α-Syn-emGFP-5Fm condensates was further confirmed by staining with AmyTracker (Fig. 4B). The phosphorylation of α-Syn-emGFP-5Fm was confirmed in cellulo by immunofluorescence (Fig. 4C). Collectively, these observations indicate that α-Syn-emGFP-5Fm condensates are remodeled microscopically upon interaction with exogenous α-Syn fibrils. This process is accompanied by the acquisition of biochemical properties that recapitulate the phenotypic markers of pathological α-Syn inclusions, including S129 phosphorylation and detergent resistance.

Liquid-to-solid transition is independent from α-Syn phosphorylation within condensates

To determine whether the phosphorylation of residue S129 within α-Syn is required for liquid-to-solid transition within α-Syn condensates, we generated α-Syn condensates where serine-129 was changed to alanine which prevented phosphorylation. Classical

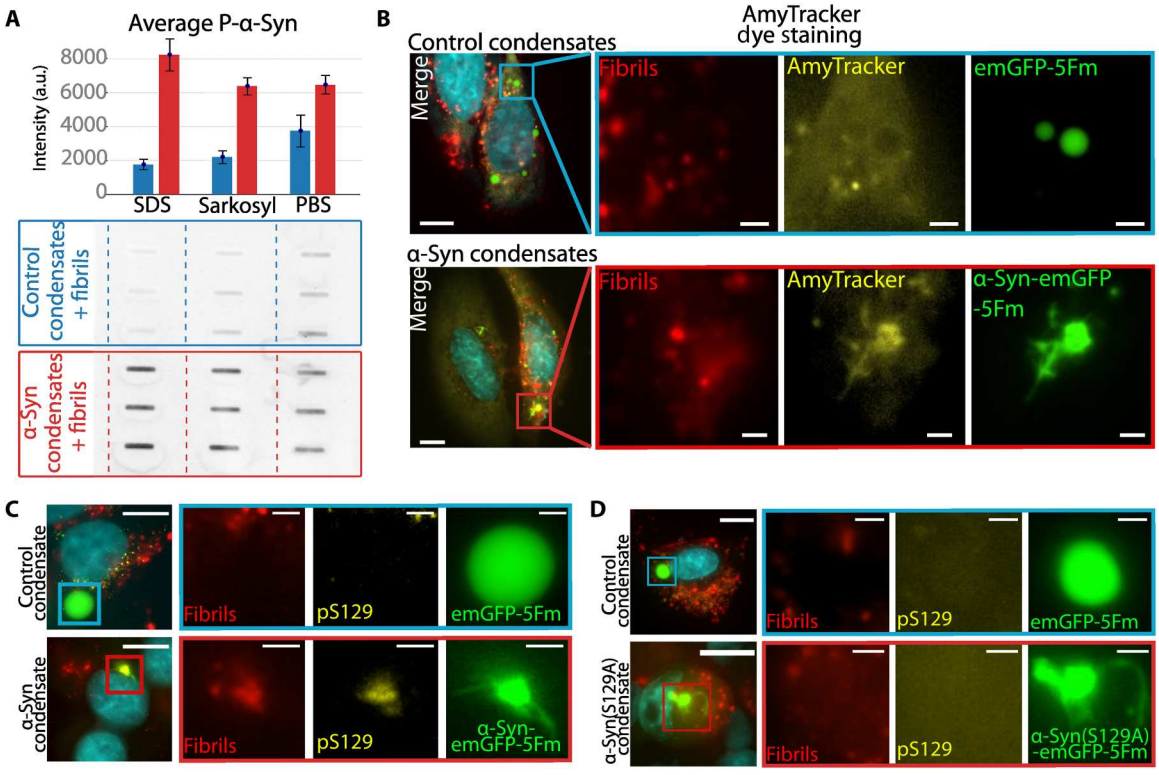

Fig. 4. Abnormally shaped α-Syn condensates are of amyloid nature. (**A**) Filter trap analysis coupled with immunoblotting against α-Syn-pS129 performed on cell lysates containing condensates incubated with preformed fibrils for 72 hours. The bar plot illustrates the chemiluminescence intensity for immunoblotting. Results from control condensates are in blue and results from α-Syn condensates are in red. For each of the three experimental conditions [SDS, sarkosyl, and phosphate-buffered saline (PBS)], $N = 3$ experiments were performed with control and α-Syn condensates. Error bars represent the SD. (**B**) AmyTracker staining on HeLa cells expressing α-Syn condensates and control condensates after 72-hour incubation with fibrils. (**C**) Epifluorescence microscopy images depicting HeLa cells exposed to wild-type α-Syn fibrils and expressing condensates after immunostaining for α-Syn-pS129. Nuclei were stained with Hoechst. (**D**) Epifluorescence microscopy images depicting HeLa cells infected with α-Syn(S129A) fibrils and expressing α-Syn(S129A) condensates after immunostaining for α-Syn-pS129. Nuclei were stained with Hoechst. Scale bars, 10 μm for whole-cell images and 2 μm for zoom-ins.

spherical condensates were observed in cells expressing α-SynS129A-emGFP-5Fm. Those condensates displayed drastic morphological changes, phenocopying those found in cells expressing wild-type (WT) α-Syn condensates upon cell exposure to exogenous S129A α-Syn fibrils (Fig. 4D, bottom). This implies that the liquid-to-solid transition of α-Syn condensates is independent of the phosphorylation of α-Syn within condensates. Furthermore, the finding that exogenous fibrils, made of α-Syn that cannot be phosphorylated, are equally potent in inducing abnormally shaped condensates within cells shows that exogenous fibril phosphorylation, which we showed not to occur, is not responsible for α-Syn condensates remodeling (*43*, *44*).

Fibrillar α-Syn polymorphism and the formation of abnormally shaped condensates

α-Syn assembles into distinct fibrillar polymorphs that bind neuronal cells and seed the aggregation of endogenous α-Syn differently (*42*). To determine whether structurally distinct α-Syn fibrillar assemblies remodel α-Syn-emGFP-5Fm condensates, we exposed cells expressing α-Syn condensates to the α-Syn fibrillar polymorph ribbons. This leads to morphological alterations within α-Syn condensates, which were not observed with control condensates, similar to those triggered by the polymorph fibrils (fig. S5 and movie S8). We conclude from this observation that structurally distinct α-Syn fibrillar polymorphs are capable of remodeling α-Syn-emGFP-5Fm condensates in a time-dependent manner (fig. S5E), most probably through a seeding process.

Preformed α-Syn fibrils triggered the evolution of liquid α-Syn condensates into solid-needle like structures in SH-SY5Y neuronal cells

To determine whether the conversion of liquid α-Syn condensates into abnormal ones may occur in other cell lines, we transposed our assay into the neuronal cells SH-SY5Y. We found that α-Syn-emGFP-5Fm expression in SH-SY5Y cells led to the formation of very large condensates dispersed throughout their cytoplasm (fig. S6A). We observed the evolution of liquid α-Syn condensates into needle-like structures in SH-SY5Y cells exposed either to fibrils or ribbons, thus phenocopying our observations in HeLa cells (fig. S6B). Abnormal condensates were also positive to the AmyTracker stain (fig. S6B) and FRAP experiments indicated that they have solid-like properties (fig. S6C).

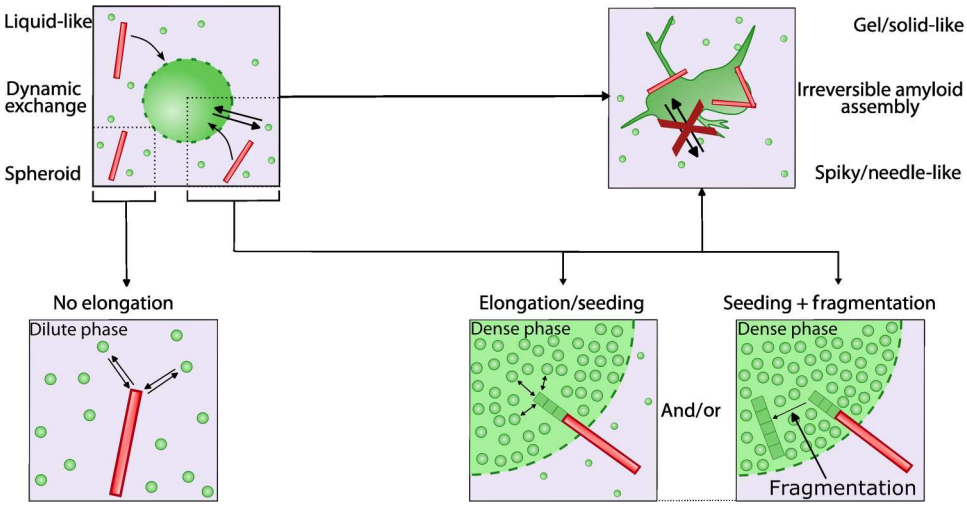

Fig. 5. Illustration of the hypothesized mechanisms underlying the liquid-to-solid transition of α-Syn condensates in the presence of fibrils. Schematic of a single α-Syn condensate (green droplet) in dynamical equilibrium with its dilute phase. Green dots are monomeric α-Syn-emGFP-5Fm exchanging between the cytosol and the condensate. The elongation of exogenous fibrillar α-Syn polymorphs (red rods) is not as efficient in an environment containing physiological concentrations of α-Syn (bottom, left). In contrast, the elongation of exogenous fibrils is explosive in the highly concentrated environment of liquid condensates (bottom, middle and right). Preformed fibrils (red) elongate rapidly by incorporation of α-Syn-emGFP-5Fm (green). Explosive elongation may lead to imperfect stacking and breakage of long fibrils into shorter ones. Other factors, known to fragment fibrils such as molecular chaperones, trapped within the condensates, may sever the fibrils leading to an increased number of fibril ends and aggregation. Last, changes in the viscoelastic properties of the condensate environment may favor the de novo aggregation of α-Syn-emGFP-5Fm. Together, these events drive a liquid-to-solid transition and the resulting changes in condensate shape.

DISCUSSION

In recent years, several proteins involved in neurodegenerative diseases, such as Tau, TDP43, FUS, huntingtin, and hnRNPA1, have been reported to form cytosolic condensates, and efforts have been made to describe the physiological and pathological consequences of this phenomenon. Little evidence supporting α-Syn PS in a cellular context has been brought so far. Nonetheless, α-Syn is predicted to undergo PS given (i) its overall low complexity and the specific abundance of charged and polar amino acid residues within its C-terminal domain (*24*, *45*, *46*), (ii) its ability to form condensates at high concentrations and in the presence of crowding factors in vitro (*27*, *28*) which have been proposed to favor fibrils formation (*27*, *47*), and (iii) its presence within Tau and synapsin condensates (*48*, *49*). Studies in cellular models have proven to be difficult, with limited reproducibility, thus motivating our design of artificial α-Syn condensates. Biophysical characterizations indicated that our artificial α-Syn condensates recapitulated the spheroid morphology, the reversibility, and the liquid-like material properties that characterize PS-derived cellular compartments. This confirmed that our artificial condensates could be instrumentalized to decipher the impact of PS on the protein.

For proteins such as FUS or Tau, phase-separated droplet formation in vitro is sufficient to trigger the spontaneous nucleation and subsequent growth of fibrillar aggregates (*15*, *20*). This temporal evolution from liquid states to more gel or solid ones has fueled the hypothesis that liquid condensates act as intermediates between diffusible monomers and stable, disease-associated aggregates by providing an aggregation-suitable environment, notably through concentrating aggregation-prone proteins (*15*, *20*). Recent in vitro studies and theoretical modeling examined how liquid condensates could modulate nucleation rate. For instance, coacervate droplets modified α-Syn aggregation properties by accelerating their formation at their surface or, in contrast, by suppressing aggregation within droplets (*50*). The interface of droplets was also shown to accelerate fibril formation of the low-complexity domain of hnRNPA1 (*46*). Studies of α-Syn droplets coupled to a thioflavin T assay suggest that aggregation within droplets could appear from primary nucleation and that secondary processes due to changes in viscosity, concentration, hydration, interface, etc. could outperform primary ones (*28*). Furthermore, theoretical predictions also showed how spatially localized aggregation within liquid condensates could emerge from weak interactions between protein monomers and the compartments that could act as continuous sinks (*47*).

In our setting, α-Syn artificial condensates behaved as highly dynamic bodies displaying no time-dependent evolution in material properties over 72 hours. These persistent liquid-like properties suggest no detectable protein aggregation events within our condensates over this time scale. Two previous studies found that α-Syn condensates could undergo maturation over time. In HeLa cells, α-Syn condensates behave as liquid-like bodies at 24 hours, with a decrease in the dynamic at 48 hours (*27*). In the nematode *C. elegans*, α-Syn condensates display liquid-like properties in young worms (up to 7 to 11 days) and evolved toward gel inclusions in aged worms (15 days) (*36*). Differences in behavior with our α-Syn artificial condensates may be due to an antiaggregation propensity of the emGFP-5Fm moieties grafted to α-Syn protein within the condensates. Together, this agrees with the idea that the initial nucleation events of fibril aggregates assembly can be viewed as a rate-limiting step for the assembly process (*51*).

Primary nucleation and subsequent growth of aggregates are not, however, the only pathways for synucleinopathy expansion. Assessment of α-Syn pathology progression in the brain using preformed α-Syn fibrils has revealed that fibrillar α-Syn can be excreted from

affected cells into the extracellular environment and taken up by naïve cells (*38*). Pieces of evidence for the active transport of fibrillar α-Syn aggregates through membranous structures between neuronal cells have also been brought (*52*, *53*). Fibrillar α-Syn multiplies by recruiting their cellular monomeric counterpart while spreading, thus contributing to disease progression via this prion-like propagation process (*39*). It remains nonetheless unclear whether fibrils could interact with α-Syn within condensates in cells and what potential outcomes could emerge from such interplay. Thanks to our assay, one could probe how fibrillar forms of α-Syn affect a monomeric α-Syn inside condensates within cells. We found that the interactions of fibrils with the condensates trigger severe changes in their morphology, which entailed the formation of micrometer-long needle-like protrusions originating from α-Syn condensates. These modifications were accompanied by a conversion of α-Syn from a dynamic liquid state to a solid-like state exhibiting the characteristics of amyloid deposits, namely, irreversibility, arrested component turnover, and resistance to SDS.

These abnormally shaped bodies originated exclusively from already-formed condensates, indicating that α-Syn within PS-derived condensates is more prone than its diffuse cytosolic counterpart to undergo conversion into amyloid fibrils. In addition, the abnormally shaped condensates stained positive for α-Syn phosphorylated at serine-129, a hallmark of pathogenic α-Syn within Lewy bodies (*23*, *54*, *55*). This further supports the view that α-Syn within the condensates can fuel α-Syn fibrils growth and multiplication and the spreading of pathology within the central nervous system. A critical aspect in α-synucleinopathies is the concept of strains where different α-Syn fibrillar polymorphs impose their intrinsic structural characteristics upon recruitment of endogenous α-Syn (*42*). As a perspective, it will be interesting to examine whether the needle-shaped amyloid structures that form in cells from the condensates retain the structural properties of the seed.

What makes α-Syn condensates more prone than the diffusing α-Syn pool to aggregate upon fibril exposure? We propose that supersaturation is achieved by α-Syn condensation (Fig. 5) (*56*, *57*). Preformed fibrils can elongate by recruiting monomeric α-Syn. Seeding and preformed fibril growth are notably less efficient in a dilute environment containing physiological α-Syn as compared to that of the highly concentrated liquid α-Syn condensates (Fig. 5). This accounts most for our observations. Furthermore, fragmentations of rapidly growing fibrils may generate additional ends, leading to further acceleration of liquid-to-solid transition and the resulting changes in α-Syn condensate shape. This phenomenon could be due to imperfect stacking of α-Syn in the fibrils, severing factors such as molecular chaperones within the condensates, and/or de novo aggregation of α-Syn-emGFP-5Fm because of changes in the viscoelastic properties of the condensate environment (Fig. 5). Although supersaturation could also lead to de novo aggregation without exogenous α-Syn fibrillar triggers, this was not observed with α-Syn condensates in the absence of preformed fibrils. This may be due to the antiaggregation propensity of the emGFP-5Fm moieties of α-Syn-emGFP-5Fm molecules within the condensates. This suggests that our α-Syn condensates are at a concentration that is high enough to substantially accelerate exogenous fibril-induced aggregation, but that does not exceed the threshold for spontaneous aggregation (*56*). It is further reasonable to hypothesize that the extent to which α-Syn conformational states compatible with fibrillar assembly formation or the elongation of preformed fibrils are populated is much higher within α-Syn condensates than in the diffusing α-Syn pool (Fig. 5). Both pictures could account for the drastic morphological changes and time-dependent evolutions of α-Syn-emGFP-5Fm condensates enabling the liquid-to-solid transition (Fig. 5).

How our observations could be related to the aggregation of α-Syn in neurons? Our artificial α-Syn condensates form micrometric bodies in HeLa and SH-SY5Y cells that are unlikely to be of similar sizes within neurons. Yet, phase-separated condensates have recently attracted strong interest in the physiology and pathophysiology of neurons (*58*). For instance, in vitro studies suggested that synaptic proteins, such as postsynaptic density or synapsin, could phase-separate, thus proposing a complementary framework to examine assemblies at synapses (*48*). In this context, it has been shown that overexpression of synapsin can trigger condensation and recruit α-Syn by partitioning, which could, in turn, potentially modulate synapsin/synaptic vesicle condensation and clustering (*48*). Therefore, the perturbation of synaptic activity described during the accumulation of insoluble α-Syn might be mediated by such condensates. In addition, it has been hypothesized that the irreversible evolution of α-Syn condensates in the presence of lipids and other cellular components in the *C. elegans* model might be linked to the formation of Lewy bodies, one of the main landmarks of Parkinson's disease (*36*). Last, the up-regulation of *SNCA* gene expression in human induced pluripotent stem cell–derived dopaminergic neurons was observed upon seeded aggregation of endogenous α-Syn (*43*) and may favor α-Syn phase transition.

Our findings show how α-Syn–enriched condensates could favor the prion-like propagation of pathogenic α-Syn fibrillar aggregates. Our ability to fine-tune seeding within our assay together with its sensitivity and robustness make it amenable to high-throughput screening of modulators of α-Syn aggregation. Furthermore, the flexibility of our system could allow the investigation of other neurodegeneration-prone proteins to address the fundamental hypothesis linking liquid condensates and aggregation.

MATERIALS AND METHODS

Cell culture

All cellular experiments were carried out in human epithelioid carcinoma HeLa (American Type Culture Collection, ccl-2) cells and SH-SY5Y(ECACC). Cells were maintained in Dulbecco's modified Eagle's medium [DMEM; with D-glucose (4.5 g/liter); Corning, 10-017-CV] supplemented with 10% fetal bovine serum (FBS; Gibco, 10270-106) and 1% penicillin/streptavidin (P/S; Sigma-Aldrich, P4333), at 37°C in a 5% CO_2-humidified incubator. Cells were tested every 2 months for mycoplasma infection. SH-SY5Y was a gift from I. Janoueix-Lesosey (Institut Curie).

Plasmids

The pcDNA3.1 (Invitrogen) backbone was used for all the plasmids transfected during this study (table S1). All plasmids contain the 6His and the Myc tag downstream of the coding sequence. The pcDNA3.1-emGFP-5Fm plasmid was created by inserting the emGFP coding sequence between the HindIII and Eco47III restriction sites from the pcDNA3.1-5Fm. The pcDNA3.1-α-Syn-emGFP-5Fm plasmid was created by replacing the seipin coding sequence from the pcDNA3.1-Seipin-emGFP-5Fm (between the HindIII and

SacII restriction sites) with the α-Syn coding sequence. The pcDNA3.1-α-Syn(S129A)-emGFP-5Fm plasmid was created from the pcDNA3.1-α-SynWT-emGFP-5Fm using a primer containing the S129A mutation through the Gibson method.

Transfection

All transfection experiments were carried out using Lipofectamine 2000 (Invitrogen) and OptiMEM (Gibco, 31985-062). Cells were seeded for 24 hours before transfection (80,000 cells per well on 12 mm diameter round coverslips for 24-well plates; 350,000 cells per well on 22 × 22 mm^2 coverslips for six-well plates and 100,000 cells per well for ibidi dishes) and placed in the incubator at 37°C and 5% CO_2. For each well, two solutions were mixed together: Solution 1 contained Lipofectamine 2000 (2 μl for 24 wells or ibidi dishes and 4 μl for 6 wells) + optiMEM (50 μl for 24 wells, 60 μl for ibidi dishes, and 150 μl for 6 wells); solution 2 contained plasmid DNA (750 ng for 24 wells, 1 μg for ibidi dishes, and 2 μg for 6 wells) + OptiMEM (same volumes as solution 1). Solution 1 was incubated for 5 min before mixing with solution 2 and incubating for another 20 min. The cells were then incubated with DNA/Lipofectamine 2000 mix for 1 hour and 30 min at 37°C and 5% CO_2, then washed twice with DMEM + Fetal Bovine Serum (FBS) + P/S and incubated for 24 to 72 hours depending on the experiment. Each of the three plasmids, i.e., pcDNA3.1-emGFP-5Fm, α-Syn-emGFP-5Fm, and α-Syn(S129A)-emGFP-5Fm, were cotransfected with the 5Fm in 1:1 stoichiometry, except for experiments carried out in six-well plates where the control emGFP-5Fm was cotransfected with 5Fm in a 2:3 stoichiometry to avoid the saturation of the images.

α-Syn seeding assays

Human WT α-Syn and a version of the protein where the phosphorylatable Ser^{129} residue was replaced by an Ala were expressed, purified, and assembled into the fibrillar polymorphs fibrils and ribbons as described previously (*42*). The fibrillar polymorphs were diluted to 0.5 nM in DMEM + SVF + P/S and added to cells for 1 hour and 30 min after transfection (at the moment when the Lipofectamine 2000 + DNA mixture was washed away).

For fixed cells experiments, 24-well plates were used. Cells were incubated for 24 hours with fibrils at 37°C and 5% CO_2 for fibril integration, then washed with fresh DMEM + FBS + P/S. They were then either fixed immediately after washing (for 24-hour fibril incubation experiments) or incubated for another 24 to 48 hours (for 48- and 72-hour fibril incubation experiments, respectively) before fixation and observation on an epifluorescence microscope. For details about the experimental setting, please refer to the "Imaging" section.

For live-microscopy experiments, ibidi μ-Dish (35 mm) was used. Cells with fibrils were followed through overnight movies at different time points: For the 0- to 24-hour interval, cells were incubated for 7 to 8 hours with fibrils, and then transferred to a confocal microscope. For 24 to 48 hours, cells were incubated for 24 hours with fibrils, washed with fresh medium, and then transferred to the confocal microscope. For 48- to 72-hour experiments, cells were incubated with fibrils for 24 hours, washed, then incubated for another 24 hours before another round of wash and the transfer to the confocal microscope. For details about the experimental setting, please refer to the "Imaging" section.

Immunofluorescence

Twenty-four to 72 hours after transfection, cells were fixed with a 4% paraformaldehyde solution (Sigma-Aldrich) for 20 min. Cells were then washed three times with phosphate-buffered saline (PBS) and permeabilized with a solution of 0.1% Triton X-100 (Sigma-Aldrich) for 10 min, washed three times for 5 min with PBS, and then incubated for 1 hour with the primary antibody anti–α-Syn-pS129 (Abcam, ab51253) diluted 1:10,000 in a solution of 1% BSA in PBS. Then, cells were washed again three times for 5 min with PBS and incubated with the secondary antibody Alexa Fluor 568 (Invitrogen, A-11011) diluted 1:1000 in a solution of 1% BSA in PBS. Cells were then washed again three times for 5 min in Dulbecco's PBS and mounted on coverslips using the Fluoromount-G mounting medium.

Dissolution and reversibility and granule formation prevention assays

For live dissolution, a 2.5 mM solution of FK506 (in dimethyl sulfoxide) was diluted in 50 μl of medium and was added to the cells such that the final concentration was 2.5 μM. Dissolution was monitored by capturing an image every 10 s starting from FK506 addition. For condensate formation prevention, FK506 at a final concentration of 2.5 μM was added to cell media 1 hour and 30 min after transfection (at washing). For condensate reversibility assays, FK506 at a final concentration of 2.5 μM was added to cell media 1 hour before fixation.

Fluorescence recovery after photobleaching

FRAP experiments were carried out in live HeLa cells in a humidified chamber maintained at 37°C and 5% CO_2, which was mounted on a confocal microscope (see details in the "Imaging" section). Condensates were scanned 10 times to establish the average level of initial fluorescence, then bleached using a 488 nm laser at 100% intensity (10 iterations). The recovery of fluorescence was then followed by acquiring an image of 512 × 512 pixels every second for 120 s. The FRAP movies were analyzed using the Fiji software where each condensate studied was integrated into a region of interest from which the average fluorescence intensity was extracted. To correct the movement of the condensates, the StackReg plugin was used on some of the movies. Analysis and fitting of the fluorescence intensity data were performed using Python. For the graphical representation, we fixed the initial fluorescence at 100% and the fluorescence at bleaching 0% and normalized the remaining points accordingly.

Western blot analysis

For Western blots, cellular pellets were resuspended in PBS buffer supplemented with 0.5% Tween 20 and lysed using a Branson Sonifier (approximately five to seven pulses of 15 s at 60% amplitude). Cell homogenates were denatured with preheated (95°C) sample buffer [50 mM tris-HCl (pH 6.8), 4% SDS, 2% ß-mercaptoethanol, 12% glycerol, and 0.01% bromophenol blue]. After a 5 min incubation at 95°C, the samples were analyzed on 12% SDS-PAGE, followed by a transfer to a polyvinylidene difluoride membrane for 2 hours at 30 V. The membranes were blocked in 5% skimmed milk and probed with the primary antibody overnight and with the secondary antibody for 1 hour (both at 4°C). Chemiluminescence was imaged and quantified using the Clarity Western ECL Substrate (Bio-Rad) in a ChemiDoc Imaging System (Bio-Rad).

Quantification of pathogenic α-Syn using Western blot analysis and filter-retention assay

Pathogenic α-Syn was quantified using both a filter retardation assay and immunoblotting and Western blot analysis. Cell homogenates in PBS, PBS containing 1% sarkosyl, and PBS containing 1% SDS (0.5 mg) were immobilized on cellulose acetate membranes (0.2 μm pore size; Millipore Corp., Bedford, MA) by filtration using a 48-slot slot-blot filtration apparatus (GE Healthcare). The membranes were blocked in 5% skimmed milk and probed with the anti-pS129 α-Syn antibody EP1536Y (Abcam, catalog no. ab51253) and a goat anti-rabbit antibody coupled to HRP (Thermo Fisher Scientific, catalog no. A27036).

Imaging

Fixed samples and dissolution movies were imaged with an epifluorescence microscope (IX81, Olympus) operated by the Micro-Manager 2.0, using an Orca-fusion camera (Hamamatsu), a 63× oil-immersion objective, and the Spectra-X Lumencor LED for illumination. For overnight live movies and FRAP, we used the Zeiss LSM 710 META laser scanning confocal microscope equipped with a humidified chamber maintained at 37°C and 5% CO_2. Samples were illuminated using a 25 mW argon laser and observed using a 63× oil-immersion objective. The microscope was operated using the LSM Zen 2012 software.

Statistical analysis

For Fig. 2D and fig. S5D, a Python script based on the scipy.stats.pearsonr function was used to determine the Pearson's coefficient describing the linear relationship between the fluorescence intensity within the fibril and condensate channels. To assess the statistical significance of the data, Student's *t* tests were performed for control and α-Syn condensates data samples from the same time point. All datasets were confirmed to be normal distributions before analysis with Student's *t* test.

Supplementary Materials

This PDF file includes:
Figs. S1 to S6
Table S1
Legends for movies S1 to S8

Other Supplementary Material for this manuscript includes the following:
Movies S1 to S8

REFERENCES AND NOTES

1. A. A. Hyman, C. A. Weber, F. Jülicher, Liquid-liquid phase separation in biology. *Annu. Rev. Cell Dev. Biol.* **30**, 39–58 (2014).
2. S. F. Banani, H. O. Lee, A. A. Hyman, M. K. Rosen, Biomolecular condensates: Organizers of cellular biochemistry. *Nat. Rev. Mol. Cell Biol.* **18**, 285–298 (2017).
3. Y. Luo, Z. Na, S. A. Slavoff, P-Bodies: Composition, properties, and functions. *Biochemistry* **57**, 2424–2431 (2018).
4. X. Liu, X. Liu, H. Wang, Z. Dou, K. Ruan, D. L. Hill, L. Li, Y. Shi, X. Yao, Phase separation drives decision making in cell division. *J. Biol. Chem.* **295**, 13419–13431 (2020).
5. J. R. Buchan, R. Parker, Eukaryotic stress granules: The ins and outs of translation. *Mol. Cell* **36**, 932–941 (2009).
6. P. Li, S. Banjade, H.-C. Cheng, S. Kim, B. Chen, L. Guo, M. Llaguno, J. V. Hollingsworth, D. S. King, S. F. Banani, P. S. Russo, Q.-X. Jiang, B. T. Nixon, M. K. Rosen, Phase transitions in the assembly of multivalent signalling proteins. *Nature* **483**, 336–340 (2012).
7. S. Boeynaems, S. Alberti, N. L. Fawzi, T. Mittag, M. Polymenidou, F. Rousseau, J. Schymkowitz, J. Shorter, B. Wolozin, L. V. D. Bosch, P. Tompa, M. Fuxreiter, Protein phase separation: A new phase in cell biology. *Trends Cell Biol.* **28**, 420–435 (2018).
8. G. A. P. de Oliveira, Y. Cordeiro, J. L. Silva, T. C. R. G. Vieira, Liquid-liquid phase transitions and amyloid aggregation in proteins related to cancer and neurodegenerative diseases. *Adv. Protein Chem. Struct. Biol.* **118**, 289–331 (2019).
9. C. Mathieu, R. V. Pappu, J. P. Taylor, Beyond aggregation: Pathological phase transitions in neurodegenerative disease. *Science* **370**, 56–60 (2020).
10. A. Zbinden, M. Pérez-Berlanga, P. De Rossi, M. Polymenidou, Phase separation and neurodegenerative diseases: A disturbance in the force. *Dev. Cell* **55**, 45–68 (2020).
11. A. Aguzzi, M. Altmeyer, Phase separation: Linking cellular compartmentalization to disease. *Trends Cell Biol.* **26**, 547–558 (2016).
12. E. Chuang, A. M. Hori, C. D. Hesketh, J. Shorter, Amyloid assembly and disassembly. *J. Cell Sci.* **131**, jcs189928 (2018).
13. W. M. Babinchak, W. K. Surewicz, Liquid-liquid phase separation and its mechanistic role in pathological protein aggregation. *J. Mol. Biol.* **432**, 1910–1925 (2020).
14. L. Jawerth, E. Fischer-Friedrich, S. Saha, J. Wang, T. Franzmann, X. Zhang, J. Sachweh, M. Ruer, M. Ijavi, S. Saha, J. Mahamid, A. A. Hyman, F. Jülicher, Protein condensates as aging Maxwell fluids. *Science* **370**, 1317–1323 (2020).
15. A. Patel, H. O. Lee, L. Jawerth, S. Maharana, M. Jahnel, M. Y. Hein, S. Stoynov, J. Mahamid, S. Saha, T. M. Franzmann, A. Pozniakovski, I. Poser, N. Maghelli, L. A. Royer, M. Weigert, E. W. Myers, S. Grill, D. Drechsel, A. A. Hyman, S. Alberti, A liquid-to-solid phase transition of the ALS protein FUS accelerated by disease mutation. *Cell* **162**, 1066–1077 (2015).
16. J. D. Camino, P. Gracia, N. Cremades, The role of water in the primary nucleation of protein amyloid aggregation. *Biophys. Chem.* **269**, 106520 (2021).
17. A. Molliex, J. Temirov, J. Lee, M. Coughlin, A. P. Kanagaraj, H. J. Kim, T. Mittag, J. P. Taylor, Phase separation by low complexity domains promotes stress granule assembly and drives pathological fibrillization. *Cell* **163**, 123–133 (2015).
18. K. A. Burke, A. M. Janke, C. L. Rhine, N. L. Fawzi, Residue-by-residue view of in vitro FUS granules that bind the C-terminal domain of RNA polymerase II. *Mol. Cell* **60**, 231–241 (2015).
19. S. Boyko, X. Qi, T.-H. Chen, K. Surewicz, W. K. Surewicz, Liquid–Liquid phase separation of tau protein: The crucial role of electrostatic interactions. *J. Biol. Chem.* **294**, 11054–11059 (2019).
20. S. Wegmann, B. Eftekharzadeh, K. Tepper, K. M. Zoltowska, R. E. Bennett, S. Dujardin, P. R. Laskowski, D. MacKenzie, T. Kamath, C. Commins, C. Vanderburg, A. D. Roe, Z. Fan, A. M. Molliex, A. Hernandez-Vega, D. Muller, A. A. Hyman, E. Mandelkow, J. P. Taylor, B. T. Hyman, Tau protein liquid–liquid phase separation can initiate tau aggregation. *EMBO J.* **37**, e98049 (2018).
21. S. Ambadipudi, J. Biernat, D. Riedel, E. Mandelkow, M. Zweckstetter, Liquid-liquid phase separation of the microtubule-binding repeats of the Alzheimer-related protein Tau. *Nat. Commun.* **8**, 275 (2017).
22. K. Uéda, H. Fukushima, E. Masliah, Y. Xia, A. Iwai, M. Yoshimoto, D. A. Otero, J. Kondo, Y. Ihara, T. Saitoh, Molecular cloning of cDNA encoding an unrecognized component of amyloid in Alzheimer disease. *Proc. Natl. Acad. Sci. U.S.A.* **90**, 11282–11286 (1993).
23. M. G. Spillantini, M. L. Schmidt, V. M. Lee, J. Q. Trojanowski, R. Jakes, M. Goedert, α-Synuclein in Lewy bodies. *Nature* **388**, 839–840 (1997).
24. H. A. Lashuel, C. R. Overk, A. Oueslati, E. Masliah, The many faces of α-synuclein: From structure and toxicity to therapeutic target. *Nat. Rev. Neurosci.* **14**, 38–48 (2013).
25. J. E. Galvin, V. M.-Y. Lee, J. Q. Trojanowski, Synucleinopathies: Clinical and pathological implications. *Arch. Neurol.* **58**, 186–190 (2001).
26. M. G. Spillantini, R. A. Crowther, R. Jakes, N. J. Cairns, P. L. Lantos, M. Goedert, Filamentous α-synuclein inclusions link multiple system atrophy with Parkinson's disease and dementia with Lewy bodies. *Neurosci. Lett.* **251**, 205–208 (1998).
27. S. Ray, N. Singh, R. Kumar, K. Patel, S. Pandey, D. Datta, J. Mahato, R. Panigrahi, A. Navalkar, S. Mehra, L. Gadhe, D. Chatterjee, A. S. Sawner, S. Maiti, S. Bhatia, J. A. Gerez, A. Chowdhury, A. Kumar, R. Padinhateeri, R. Riek, G. Krishnamoorthy, S. K. Maji, α-Synuclein aggregation nucleates through liquid–Liquid phase separation. *Nat. Chem.* **12**, 705–716 (2020).
28. S. T. Dada, M. C. Hardenberg, L. K. Mrugalla, M. O. McKeon, E. Klimont, T. C. T. Michaels, M. Vendruscolo, Spontaneous nucleation and fast aggregate-dependent proliferation of α-synuclein aggregates within liquid condensates at physiological pH. bioRxiv 2021.09.26.461836 [Preprint] (6 September 2021). https://doi.org/10.1101/2021.09.26.461836.
29. A. S. Sawner, S. Ray, P. Yadav, S. Mukherjee, R. Panigrahi, M. Poudyal, K. Patel, D. Ghosh, E. Kummerant, A. Kumar, R. Riek, S. K. Maji, Modulating α-synuclein liquid–liquid phase separation: Published as part of the *Biochemistry* virtual special issue "Protein Condensates". *Biochemistry* **60**, 3676–3696 (2021).
30. S. Huang, B. Xu, Y. Liu, Calcium promotes α-synuclein liquid-liquid phase separation to accelerate amyloid aggregation. *Biochem. Biophys. Res. Commun.* **603**, 13–20 (2022).

31. B. Xu, S. Huang, Y. Liu, C. Wan, Y. Gu, D. Wang, H. Yu, Manganese promotes α-synuclein amyloid aggregation through the induction of protein phase transition. *J. Biol. Chem.* **298**, 101469 (2022).
32. S. Ray, T. O. Mason, L. Boyens-Thiele, N. Jahnke, A. K. Buell, Mass photometric detection and quantification of nanoscale α-synuclein phase separation. bioRxiv 2022.05.03.490467 [Preprint] (4 May 2022). https://doi.org/10.1101/2022.05.03.490467.
33. A. Cochard, M. Garcia-Jove Navarro, L. Piroska, S. Kashida, M. Kress, D. Weil, Z. Gueroui, RNA at the surface of phase-separated condensates impacts their size and number. *Biophys. J.* **121**, 1675–1690 (2022).
34. W. P. Flavin, L. Bousset, Z. C. Green, Y. Chu, S. Skarpathiotis, M. J. Chaney, J. H. Kordower, R. Melki, E. M. Campbell, Endocytic vesicle rupture is a conserved mechanism of cellular invasion by amyloid proteins. *Acta Neuropathol. (Berl.)* **134**, 629–653 (2017).
35. J. Labbadia, R. I. Morimoto, The biology of proteostasis in aging and disease. *Annu. Rev. Biochem.* **84**, 435–464 (2015).
36. M. C. Hardenberg, T. Sinnige, S. Casford, S. T. Dada, C. Poudel, E. A. Robinson, M. Fuxreiter, C. F. Kaminksi, G. S. Kaminski Schierle, E. A. A. Nollen, C. M. Dobson, M. Vendruscolo, Observation of an α-synuclein liquid droplet state and its maturation into Lewy body-like assemblies. *J. Mol. Cell Biol.* **13**, 282–294 (2021).
37. A. Cochard, A. Safieddine, P. Combe, M.-N. Benassy, D. Weil, Z. Gueroui, Condensate functionalization with motors directs their nucleation in space and allows manipulating RNA localization. bioRxiv 2022.07.10.499452 [Preprint] (10 July 2022). https://doi.org/10.1101/2022.07.10.499452.
38. S. Gribaudo, P. Tixador, L. Bousset, A. Fenyi, P. Lino, R. Melki, J.-M. Peyrin, A. L. Perrier, Propagation of α-synuclein strains within human reconstructed neuronal network. *Stem Cell Rep.* **12**, 230–244 (2019).
39. C. Hansen, E. Angot, A.-L. Bergström, J. A. Steiner, L. Pieri, G. Paul, T. F. Outeiro, R. Melki, P. Kallunki, K. Fog, J.-Y. Li, P. Brundin, α-Synuclein propagates from mouse brain to grafted dopaminergic neurons and seeds aggregation in cultured human cells. *J. Clin. Invest.* **121**, 715–725 (2011).
40. M. Garcia-Jove Navarro, S. Kashida, R. Chouaib, S. Souquere, G. Pierron, D. Weil, Z. Gueroui, RNA is a critical element for the sizing and the composition of phase-separated RNA-protein condensates. *Nat. Commun.* **10**, 3230 (2019).
41. J. J. Barrero, E. Papanikou, J. C. Casler, K. J. Day, B. S. Glick, An improved reversibly dimerizing mutant of the FK506-binding protein FKBP. *Cell Logist.* **6**, e1204848 (2016).
42. L. Bousset, L. Pieri, G. Ruiz-Arlandis, J. Gath, P. H. Jensen, B. Habenstein, K. Madiona, V. Olieric, A. Böckmann, B. H. Meier, R. Melki, Structural and functional characterization of two alpha-synuclein strains. *Nat. Commun.* **4**, 2575 (2013).
43. B. Tanudjojo, S. S. Shaikh, A. Fenyi, L. Bousset, D. Agarwal, J. Marsh, C. Zois, S. Heman-Ackah, R. Fischer, D. Sims, R. Melki, G. K. Tofaris, Phenotypic manifestation of α-synuclein strains derived from Parkinson's disease and multiple system atrophy in human dopaminergic neurons. *Nat. Commun.* **12**, 3817 (2021).
44. A. N. Shrivastava, L. Bousset, M. Renner, V. Redeker, J. Savistchenko, A. Triller, R. Melki, Differential membrane binding and seeding of distinct α-synuclein fibrillar polymorphs. *Biophys. J.* **118**, 1301–1320 (2020).
45. M. Hardenberg, A. Horvath, V. Ambrus, M. Fuxreiter, M. Vendruscolo, Widespread occurrence of the droplet state of proteins in the human proteome. *Proc. Natl. Acad. Sci. U.S.A.* **117**, 33254–33262 (2020).
46. M. Linsenmeier, L. Faltova, U. C. Palmiero, C. Seiffert, A. M. Küffner, D. Pinotsi, J. Zhou, R. Mezzenga, P. Arosio, The interface of condensates of the hnRNPA1 low complexity domain promotes formation of amyloid fibrils. bioRxiv 2022.05.23.493075 [Preprint] (23 May 2022). https://doi.org/10.1101/2022.05.23.493075.
47. C. Weber, T. Michaels, L. Mahadevan, Spatial control of irreversible protein aggregation. *eLife* **8**, e42315 (2019).
48. C. Hoffmann, R. Sansevrino, G. Morabito, C. Logan, R. M. Vabulas, A. Ulusoy, M. Ganzella, D. Milovanovic, Synapsin condensates recruit alpha-synuclein. *J. Mol. Biol.* **433**, 166961 (2021).
49. A. Siegert, M. Rankovic, F. Favretto, T. Ukmar-Godec, T. Strohäker, S. Becker, M. Zweckstetter, Interplay between tau and α-synuclein liquid-liquid phase separation. *Protein Sci.* **30**, 1326–1336 (2021).
50. W. P. Lipiński, B. S. Visser, I. Robu, M. A. A. Fakhree, S. Lindhoud, M. M. A. E. Claessens, E. Spruijt, Biomolecular condensates can both accelerate and suppress aggregation of α-synuclein. *Sci. Adv.* **8**, eabq6495 (2022).
51. R. Crespo, F. A. Rocha, A. M. Damas, P. M. Martins, A generic crystallization-like model that describes the kinetics of amyloid fibril formation. *J. Biol. Chem.* **287**, 30585–30594 (2012).
52. S. Abounit, L. Bousset, F. Loria, S. Zhu, F. de Chaumont, L. Pieri, J.-C. Olivo-Marin, R. Melki, C. Zurzolo, Tunneling nanotubes spread fibrillar α-synuclein by intercellular trafficking of lysosomes. *EMBO J.* **35**, 2120–2138 (2016).
53. H. Scheiblich, C. Dansokho, D. Mercan, S. V. Schmidt, L. Bousset, L. Wischhof, F. Eikens, A. Odainic, J. Spitzer, A. Griep, S. Schwartz, D. Bano, E. Latz, R. Melki, M. T. Heneka, Microglia jointly degrade fibrillar α-synuclein cargo by distribution through tunneling nanotubes. *Cell* **184**, 5089–5106.e21 (2021).
54. J. Zhang, X. Li, J.-D. Li, The roles of post-translational modifications on α-synuclein in the pathogenesis of Parkinson's diseases. *Front. Neurosci.* **13**, 381 (2019).
55. J. P. Anderson, D. E. Walker, J. M. Goldstein, R. de Laat, K. Banducci, R. J. Caccavello, R. Barbour, J. Huang, K. Kling, M. Lee, L. Diep, P. S. Keim, X. Shen, T. Chataway, M. G. Schlossmacher, P. Seubert, D. Schenk, S. Sinha, W. P. Gai, T. J. Chilcote, Phosphorylation of Ser-129 is the dominant pathological modification of alpha-synuclein in familial and sporadic Lewy body disease. *J. Biol. Chem.* **281**, 29739–29752 (2006).
56. F. Oosawa, S. Asakura, Thermodynamics of the polymerization of protein, B. Horecker, N.O. Kaplan, J. Matmur, H.A. Scheraga, (Eds.), pp.41–55 (Academic Press, London, 1975).
57. P. Ciryam, G. G. Tartaglia, R. I. Morimoto, C. Dobson, M. Vendruscolo, Widespread aggregation and neurodegenerative diseases are associated with supersaturated proteins. *Cell Rep.* **5**, 781–790 (2013).
58. X. Wu, H. Qiu, M. Zhang, Interactions between membraneless condensates and membranous organelles at the presynapse: A phase separation view of synaptic vesicle cycle. *J. Mol. Biol.* **435**, 167629 (2023).

Acknowledgments: We thank A. Cochard for helping along the project, A. Triller for fruitful discussion, and C. Amari for helping in the implementation of quantification processes. **Funding:** This work was supported by FRM (MND202003011470) to Z.G. and FRM (ALZ201912009776) and France Parkinson Association to R.M. L.P. was supported by a Sorbonne University PhD fellowship. **Author contributions:** L.P., R.M., and Z.G. conceived the project. L.P. conducted the majority of the experiments. A.F. and R.M. produced α-Syn fibrils and performed biochemical experiments characterizing amyloid-like assemblies. S.T. and M.-A.P. contributed to performed biochemical characterizations. V.R. provided reagents. All authors analyzed the data. L.P., R.M., and Z.G. wrote the manuscript. All authors discussed the results and commented on the manuscript. **Competing interests:** The authors declare that they have no competing interests. **Data and materials availability:** All data needed to evaluate the conclusions in the paper are present in the paper and/or the Supplementary Materials. The plasmids used in this study can be provided by Z.G. pending proper completed material transfer agreement.

Submitted 6 January 2023
Accepted 13 July 2023
Published 16 August 2023
10.1126/sciadv.adg5663

ScienceAdvances

#-Synuclein liquid condensates fuel fibrillar #-synuclein growth

Leonard Piroska, Alexis Fenyi, Scott Thomas, Marie-Aude Plamont, Virginie Redeker, Ronald Melki, and Zoher Gueroui

Sci. Adv. **9** (33), eadg5663. DOI: 10.1126/sciadv.adg5663

Science Advances
AAAS

Supplementary Materials for

α-Synuclein liquid condensates fuel fibrillar α-synuclein growth

Leonard Piroska *et al.*

Corresponding author: Ronald Melki, ronald.melki@cnrs.fr; Zoher Gueroui, zoher.gueroui@ens.fr

Sci. Adv. **9**, eadg5663 (2023)
DOI: 10.1126/sciadv.adg5663

The PDF file includes:

Other Supplementary Material for this manuscript includes the following:

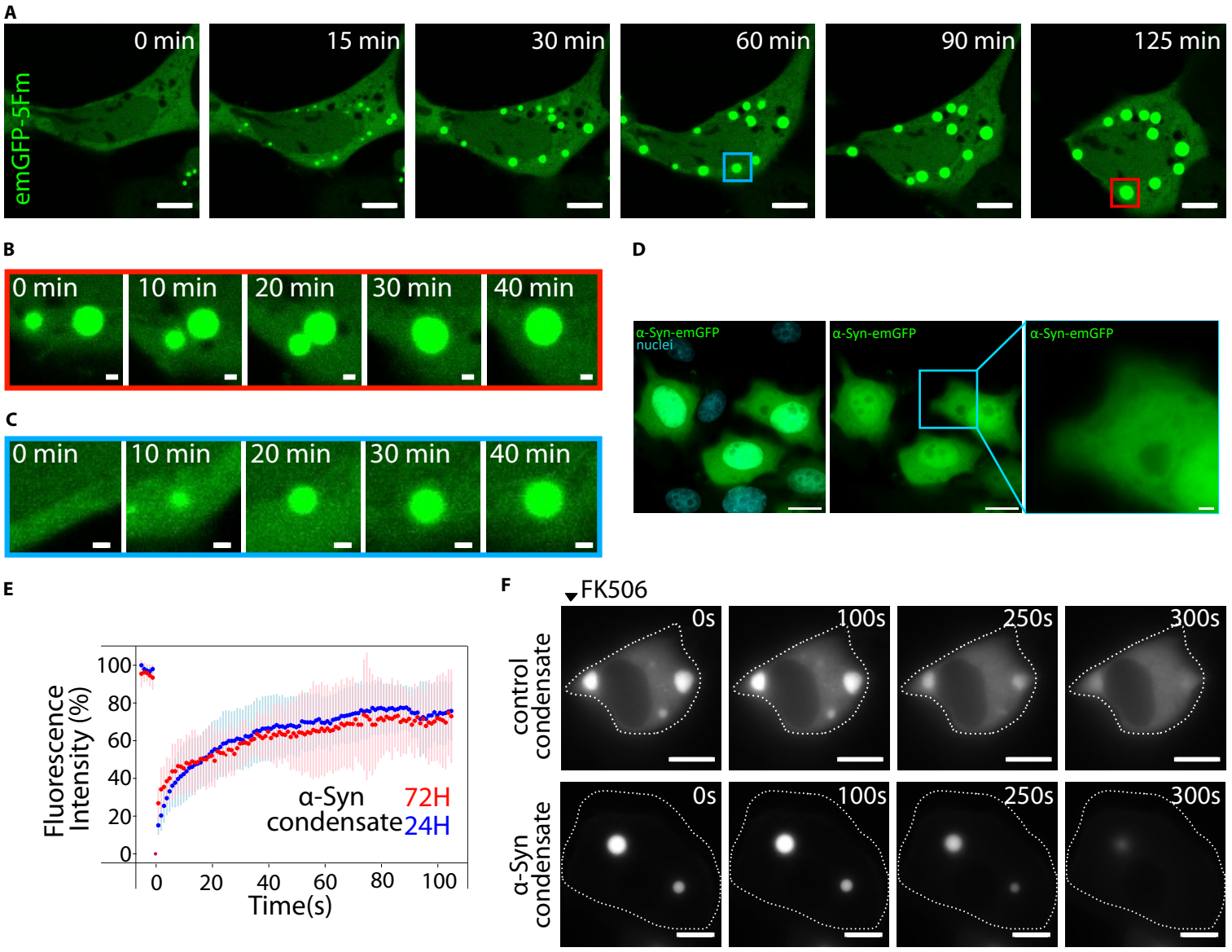

Fig. S1. Artificial α-Syn and control condensates with liquid-like properties

(**A**) Time-lapse confocal imaging of the formation of control condensates in HeLa cells starting from 10h after transfection. Bar, 10µm. (**B**) and (**C**) Enlarged regions extract from the timelapse (**A**) displaying growth of condensates mediated by coalescence (**B**) or subunit addition (**C**). Bars, 2µm. (**D**) Epi-fluorescence microscopy images of HeLa cells expessing the α-Syn-emGFP fusion. Bar, 10µm for whole cell images and 2µm for zoom-ins. (**E**) FRAP curves displaying the fluorescence recovery of α-Syn-enriched condensates 24H (blue, 10 cells) and 72H (red, 15 cells) after cell transfection with the α-Syn_emGFP_5Fm scaffold. Dotted line in bold represents the mean and the error bar represents the standard deviation. Aquisitions were made every second. Pre-bleaching fluorescence intensity was set at 100 and the post-bleach fluorescence was normalized at 0 for all experiments. (**F**) Time-lapse imaging of the dissolution of 72H-old control (Upper row) and α-Syn (Lower row) condensates upon the addition of FK506. Bar, 10µm.

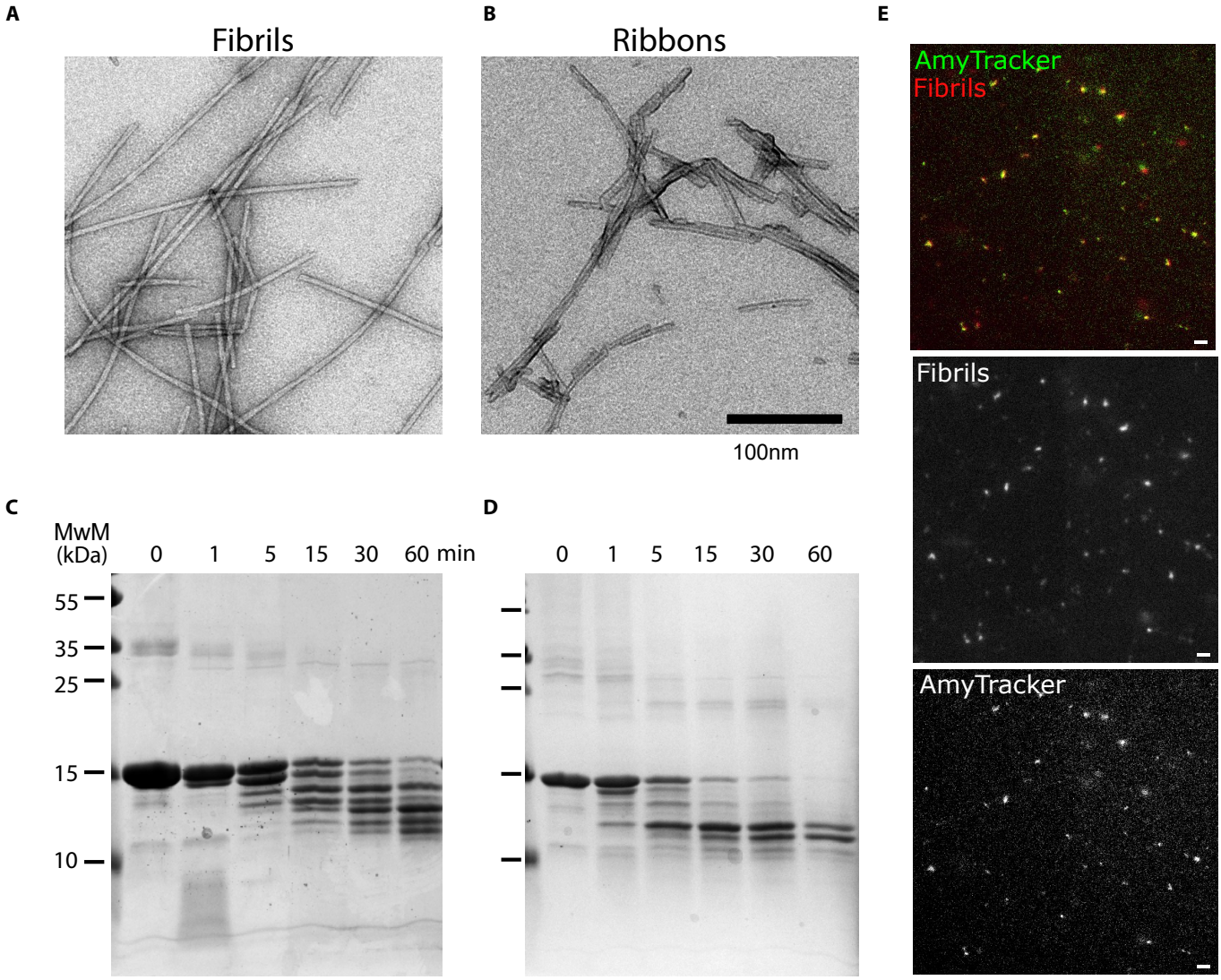

Fig. S2 Characterization of the α-syn fibrillar polymorphs.
Fibrils and Ribbons used throughout this study. Transmission electron micrographs of the polymorphs Fibrils and Ribbons after negative staining with uranyl acetate (panels **A** and **B**). Time course of proteolysis of the polymorphs Fibrils and Ribbons by proteinase K (3.8 µg/mL) after PAGE and staining with Coomassie blue (panels **C** and **D**). Bar, 100nm. The time is in min and the molecular weight markers, in kDa, are indicated on the top and left of each polyacrylamide gel. (**E**) Observation of preformed fibrils (0.5nM) stained with AmyTracker. Bar, 2µm.

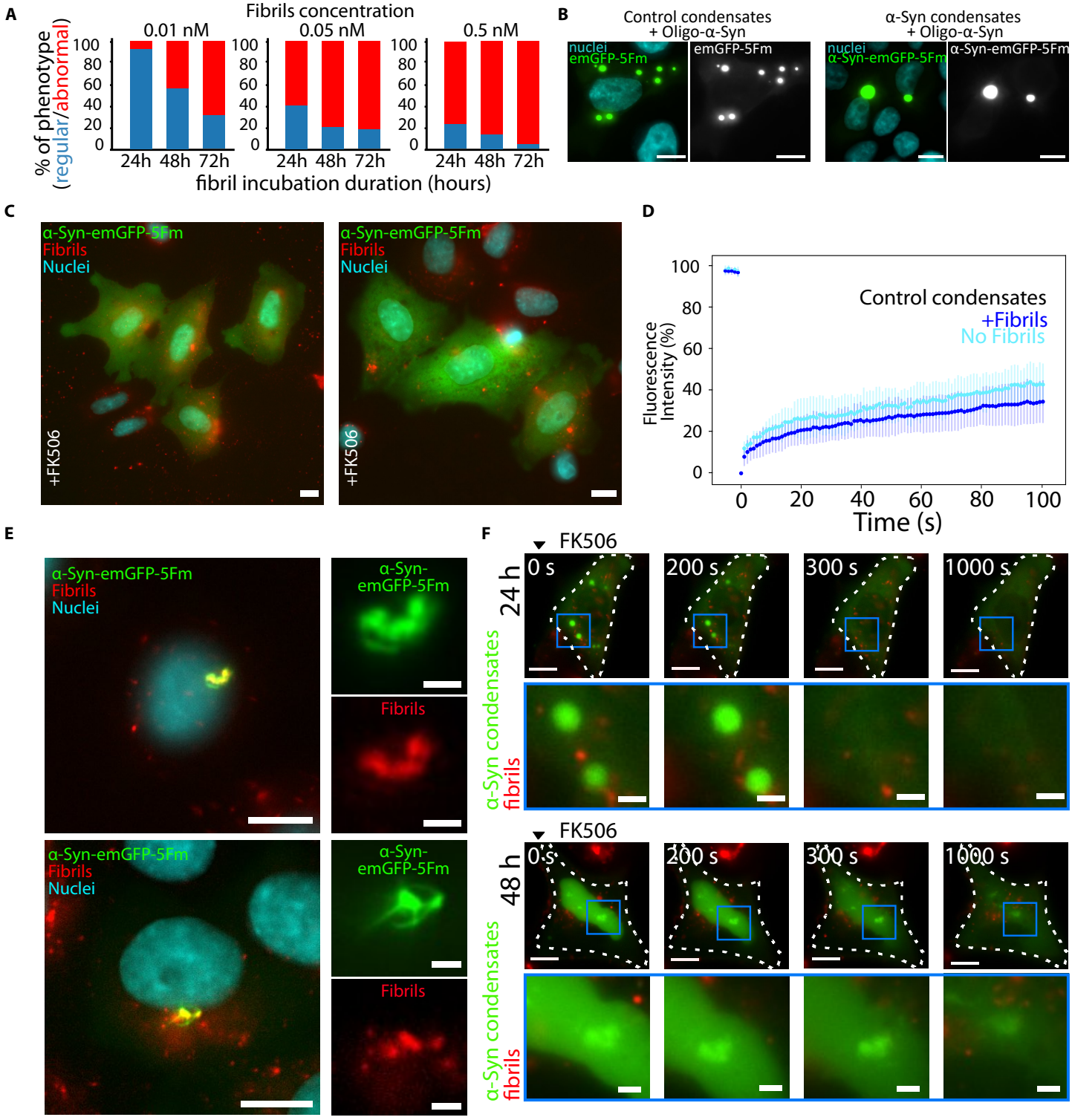

Fig. S3. Abnormally-shaped condensates occur only from α-Syn condensates exposed to fibrils
(**A**)Quantification of the percentage of cells with condensates expressing the two different phenotypes: "Regular"– blue; "Abnormal" – red. as a function of time and concentration of preformed fibrils. HeLa cells expressing α-Syn-emGFP-5Fm (for 24 hours, 48 hours and 72 hours) were exposed to increasing concentration of preformed fibrils (0.01 nM, 0.1 nM and 0.5 nM). The graph is the sum of N=2 experiments. (**B**) HeLa cells expressing control (left) and α-Syn (right) condensates and exposed for 72 hours to preformed α-Syn oligomers (0.5 nM). (**C**) HeLa cells expressing α-Syn-emGFP-5Fm scaffold (green) and exposed to preformed α-Syn fibrils (red) for 72 hours in presence of FK506. Nuclei (cyan) were stained with Hoechst. Bars, 10 µm (**D**) FRAP analysis of control condensates from cells exposed (dark blue, 8 cells) or not (light blue, 15 cells) to fibrils. Pre-bleaching fluorescence intensity was set at 100 and the post-bleach fluorescence was normalized at 0 for all experiments. An acquisition was made every second. Error bars correspond to the standard deviation. (**E**) HeLa cells expressing α-Syn condensates (green) and exposed to preformed α-Syn fibrils (red) for 72 hours after incubation with FK506 for 1 hour. Nuclei (cyan) were stained with Hoechst. Bars, 10 µm for full-cell images and 2 µm for zoom-ins. (**F**) Live confocal microscopy frames depicting the FK506-driven dissolution patterns of 24 hours-old (upper pannel) and 48 hours-old (lower pannel) α-syn condensates (green) from HeLa cells exposed to fibrils (red). Different timepoints are shown, with 0 s being pinpointed at the moment when FK506 was added. Bars, 10 µm for whole cell frames and 2 µm for zoom-ins.

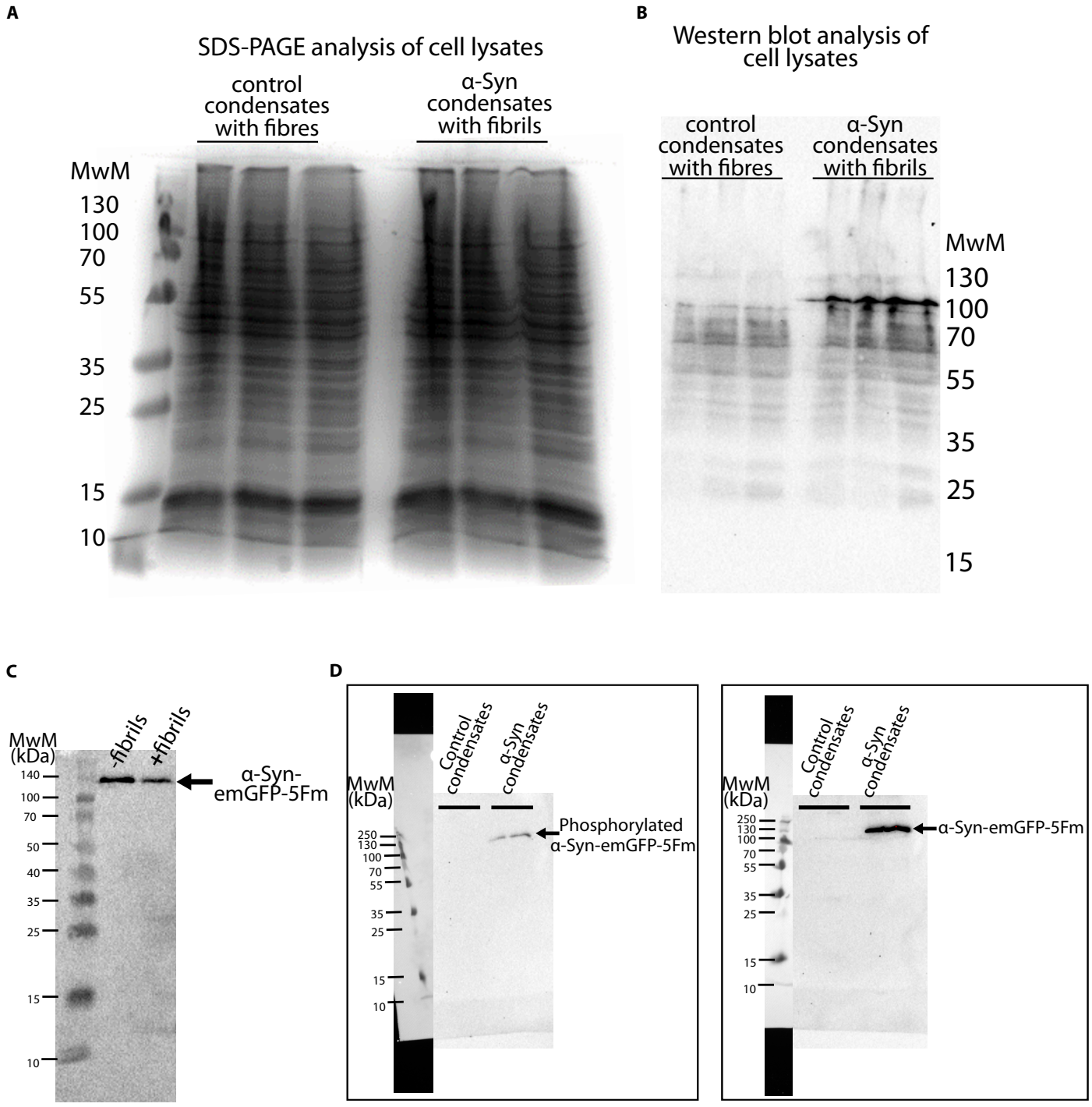

Fig. S4. Biochemical analysis of condensates with and without fibrils

(**A**) SDS-PAGE analysis of lysates used for western blot and filter trap assay. First three lanes to the left: cells expressing control condensates. Next three lanes: cells expressing α-Syn condensates. (**B**) Western Blot performed with an anti α-Syn-PS129 antibody (EP1536Y) on lysates from cells expressing control condensates (first three lanes to the left) and α-Syn condensates (fourth to sixth lanes). (**C**) Western blot performed with a anti-α-Syn primary antibody (BD Biosciences 610787) illustating the α-Syn-emGFP-5Fm construct from lysates of cells exposed or not to fibrils. (**D**) Western Blots performed with anti α-Syn (BD Biosciences 610787, MABN633 Sigma, MABN389 Sigma, # MA1-90346 Invitrogen) and an anti α-Syn-PS129 (EP1536Y) antibody on lysates from cells expressing control condensates and α-Syn condensates in presence of fibrils.

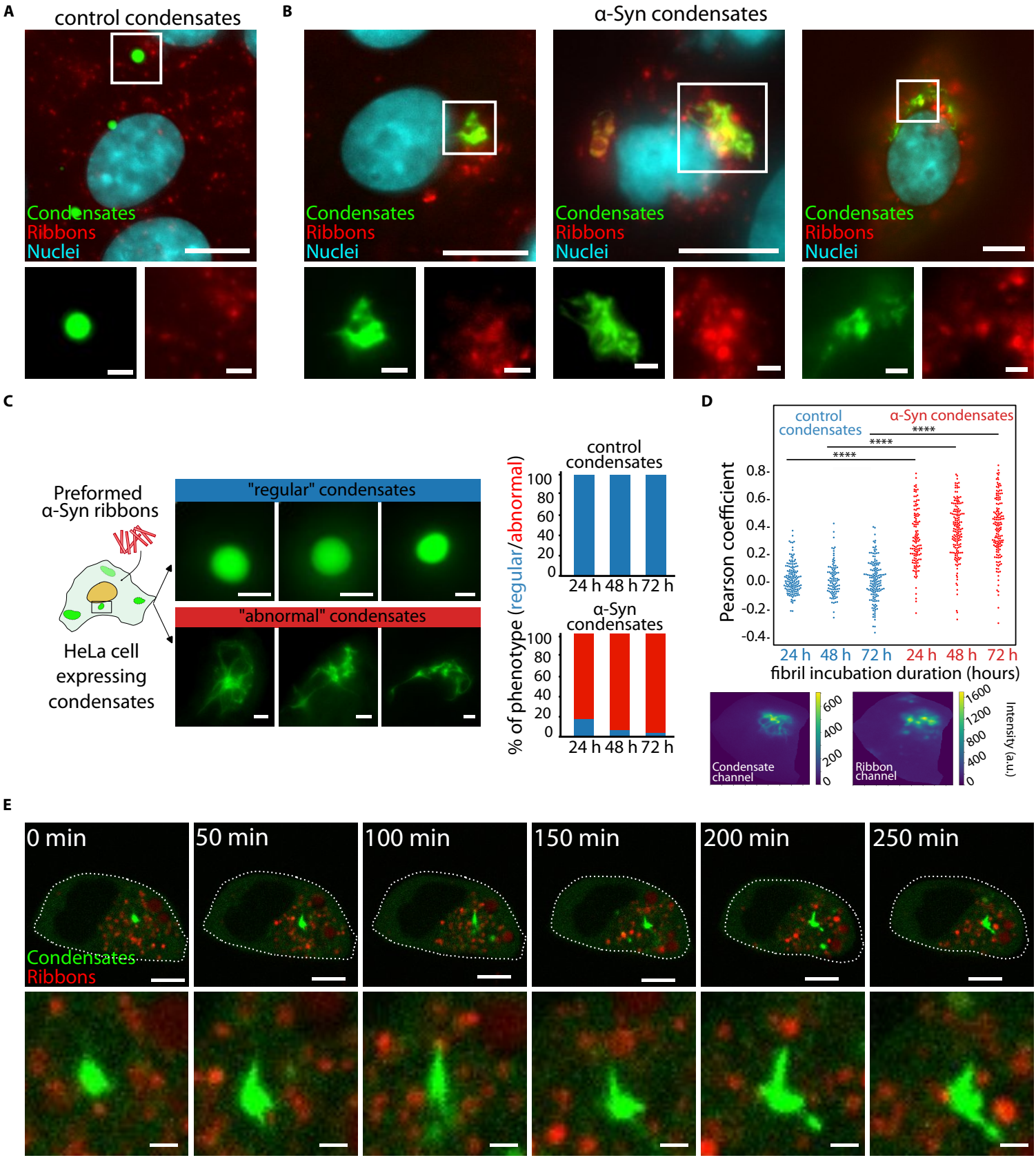

Fig. S5. α-Syn condensates are perturbed by preformed ribbons

Representative epifluorescence images of HeLa cells exposed to preformed α-Syn ribbons (red) and expressing control (**A**) and α-Syn (**B**) condensates (green). Nuclei (cyan) were stained with Hoechst. Bars, 10 μm for full-cell images and 2 μm for zoom-ins. (**C**) Quantification of the percentage of cells with condensates expressing the two different phenotypes: "regular"– blue; "abnormal" – red. The graph is the sum of N=3 experiments. (**D**) Quantification of the Pearson coefficient calculated for the correlation between the fluorescence intensities of the ribbon and condensate channels in microscopy images that were cropped to match the shape of the cell. Each point represents a cell. The graph is the sum of N=3 experiments. Differences between conditions with control and α-Syn condensates were statistically significant (p-values < 10-7 using a Student's t-test). a.u. stands for arbitrary unit. (**E**) Live confocal microscopy frames depicting HeLa cells expressing α-Syn condensates (green) changing morphology upon exposure to ribbons (red). Bars, 10 μm for full-cell images and 2 μm for zoom-ins.

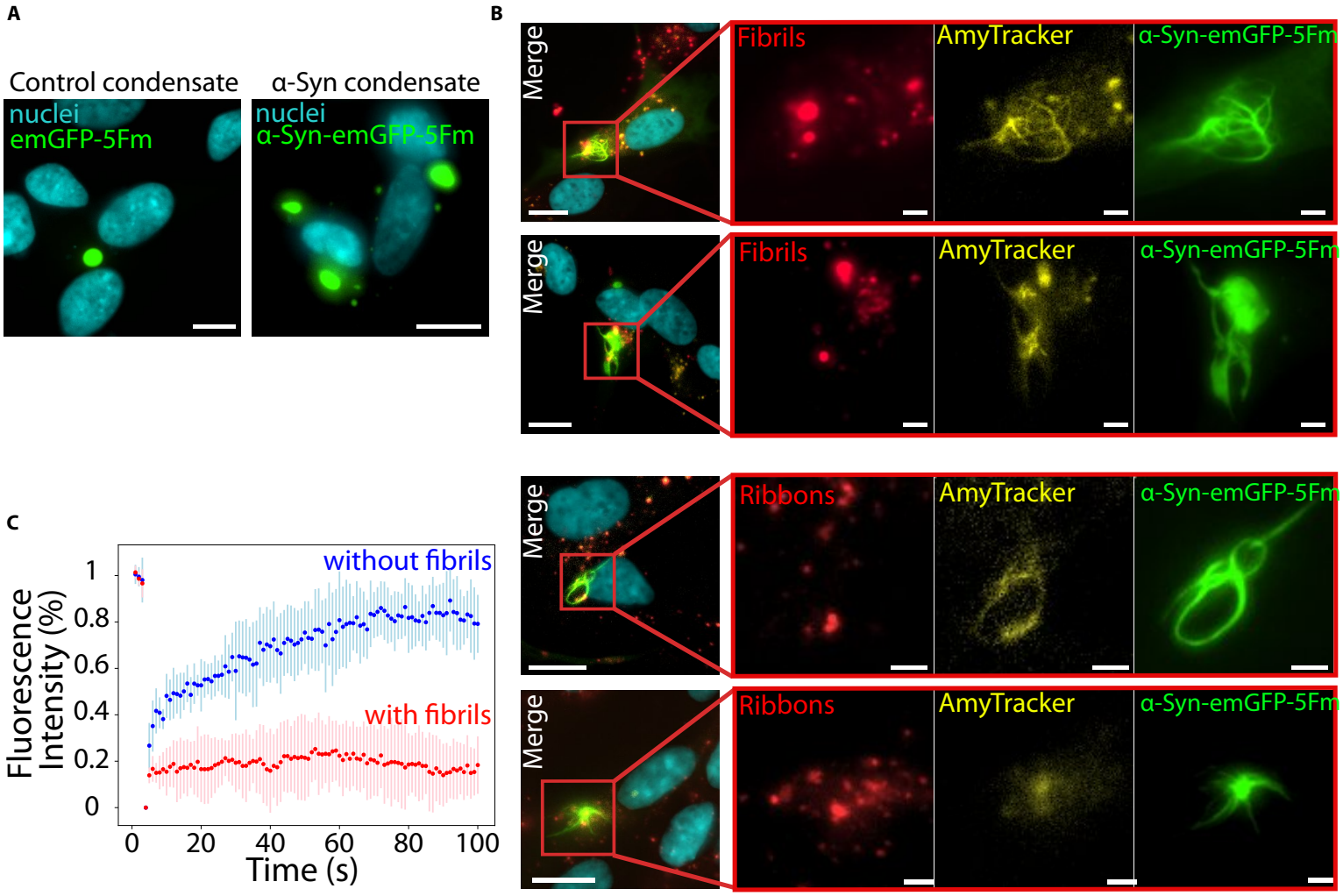

Fig. S6. Preformed α-Syn fibrils triggered the evolution of liquid α-Syn condensates into solid-needle like structures in SH-SY5Y neuronal cells.

Representative epifluorescence images of SHSY-5Y cells infected with preformed α-Syn fibrils (red) and expressing control **(A)** and α-Syn **(B)** condensates (green). Nuclei (cyan) were stained with Hoechst. AmyTracker staining on SHSY-5Y cells expressing α-Syn condensates after 72 hours incubation with fibres. Bars, 10 µm for full-cell images and 2 µm for zoom-ins. **(C)** FRAP analysis of abnormally-shaped condensates. The graph comprises the average of 10 different experiments for the condition with fibrils and 7 different experiments for the condition without fibirls . Pre-bleaching fluorescence intensity was set at 100% and the post-bleach fluorescence was normalized at 0 for all experiments. An acquisition was made every second. Error bars correspond to the standard deviation.

Construct	Oligo Name	Sequence
pcDNA3.1 α-Syn-emGFP-5Fm	LP029 HindIII_KozaK+ATG_α-SynWT	actgacaAGCTTgccaccATGGATGTATTCATGAAAGGACTTTCAAAGG
pcDNA3.1 α-Syn-emGFP-5Fm	LP030 3' SacII_α-Syn	TCAGTCCGCGGGGCTTCAGGTTCGTAGTCTTGATACC
pcDNA3.1 α-Syn(S129A)-emGFP-5Fm	ACC031 Kan Fw	CGAGCGAGCACGTACTCGGA
pcDNA3.1 α-Syn(S129A)-emGFP-5Fm	ACC032 Kan Rv	TCCGAGTACGTGCTCGCTCG
pcDNA3.1 α-Syn(S129A)-emGFP-5Fm	LP036 α-Syn for	TATGAAATGCCTGCTGAGGAAGGGTATCA
pcDNA3.1 α-Syn(S129A)-emGFP-5Fm	LP037 α-Syn Rev	TGATACCCTTCCTCAGCAGGCATTTCATA

Supplementary table 1.
List of DNA primers used for the cloning of the pcDNA3.1 α-Syn-emGFP-5Fm and pcDNA3.1 α-Syn(S129A)-emGFP-5Fm

Supplementary movies

Movie S1: Time-lapse confocal microscopy of the formation of α-Syn condensates. Acquisitions were taken every 5 minutes.

Movie S2: Time-lapse confocal microscopy of the formation of control condensates. Acquisitions were taken every 5 minutes.

Movie S3: Time-lapse epifluorescence microscopy of the dissolution of 24H-old α-Syn condensates. FK506 was added 30 seconds in. Acquisitions were taken every 10 seconds.

Movie S4: Time-lapse epifluorescence microscopy of the dissolution of 72H-old α-Syn condensates. FK506 was added 30 seconds in. Acquisitions were taken every 10 seconds.

Movie S5: Time-lapse confocal microscopy of the evolution of α-Syn condensates (green) from "regular" to "abnormal" phenotype in presence of fibres (red). Acquisitions were started 48 hours after cell exposure to fibrils and images were taken every 5 minutes.

Movie S6: Time-lapse epifluorescence microscopy of the dissolution of 72H-old α-Syn condensates (green) with fibres (red). FK506 was added 30 seconds in. Acquisitions were taken every 10 seconds.

Movie S7: Time-lapse confocal microscopy of the growth of α-Syn condensates (green) in presence of fibres (red). Acquisitions were taken every 5 minutes.

Movie S8: Time-lapse confocal microscopy of the evolution of α-Syn condensates (green) from "regular" to "abnormal" phenotype in presence of ribbons (red). Acquisitions were started 48 hours after cell exposure to ribbons and images were taken every 5 minutes

CHAPTER III: α-SYN AND SYNAPSIN I MIXED CONDENSATES. LIQUID-TO-FIBRILLAR SOLID TRANSITION MEDIATED BY PREFORMED α-SYN FIBRILS

III.1 Introduction

III.1.1 Towards the creation of condensates with more relevant compositions

The previous chapter explored how the cellular condensed liquid phase of α-Syn can be converted into amyloid-containing fibres upon interaction with preformed fibrils. A hypothesis that can be derived from this data is that, in conditions of pathological aggregate spreading, neuronal liquid condensates containing α-Syn could be vulnerable spots with respect to the prion-like propagation of the fibrillar amyloid state. Thus, a study of α-Syn in the context of condensates that are closer to those found in its natural neuronal environment is of great utility. A region of particular interest when looking for examples of potential "natural" α-Syn condensates is the presynaptic termini of neurons, where the protein is the most abundant (*139*). For this reason, the current chapter will focus on presynaptic proteins, namely α-Syn and synapsin I. First, I will provide a brief description of biomolecular condensates from the presynaptic space, then I will develop in more detail one such condensate that is closely related to α-Syn. Most importantly, I will describe how our controlled PS system provided more insight about this condensate, notably in a context related to their interactions with preformed fibrils.

III.1.2 The presynaptic environment and its biomolecular condensates

The presynaptic terminal, also known as presynaptic bouton, is a specialized structure located at the end of a neuron's axon. It plays a role in transmitting signals between two neurons (presynaptic and postsynaptic) via the release of neurotransmitters into the small gap between them, called the synaptic cleft. Neurotransmitters are stored in small membrane-enclosed compartments called synaptic vesicles (SVs), which are distributed in the presynaptic terminal in discrete pools, each bearing distinct functional significance in modulating the efficacy of synaptic signalling (*182*). First, there is the readily releasable pool, which consists of a group of SVs that sit close to the membrane, in a region called the active zone. They can quickly fuse to the membrane in response to single action potentials, releasing the neurotransmitter into the synapse. Second, there is the reserve pool, which is an SV cluster that sits further back in the synaptic terminal. This pool is unresponsive to single action potentials, but can act as a reservoir that supplies SVs to the active zone during periods of high-frequency neural activity, ensuring sustained neurotransmitter release (*182*). Third, there is the recyclable pool, which contains the

SVs that have been endocytosed and refilled with neurotransmitters. These SVs can shuttle either to the reserve pool, or to the readily-releasable pool for additional rounds of neurotransmitter release in case of moderate-frequency stimuli (*182*).

Recent studies report that PS could play a role in the assembly and functioning of these SV pools (**Figure III.1**). For example, two major scaffold proteins of the active zone: IDPs Rab3 Interacting Molecule (RIM) and RIM-binding protein (RIM-BP), were shown to undergo PS *in vitro*, suggesting that the readily releasable pool could be part of a biomolecular condensate structure (*183*). Moreover, studies in *C. elegans* later reported that the assembly of the active zone *in vivo* is dependent on the phase separation of two proteins: SYD-2/Liprin-α and ELKS. However, no interplay between the two protein pairs in the context of PS was discovered to date. Alternately, the protein EndoA1, which is a factor that plays a role in the recycling of depleted SVs through endocytosis, was also shown to undergo PS in hippocampal neurons (*184*). Therein, it colocalizes with SV clusters, hinting at the existence of an endocytic condensate (*184*).

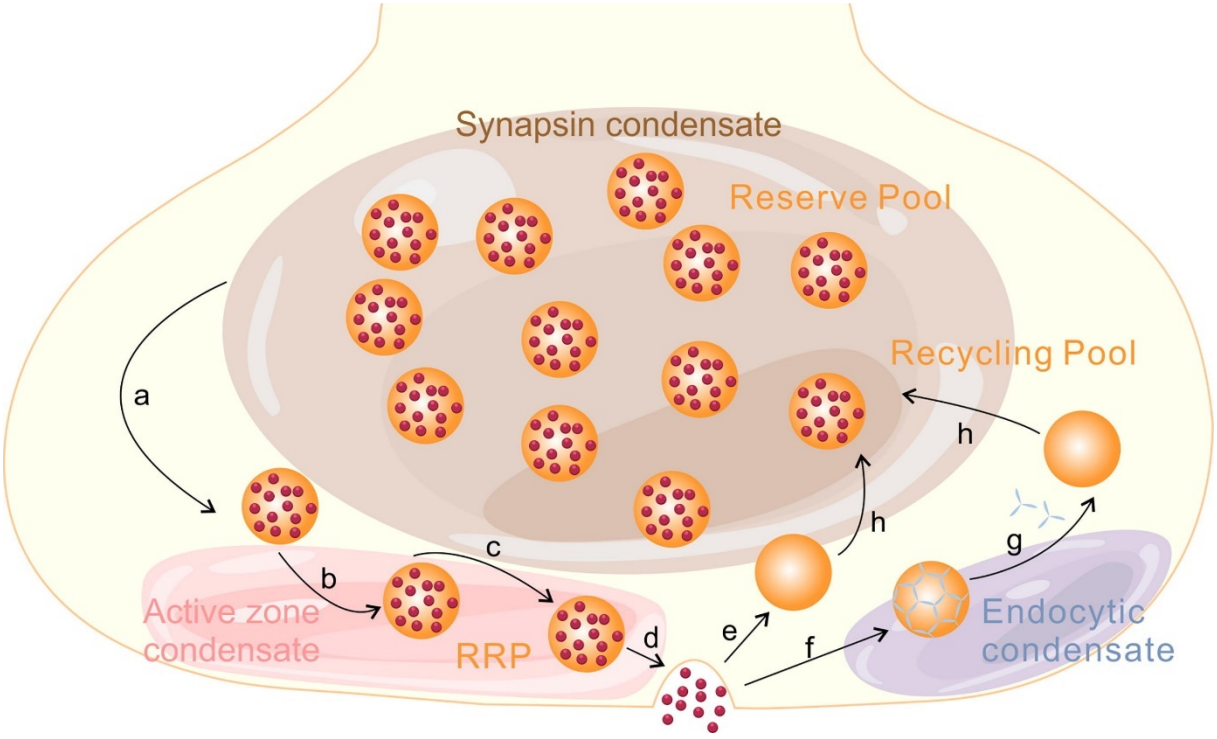

Figure III.1 Biomolecular condensates at the presynaptic terminal. *The active zone condensate is proposed to be scaffolded by RIM/RIM-BP. The endocytosis of used SVs is also hypothesized to happen within a condensate. Within the reserve pool, a synapsin I condensate was proposed to ensure the clustering of SVs. Adapted from* (*185*).

The reserve pool is also a condensate, mainly associated with the PS of the protein synapsin I (*176*). This protein, encoded by the *SYN1* gene in humans, plays a critical role in controlling the SV storage in/release from the reserve pool as a function of neural activity patterns (*186*). A mechanism for this process was already proposed before its connection to PS. In periods of rest, synapsin I clusters SVs together by selectively binding to them through its C-terminal domain, and tethering them to a complex matrix, which containing multiple proteins (*187*) and, potentially, cytoskeleton elements such as actin filaments and microtubules (*188*, *189*). Upon sustained stimulation, however, the Ca^{2+} influx activates the calcium/calmodulin-dependent protein kinase II (CaMKII), which phosphorylates synapsin I. This, in turn, impairs binding of synapsin I to SV, thereby triggering their release (*190*).

The first time PS was proposed to be involved in this process was in 2018, when Milovanovic et al. reported how synapsin I could form a distinct liquid phase in an *in vitro* aqueous environment (**Figure III.2**) (*176*). In this study, they report that the synapsin I condensate concentrates small lipid vesicles, which they use as mimics of SVs, and these vesicles display high degrees of mobility within the condensed phase. Moreover, CaMKII also partitions into the condensate, and addition of ATP, which is a necessary substrate for the kinase activity of CaMKII, triggers the dissolution of the synapsin I/CaMKII condensate (*176*). The reconstitution of SV clusters with a minimal synapsin I/vesicle/CaMKII condensate system has reshaped the conventional perspective on SV clusters, now considering PS as a potential organizational principle.

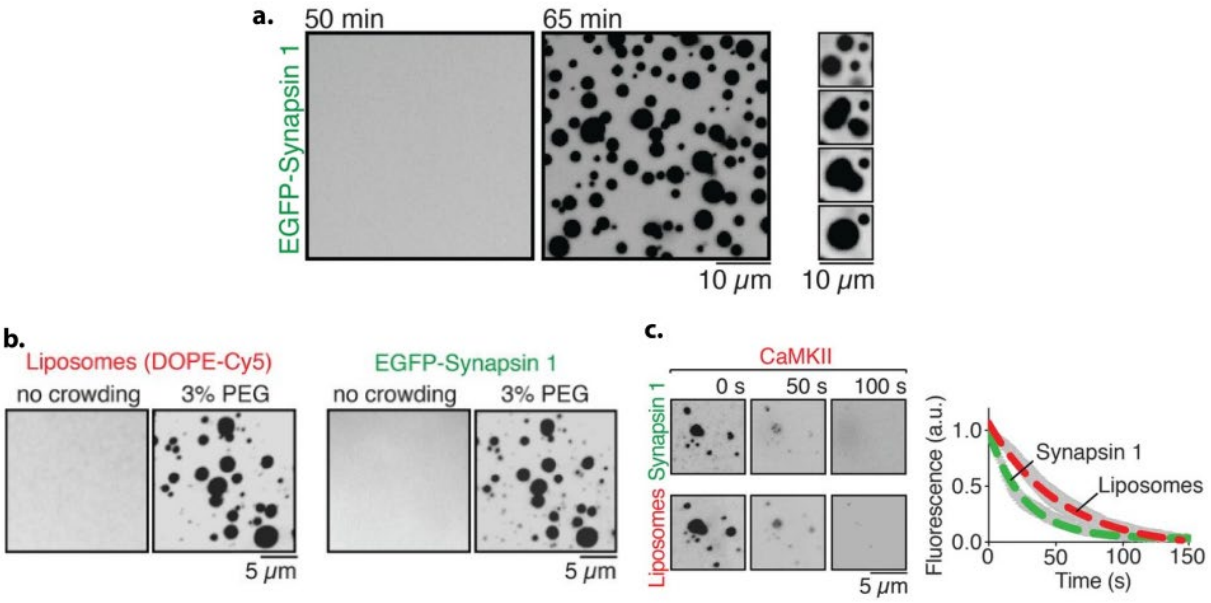

Figure III.2 In vitro reconstituted synapsin condensates. a. *Left panel: Fluorescence microscopy images of EGFP-tagged Synapsin I incubated at 10μM. After 1 hour, condensates appear. Right panel: Synapsin I droplets fuse and relax into spherical shapes, indicating a liquid-like behaviour.* ***b.*** *EGFP-synapsin I incubated with DOPE-Cy5-tagged lipid vesicles in the presence of 3 % PEG-8000. Synapsin I droplets form, that accumulate lipid vesicles.* ***c.*** *Left panel: time-frames of the dissolution of EGFP-synapsin I/lipid vesicle condensates in presence of CaMKII and 200 μM ATP. Right panel: quantification of the decrease in droplet fluorescence upon exposure to CaMKII/ATP. Adapted from (176).*

III.1.3 α-Syn/synapsin I interplay in the context of LLPS

In the context of our study, the synapsin I presynaptic droplets are relevant, because they have been reported to concentrate α-Syn in 2021, when Hoffmann et al. described how the co-expression of mCherry-synapsin I and α-Syn-BFP in HEK293T cells yielded liquid-like droplets where the two protein constructs colocalized (**Figure III.3**) (*110*). Interestingly, they reported that the overexpression of mCherry-synapsin I alone did not result in such intracellular objects, and thus revealed that, at least *in cellula*, synapsin I did not possess the properties of a full PS "scaffold" protein, and that its phase separation was dependent on its interaction with α-Syn. The study additionally examined other factors influencing the formation of synapsin I/α-Syn condensates *in vitro*. It was presented that the presence of native SVs isolated from rats substantially enhanced the phase separation capability of synapsin I alone, as well as of

synapsin I/α-Syn mixes. Indeed, they observed an SV dose-dependent increase in turbidity - which indicates supramolecular assemblies - within synapsin I + α-Syn solutions which were outside the PS concentration regimes.

Interestingly, the presence of α-Syn within synapsin I condensates appears to have a drastic effect. Hoffmann et al.'s study emphasized the critical role of the stoichiometric ratio between the two proteins on phase separation, showing that an excess of α-Syn (α-Syn at 6 μM and synapsin I at 2 μM, corresponding to a ratio of 3:1) substantially reduced synapsin I's ability to form droplets, even in the presence of PS-enhancing SVs (*110*). Conversely, a more moderate amount of α-Syn (equimolar to synapsin I) was reported to allow phase separation (*110*). However, the opposite scenario, meaning absence of α-Syn, did not perturb the PS of synapsin I + rat SVs, suggesting that α-Syn might not be a driver of phase separation for this condensate. This was in agreement with previous studies in triple synuclein knockout hippocampal neurons, where SV clustering, which likely occurs through synapsin I PS, was not impaired (*177*). However, in this system, α-Syn depletion also had diminishing effect on synaptic boutons size and resulted in a tighter packing of SVs within the clusters (*177*). Thus, α-Syn's partition into synapsin I's condensate in the right quantities could potentially enable the maintenance of specific physical properties, which in turn affect synaptic vesicle mobility and facilitate neurotransmitter release. This facet of the interaction between the two proteins remains, however, largely unexplored.

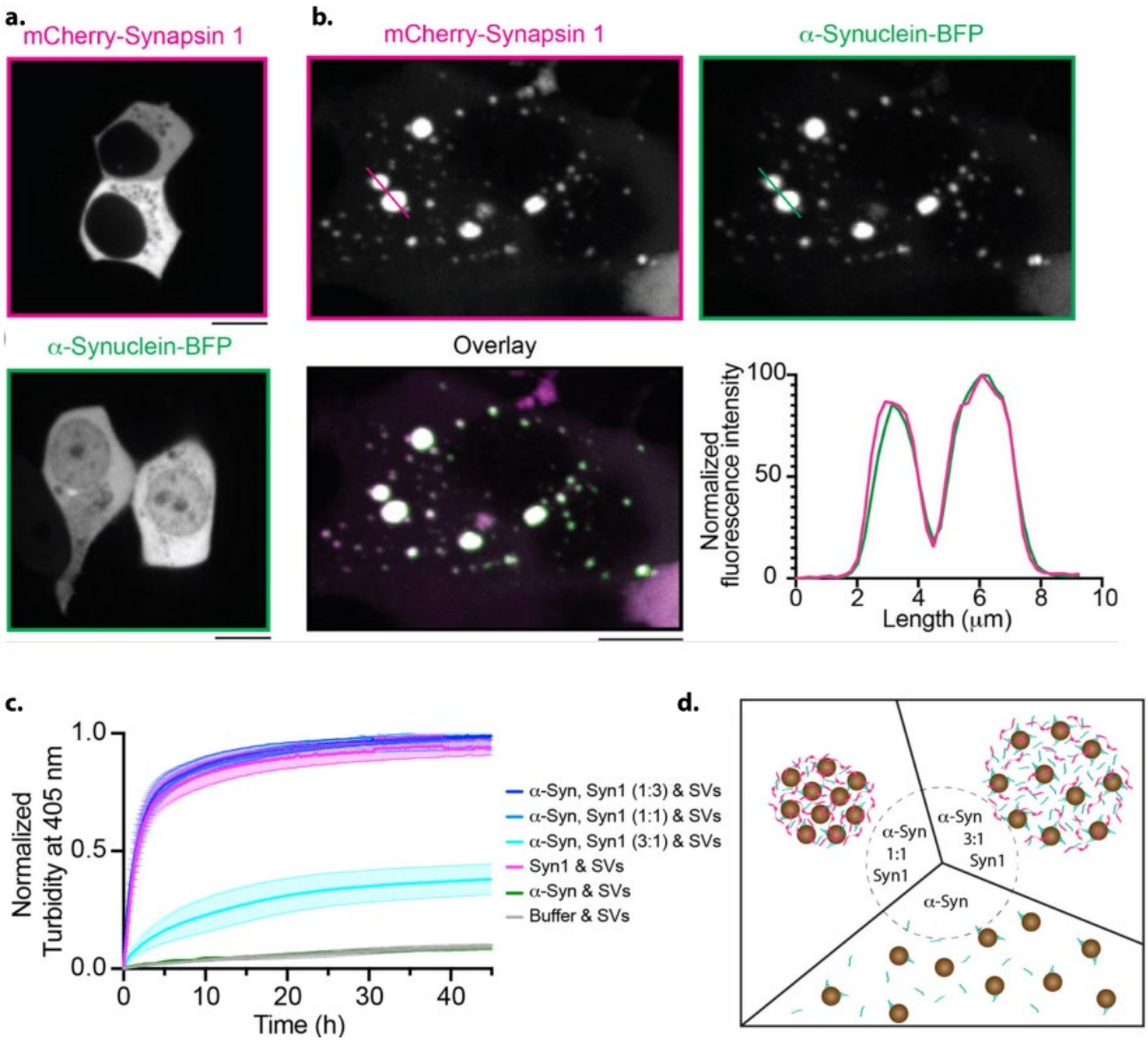

Figure III.3 Mixed α-Syn/synapsin I condensates in cells. *a. HEK293 cells overexpressing α-Syn-BFP or mCherry-synapsin I separately display a diffuse pattern of expression of the two proteins.* ***b.*** *Co-expression of the two proteins yields micrometric puncta enriched in both of them.* ***c.*** *Kinetics of condensate formation (assessed through turbidity measurements) as a function of the added quantity of SVs.* ***d.*** *Schematic of the observations related to the influence of α-Syn/synapsin I stoichiometry on PS. Equimolar quantities of the two proteins allow PS, whereas an excess of α-Syn impairs it. Adapted from* (*110*).

III.1.4 Aims and motivations of the study

In this chapter, we aim to expand our insight surrounding α-Syn and synapsin I in the framework of PS. To this end, we have set several goals: (i) to reconstitute synapsin I condensates and analyse their properties, (ii) to design an α-Syn client molecule, that can partition into synapsin I condensates to create a mixed α-Syn/synapsin I condensates, and (iii) to investigate whether α-Syn/synapsin I mixed condensates can undergo a conversion towards fibrillar aggregates upon exposure to preformed α-Syn fibrils.

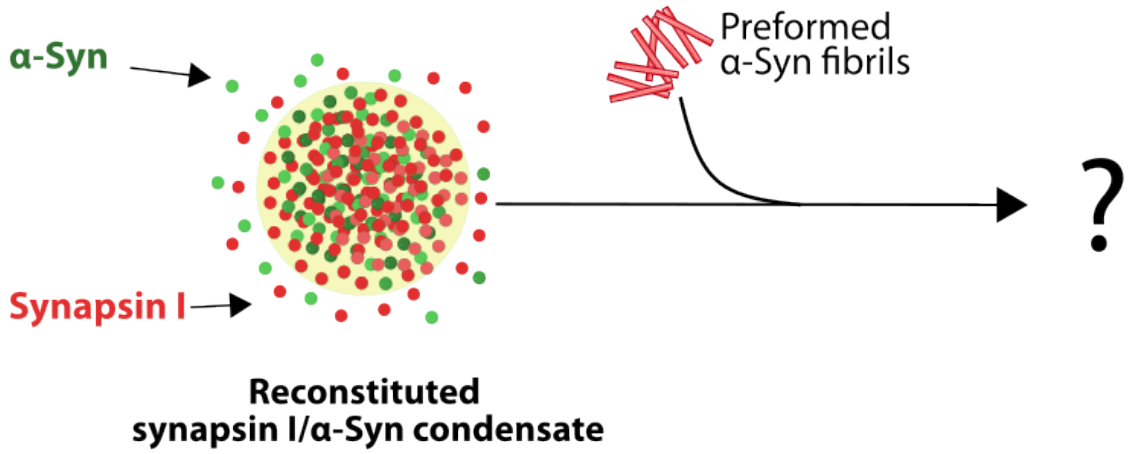

Figure III.4 Schematic representation of the motivations of the study

III.2. Results

The current section presents results from an ongoing study, that is close to being complete. The existing dataset is composed of qualitative and some quantitative data which permit us to draw preliminary conclusions. However, we estimate that a set of additional controls and quantifications would be of great value in consolidating our results and allowing us to draw robust conclusions. A summary of the remaining experiments that have been planned for the completion of this study will be provided at the end of this section, after the presentation of the existing data.

III.2.1. Phase separation of overexpressed synapsin I

To assess the baseline PS propensity of synapsin I in our experimental setting, we overexpressed the mCherry-synapsin I construct in HeLa cells, conserving the N_{ter} placement of the fluorescent reporter that was used in previous studies on synapsin phase separation (*110*). The expression pattern of this construct in our setting was diffuse in the large majority of transfected cells, which is accordance with an earlier finding that synapsin I overexpression alone did not lead to detectable levels of condensation (**Figure III.5.a left column**) (*110*). In rare cases, cells would display small puncta (around 1 µm in diameter) that could correspond to mCherry-synapsin I assemblies, however these were too scarce to support any conclusion (**Figure III.5.a right column**). In co-overexpression with α-Syn-emGFP, mCherry-synapsin I assemblies became more frequent, and larger (**Figure III.5.b**). Interestingly, however, with our current microscopy setup, we could not detect a partitioning of α-Syn-emGFP within these condensates. This aspect raises questions about the interplay of the two proteins *in cellula,* and underscores the need for a system that provides enhanced control over synapsin I's PS and over the partition of α-Syn within its condensates.

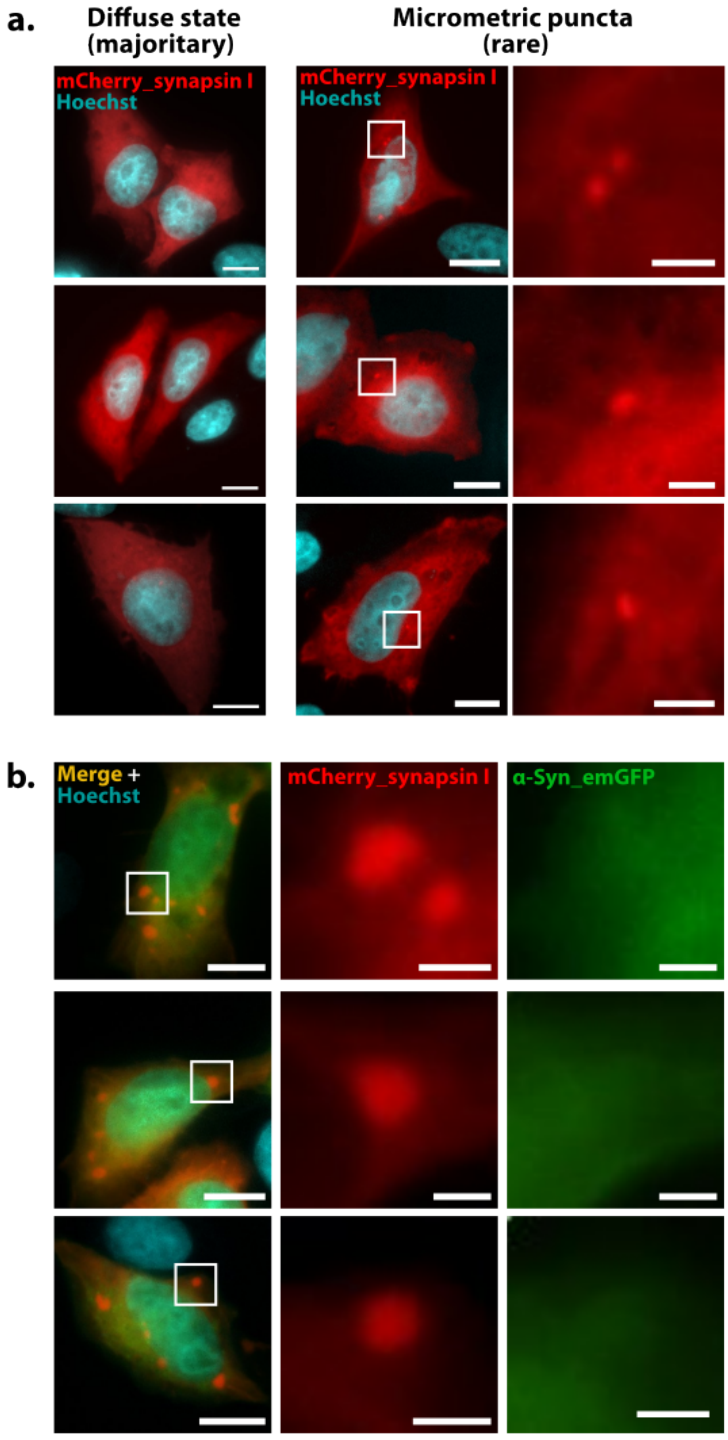

Figure III.5 mCherry-synapsin I PS. a. *Representative epifluorescence images of HeLa cells overexpressing mCherry-synapsin I. Most cells displayed a diffuse fluorescent signal (left column). On rare occasions, cells would display small puncta around 1µm in diameter (right column).* ***b.*** *Co-overexpression of mCherry-synapsin I with α-Syn-emGFP. Micrometric assemblies appear. α-Syn-emGFP conserved a diffuse pattern of expression. Scale bars, 10 µm for whole-cell images and 2 µm for zoom-ins.*

III.2.2 5Fm-mCherry-synapsin I yields two distinct types of assemblies

For the reconstitution of synapsin I condensates, we have genetically fused the protein to mCherry and 5Fm – a protein scaffold that we previously designed for the generation of artificial condensates (*175*, *181*) (**Figure III.6.a**). In HeLa cells, the 5Fm-mCherry-synapsin I construct exhibited two different patterns of expression: spherical bodies and filiform assemblies (**Figure III.6.b**). Spherical bodies were small (1-3 µm in diameter) and dispersed throughout the cytosolic space. They were morphologically reminiscent of condensates made with the control "neutral" scaffold 5Fm-mCherry (**Figure III.6.c**). Filiform patterns presented as thin, elongated structures that spanned over several micrometres. They were either long threads interlaced with each other in a spider web pattern, or curving around the edges of nuclei. To assess the influence of synapsin I into the occurrence of the filiform assemblies, we have co-expressed 5Fm-mCherry-synapsin I with the neutral scaffold 5Fm in different stoichiometries, such that the concentration of synapsin I within the condensates was varied. We found that as the ratio of 5Fm to 5Fm-mCherry-synapsin I increased, cells became less likely to exhibit a "filiform" phenotype. Whereas 58 % of cells with displayed a filiform phenotype when expressing solely the 5Fm-mCherry-synapsin I scaffold, the percentage drops at 38% with equimolar 5Fm and 5Fm-mCherry-synapsin I, and to 22 % when the ratio is at 3:1. For a 10:1 ratio of transfected Fm to 5Fm-mCherry-synapsin I, the filiform phenotype was not at all observed (**Figure III.6.d**). Thus, we hypothesize 5Fm-mCherry-synapsin I's self-assembly could be driven by two different forces: (i) the 5Fm cohesive interactions and (ii) interactions between synapsin I and a fibre-shaped cellular structures, reminiscent of cytoskeletal elements. We propose that when the former interactions are prevalent a 3D spherical morphology is favoured, whereas the latter drives the system towards a 1D filiform phenotype (**Figure III.6.d**).

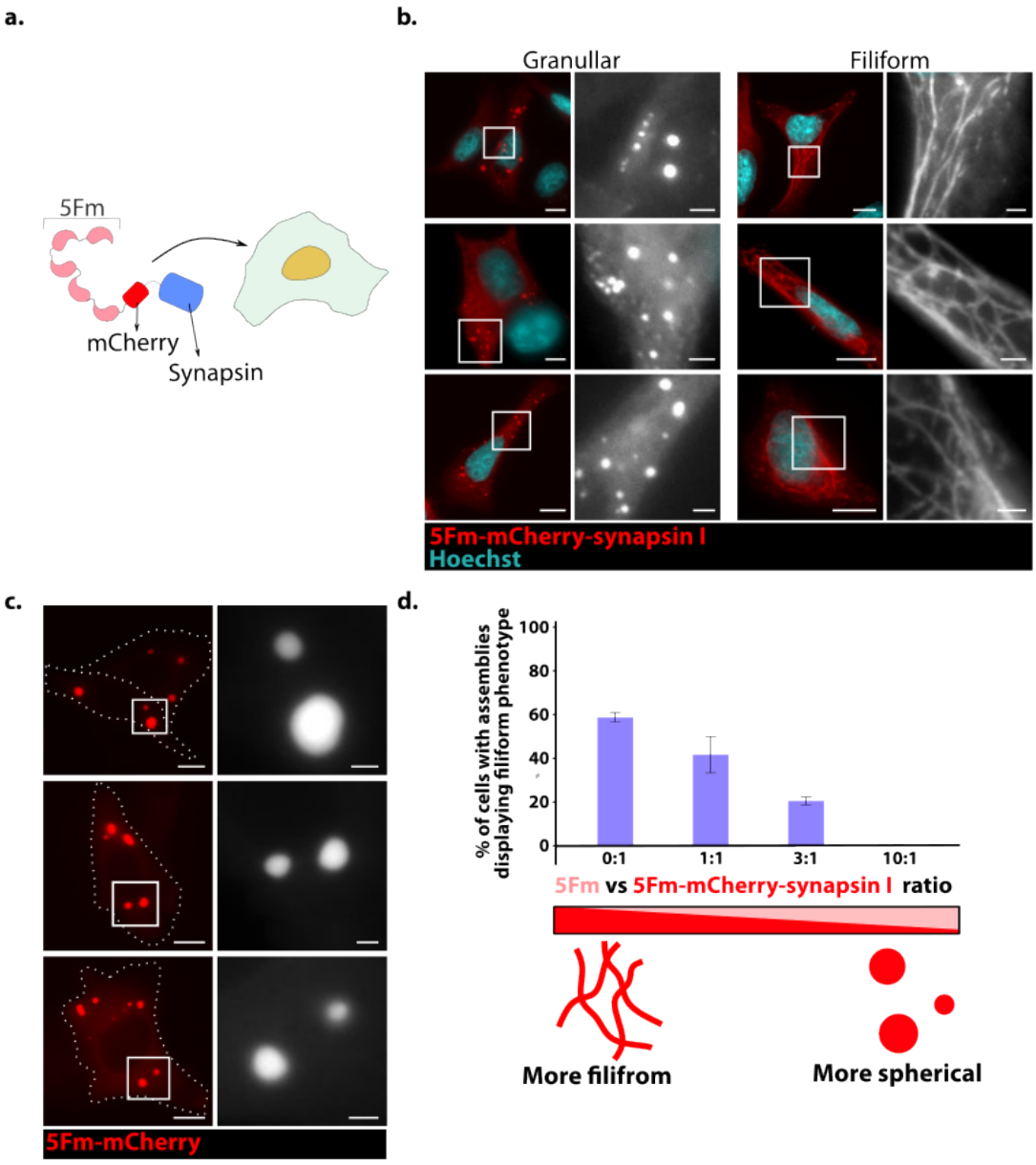

Figure III.6 Reconstitution of synapsin I condensates a. *Schematic representation of the 5Fm-mCherry-synapsin I scaffold.* ***b.*** *Epifluorescence microscopy images depicting HeLa cells expressing 5Fm-mCherry-synapsin I (red in whole-cell images, greys in zoom-ins). Left column: spherical condensates; Right column: filiform condensates. Nuclei are in cyan.* ***c.*** *Epifluorescence microscopy images depicting HeLa cells expressing 5Fm-mCherry (red in whole-cell images, greys in zoom-ins). Dashed lines indicate cell outlines.* ***d.*** *Bar plot showing the percentage of cells with assemblies that display the filiform phenotype, at different ratios of 5Fm to 5Fm-mCherry-synapsin I (in terms of transfected DNA). N=2 experiments. Error bars are standard deviations. For all images: scale bars, 10 µm for whole-cell frames and 2 µm for zoom-ins.*

III.2.3. Reversibility of the synapsin I assemblies

To test our hypothesis, we set to assess the reversibility of the two types of assemblies by using the FK506 assay. This method enables us to analyse the interactions within 5Fm-mCherry-synapsin I assemblies, as it triggers the dispersal of 5Fm-based cohesive forces while preserving other interactions (*175*, *181*). To provide a more faithful comparison between the two, we have chosen to look at the dissolution patterns of granular and filiform patterns within the same cell, which allowed us to rule out differences in the diffusion of FK506 through the cytosol. We noted that spherical bodies completely dissolved within a minute after addition of FK506, whereas the filiform ones underwent a partial dissolution. Whilst the fluorescence intensity of filiform assemblies substantially decreased as an effect of FK506, a small fraction persisted on consequentially longer timescales (more than 10 minutes) (**Figure III.7**). Experiments in fixed cells were consistent with this finding: cells exposed to FK506 1 h before fixation (late timepoint) displayed remainders of filiform assemblies, whereas when FK506 was added at wash 1h30 after transfection (early timepoint), cells rarely expressed small puncta, similarly to the expression of mCherry-synapsin I alone (**Figure III.8**). Two main conclusions can be drawn from these observations. Firstly, both spherical and filiform assemblies feature reversible cohesive forces driven by our 5Fm scaffold, exhibiting component dynamics characteristic of condensates. Secondly, filiform condensates involve an additional type of interaction, which we hypothesize could be between synapsin I and an endogenous cytoskeletal element such as microtubules (MTs) or actin fibres.

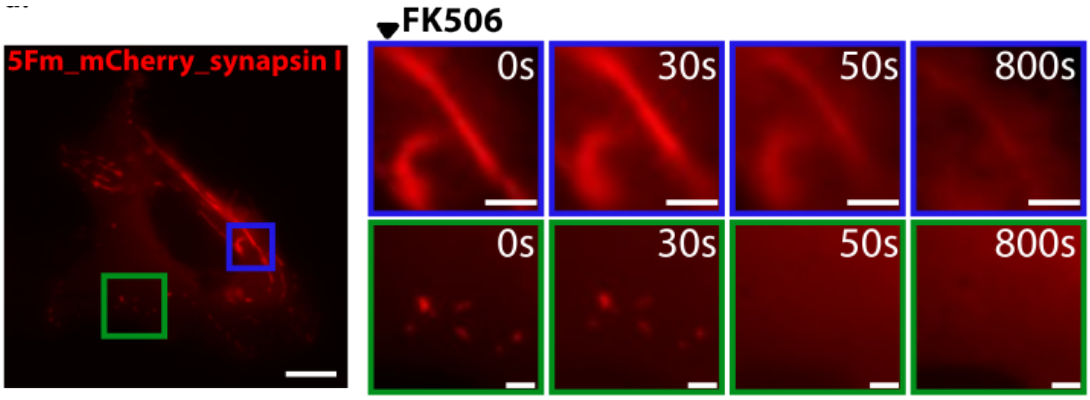

Figure III.7 Live dissolution assay with FK506 on HeLa cells expressing 5Fm-mCherry-synapsin I. *Microscopy frames from a movie following the dissolution of 5Fm-mCherry-synapsin I condensates upon exposure to FK506 (2.5 µM). The 0 s timepoint was set at the moment when FK506 was added. Upper row: zoom-in onto filiform condensates. Lower row: zoom on spherical condensates.*

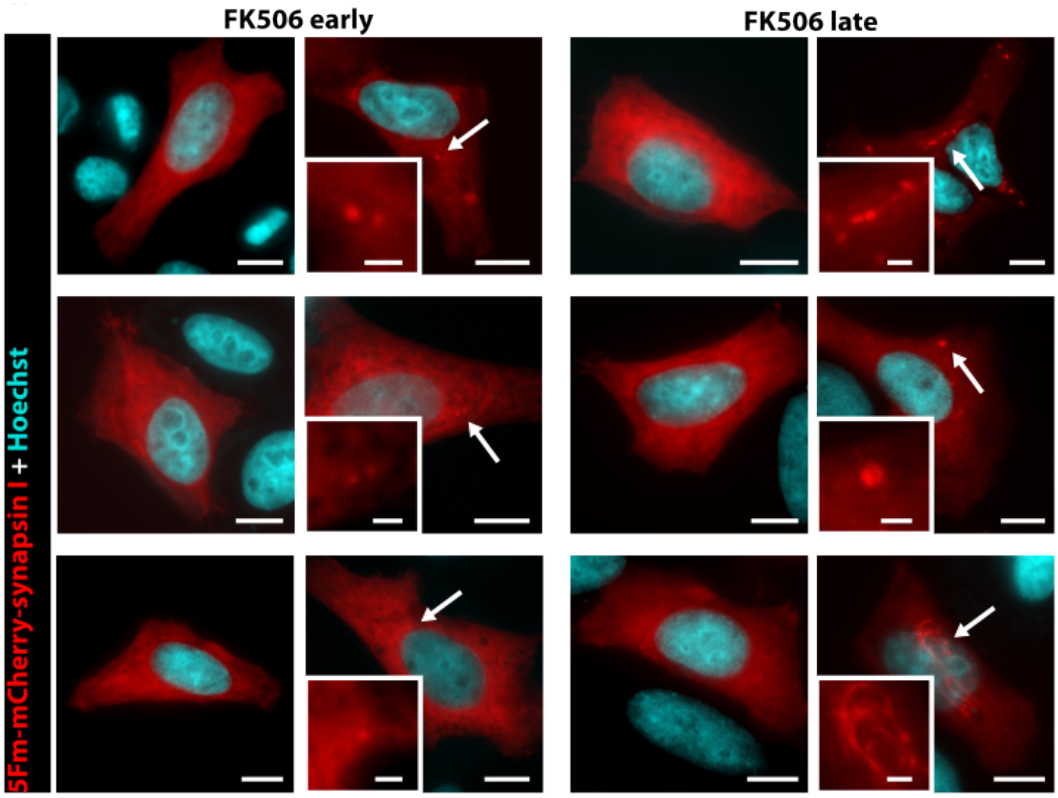

Figure III.8 Early vs. late exposure of 5Fm-mCherry-synapsin I to FK506. Left half: *Early exposure to FK506 (1h30 after transfection). Left column: cells with diffuse fluorescence. Right column: cells with small puncta.* ***Right half:*** *Late exposure to FK506 (1h before fixation). Left column depicts cells with diffuse fluorescence. Right column depicts cells with remains of synapsin I condensates that were only partially dissolved. For all images in the figure: scale bars, 10 µm for whole-cell images and 2 µm for zoom-ins.*

III.2.4 Interaction of synapsin I condensates with microtubules

We next aimed to determine whether the filiform patterns could be the result of an interaction with microtubules, building on previous evidence suggesting that synapsin I interacts with this cellular structure (*189*). To investigate this, we have performed an anti-α-Tubulin immunostaining on cells expressing 5Fm-mCherry-synapsin I condensates (**Figure III.9**). We observed indeed that filiform condensates formed in areas corresponding to an increased anti-α-Tubulin signal. Intriguingly, spherical condensates also appeared to decorate microtubule strands in a similar manner to droplets on a spider web. These results suggest that our reconstituted synapsin I condensates may interact with MT, and that this interaction influences their morphology. We propose a model where condensates wet the MT: a "partial" wetting could result in the 3D spherical morphologies, whereas a "total" wetting could yield 1D condensates which are characterized by filiform morphologies (**Figure III.9.b**).

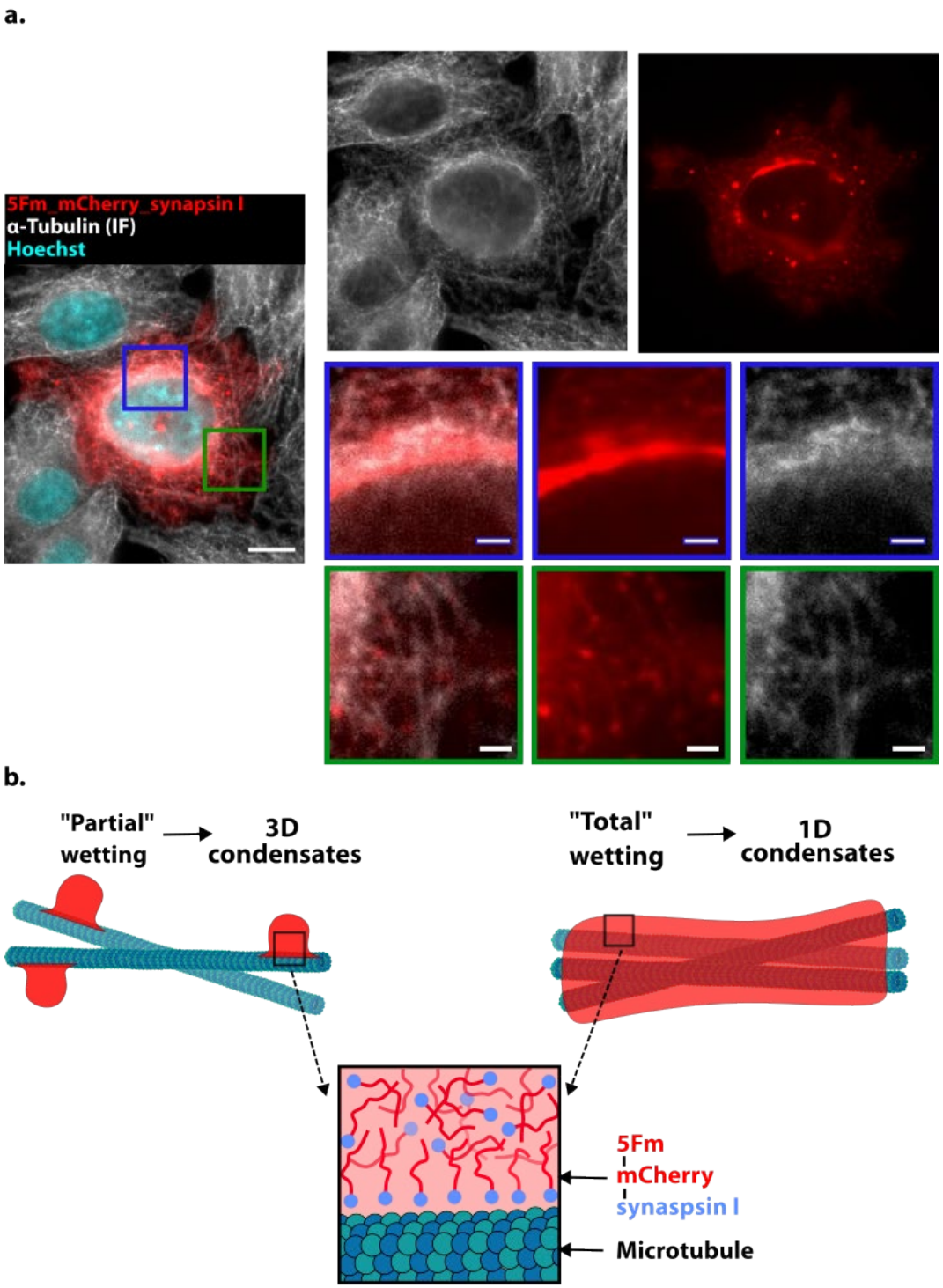

Figure III.9 Interaction of synapsin I condensates with microtubules. a. *Left: Representative epifluorescence microscopy image of the anti-α-Tubulin immunostaining (greys) on cells expressing 5Fm-mCherry-synapsin I condensates (red). Right side, upper row: Separated channels. Right side, middle row: zoom-in on a section of a filiform condensate. Right side, lower row: zoom-in on spherical condensates. Scale bar, 10 µm for whole-cell frames and 2 µm for zoom-ins.* ***b.*** *Schematic representation of the hypothesized "wetting" of synapsin I condensates (spherical and filiform) and microtubules.*

III.2.5 Mixed synapsin I/α-Syn condensates

To gain more insight on the interplay between α-Syn and synapsin I, we have set to create a mixed synapsin I / α-Syn condensate. To achieve this, we first tried co-overexpressing emGFP-tagged α-Syn together with the 5Fm-mCherry-synapsin I scaffold. In contrast to what we expected, we did not observe a partition of α-Syn-emGFP into our synapsin I condensate. The divergence between our findings and those of an earlier study (*110*) could be due to an effect of the voluminous 5Fm-mCherry tag that we attached to synapsin I. (**Figure III.10**).

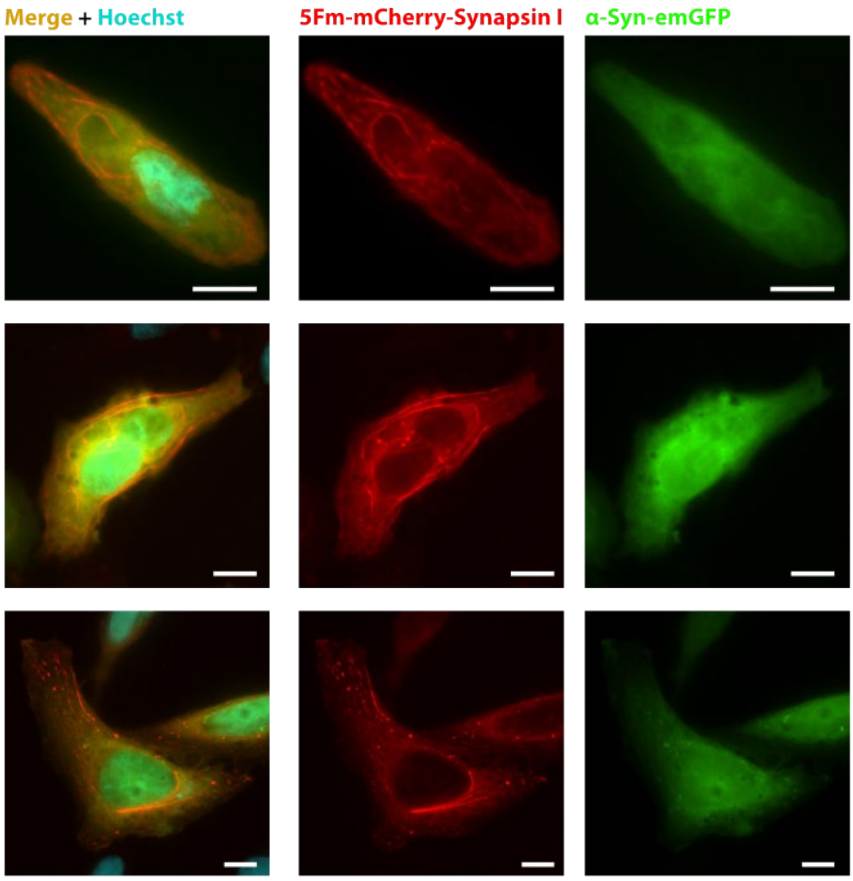

Figure III.10 5Fm-mCherry-synapsin I co-overexpression with α-Syn-emGFP. *Microscopy images depicting HeLa cells expressing 5Fm-mCherry-synapsin I (red) and α-Syn-emGFP (green). Scale bars, 10 µm.*

To mimic the recruitment of α-Syn within our synapsin I condensates, we have created an α-Syn construct that would fit into the category of a "client" molecule, according to Banani et al.'s classification (*120*). To achieve this, we have reduced the number of Fm repetitions, such that PS would not spontaneously happen in cells upon overexpression, but that enough Fm valences are available for a preferential partition of the construct within a 5Fm-based condensate. We found that a fusion of 2 Fm moieties fits the best into this description (see Annex for more details about our "client" constructs), leading to the α-Syn-emGFP-2Fm

construct. For the sake of simplicity, I will from now on refer to condensates containing both α-Syn-emGFP-2Fm and 5Fm-mCherry-synapsin I as "mixed α-Syn/ synapsin I condensates".

In accordance with the behaviour of a "client" molecule, overexpression of α-Syn-emGFP-2Fm alone does not result in the formation of any condensates (**Figure III.11**). However, when co-overexpressed with the synapsin I "scaffold" molecule 5Fm-mCherry-synapsin I, α-Syn-emGFP-2Fm readily partitioned into the resulting condensates (**Figure III.12**). To establish whether the presence of the α-Syn client had an influence on the properties of the synapsin I condensates, we have performed the FK506 dissolution assay on mixed condensates. Upon exposure to this molecule, the α-Syn client readily diffuses out of the condensate. On the contrary, synapsin I condensates that had accommodated α-Syn clients exhibited an incomplete dissolution, as even after 1000 s, faintly fluorescent "ghost" condensates that needed a contrasting increase to be observed, were still present (**Figure III.12.c**). This in contrast with condensates of simple synapsin I condensates, which were completely dissolved when they presented a spherical shape. Consistent with the fast dispersion of the fluorescence during the dissolution assay, FRAP experiments displayed a quick recovery of nearly all of the fluorescence intensity of α-Syn-emGFP-2Fm within a minute, indicating a high motility of the α-Syn clients within the synapsin I condensates (**Figure III.12.d**). Overall, these results indicate that the α-Syn-emGFP-2Fm construct is a "client" of synapsin I condensates. Furthermore, the mixed synapsin I/ α-Syn condensate exhibits a partial reversibility, reminiscent of the interactions found in homotypic synapsin I filiform condensates, that go beyond those involving 5Fm.

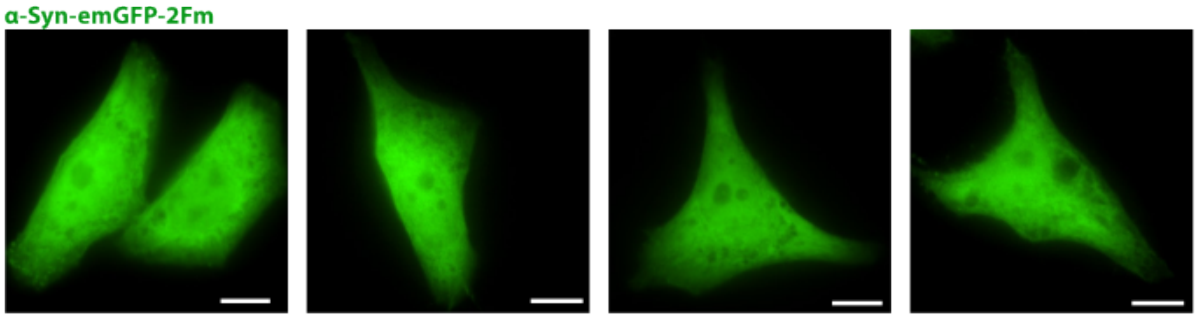

Figure III.11 α-Syn-emGFP-2Fm does not phase separate alone. *Representative epifluorescence microscopy images depicting HeLa cells expressing α-Syn-emGFP-2Fm (green). Scale bars, 10 µm.*

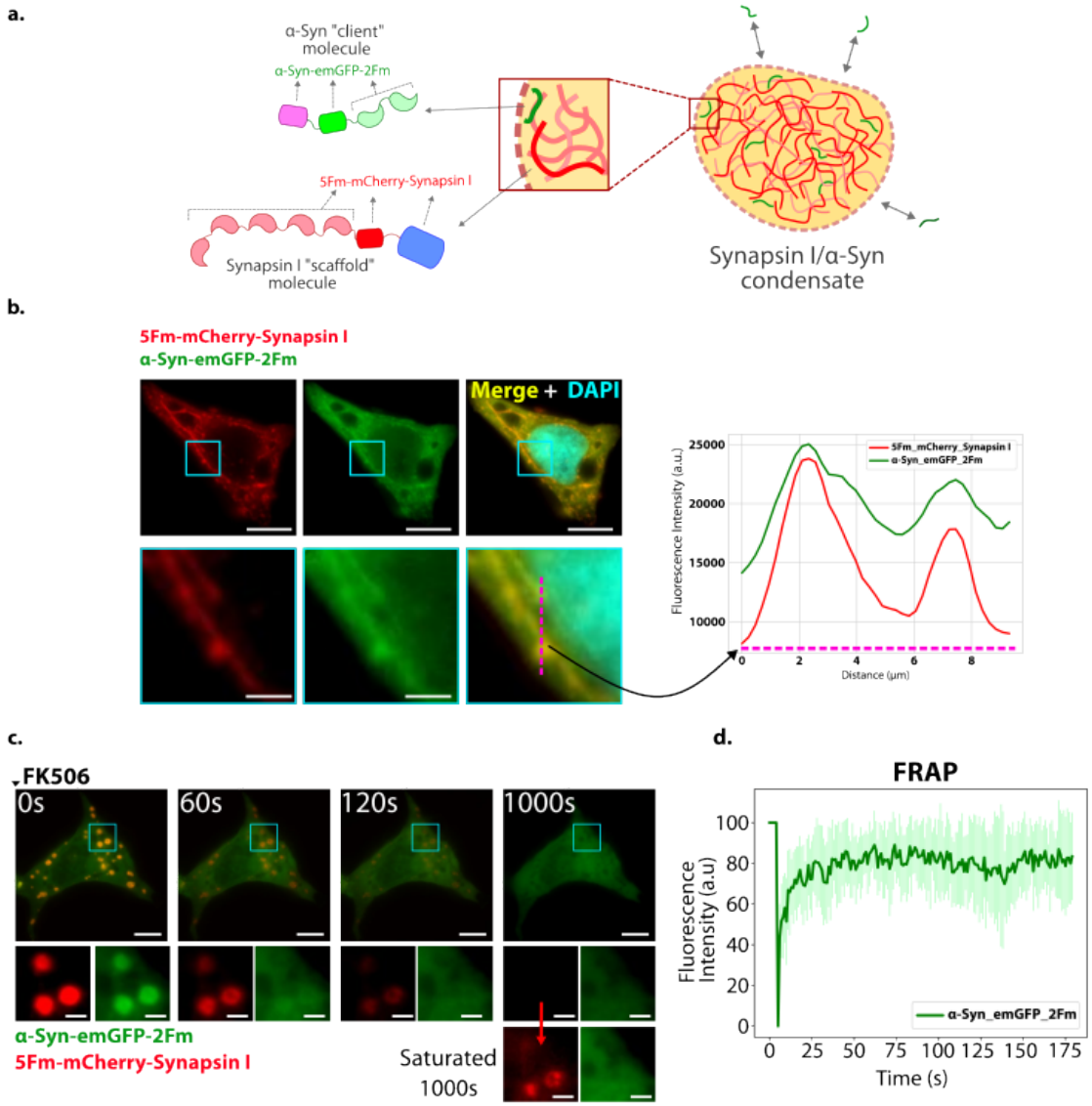

Figure III.12 Mixed synapsin I/α-Syn condensates a. *Schematic representation of the "mixed" condensate.* ***b.*** *Left side: Epifluorescence microscopy images of HeLa cells expressing 5Fm-mCherry-synapsin I (red) and α-Syn-emGFP-2Fm (green). Nuclei are in cyan. Right side: Plot superposing the fluorescence intensity of mCherry (red) and emGFP (green) across the condensates (pink dashed line). Coordinated spikes in fluorescence indicate partition of α-Syn-emGFP-2Fm into the 5Fm-mCherry-synapsin I condensate.* ***c.*** *Frames from a live movie following the dissolution of 5Fm-mixed synapsin I/α-Syn condensates upon exposure to FK506 (2.5 µM). The 0 s time was set at the moment when FK506 was added. For the 1000 s timepoint, as saturated version is provided below.* ***d.*** *FRAP of α-Syn-emGFP-2Fm within synapsin I/α-Syn mixed condensates. Fluorescence intensity unit was set at 100 for pre-bleach, 0 for just after the bleaching, and the rest was normalized accordingly. Dark green line represents mean of 9 different condensates and light green error bars are the standard deviation. For all images in the figure: Scale bar, 10 µm for whole-cell frames and 2 µm for zoom-ins.*

III.2.6 Preformed α-Syn fibrils perturb α-Syn/synapsin I mixed condensates

We recently showed how α-Syn from α-Syn condensates can readily convert into amyloid-containing solid structures upon exposure to preformed α-Syn fibrils (*175*). Naturally, we set to establish whether such an effect could be reproduced in synapsin I condensates where α-Syn is solely partitioning as a client. Thus, we incubated cells co-expressing the 5Fm-mCherry-synapsin I and the α-Syn-emGFP-2Fm constructs with the same concentration of fibrils that would trigger the amyloid transition in simple α-Syn condensates, that is 0.5 nM (**Figure III.13.a**). After 24 h of exposure to fibrils, mixed condensates readily underwent a morphological conversion that was reminiscent to that presented in the previous chapter when describing "abnormally-shaped" condensates: they became bright spots with multiple fibril-like protrusions (**Figure III.13.b**). Intriguingly these morphological transitions were not observed with condensates composed of 5Fm-mCherry-synapsin I alone, suggesting that the α-Syn client was a necessary condition for this to occur (**Figure III.14**). Despite the presence of filamentous structures, "abnormally-shaped" condensates are easily distinguishable from filiform ones. Filiform condensates are much longer (up to 20 μm in length), and often appear in intertwined web-like structures that cover great areas of the cytosol, whereas abnormally-shaped ones are substantially smaller (2 to 5 μm) and often present a distinct pattern of thorny protrusions that sprout from a central point.

Modified condensates were visible in both the mCherry and emGFP channels, meaning that, 5Fm-mCherry-synapsin I suffered an alteration along with the α-Syn-emGFP-2Fm construct. It is important to note that when cells expressing the two constructs were incubated with FK506 as well as with preformed fibrils, no condensates (regular or "abnormally-shaped") were observed (**Figure III.15**), meaning that the presence of the condensates was a precondition for the apparition of "abnormally-shaped" condensates. Overall, these observations lead us to conclude that mixed α-Syn/ synapsin I condensates undergo a morphological alteration upon exposure to fibrils, that is qualitatively identical to that observed with α-Syn condensates.

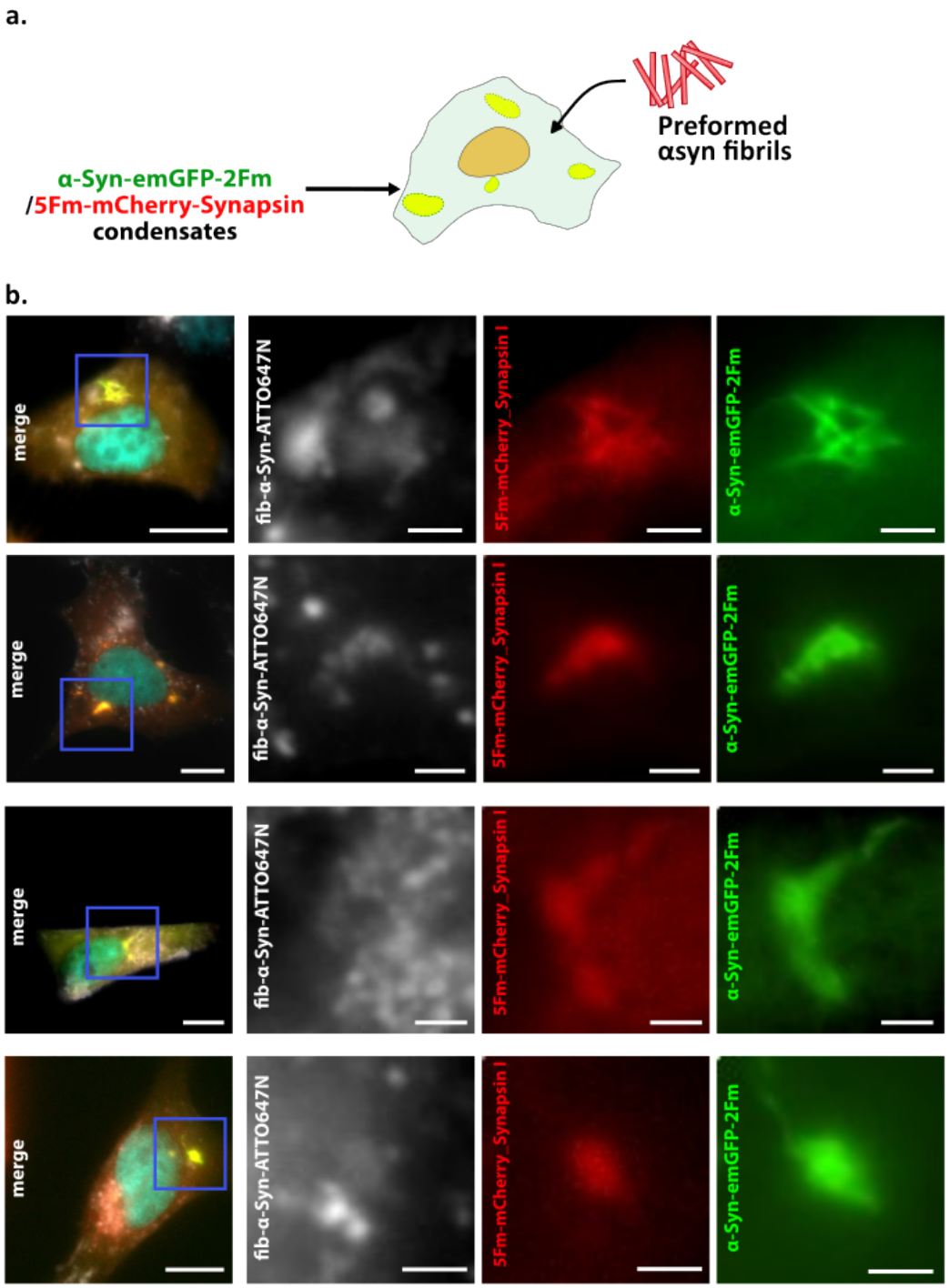

Figure III.13 α-Syn/synapsin I mixed condensates are perturbed by preformed α-Syn fibrils. ***a.*** *Schematic representation of the fibril exposure assay.* ***b.*** *Representative epifluorescence microscopy images depicting HeLa cells expressing 5Fm-mCherry-synapsin I (red) and α-Syn-emGFP-2Fm (green) and exposed to preformed α-Syn fibrils tagged with the ATTO647N fluorophore (greys). Nuclei are in cyan. For all images in the figure: Scale bar, 10 µm for whole-cell frames and 2 µm for zoom-ins.*

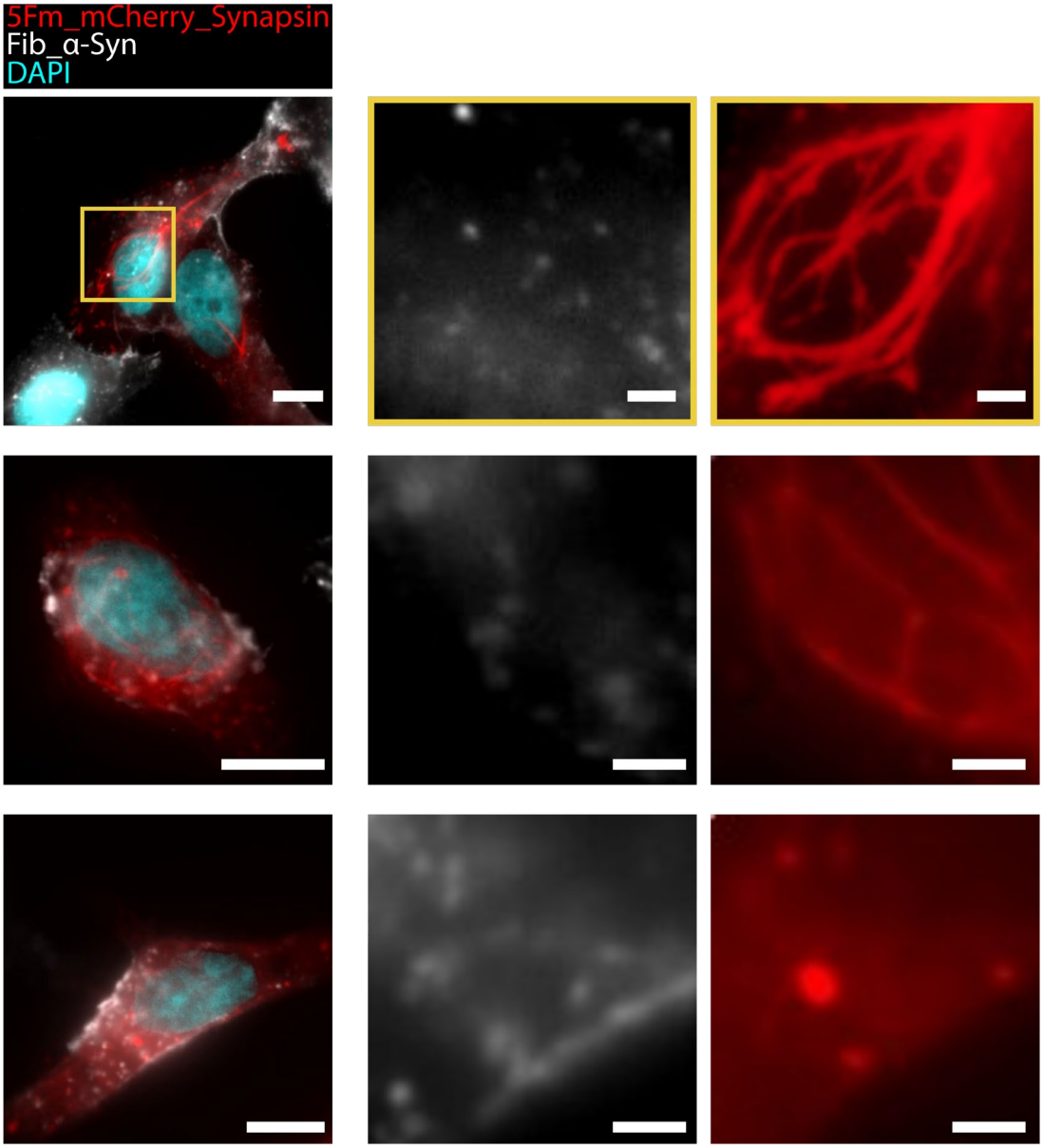

Figure III.14 synapsin I condensates are not perturbed by preformed α-Syn fibrils. *Representative epifluorescence microscopy images depicting HeLa cells expressing 5Fm-mCherry-synapsin I (red) and exposed to preformed α-Syn fibrils tagged with the ATTO647N fluorophore (grays). Nuclei are in cyan. Scale bar, 10 µm for whole-cell frames and 2 µm for zoom-ins.*

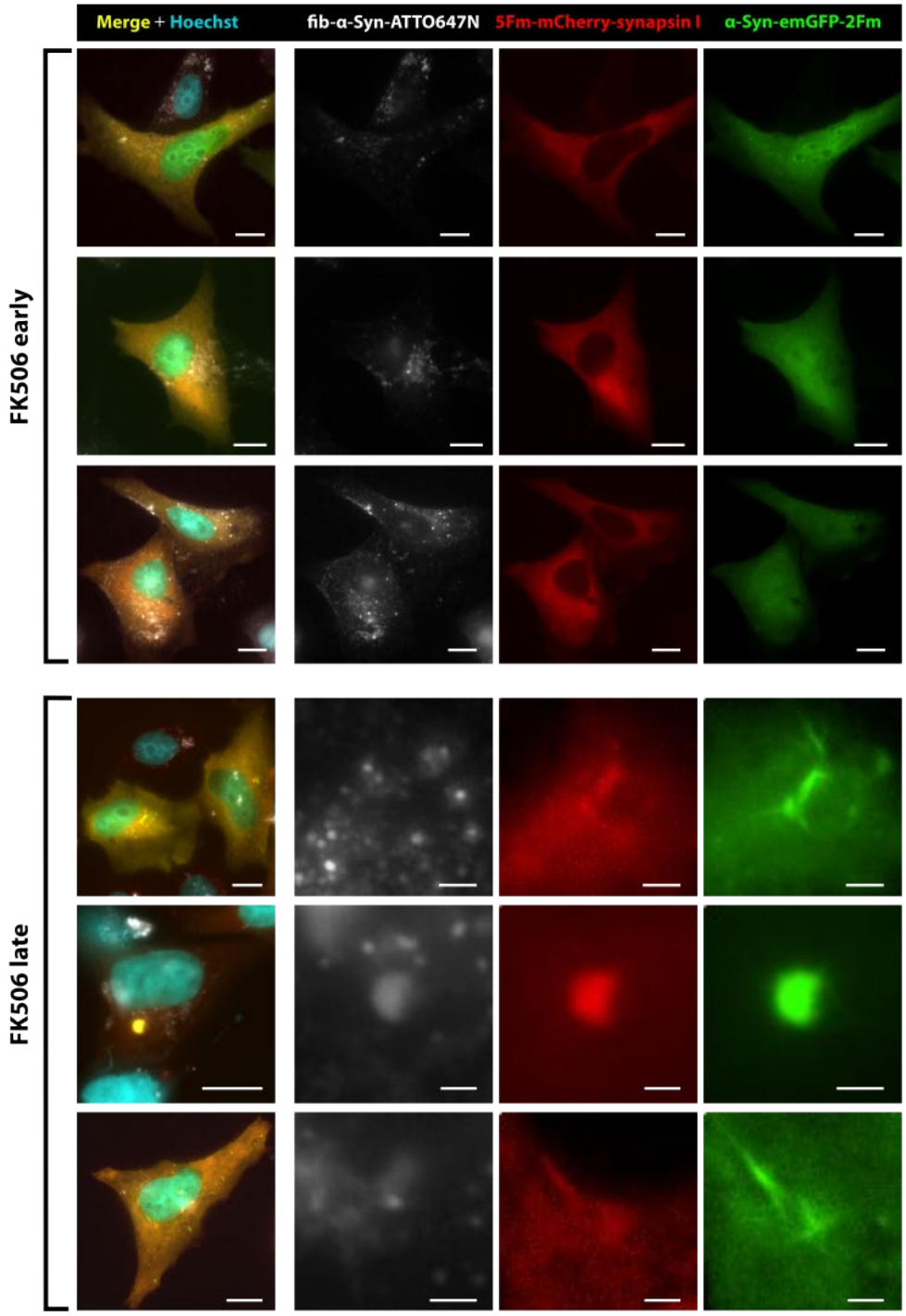

Figure III.15 Dissolution assay with FK506 on HeLa cells expressing α-Syn/synapsin I mixed condensates and exposed to α-Syn fibrils. *Upper half: Early exposure to FK506 (1h30 after transfection, during the washing of the Lipofectamine). No condensates were observed. Lower half: Late exposure to FK506 (1h before fixation). "Abnormally-shaped" condensates were observed, that resisted dissolution against FK506. Scale bars, 10 µm for whole-cell images and 2 µm for zoom-ins.*

III.2.7 α-Syn/synapsin I mixed condensates modified by fibrils have solid-like material properties.

We conducted a biophysical analysis of these modified mixed α-Syn/synapsin I condensates, to determine whether they exhibited solid-like properties similar to amyloid-containing altered α-Syn condensates, to which they resemble morphologically. First, we followed the dissolution pattern of mixed condensates upon exposure to FK506, using live epifluorescence microscopy. We find that, in presence of fibrils, mixed condensates became irreversible (**Figure III.16.a**). As opposed to the condition without fibrils, the fluorescence corresponding to α-Syn clients within condensates persisted after very long timescales (up to 30 min). Interestingly, the dispersion of the 5Fm-mCherry-synapsin I from the condensate was also slowed down, with a faint residue of the condensate also persisting after 30 minutes. Moreover, FRAP experiments confirmed the acquisition of solid-like properties of α-Syn within the mixed condensate, as the exposure to fibrils for 24 hours results in a complete loss of the fluorescence recovery (**Figure III.16.b**). Overall, these results suggest that the exposure to fibrils triggers a transition of the material properties of mixed synapsin I/α-Syn condensates from a liquid to a gel-like or solid-like state.

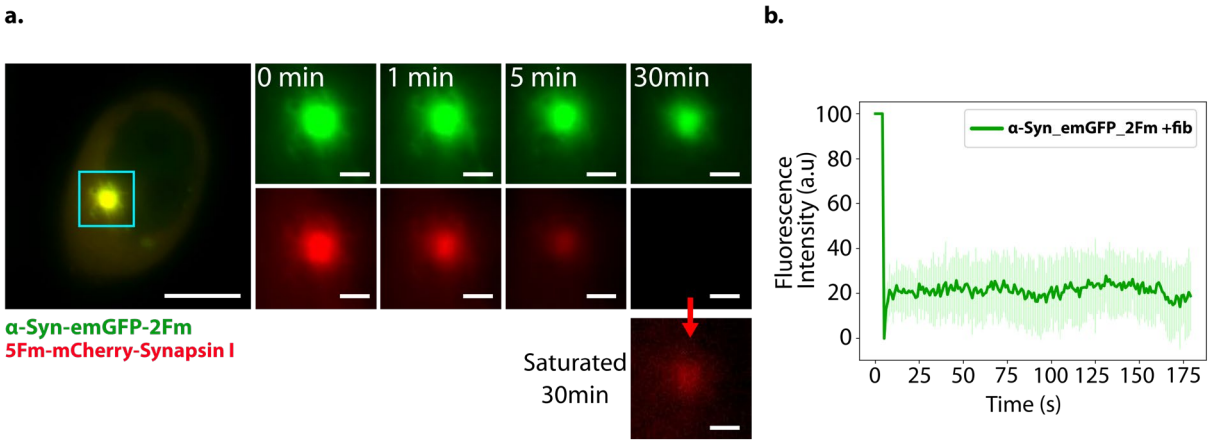

Figure III.16 α-Syn/synapsin I mixed condensates modified by fibrils have solid-like material properties. ***a.*** *Microscopy frames from a live movie following the dissolution of 5Fm-mixed synapsin I/α-Syn condensates exposed to preformed fibrils (0.5 nM) for 24 h, using FK506 (2.5 µM). The 0 min timepoint is the moment when FK506 was added. For the 30 min timepoint, as saturated version is provided below.* ***b.*** *FRAP of α-Syn-emGFP-2Fm within synapsin I/α-Syn mixed condensates exposed to fibrils (0.5 nM) for 24 h. Fluorescence intensity unit was set at 100 for pre-bleach, 0 for just after the bleaching, and the rest was normalized accordingly. The dark green line is the mean of N=10 different condensates and light green error bars are the standard deviation. Scale bar, 10 µm for whole-cell frames and 2 µm for zoom-ins.*

III.2.8 Future experiments

As stated as the beginning of this section, a certain set of experiments are planned for the future, to improve the robustness of the study. Concerning synapsin I condensates, we aim at studying their potential interaction with other elements of the cytoskeleton, such as actin filaments, which were reported to interact with synapsin I as part of its physiological role (*188*). We also plan to perform live microscopy, to follow the formation of spherical and filiform condensates, and to potentially elucidate more in-depth the origins of their distinctiveness. This live microscopy approach would also allow us to observe the transition of mixed synapsin I/ α-Syn condensates into fibrillar "abnormally-shaped" assemblies, upon exposure to preformed α-Syn fibrils. Furthermore, we set to perform a biochemical analysis of these "abnormally-shaped" condensates, to establish whether they contain amyloids. We also plan to enhance the robustness of our system, by validating in a more relevant cellular model, such as the SH-SY5Y neuroblastoma cell line.

III.3 Discussion

An increasing amount of evidence, particularly from *in vitro* studies, is beginning to substantiate that phase separated condensates may serve as intermediates in protein aggregation events linked to neurodegenerative diseases (*191–193*). For α-Syn, *in vitro* PS-derived condensates were suggested to progress into potentially cytotoxic aggregates (*133*, *168*, *169*). We recently reconstituted intracellular α-Syn condensates, and showed that they were readily converted into amyloid-containing fibrillar aggregates as a result of an interaction with preformed α-Syn fibrils (*175*). The goal of the present study was to evaluate the link between α-Syn PS and fibril-mediated aggregation, in the context of a condensate that features heterotypic interactions involving α-Syn. We have focused on α-Syn and synapsin I, based on a recent report suggesting that the two proteins co-phase separate (*110*).

Within our HeLa overexpression system, the occurrence of phase separation in synapsin I was nearly non-existent, in accordance with previous reports (*110*). Conversely, the overexpression of the 5Fm-mCherry-synapsin I scaffold yielded condensates, that we classified in two different morphological categories: spherical and filiform. Considering the morphology of filiform condensates, we hypothesized that these assemblies may form around microtubules, which are an element of the cytoskeleton that synapsin I was reported to bind (*189*). This hypothesis was favoured by data obtained from immunofluorescence staining for the microtubule building block α-Tubulin, and by the observation that filiform condensates partially resisted FK506 dissolution, suggesting that a novel bond involving synapsin I had formed. Moreover, a "wetting" behaviour of condensates on the surface of microtubules has already been observed *in vitro,* with droplets of the microtubule-associated protein tau (*194*).

The synapsin I condensate served as a base for the formation of mixed synapsin I/α-Syn condensates. The study of a composite separated phase containing α-Syn seemed of significant interest because, *in cellula*, α-Syn condensates could not be obtained through overexpression of the protein alone (*110*, *175*), and *in vitro* evidence suggests that heterotypic interactions could favour the engagement of the protein in PS (*171*, *172*). The choice of synapsin I as a partner in the mixed condensate was supported by multiple factors. Synapsin I was shown to form liquid droplets *in vitro*, and PS was proposed as a potential model for the synapsin I-mediated regulation of SV trafficking (*176*). Moreover, synapsin I was reported to co-phase separate with α-Syn, in an overexpression system in HEK293T cells (*110*). Furthermore, in physiological conditions, α-Syn and synapsin I are both abundantly expressed in the presynaptic termini of

neurons, where they are hypothesized to interact with each other (*139*, *195*). Intriguingly, mixed synapsin I/α-Syn condensates (spherical and filiform) displayed a slight resistance to our condensate reversibility assay, in contrast to spherical synapsin I condensates. This could potentially originate in the interaction with MTs, as seen with synapsin I filiform condensates. Since we also observed this with spherical mixed condensates, we hypothesize that this might also be the result of synapsin I - α-Syn interactions, which are inert to the effects of FK506. Further studies would be necessary to establish whether such an interaction takes place.

In a similar way to α-Syn condensates (*175*), mixed synapsin I/α-Syn separated phases underwent drastic changes after being exposed to preformed α-Syn fibrils. These alterations manifested through a complete change of morphology, with condensates growing micrometric fibrillar protrusions, reminiscing those described previously with α-Syn condensates (*175*). Moreover, α-Syn "clients" within these condensates completely lost their characteristic dynamic properties, and became resistant to our reversibility assay, which is indicative of an amyloid transition of α-Syn within the synapsin I/α-Syn condensate. Importantly, none of these alterations were observed when "simple" synapsin I condensates were exposed to preformed α-Syn fibrils. These observations imply that a heterotypic condensate where α-Syn partitions as a "client" molecule, can accommodate an accelerated response of the protein fibril-induced amyloid transition, similar to an α-Syn condensate (*175*). Moreover, the transition did not occur when the formation of condensates was averted by incubating with FK506 throughout the whole duration of the experiment. We thus suggest that the partition of the α-Syn "client" into a condensate is necessary for this transition, as an imposed diffuse state remained inert to fibril exposure.

Interestingly, the loss in reversibility was also partially characteristic of the synapsin I population of the condensate. Since, contrary to α-Syn, synapsin I is not known to form amyloid structures, we hypothesize that this prolonged persistence of synapsin I within the mixed condensates could be either (or both) of two possibilities: (i) the partition of α-Syn "clients" changed the synapsin I condensate's properties, as evidenced with mixed condensates that were not exposed to preformed fibrils, and (ii) synapsin I is trapped in *de novo* aggregates that formed with α-Syn "clients" through prion-like transition mediated by fibrils. Indeed, Lewy Bodies have been shown to feature a hugely complex composition (*24*), suggesting that proximal cellular factors and interactors can become enmeshed in the tangles of α-Syn amyloid fibrils during the aggregation process.

What could be the implications of these observations in the context of neurodegeneration? Our observations bring a new vantage point for the study of the effects of synucleinopathies at the synapse. Indeed, one of the pathological signs associated with α-Syn amyloid inclusions are disruptions at the synapse (*156*, *196*). Building on previous hypotheses about a presynaptic synapsin I phase enriched in α-Syn (*110*), the results presented herein hint at the possibility that such a condensate could be a sensitive spot in the propagation of aggregates. This would be in phase with data suggesting that the vast majority of small incipient α-Syn aggregates are localized in the presynaptic space (*197*), but also with the finding that a considerable proportion of the non-α-Syn components of Lewy Bodies corresponds to SV-associated factors (*198*). The adaptability of our system may enable, for future studies, a more in-depth exploration of these aspects, for example through the exploration of the impact of lipids and/or vesicles on the mixed α-Syn/synapsin I condensate in the context of fibril-mediated aggregation.

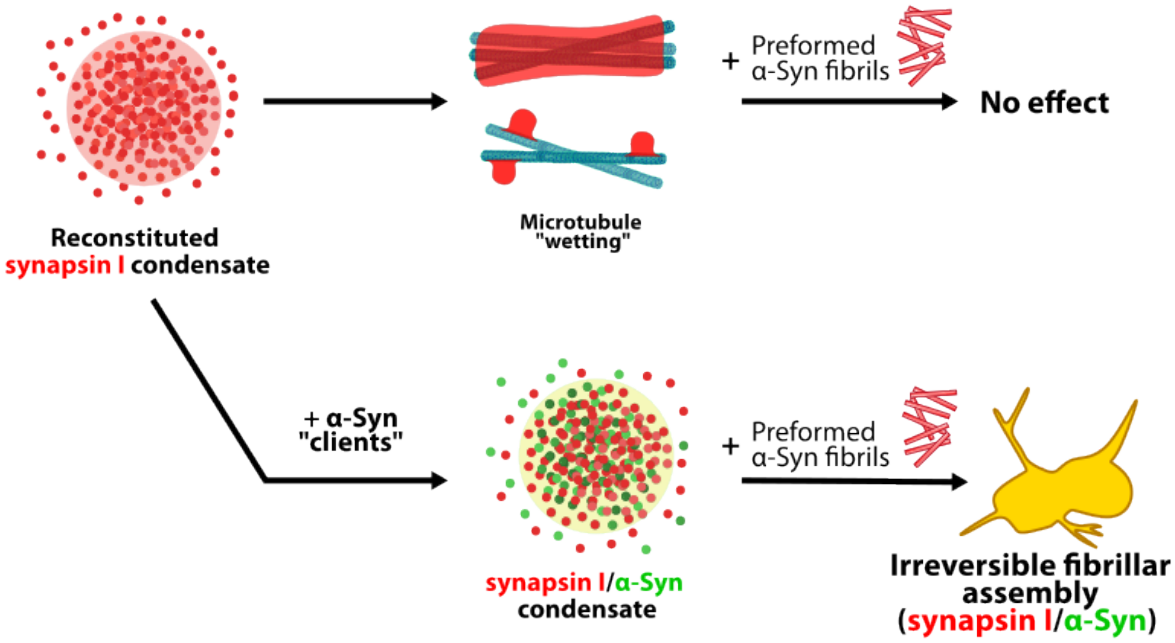

Figure III.17 Schematic summary of the conclusions of this chapter.

III.4 Materials and methods

Cell Culture:

All cellular experiments presented in this section were conducted in HeLa cells (human epithelioid carcinoma, American Type Culture Collection, ccl-2) and SH-SY5Y cells (ECACC). Cells were cultivated in Dulbecco's modified Eagle's medium (DMEM) supplemented with 10% foetal bovine serum (FBS) and 1% penicillin/streptavidin (P/S) at 37°C within a 5% CO2-humidified incubator. Regular mycoplasma infection tests were performed every 2 months on both cell cultures, to ensure lack of contamination.

Plasmids:

For the experiments presented here, we utilized plasmids with the pcDNA3.1 (Invitrogen) backbone. All plasmids featured the 6His and Myc tags downstream of the genes of interest. The pcDNA3.1-5F_mCherry_synaspin I plasmid was specifically engineered by inserting the synapsin I coding sequence between the XbaI and Eco47III restriction sites in the pcDNA3.1 5Fm-mCherry plasmid. The pcDNA3.1 emGFP_2Fm construct was created through the insertion of the emGFP coding sequence between the NheI and Eco47III restriction sites in the vector pcDNA3.1 2Fm. The pcDNA3.1- α-Syn-emGFP-2Fm plasmid was created by inserting the α-Syn coding sequence between the NheI and XhoI restriction sites in the pcDNA3.1-emGFP-2Fm plasmid.

Transfection:

All transfection experiments were carried out using the Lipofectamine 2000 reagent (Invitrogen) and OptiMEM (Gibco, 31985-062). Twenty-four hours prior to transfection, cells were seeded in different numbers depending on the cell culture plates used, as follows: 80,000 cells per well on 12 mm diameter round coverslips for 24-well plates; 350,000 cells per well on 22 × 22 mm2 coverslips for six-well plates and 100,000 cells per well for ibidi dishes. On transfection day, for each well, two solutions were mixed together: Solution 1 contained Lipofectamine 2000 (2 µl for 24 wells or ibidi dishes and 5 µL for 6 wells) + optiMEM (50 µL for 24 wells, 60µL for ibidi dishes, and 150 µL for 6 wells); solution 2 contained plasmid DNA (750 ng for 24 wells, 1 µg for ibidi dishes, and 2.5 µg for 6 wells) + OptiMEM (same volumes as solution 1). Solution 1 was incubated for 5 min before mixing with solution 2 and incubating

for another 20 min at room temperature. The cells were then incubated with DNA/Lipofectamine 2000 mix for 1 hour and 30 min at 37°C and 5% CO2, then washed twice with DMEM + FBS + P/S and incubated for an additional 24 hours. After the 24-hour incubation, cells were fixed in 4% formaldehyde solutions for 20 minutes. Subsequently, cells were washed in PBS, and the coverslips were mounted on microscopy glass slides using Fluoromount-G mounting medium. Coverslips were also sealed using a transparent nail polish.

α-Syn seeding assays:

Human WT α-Syn were expressed, purified, and assembled into the fibrillar polymorphs fibrils by our collaborator Ronald Melki, following a previously reported protocol (*58*). The tubes containing fibrils were thawed by being placed in a 37°C heated bath immediately after exiting the -80°C refrigerator, then diluted to a concentration of 0.5 nM in DMEM + SVF + P/S and added to cells at the washing moment (1 hour and 30 min after transfection). For fixed cells experiments, 6-well plates were used. Cells were incubated for 24 hours with fibrils at 37°C and 5% CO2 for fibril integration, then washed with fresh DMEM + FBS + P/S, before being fixed and mounted on slides as described previously.

Immunofluorescence:

Twenty-four hours after transfection, cells were fixed with a 4% paraformaldehyde solution (Sigma-Aldrich) for 20 minutes. Subsequently, cells underwent three washes with phosphate-buffered saline (PBS) and were permeabilized with a 0.1% Triton X-100 solution (Sigma-Aldrich) for 10 minutes, followed by three additional 5-minute washes with PBS. Cells were then incubated for 1 hour with the primary antibody anti-alphaTubulin (DM1A) at a 1/1000 dilution in a 1% BSA-PBS solution. Following this, cells were subjected to another three 5-minute washes with PBS and then incubated with the secondary antibody AF647 – AffiniPure Goat AntiMouse JIR115-605 at a 1/1000 dilution in a 1% BSA-PBS solution. After a final set of three 5-minute washes in Dulbecco's PBS, cells were mounted onto glass microscopy slides using Fluoromount-G (Thermo Fisher) mounting medium.

Dissolution and Reversibility, and Granule Formation Prevention Assays:

For live dissolution experiments, a 2.5 mM solution of FK506 (in dimethyl sulfoxide) was diluted in 50 µL of medium and added to the cells to achieve a final concentration of 2.5 µM. The dissolution process was monitored by capturing an image every 10 seconds immediately

following the addition of FK506. For condensate reversibility assays, FK506 at a final concentration of 2.5 μM was included in the cell media 1 hour prior to fixation.

Fluorescence Recovery After Photobleaching (FRAP):

FRAP experiments were conducted on live HeLa cells placed in a humidified chamber at 37°C and 5% CO2, mounted on a confocal microscope (for detailed information, refer to the "Imaging" section). The condensates were scanned 5 times to establish the average initial fluorescence level, after which they were bleached using a 488 nm laser at 100% intensity (10 iterations). Fluorescence recovery was subsequently tracked by capturing images of the bleached condensates every second for a duration of 180 seconds. The FRAP movies underwent analysis using Fiji software, with each condensate integrated into a region of interest to extract the average fluorescence intensity. To account for condensate movement, the StackReg plugin was applied to some of the movies. Analysis and fitting of the fluorescence intensity data were conducted using Python. For graphical representation, the initial fluorescence was set at 100%, the fluorescence at bleaching at 0%, and the remaining points were normalized accordingly.

Imaging:

For samples fixed on coverslips as well as for live FK506 dissolution assay movies we used an epifluorescence microscope (IX81, Olympus), which was controlled by the Micro-Manager 2.0 software. This microscope featured an Orca-fusion camera (Hamamatsu), a 63× oil-immersion objective, and utilized the Spectra-X Lumencor LED for illumination.

For Fluorescence Recovery After Photobleaching (FRAP) experiments, we employed the Zeiss LSM 710 META laser scanning confocal microscope, which we piloted using the LSM Zen 2012 Software. This system was equipped with a humidified chamber, maintaining conditions at 37°C and 5% CO2 for optimal sample viability. Illumination was provided by a 25 mW argon laser, and observations were made using a 63× oil-immersion objective.

III.5 Annex – Client molecules

The study of cellular LLPS implies considering both types of molecules that can compose biomolecular condensates: scaffolds and clients. Scaffolds are macromolecules whose multivalent valences allow them to be drivers of phase separation, via the multiplicity of interactions that they engage in. Clients, on the contrary, are molecules that can partition into already formed condensates by binding to scaffolds, but that cannot undergo PS. The compositional conditions that lead to the partition of scaffolds in condensates has been previously documented (*120*). In a two-scaffold system, the client molecules that partition more efficiently into the condensate are the ones binding the scaffold in stoichiometric excess. This is because some of the sticky domains of this scaffold remain unbound within the condensate. On the contrary, the limiting scaffold will have virtually all its binding sites saturated and thus will not recruit binding clients as efficiently (*120*). Our system for the reconstitution of condensates is based on one single scaffold, that engages in homotypic interactions. Thus, to partition into the condensate, a client needs to compete with the binding of the scaffold to itself. To design an efficient client, the valency needs to be high enough to allow it to competitively bind scaffolds and partition into condensates, but low enough to not undergo LLPS by itself. We experimentally found that a 2Fm fusion is appropriate for that scope (**Figure III.18**).

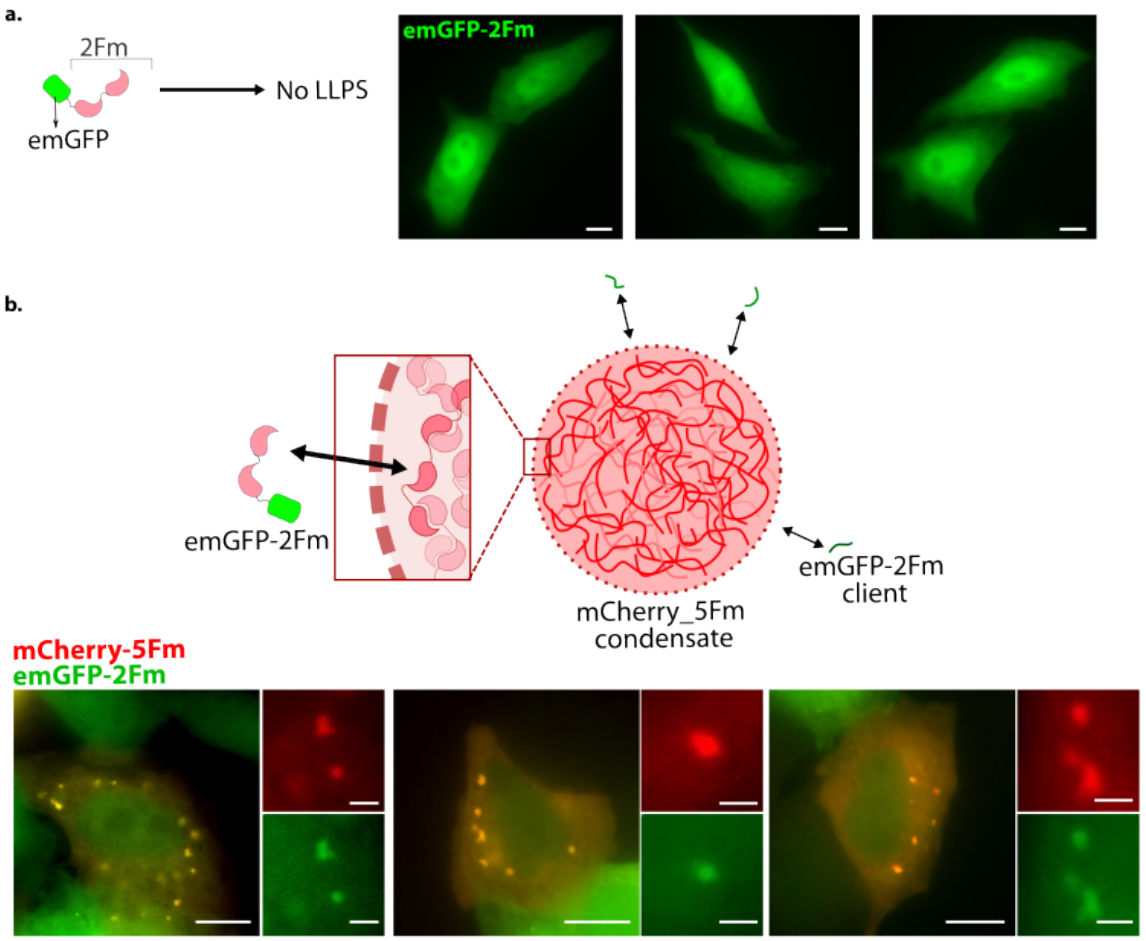

Figure III.18 Client molecules for the 5Fm system a. Left: *Schematic representation of the emGFP-2Fm construct. Right: Representative epifluorescence microscopy images depicting HeLa cells expressing the emGFP-2Fm construct. No condensates were observed. Scale bar, 10 µm* ***b.*** *Upper part : Schematic representation of the partition of the emGFP-2Fm client into a mCherry-5Fm condensate. Lower part: Representative epifluorescence microscopy images depicting HeLa cells expressing the emGFP-2Fm client and the mCherry-5Fm scaffold. The emGFP-2Fm clients partition into the mCherry-5Fm condensates. Scale bars, 10 µm for whole-cell images and 2 µm for zoom-ins.*

IV. CONCLUSION AND PERSPECTIVES

The present work was situated at the crossroads between two distinct but interconnected domains: the intricate biological processes underpinning protein aggregation in neurodegenerative diseases and the fundamental physical chemistry principles of phase separation. Whilst the evidences about a connection between the two keeps getting more solid, some limitations persist, that interfere with our ability to piece together an accurate depiction of this relationship. Notably, intracellular phase separation of proteins results in intricate objects called biomolecular condensates, whose study *in vivo* is very challenging, and whose complexity impairs accurate mimicking *in vitro.* Herein, I presented two studies involving the reconstitution of cellular biomolecular condensates. These reconstituted systems were more "accessible" for study than naturally occurring condensates, owing to their controlled formation and simplified composition. Thus, a series of inquiries related to PS in the context of neurodegeneration were addressed.

The first part was focused on the reconstitution of a biomolecular condensate enriched in α-Syn - a neurodegeneration-linked factor whose position with regards to phase separation remains unclear. In this part, we aimed at addressing the uncertainties related to the involvement of a putative α-Syn droplet state in the development of synucleinopathies, a topic that has remained ambiguous due to the extremely limited number of cell-based studies. First, our artificial condensate toolbox successfully yielded liquid-like α-Syn droplets in HeLa and SH-SY5Y cells. These droplets recapitulated the properties of phase separated condensates on multiple levels: (i) their formation was concentration-dependent, (ii) they were reversible, as illustrated with our controlled dissolution assay, and (iii) they exhibited liquid-like behaviour. We used these reconstituted condensates as a platform to investigate the hypothesis that the α-Syn separated phase could accommodate intracellular pathological aggregation. We reported that, upon exposure to preformed α-Syn fibrils, the condensates underwent a transition towards fibrillar solid-like aggregates. On the contrary, the diffuse state of the protein did not exhibit this response. A closer investigation allowed us to conclude that preformed fibrils triggered an amyloid transition within condensates, which was likely kinetically boosted by the high concentration of α-Syn within the condensate.

In the second part, we sought to increase the complexity of the artificial α-Syn droplet. Recent reports suggest that, in a cellular context, α-Syn might be linked to PS via a partition

into a putative droplet state of synapsin I in the context of presynaptic SV clusters. To study this phenomenon, we have developed an artificial system that emulates this composite condensate. The first step was to create a synapsin I condensate. We hypothesized that this condensate is shaped by the interaction between the synapsin I and microtubules, in addition to the interactions engaging our PS-inducing protein scaffold. The second step was to create an α-Syn client for the synapsin I condensate, which would mimic the previously proposed pathway for the co-phase separation of the two proteins. Preliminary data allowed us to hypothesize that heterotypic α-Syn - synapsin I interactions may form within these condensates. We naturally also explored the possibility of an amyloid conversion of α-Syn within these mixed condensates, in light of the results from our first study. Our data suggests that preformed α-Syn fibrils triggered a transition of the composite condensate from a liquid phase to a solid fibrillar state, and that these modified biophysical properties affected not only the intra-condensate α-Syn, but also the synapsin I component. This observation has two implications: (i) α-Syn in heterotypic condensates can undergo a fibrillar aggregate transition upon exposure to preformed fibrils, and (ii) α-Syn aggregates issued form the fibrillar conversion of condensates can trap other components of the condensate.

The two studies leave plenty of room for further investigations. In the context of α-Syn condensates that were converted into amyloids, an inquiry worthy of future attention is whether this has any impact on cell viability, or more generally whether any forms of cytotoxicity could be attributed to the presence of such condensate-derived aggregates. Such a study could bring valuable data regarding the topic of the causality between aggregation and pathology, which remains under discussion. Moreover, the artificial condensates could be used as a platform for the efficacy assessment of aggregation-inhibiting agents, such as small molecules or peptides. The system could also be used to explore the influence of different factors, such as lipids or metal ions, on the droplet state of α-Syn. With regards to the composite α-Syn/synapsin I condensates, an additional layer of complexity could be explored, by searching for a way to integrate SV mimics. This would bring the condensate one step closer to a potential naturally occurring α-Syn/synapsin I presynaptic droplet, and could allow a more in-depth analysis of its potential disfunctions and relationships to pathology. Moreover, it could be of great value to analyse the composition of condensates converted to fibrillar aggregate, to determine the nature of the cellular factors that can be trapped inside during the aggregation process. Lastly, our versatile condensate scaffold could be functionalized with other neurodegeneration-related proteins, paving the way for similar studies with applications in different proteinopathies.

V. REFERENCES

1. Key figures, *Institut du Cerveau*. https://institutducerveau-icm.org/en/key-figures/.

2. Y. Hou, X. Dan, M. Babbar, Y. Wei, S. G. Hasselbalch, D. L. Croteau, V. A. Bohr, Ageing as a risk factor for neurodegenerative disease. *Nat. Rev. Neurol.* **15**, 565–581 (2019).

3. A. E. Raftery, N. Li, H. Ševčíková, P. Gerland, G. K. Heilig, Bayesian probabilistic population projections for all countries. *Proc. Natl. Acad. Sci.* **109**, 13915–13921 (2012).

4. G. Cipriani, C. Dolciotti, L. Picchi, U. Bonuccelli, Alzheimer and his disease: a brief history. *Neurol. Sci.* **32**, 275–279 (2011).

5. F. Boller, M. M. Forbes, History of dementia and dementia in history: An overview. *J. Neurol. Sci.* **158**, 125–133 (1998).

6. P. J. García Ruiz, [Prehistory of Parkinson's disease]. *Neurol. Barc. Spain* **19**, 735–737 (2004).

7. P. Pinel, *Medico-Philosophical Treatise on Mental Alienation* (John Wiley & Sons, Ltd, Chichester, UK, 2008; http://doi.wiley.com/10.1002/9780470712238).

8. J. Parkinson, An Essay on the Shaking Palsy. *J Neuropsychiatry Clin Neurosci* (2002).

9. K. Seidel, J. Mahlke, S. Siswanto, R. Krüger, H. Heinsen, G. Auburger, M. Bouzrou, L. T. Grinberg, H. Wicht, H. Korf, W. den Dunnen, U. Rüb, The Brainstem Pathologies of Parkinson's Disease and Dementia with Lewy Bodies. *Brain Pathol.* **25**, 121–135 (2014).

10. H. Braak, U. Rüb, W. P. Gai, K. Del Tredici, Idiopathic Parkinson's disease: possible routes by which vulnerable neuronal types may be subject to neuroinvasion by an unknown pathogen. *J. Neural Transm.* **110**, 517–536 (2003).

11. G. Huntington, On Chorea. *J. Neuropsychiatry Clin. Neurosci.* **15**, 109–112 (2003).

12. T. Uchihara, Silver diagnosis in neuropathology: principles, practice and revised interpretation. *Acta Neuropathol. (Berl.)* **113**, 483–499 (2007).

13. A. Alzheimer, R. A. Stelzmann, H. N. Schnitzlein, F. R. Murtagh, An English translation of Alzheimer's 1907 paper, "Uber eine eigenartige Erkankung der Hirnrinde." *Clin. Anat. N. Y. N* **8**, 429–431 (1995).

14. M. Goedert, M. G. Spillantini, K. Del Tredici, H. Braak, 100 years of Lewy pathology. *Nat. Rev. Neurol.* **9**, 13–24 (2013).

15. M. DiFiglia, E. Sapp, K. O. Chase, S. W. Davies, G. P. Bates, J. P. Vonsattel, N. Aronin, Aggregation of Huntingtin in Neuronal Intranuclear Inclusions and Dystrophic Neurites in Brain. *Science* **277**, 1990–1993 (1997).

16. T. Arai, M. Hasegawa, H. Akiyama, K. Ikeda, T. Nonaka, H. Mori, D. Mann, K. Tsuchiya, M. Yoshida, Y. Hashizume, T. Oda, TDP-43 is a component of ubiquitin-positive tau-negative inclusions in frontotemporal lobar degeneration and amyotrophic lateral sclerosis. *Biochem. Biophys. Res. Commun.* **351**, 602–611 (2006).

17. G. G. Glenner, C. W. Wong, Alzheimer's disease: initial report of the purification and characterization of a novel cerebrovascular amyloid protein. *Biochem. Biophys. Res. Commun.* **120**, 885–890 (1984).

18. C. L. Masters, G. Simms, N. A. Weinman, G. Multhaup, B. L. McDonald, K. Beyreuther, Amyloid plaque core protein in Alzheimer disease and Down syndrome. *Proc. Natl. Acad. Sci. U. S. A.* **82**, 4245–4249 (1985).

19. E. Scherzinger, R. Lurz, M. Turmaine, L. Mangiarini, B. Hollenbach, R. Hasenbank, G. P. Bates, S. W. Davies, H. Lehrach, E. E. Wanker, Huntingtin-encoded polyglutamine expansions form amyloid-like protein aggregates in vitro and in vivo. *Cell* **90**, 549–558 (1997).

20. M. G. Spillantini, M. L. Schmidt, V. M.-Y. Lee, J. Q. Trojanowski, R. Jakes, M. Goedert, α-Synuclein in Lewy bodies. *Nature* **388**, 839–840 (1997).

21. C. A. Ross, M. A. Poirier, Protein aggregation and neurodegenerative disease. *Nat. Med.* **10 Suppl**, S10-17 (2004).

22. C. Pellegrini, L. Antonioli, R. Colucci, C. Blandizzi, M. Fornai, Interplay among gut microbiota, intestinal mucosal barrier and enteric neuro-immune system: a common path to neurodegenerative diseases? *Acta Neuropathol. (Berl.)* **136**, 345–361 (2018).

23. L. O. Narhi, J. Schmit, K. Bechtold-Peters, D. Sharma, Classification of Protein Aggregates1. *J. Pharm. Sci.* **101**, 493–498 (2012).

24. M. B. Fares, S. Jagannath, H. A. Lashuel, Reverse engineering Lewy bodies: how far have we come and how far can we go? *Nat. Rev. Neurosci.* **22**, 111–131 (2021).

25. M. Hasegawa, T. Nonaka, H. Tsuji, A. Tamaoka, M. Yamashita, F. Kametani, M. Yoshida, T. Arai, H. Akiyama, Molecular Dissection of TDP-43 Proteinopathies. *J. Mol. Neurosci.* **45**, 480–485 (2011).

26. C. S. Atwood, R. N. Martins, M. A. Smith, G. Perry, Senile plaque composition and posttranslational modification of amyloid-β peptide and associated proteins. *Peptides* **23**, 1343–1350 (2002).

27. L. Breydo, V. N. Uversky, Structural, morphological, and functional diversity of amyloid oligomers. *FEBS Lett.* **589**, 2640–2648 (2015).

28. Y. Kuroda, Biophysical studies of amorphous protein aggregation and in vivo immunogenicity. *Biophys. Rev.* **14**, 1495–1501 (2022).

29. J. Wu, N. Österlund, H. Wang, R. Sternke-Hoffmann, H. Pupart, L. L. Ilag, A. Gräslund, J. Luo, Identifying the role of co-aggregation of Alzheimer's amyloid-β with amorphous protein aggregates of non-amyloid proteins. *Cell Rep. Phys. Sci.* **3**, 101028 (2022).

30. Y. Li, C. Zhao, F. Luo, Z. Liu, X. Gui, Z. Luo, X. Zhang, D. Li, C. Liu, X. Li, Amyloid fibril structure of α-synuclein determined by cryo-electron microscopy. *Cell Res.* **28**, 897–903 (2018).

31. J. Hardy, D. J. Selkoe, The Amyloid Hypothesis of Alzheimer's Disease: Progress and Problems on the Road to Therapeutics. *Science* **297**, 353–356 (2002).

32. M. G. Iadanza, M. P. Jackson, E. W. Hewitt, N. A. Ranson, S. E. Radford, A new era for understanding amyloid structures and disease. *Nat. Rev. Mol. Cell Biol.* **19**, 755–773 (2018).

33. L. C. Serpell, J. M. Smith, Direct visualisation of the β-sheet structure of synthetic Alzheimer's amyloid11Edited by F. E. Cohen. *J. Mol. Biol.* **299**, 225–231 (2000).

34. A. Schmidt, K. Annamalai, M. Schmidt, N. Grigorieff, M. Fändrich, Cryo-EM reveals the steric zipper structure of a light chain-derived amyloid fibril. *Proc. Natl. Acad. Sci.* **113**, 6200–6205 (2016).

35. D. Li, C. Liu, Conformational strains of pathogenic amyloid proteins in neurodegenerative diseases. *Nat. Rev. Neurosci.* **23**, 523–534 (2022).

36. J. Zhou, L. Venturelli, L. Keiser, S. K. Sekatskii, F. Gallaire, S. Kasas, G. Longo, T. P. J. Knowles, F. S. Ruggeri, G. Dietler, Environmental Control of Amyloid Polymorphism by Modulation of Hydrodynamic Stress. *ACS Nano* **15**, 944–953 (2021).

37. K. Zhao, Y. Li, Z. Liu, H. Long, C. Zhao, F. Luo, Y. Sun, Y. Tao, X. Su, D. Li, X. Li, C. Liu, Parkinson's disease associated mutation E46K of α-synuclein triggers the formation of a distinct fibril structure. *Nat. Commun.* **11**, 2643 (2020).

38. L. Vugmeyster, D. F. Au, D. Ostrovsky, B. Kierl, R. Fu, Z. Hu, W. Qiang, Effect of Post-Translational Modifications and Mutations on Amyloid-β Fibrils Dynamics at N Terminus. *Biophys. J.* **117**, 1524–1535 (2019).

39. Y. Shi, W. Zhang, Y. Yang, A. G. Murzin, B. Falcon, A. Kotecha, M. van Beers, A. Tarutani, F. Kametani, H. J. Garringer, R. Vidal, G. I. Hallinan, T. Lashley, Y. Saito, S. Murayama, M. Yoshida, H. Tanaka, A. Kakita, T. Ikeuchi, A. C. Robinson, D. M. A. Mann, G. G. Kovacs, T. Revesz, B. Ghetti, M. Hasegawa, M. Goedert, S. H. W. Scheres, Structure-based classification of tauopathies. *Nature* **598**, 359–363 (2021).

40. J. Vaquer-Alicea, M. I. Diamond, L. A. Joachimiak, Tau strains shape disease. *Acta Neuropathol. (Berl.)* **142**, 57 (2021).

41. W. Peelaerts, L. Bousset, A. Van der Perren, A. Moskalyuk, R. Pulizzi, M. Giugliano, C. Van den Haute, R. Melki, V. Baekelandt, α-Synuclein strains cause distinct synucleinopathies after local and systemic administration. *Nature* **522**, 340–344 (2015).

42. C. Peng, R. J. Gathagan, V. M.-Y. Lee, Distinct α-Synuclein strains and implications for heterogeneity among α-Synucleinopathies. *Neurobiol. Dis.* **109**, 209–218 (2018).

43. W. Wang, S. Nema, D. Teagarden, Protein aggregation--pathways and influencing factors. *Int. J. Pharm.* **390**, 89–99 (2010).

44. C. Soto, Unfolding the role of protein misfolding in neurodegenerative diseases. *Nat. Rev. Neurosci.* **4**, 49–60 (2003).

45. N. Sabath, F. Levy-Adam, A. Younis, K. Rozales, A. Meller, S. Hadar, S. Soueid-Baumgarten, R. Shalgi, Cellular proteostasis decline in human senescence. *Proc. Natl. Acad. Sci. U. S. A.* **117**, 31902–31913 (2020).

46. R. E. Mrak, W. S. T. Griffin, D. I. Graham, Aging-associated Changes in Human Brain. *J. Neuropathol. Exp. Neurol.* **56**, 1269–1275 (1997).

47. Y. Decker, E. Németh, R. Schomburg, A. Chemla, L. Fülöp, M. D. Menger, Y. Liu, K. Fassbender, Decreased pH in the aging brain and Alzheimer's disease. *Neurobiol. Aging* **101**, 40–49 (2021).

48. A. K. Buell, Stability matters, too – the thermodynamics of amyloid fibril formation. *Chem. Sci.* **13**, 10177–10192 (2022).

49. A. Sicorello, S. Torrassa, G. Soldi, S. Gianni, C. Travaglini-Allocatelli, N. Taddei, A. Relini, F. Chiti, Agitation and High Ionic Strength Induce Amyloidogenesis of a Folded PDZ Domain in Native Conditions. *Biophys. J.* **96**, 2289–2298 (2009).

50. V. N. Uversky, Intrinsic disorder in proteins associated with neurodegenerative diseases. *Front. Biosci.-Landmark* **14**, 5188–5238 (2009).

51. H. J. Dyson, P. E. Wright, Intrinsically unstructured proteins and their functions. *Nat. Rev. Mol. Cell Biol.* **6**, 197–208 (2005).

52. L. Zhang, D. Lu, Z. Liu, How native proteins aggregate in solution: A dynamic Monte Carlo simulation. *Biophys. Chem.* **133**, 71–80 (2008).

53. M. Törnquist, T. C. T. Michaels, K. Sanagavarapu, X. Yang, G. Meisl, S. I. A. Cohen, T. P. J. Knowles, S. Linse, Secondary nucleation in amyloid formation. *Chem. Commun.* **54**, 8667–8684 (2018).

54. J. D. Harper, S. S. Wong, C. M. Lieber, P. T. Lansbury, Assembly of Aβ Amyloid Protofibrils: An in Vitro Model for a Possible Early Event in Alzheimer's Disease. *Biochemistry* **38**, 8972–8980 (1999).

55. S. I. A. Cohen, S. Linse, L. M. Luheshi, E. Hellstrand, D. A. White, L. Rajah, D. E. Otzen, M. Vendruscolo, C. M. Dobson, T. P. J. Knowles, Proliferation of amyloid-β42 aggregates occurs through a secondary nucleation mechanism. *Proc. Natl. Acad. Sci. U. S. A.* **110**, 9758–9763 (2013).

56. Y. S. Eisele, U. Obermüller, G. Heilbronner, F. Baumann, S. A. Kaeser, H. Wolburg, L. C. Walker, M. Staufenbiel, M. Heikenwalder, M. Jucker, Peripherally Applied Aβ-Containing Inoculates Induce Cerebral β-Amyloidosis. *Science* **330**, 980–982 (2010).

57. K. C. Luk, V. M. Kehm, B. Zhang, P. O'Brien, J. Q. Trojanowski, V. M. Y. Lee, Intracerebral inoculation of pathological α-synuclein initiates a rapidly progressive neurodegenerative α-synucleinopathy in mice. *J. Exp. Med.* **209**, 975–986 (2012).

58. L. Bousset, L. Pieri, G. Ruiz-Arlandis, J. Gath, P. H. Jensen, B. Habenstein, K. Madiona, V. Olieric, A. Böckmann, B. H. Meier, R. Melki, Structural and functional characterization of two alpha-synuclein strains. *Nat. Commun.* **4**, 2575 (2013).

59. B. Frost, M. I. Diamond, Prion-like mechanisms in neurodegenerative diseases. *Nat. Rev. Neurosci.* **11**, 155–159 (2010).

60. S. B. Prusiner, Novel Proteinaceous Infectious Particles Cause Scrapie. *Science* **216**, 136–144 (1982).

61. M. Yonetani, T. Nonaka, M. Masuda, Y. Inukai, T. Oikawa, S. Hisanaga, M. Hasegawa, Conversion of Wild-type α-Synuclein into Mutant-type Fibrils and Its Propagation in the Presence of A30P Mutant. *J. Biol. Chem.* **284**, 7940–7950 (2009).

62. B. B. Holmes, M. I. Diamond, Prion-like Properties of Tau Protein: The Importance of Extracellular Tau as a Therapeutic Target. *J. Biol. Chem.* **289**, 19855–19861 (2014).

63. T. Nonaka, M. Masuda-Suzukake, T. Arai, Y. Hasegawa, H. Akatsu, T. Obi, M. Yoshida, S. Murayama, D. M. A. Mann, H. Akiyama, M. Hasegawa, Prion-like Properties of Pathological TDP-43 Aggregates from Diseased Brains. *Cell Rep.* **4**, 124–134 (2013).

64. G. S. Victoria, C. Zurzolo, The spread of prion-like proteins by lysosomes and tunneling nanotubes: Implications for neurodegenerative diseases. *J. Cell Biol.* **216**, 2633–2644 (2017).

65. K. C. Luk, V. Kehm, J. Carroll, B. Zhang, P. O'Brien, J. Q. Trojanowski, V. M.-Y. Lee, Pathological α-Synuclein Transmission Initiates Parkinson-like Neurodegeneration in Non-transgenic Mice. *Science* **338**, 949–953 (2012).

66. A.-L. Mougenot, S. Nicot, A. Bencsik, E. Morignat, J. Verchère, L. Lakhdar, S. Legastelois, T. Baron, Prion-like acceleration of a synucleinopathy in a transgenic mouse model. *Neurobiol. Aging* **33**, 2225–2228 (2012).

67. M. Masuda-Suzukake, T. Nonaka, M. Hosokawa, T. Oikawa, T. Arai, H. Akiyama, D. M. A. Mann, M. Hasegawa, Prion-like spreading of pathological α-synuclein in brain. *Brain* **136**, 1128–1138 (2013).

68. S. Wegmann, E. A. Maury, M. J. Kirk, L. Saqran, A. Roe, S. L. DeVos, S. Nicholls, Z. Fan, S. Takeda, O. Cagsal-Getkin, C. M. William, T. L. Spires-Jones, R. Pitstick, G. A. Carlson, A. M. Pooler, B. T. Hyman, Removing endogenous tau does not prevent tau propagation yet reduces its neurotoxicity. *EMBO J.* **34**, 3028–3041 (2015).

69. S. Lam, F. Petit, A.-S. Hérard, S. Boluda, S. Eddarkaoui, M. Guillermier, F. Letournel, M.-L. Martin-Négrier, M. Faisant, C. Godfraind, J. Boutonnat, C.-A. Maurage, V. Deramecourt, M. Duchesne, D. Meyronet, T. Fenouil, A. M. de Paula, V. Rigau, F. Vandenbos-Burel, D. Seilhean, C. Duyckaerts, S. Boluda, I. Plu, D. C. Chiforeanu, A. Laquerrière, F. Marguet, B. Lannes, B. Lhermitte, L. Buée, C. Duyckaerts, S. Haïk, J.-L. Picq, M. Dhenain, The Brain Bank Neuro-C. E. B. Neuropathology Network,

Transmission of amyloid-beta and tau pathologies is associated with cognitive impairments in a primate. *Acta Neuropathol. Commun.* **9**, 165 (2021).

70. M. D. Kane, W. J. Lipinski, M. J. Callahan, F. Bian, R. A. Durham, R. D. Schwarz, A. E. Roher, L. C. Walker, Evidence for Seeding of β-Amyloid by Intracerebral Infusion of Alzheimer Brain Extracts in β-Amyloid Precursor Protein-Transgenic Mice. *J. Neurosci.* **20**, 3606–3611 (2000).

71. H. Braak, K. D. Tredici, U. Rüb, R. A. I. de Vos, E. N. H. Jansen Steur, E. Braak, Staging of brain pathology related to sporadic Parkinson's disease. *Neurobiol. Aging* **24**, 197–211 (2003).

72. J. E. Duda, V. M.-Y. Lee, J. Q. Trojanowski, Neuropathology of synuclein aggregates: New insights into mechanisms of neurodegenerative diseases. *J. Neurosci. Res.* **61**, 121–127 (2000).

73. T. G. Beach, C. H. Adler, L. Lue, L. I. Sue, J. Bachalakuri, J. Henry-Watson, J. Sasse, S. Boyer, S. Shirohi, R. Brooks, J. Eschbacher, C. L. White, H. Akiyama, J. Caviness, H. A. Shill, D. J. Connor, M. N. Sabbagh, D. G. Walker, Unified Staging System for Lewy Body Disorders: Correlation with Nigrostriatal Degeneration, Cognitive Impairment and Motor Dysfunction. *Acta Neuropathol. (Berl.)* **117**, 613–634 (2009).

74. D. R. Thal, T. G. Beach, M. Zanette, K. Heurling, A. Chakrabarty, A. Ismail, A. P. L. Smith, C. Buckley, [18F]flutemetamol amyloid positron emission tomography in preclinical and symptomatic Alzheimer's disease: Specific detection of advanced phases of amyloid-β pathology. *Alzheimers Dement.* **11**, 975–985 (2015).

75. W. R. Bevan-Jones, T. E. Cope, P. S. Jones, S. S. Kaalund, L. Passamonti, K. Allinson, O. Green, Y. T. Hong, T. D. Fryer, R. Arnold, J. P. Coles, F. I. Aigbirhio, A. J. Larner, K. Patterson, J. T. O'Brien, J. B. Rowe, Neuroinflammation and protein aggregation co-localize across the frontotemporal dementia spectrum. *Brain* **143**, 1010–1026 (2020).

76. M. E. MacDonald, C. M. Ambrose, M. P. Duyao, R. H. Myers, C. Lin, L. Srinidhi, G. Barnes, S. A. Taylor, M. James, N. Groot, H. MacFarlane, B. Jenkins, M. A. Anderson, N. S. Wexler, J. F. Gusella, G. P. Bates, S. Baxendale, H. Hummerich, S. Kirby, M. North, S. Youngman, R. Mott, G. Zehetner, Z. Sedlacek, A. Poustka, A.-M. Frischauf, H. Lehrach, A. J. Buckler, D. Church, L. Doucette-Stamm, M. C. O'Donovan, L. Riba-Ramirez, M. Shah, V. P. Stanton, S. A. Strobel, K. M. Draths, J. L. Wales, P. Dervan, D. E. Housman, M. Altherr, R. Shiang, L. Thompson, T. Fielder, J. J. Wasmuth, D. Tagle, J. Valdes, L. Elmer, M. Allard, L. Castilla, M. Swaroop, K. Blanchard, F. S. Collins, R. Snell, T. Holloway, K. Gillespie, N. Datson, D. Shaw, P. S. Harper, A novel gene containing a trinucleotide repeat that is expanded and unstable on Huntington's disease chromosomes. *Cell* **72**, 971–983 (1993).

77. K. Zhao, Y. Li, Z. Liu, H. Long, C. Zhao, F. Luo, Y. Sun, Y. Tao, X. Su, D. Li, X. Li, C. Liu, Parkinson's disease associated mutation E46K of α-synuclein triggers the formation of a distinct fibril structure - Nat. Commun. 11, 2643 (2020).

78. N. Ostrerova-Golts, L. Petrucelli, J. Hardy, J. M. Lee, M. Farer, B. Wolozin, The A53T α-Synuclein Mutation Increases Iron-Dependent Aggregation and Toxicity. *J. Neurosci.* **20**, 6048–6054 (2000).

79. D. Chen, K. W. Drombosky, Z. Hou, L. Sari, O. M. Kashmer, B. D. Ryder, V. A. Perez, D. R. Woodard, M. M. Lin, M. I. Diamond, L. A. Joachimiak, Tau local structure shields an amyloid-forming motif and controls aggregation propensity. *Nat. Commun.* **10**, 2493 (2019).

80. D. F. Lázaro, E. F. Rodrigues, R. Langohr, H. Shahpasandzadeh, T. Ribeiro, P. Guerreiro, E. Gerhardt, K. Kröhnert, J. Klucken, M. D. Pereira, B. Popova, N. Kruse, B. Mollenhauer, S. O. Rizzoli, G. H. Braus, K. M. Danzer, T. F. Outeiro, Systematic Comparison of the Effects of Alpha-synuclein Mutations on Its Oligomerization and Aggregation. *PLOS Genet.* **10**, e1004741 (2014).

81. H. Deng, K. Gao, J. Jankovic, The role of FUS gene variants in neurodegenerative diseases. *Nat. Rev. Neurol.* **10**, 337–348 (2014).

82. W. J. Jansen, R. Ossenkoppele, D. L. Knol, B. M. Tijms, P. Scheltens, F. R. J. Verhey, P. J. Visser, P. Aalten, D. Aarsland, D. Alcolea, M. Alexander, I. S. Almdahl, S. E. Arnold, I. Baldeiras, H. Barthel, B. N. M. Van Berckel, K. Bibeau, K. Blennow, D. J. Brooks, M. A. Van Buchem, V. Camus, E. Cavedo, K. Chen, G. Chetelat, A. D. Cohen, A. Drzezga, S. Engelborghs, A. M. Fagan, T. Fladby, A. S. Fleisher, W. M. Van Der Flier, L. Ford, S. Förster, J. Fortea, N. Foskett, K. S. Frederiksen, Y. Freund-Levi, G. B. Frisoni, L. Froelich, T. Gabryelewicz, K. D. Gill, O. Gkatzima, E. Gómez-Tortosa, M. F. Gordon, T. Grimmer, H. Hampel, L. Hausner, S. Hellwig, S.-K. Herukka, H. Hildebrandt, L. Ishihara, A. Ivanoiu, W. J. Jagust, P. Johannsen, R. Kandimalla, E. Kapaki, A. Klimkowicz-Mrowiec, W. E. Klunk, S. Köhler, N. Koglin, J. Kornhuber, M. G. Kramberger, K. Van Laere, S. M. Landau, D. Y. Lee, M. De Leon, V. Lisetti, A. Lleó, K. Madsen, W. Maier, J. Marcusson, N. Mattsson, A. De Mendonça, O. Meulenbroek, P. T. Meyer, M. A. Mintun, V. Mok, J. L. Molinuevo, H. M. Møllergård, J. C. Morris, B. Mroczko, S. Van Der Mussele, D. L. Na, A. Newberg, A. Nordberg, A. Nordlund, G. P. Novak, G. P. Paraskevas, L. Parnetti, G. Perera, O. Peters, J. Popp, S. Prabhakar, G. D. Rabinovici, I. H. G. B. Ramakers, L. Rami, C. Resende De Oliveira, J. O. Rinne, K. M. Rodrigue, E. Rodríguez-Rodríguez, C. M. Roe, U. Rot, C. C. Rowe, E. Rüther, O. Sabri, P. Sanchez-Juan, I. Santana, M. Sarazin, J. Schröder, C. Schütte, S. W. Seo, F. Soetewey, H. Soininen, L. Spiru, H. Struyfs, C. E. Teunissen, M. Tsolaki, R. Vandenberghe, M. M. Verbeek, V. L. Villemagne, S. J. B. Vos, L. J. C. Van Waalwijk Van Doorn, G. Waldemar, A. Wallin, Å. K. Wallin, J. Wiltfang, D. A. Wolk, M. Zboch, H. Zetterberg, Prevalence of Cerebral Amyloid Pathology in Persons Without Dementia: A Meta-analysis. *JAMA* **313**, 1924 (2015).

83. G. Chételat, R. La Joie, N. Villain, A. Perrotin, V. de La Sayette, F. Eustache, R. Vandenberghe, Amyloid imaging in cognitively normal individuals, at-risk populations and preclinical Alzheimer's disease. *NeuroImage Clin.* **2**, 356–365 (2013).

84. A. DelleDonne, K. J. Klos, H. Fujishiro, Z. Ahmed, J. E. Parisi, K. A. Josephs, R. Frigerio, M. Burnett, Z. K. Wszolek, R. J. Uitti, J. E. Ahlskog, D. W. Dickson, Incidental Lewy Body Disease and Preclinical Parkinson Disease. *Arch. Neurol.* **65**, 1074–1080 (2008).

85. D. M. Rentz, J. J. Locascio, J. A. Becker, E. K. Moran, E. Eng, R. L. Buckner, R. A. Sperling, K. A. Johnson, Cognition, Reserve, and Amyloid Deposition in Normal Aging. *Ann. Neurol.* **67**, 353–364 (2010).

86. R. Cascella, S. W. Chen, A. Bigi, J. D. Camino, C. K. Xu, C. M. Dobson, F. Chiti, N. Cremades, C. Cecchi, The release of toxic oligomers from α-synuclein fibrils induces dysfunction in neuronal cells. *Nat. Commun.* **12**, 1814 (2021).

87. U. Sengupta, A. N. Nilson, R. Kayed, The Role of Amyloid-β Oligomers in Toxicity, Propagation, and Immunotherapy. *EBioMedicine* **6**, 42–49 (2016).

88. Y.-S. Fang, K.-J. Tsai, Y.-J. Chang, P. Kao, R. Woods, P.-H. Kuo, C.-C. Wu, J.-Y. Liao, S.-C. Chou, V. Lin, L.-W. Jin, H. S. Yuan, I. H. Cheng, P.-H. Tu, Y.-R. Chen, Full-length TDP-43 forms toxic amyloid oligomers that are present in frontotemporal lobar dementia-TDP patients. *Nat. Commun.* **5**, 4824 (2014).

89. H. A. Lashuel, P. T. Lansbury, Are amyloid diseases caused by protein aggregates that mimic bacterial pore-forming toxins? *Q. Rev. Biophys.* **39**, 167–201 (2006).

90. S. M. Yatin, M. Aksenova, M. Aksenov, W. R. Markesbery, T. Aulick, D. A. Butterfield, Temporal relations among amyloid beta-peptide-induced free-radical oxidative stress, neuronal toxicity, and neuronal defensive responses. *J. Mol. Neurosci. MN* **11**, 183–197 (1998).

91. Q. Zheng, T. Huang, L. Zhang, Y. Zhou, H. Luo, H. Xu, X. Wang, Dysregulation of Ubiquitin-Proteasome System in Neurodegenerative Diseases. *Front. Aging Neurosci.* **8** (2016).

92. E. J. Bennett, N. F. Bence, R. Jayakumar, R. R. Kopito, Global Impairment of the Ubiquitin-Proteasome System by Nuclear or Cytoplasmic Protein Aggregates Precedes Inclusion Body Formation. *Mol. Cell* **17**, 351–365 (2005).

93. A. J. Espay, J. A. Vizcarra, L. Marsili, A. E. Lang, D. K. Simon, A. Merola, K. A. Josephs, A. Fasano, F. Morgante, R. Savica, J. T. Greenamyre, F. Cambi, T. R. Yamasaki, C. M. Tanner, Z. Gan-Or, I. Litvan, I. F. Mata, C. P. Zabetian, P. Brundin, H. H. Fernandez, D. G. Standaert, M. A. Kauffman, M. A. Schwarzschild, S. P. Sardi, T. Sherer, G. Perry, J. B. Leverenz, Revisiting protein aggregation as pathogenic in sporadic Parkinson and Alzheimer diseases. *Neurology* **92**, 329–337 (2019).

94. A. Patel, H. O. Lee, L. Jawerth, S. Maharana, M. Jahnel, M. Y. Hein, S. Stoynov, J. Mahamid, S. Saha, T. M. Franzmann, A. Pozniakovski, I. Poser, N. Maghelli, L. A. Royer, M. Weigert, E. W. Myers, S. Grill, D. Drechsel, A. A. Hyman, S. Alberti, A Liquid-to-Solid Phase Transition of the ALS Protein FUS Accelerated by Disease Mutation. *Cell* **162**, 1066–1077 (2015).

95. N. M. Kanaan, C. Hamel, T. Grabinski, B. Combs, Liquid-liquid phase separation induces pathogenic tau conformations in vitro. *Nat. Commun.* **11**, 2809 (2020).

96. A. E. Conicella, G. H. Zerze, J. Mittal, N. L. Fawzi, ALS mutations disrupt phase separation mediated by -helical structure in the TDP-43 low complexity C-terminal domain. *Struct. Lond. Engl. 1993* **24**, 1537–1549 (2016).

97. A. Molliex, J. Temirov, J. Lee, M. Coughlin, A. P. Kanagaraj, H. J. Kim, T. Mittag, J. P. Taylor, Phase Separation by Low Complexity Domains Promotes Stress Granule Assembly and Drives Pathological Fibrillization. *Cell* **163**, 123–133 (2015).

98. P. R. ten Wolde, D. Frenkel, Enhancement of Protein Crystal Nucleation by Critical Density Fluctuations. *Science* **277**, 1975–1978 (1997).

99. K.-W. Fong, Y. Li, W. Wang, W. Ma, K. Li, R. Z. Qi, D. Liu, Z. Songyang, J. Chen, Whole-genome screening identifies proteins localized to distinct nuclear bodies. *J. Cell Biol.* **203**, 149–164 (2013).

100. A. Hubstenberger, M. Courel, M. Bénard, S. Souquere, M. Ernoult-Lange, R. Chouaib, Z. Yi, J.-B. Morlot, A. Munier, M. Fradet, M. Daunesse, E. Bertrand, G. Pierron, J. Mozziconacci, M. Kress, D. Weil, P-Body Purification Reveals the Condensation of Repressed mRNA Regulons. *Mol. Cell* **68**, 144-157.e5 (2017).

101. S. F. Banani, H. O. Lee, A. A. Hyman, M. K. Rosen, Biomolecular condensates: Organizers of cellular biochemistry. *Nat. Rev. Mol. Cell Biol.* **18**, 285–298 (2017).

102. T. Pederson, The nucleolus. *Cold Spring Harb. Perspect. Biol.* **3**, a000638 (2011).

103. C. P. Brangwynne, C. R. Eckmann, D. S. Courson, A. Rybarska, C. Hoege, J. Gharakhani, F. Jülicher, A. A. Hyman, Germline P Granules Are Liquid Droplets That Localize by Controlled Dissolution/Condensation. *Science* **324**, 1729–1732 (2009).

104. C. F. Lee, C. P. Brangwynne, J. Gharakhani, A. A. Hyman, F. Jülicher, Spatial Organization of the Cell Cytoplasm by Position-Dependent Phase Separation. *Phys. Rev. Lett.* **111**, 088101 (2013).

105. D. S. W. Protter, R. Parker, Principles and Properties of Stress granules. *Trends Cell Biol.* **26**, 668–679 (2016).

106. D. Staněk, Cajal bodies and snRNPs - friends with benefits. *RNA Biol.* **14**, 671–679 (2016).

107. E. Boke, M. Ruer, M. Wühr, M. Coughlin, R. Lemaitre, S. P. Gygi, S. Alberti, D. Drechsel, A. A. Hyman, T. J. Mitchison, Amyloid-like Self-Assembly of a Cellular Compartment. *Cell* **166**, 637–650 (2016).

108. F. Gasset-Rosa, S. Lu, H. Yu, C. Chen, Z. Melamed, L. Guo, J. Shorter, S. D. Cruz, D. W. Cleveland, Cytoplasmic TDP-43 de-mixing independent of stress granules drives inhibition of nuclear import, loss of nuclear TDP-43, and cell death. *Neuron* **102**, 339 (2019).

109. R. Tan, A. J. Lam, T. Tan, J. Han, D. W. Nowakowski, M. Vershinin, S. Simó, K. M. Ori-McKenney, R. J. McKenney, Microtubules Gate Tau Condensation to Spatially Regulate Microtubule Functions. *Nat. Cell Biol.* **21**, 1078–1085 (2019).

110. C. Hoffmann, R. Sansevrino, G. Morabito, C. Logan, R. M. Vabulas, A. Ulusoy, M. Ganzella, D. Milovanovic, Synapsin Condensates Recruit alpha-Synuclein. *J. Mol. Biol.* **433**, 166961 (2021).

111. S. Maharana, J. Wang, D. K. Papadopoulos, D. Richter, A. Pozniakovsky, I. Poser, M. Bickle, S. Rizk, J. Guillén-Boixet, T. M. Franzmann, M. Jahnel, L. Marrone, Y.-T. Chang, J. Sterneckert, P. Tomancak, A. A. Hyman, S. Alberti, RNA buffers the phase separation behavior of prion-like RNA binding proteins. *Science* **360**, 918–921 (2018).

112. S. Wegmann, B. Eftekharzadeh, K. Tepper, K. M. Zoltowska, R. E. Bennett, S. Dujardin, P. R. Laskowski, D. MacKenzie, T. Kamath, C. Commins, C. Vanderburg, A. D. Roe, Z. Fan, A. M. Molliex, A. Hernandez-Vega, D. Muller, A. A. Hyman, E. Mandelkow, J. P. Taylor, B. T. Hyman, Tau protein liquid–liquid phase separation can initiate tau aggregation. *EMBO J.* **37** (2018).

113. M. C. Hardenberg, T. Sinnige, S. Casford, S. T. Dada, C. Poudel, E. A. Robinson, M. Fuxreiter, C. F. Kaminksi, G. S. Kaminski Schierle, E. A. A. Nollen, C. M. Dobson, M. Vendruscolo, Observation of an α-synuclein liquid droplet state and its maturation into Lewy body-like assemblies. *J. Mol. Cell Biol.* **13**, 282–294 (2021).

114. C. P. Brangwynne, P. Tompa, R. V. Pappu, Polymer physics of intracellular phase transitions. *Nat. Phys.* **11**, 899–904 (2015).

115. S. Alberti, A. Gladfelter, T. Mittag, Considerations and Challenges in Studying Liquid-Liquid Phase Separation and Biomolecular Condensates. *Cell* **176**, 419–434 (2019).

116. K. A. Burke, A. M. Janke, C. L. Rhine, N. L. Fawzi, Residue-by-Residue View of In Vitro FUS Granules that Bind the C-Terminal Domain of RNA Polymerase II. *Mol. Cell* **60**, 231–241 (2015).

117. H.-R. Li, T.-C. Chen, C.-L. Hsiao, L. Shi, C.-Y. Chou, J. Huang, The physical forces mediating self-association and phase-separation in the C-terminal domain of TDP-43. *Biochim. Biophys. Acta BBA - Proteins Proteomics* **1866**, 214–223 (2018).

118. C. W. Pak, M. Kosno, A. S. Holehouse, S. B. Padrick, A. Mittal, R. Ali, A. A. Yunus, D. R. Liu, R. V. Pappu, M. K. Rosen, Sequence Determinants of Intracellular Phase Separation by Complex Coacervation of a Disordered Protein. *Mol. Cell* **63**, 72–85 (2016).

119. J.-M. Choi, A. S. Holehouse, R. V. Pappu, Physical Principles Underlying the Complex Biology of Intracellular Phase Transitions. *Annu. Rev. Biophys.* **49**, 107–133 (2020).

120. S. F. Banani, A. M. Rice, W. B. Peeples, Y. Lin, S. Jain, R. Parker, M. K. Rosen, Compositional Control of Phase-Separated Cellular Bodies. *Cell* **166**, 651–663 (2016).

121. S. Xiang, M. Kato, L. Wu, Y. Lin, M. Ding, Y. Zhang, Y. Yu, S. L. McKnight, The LC Domain of hnRNPA2 Adopts Similar Conformations in Hydrogel Polymers, Liquid-like Droplets and Nuclei. *Cell* **163**, 829–839 (2015).

122. M. Kodaka, Interpretation of concentration-dependence in aggregation kinetics. *Biophys. Chem.* **109**, 325–332 (2004).

123. D. Ubbiali, M. Fratini, L. Piersimoni, C. H. Ihling, M. Kipping, I. Heilmann, C. Iacobucci, A. Sinz, Direct Observation of "Elongated" Conformational States in α-Synuclein upon Liquid-Liquid Phase Separation. *Angew. Chem. Int. Ed Engl.* **61**, e202205726 (2022).

124. J. Wen, L. Hong, G. Krainer, Q.-Q. Yao, T. P. J. Knowles, S. Wu, S. Perrett, Conformational Expansion of Tau in Condensates Promotes Irreversible Aggregation. *J. Am. Chem. Soc.* **143**, 13056–13064 (2021).

125. T. Murakami, S. Qamar, J. Q. Lin, G. S. K. Schierle, E. Rees, A. Miyashita, A. R. Costa, R. B. Dodd, F. T. S. Chan, C. H. Michel, D. Kronenberg-Versteeg, Y. Li, S.-P. Yang, Y. Wakutani, W. Meadows, R. R. Ferry, L. Dong, G. G. Tartaglia, G. Favrin, W.-L. Lin, D. W. Dickson, M. Zhen, D. Ron, G. Schmitt-Ulms, P. E. Fraser, N. A. Shneider, C. Holt, M. Vendruscolo, C. F. Kaminski, P. St George-Hyslop, ALS/FTD Mutation-Induced Phase Transition of FUS Liquid Droplets and Reversible Hydrogels into Irreversible Hydrogels Impairs RNP Granule Function. *Neuron* **88**, 678–690 (2015).

126. J. R. Buchan, R.-M. Kolaitis, J. P. Taylor, R. Parker, Eukaryotic stress granules are cleared by autophagy and Cdc48/VCP function. *Cell* **153**, 1461–1474 (2013).

127. S. P. Shevtsov, M. Dundr, Nucleation of nuclear bodies by RNA. *Nat. Cell Biol.* **13**, 167–173 (2011).

128. Polar Positioning of Phase-Separated Liquid Compartments in Cells Regulated by an mRNA Competition Mechanism - PubMed. https://pubmed.ncbi.nlm.nih.gov/27594427/.

129. A. Cochard, M. Garcia-Jove Navarro, L. Piroska, S. Kashida, M. Kress, D. Weil, Z. Gueroui, RNA at the surface of phase-separated condensates impacts their size and number. *Biophys. J.* **121**, 1675–1690 (2022).

130. M. Garcia-Jove Navarro, S. Kashida, R. Chouaib, S. Souquere, G. Pierron, D. Weil, Z. Gueroui, RNA is a critical element for the sizing and the composition of phase-separated RNA-protein condensates. *Nat. Commun.* **10**, 3230 (2019).

131. J. P. Taylor, R. H. Brown, D. W. Cleveland, Decoding ALS: from genes to mechanism. *Nature* **539**, 197–206 (2016).

132. P. Li, S. Banjade, H.-C. Cheng, S. Kim, B. Chen, L. Guo, M. Llaguno, J. V. Hollingsworth, D. S. King, S. F. Banani, P. S. Russo, Q.-X. Jiang, B. T. Nixon, M. K. Rosen, Phase transitions in the assembly of multivalent signalling proteins. *Nature* **483**, 336–340 (2012).

133. S. Ray, N. Singh, R. Kumar, K. Patel, S. Pandey, D. Datta, J. Mahato, R. Panigrahi, A. Navalkar, S. Mehra, L. Gadhe, D. Chatterjee, A. S. Sawner, S. Maiti, S. Bhatia, J. A. Gerez, A. Chowdhury, A. Kumar, R. Padinhateeri, R. Riek, G. Krishnamoorthy, S. K. Maji, α-Synuclein aggregation nucleates through liquid–liquid phase separation. *Nat. Chem.* **12**, 705–716 (2020).

134. L. J. Bugaj, A. T. Choksi, C. K. Mesuda, R. S. Kane, D. V. Schaffer, Optogenetic protein clustering and signaling activation in mammalian cells. *Nat. Methods* **10**, 249–252 (2013).

135. Y. Shin, J. Berry, N. Pannucci, M. P. Haataja, J. E. Toettcher, C. P. Brangwynne, Spatiotemporal control of intracellular phase transitions using light-activated optoDroplets. *Cell* **168**, 159-171.e14 (2017).

136. J. R. Mann, A. M. Gleixner, J. C. Mauna, E. Gomes, M. R. DeChellis-Marks, P. G. Needham, K. E. Copley, B. Hurtle, B. Portz, N. J. Pyles, L. Guo, C. B. Calder, Z. P. Wills, U. B. Pandey, J. K. Kofler, J. L. Brodsky, A. Thathiah, J. Shorter, C. J. Donnelly,

RNA Binding Antagonizes Neurotoxic Phase Transitions of TDP-43. *Neuron* **102**, 321-338.e8 (2019).

137. H. Nakamura, A. A. Lee, A. S. Afshar, S. Watanabe, E. Rho, S. Razavi, A. Suarez, Y.-C. Lin, M. Tanigawa, B. Huang, R. DeRose, D. Bobb, W. Hong, S. B. Gabelli, J. Goutsias, T. Inoue, Intracellular production of hydrogels and synthetic RNA granules by multivalent molecular interactions. *Nat. Mater.* **17**, 79–89 (2018).

138. J. Burré, M. Sharma, T. C. Südhof, Cell Biology and Pathophysiology of α-Synuclein. *Cold Spring Harb. Perspect. Med.* **8**, a024091 (2018).

139. J. E. Galvin, T. M. Schuck, V. M.-Y. Lee, J. Q. Trojanowski, Differential Expression and Distribution of α-, β-, and γ-Synuclein in the Developing Human Substantia Nigra. *Exp. Neurol.* **168**, 347–355 (2001).

140. W. S. Davidson, A. Jonas, D. F. Clayton, J. M. George, Stabilization of alpha-synuclein secondary structure upon binding to synthetic membranes. *J. Biol. Chem.* **273**, 9443–9449 (1998).

141. G. Fusco, A. De Simone, T. Gopinath, V. Vostrikov, M. Vendruscolo, C. M. Dobson, G. Veglia, Direct observation of the three regions in α-synuclein that determine its membrane-bound behaviour. *Nat. Commun.* **5**, 3827 (2014).

142. T.-S. Fan, S. C.-H. Liu, R.-M. Wu, Alpha-Synuclein and Cognitive Decline in Parkinson Disease. *Life* **11**, 1239 (2021).

143. R. J. Perrin, W. S. Woods, D. F. Clayton, J. M. George, Interaction of Human α-Synuclein and Parkinson's Disease Variants with Phospholipids: STRUCTURAL ANALYSIS USING SITE-DIRECTED MUTAGENESIS *. *J. Biol. Chem.* **275**, 34393–34398 (2000).

144. R. Sharon, M. S. Goldberg, I. Bar-Josef, R. A. Betensky, J. Shen, D. J. Selkoe, α-Synuclein occurs in lipid-rich high molecular weight complexes, binds fatty acids, and shows homology to the fatty acid-binding proteins. *Proc. Natl. Acad. Sci. U. S. A.* **98**, 9110–9115 (2001).

145. O. S. Gorbatyuk, S. Li, F. N. Nguyen, F. P. Manfredsson, G. Kondrikova, L. F. Sullivan, C. Meyers, W. Chen, R. J. Mandel, N. Muzyczka, α-Synuclein Expression in Rat Substantia Nigra Suppresses Phospholipase D2 Toxicity and Nigral Neurodegeneration. *Mol. Ther.* **18**, 1758–1768 (2010).

146. S. Yu, X. Zuo, Y. Li, C. Zhang, M. Zhou, Y. A. Zhang, K. Uéda, P. Chan, Inhibition of tyrosine hydroxylase expression in α-synuclein-transfected dopaminergic neuronal cells. *Neurosci. Lett.* **367**, 34–39 (2004).

147. J. Burré, M. Sharma, T. Tsetsenis, V. Buchman, M. R. Etherton, T. C. Südhof, a-Synuclein Promotes SNARE-Complex Assembly in Vivo and in Vitro. **329**, 5 (2010).

148. R. Khounlo, B. J. D. Hawk, T.-M. Khu, G. Yoo, N. K. Lee, J. Pierson, Y.-K. Shin, Membrane Binding of α-Synuclein Stimulates Expansion of SNARE-Dependent Fusion Pore. *Front. Cell Dev. Biol.* **9**, 663431 (2021).

149. G. Fusco, T. Pape, A. D. Stephens, P. Mahou, A. R. Costa, C. F. Kaminski, G. S. Kaminski Schierle, M. Vendruscolo, G. Veglia, C. M. Dobson, A. De Simone, Structural basis of synaptic vesicle assembly promoted by α-synuclein. *Nat. Commun.* **7**, 12563 (2016).

150. D. Scott, S. Roy, α-Synuclein Inhibits Intersynaptic Vesicle Mobility and Maintains Recycling-Pool Homeostasis. *J. Neurosci.* **32**, 10129–10135 (2012).

151. M. Sharma, J. Burré, α-Synuclein in synaptic function and dysfunction. *Trends Neurosci.* **46**, 153–166 (2023).

152. M. H. Polymeropoulos, C. Lavedan, E. Leroy, S. E. Ide, A. Dehejia, A. Dutra, B. Pike, H. Root, J. Rubenstein, R. Boyer, E. S. Stenroos, S. Chandrasekharappa, A. Athanassiadou, T. Papapetropoulos, W. G. Johnson, A. M. Lazzarini, R. C. Duvoisin, G. Di Iorio, L. I. Golbe, R. L. Nussbaum, Mutation in the alpha-synuclein gene identified in families with Parkinson's disease. *Science* **276**, 2045–2047 (1997).

153. L. M. A. Oliveira, T. Gasser, R. Edwards, M. Zweckstetter, R. Melki, L. Stefanis, H. A. Lashuel, D. Sulzer, K. Vekrellis, G. M. Halliday, J. J. Tomlinson, M. Schlossmacher, P. H. Jensen, J. Schulze-Hentrich, O. Riess, W. D. Hirst, O. El-Agnaf, B. Mollenhauer, P. Lansbury, T. F. Outeiro, Alpha-synuclein research: defining strategic moves in the battle against Parkinson's disease. *Npj Park. Dis.* **7**, 1–23 (2021).

154. J. B. Leverenz, I. Umar, Q. Wang, T. J. Montine, P. J. McMillan, D. W. Tsuang, J. Jin, C. Pan, J. Shin, D. Zhu, J. Zhang, Proteomic Identification of Novel Proteins in Cortical Lewy Bodies. *Brain Pathol.* **17**, 139–145 (2007).

155. Y. C. Wong, D. Krainc, α-synuclein toxicity in neurodegeneration: mechanism and therapeutic strategies. *Nat. Med.* **23**, 1–13 (2017).

156. A.-L. Mahul-Mellier, J. Burtscher, N. Maharjan, L. Weerens, M. Croisier, F. Kuttler, M. Leleu, G. W. Knott, H. A. Lashuel, The process of Lewy body formation, rather than simply α-synuclein fibrillization, is one of the major drivers of neurodegeneration. *Proc. Natl. Acad. Sci.* **117**, 4971–4982 (2020).

157. α-Synuclein Locus Triplication Causes Parkinson's Disease. https://www.science.org/doi/10.1126/science.1090278?url_ver=Z39.88-2003&rfr_id=ori:rid:crossref.org&rfr_dat=cr_pub%20%200pubmed.

158. M.-B. Fares, B. Maco, A. Oueslati, E. Rockenstein, N. Ninkina, V. L. Buchman, E. Masliah, H. A. Lashuel, Induction of de novo α-synuclein fibrillization in a neuronal model for Parkinson's disease. *Proc. Natl. Acad. Sci. U. S. A.* **113**, E912-921 (2016).

159. N. de O. Manzanza, L. Sedlackova, R. N. Kalaria, Alpha-Synuclein Post-translational Modifications: Implications for Pathogenesis of Lewy Body Disorders. *Front. Aging Neurosci.* **13**, 690293 (2021).

160. H. Fujiwara, M. Hasegawa, N. Dohmae, A. Kawashima, E. Masliah, M. S. Goldberg, J. Shen, K. Takio, T. Iwatsubo, α-Synuclein is phosphorylated in synucleinopathy lesions. *Nat. Cell Biol.* **4**, 160–164 (2002).

161. J. P. Anderson, D. E. Walker, J. M. Goldstein, R. de Laat, K. Banducci, R. J. Caccavello, R. Barbour, J. Huang, K. Kling, M. Lee, L. Diep, P. S. Keim, X. Shen, T. Chataway, M. G. Schlossmacher, P. Seubert, D. Schenk, S. Sinha, W. P. Gai, T. J. Chilcote, Phosphorylation of Ser-129 is the dominant pathological modification of alpha-synuclein in familial and sporadic Lewy body disease. *J. Biol. Chem.* **281**, 29739–29752 (2006).

162. S. Tenreiro, K. Eckermann, T. F. Outeiro, Protein phosphorylation in neurodegeneration: friend or foe? *Front. Mol. Neurosci.* **7**, 42 (2014).

163. T. Bartels, J. G. Choi, D. J. Selkoe, α-Synuclein occurs physiologically as a helically folded tetramer that resists aggregation. *Nature* **477**, 107–110 (2011).

164. J. Burré, M. Sharma, T. C. Südhof, Definition of a Molecular Pathway Mediating α-Synuclein Neurotoxicity. *J. Neurosci.* **35**, 5221–5232 (2015).

165. M. Hardenberg, A. Horvath, V. Ambrus, M. Fuxreiter, M. Vendruscolo, Widespread occurrence of the droplet state of proteins in the human proteome. *Proc. Natl. Acad. Sci.* **117**, 33254–33262 (2020).

166. S. Ray, T. O. Mason, L. Boyens-Thiele, A. Farzadfard, J. A. Larsen, R. K. Norrild, N. Jahnke, A. K. Buell, Mass photometric detection and quantification of nanoscale α-synuclein phase separation. *Nat. Chem.* **15**, 1306–1316 (2023).

167. B. Xu, S. Huang, Y. Liu, C. Wan, Y. Gu, D. Wang, H. Yu, Manganese promotes α-synuclein amyloid aggregation through the induction of protein phase transition. *J. Biol. Chem.* **298**, 101469 (2022).

168. E. G. P. Stender, S. Ray, R. K. Norrild, J. A. Larsen, D. Petersen, A. Farzadfard, C. Galvagnion, H. Jensen, A. K. Buell, Capillary flow experiments for thermodynamic and kinetic characterization of protein liquid-liquid phase separation. *Nat. Commun.* **12** (2021).

169. S. T. Dada, M. C. Hardenberg, Z. Toprakcioglu, L. K. Mrugalla, M. P. Cali, M. O. McKeon, E. Klimont, T. C. T. Michaels, T. P. J. Knowles, M. Vendruscolo, Spontaneous nucleation and fast aggregate-dependent proliferation of α-synuclein aggregates within liquid condensates at neutral pH. *Proc. Natl. Acad. Sci.* **120**, e2208792120 (2023).

170. B. G. Wilhelm, S. Mandad, S. Truckenbrodt, K. Kröhnert, C. Schäfer, B. Rammner, S. J. Koo, G. A. Claßen, M. Krauss, V. Haucke, H. Urlaub, S. O. Rizzoli, Composition of isolated synaptic boutons reveals the amounts of vesicle trafficking proteins. *Science* **344**, 1023–1028 (2014).

171. A. Agarwal, L. Arora, S. K. Rai, A. Avni, S. Mukhopadhyay, Spatiotemporal modulations in heterotypic condensates of prion and α-synuclein control phase transitions and amyloid conversion. *Nat. Commun.* **13**, 1154 (2022).

172. P. Gracia, D. Polanco, J. Tarancón-Díez, I. Serra, M. Bracci, J. Oroz, D. V. Laurents, I. García, N. Cremades, Molecular mechanism for the synchronized electrostatic coacervation and co-aggregation of alpha-synuclein and tau. *Nat. Commun.* **13**, 4586 (2022).

173. Q. Chen, Y. Chen, Y. Zhang, F. Wang, H. Yu, C. Zhang, Z. Jiang, W. Luo, Iron deposition in Parkinson's disease by quantitative susceptibility mapping. *BMC Neurosci.* **20**, 23 (2019).

174. A. Reinert, M. Morawski, J. Seeger, T. Arendt, T. Reinert, Iron concentrations in neurons and glial cells with estimates on ferritin concentrations. *BMC Neurosci.* **20**, 25 (2019).

175. L. Piroska, A. Fenyi, S. Thomas, M.-A. Plamont, V. Redeker, R. Melki, Z. Gueroui, α-Synuclein liquid condensates fuel fibrillar α-synuclein growth. *Sci. Adv.* **9**, eadg5663 (2023).

176. D. Milovanovic, Y. Wu, X. Bian, P. De Camilli, A liquid phase of synapsin and lipid vesicles. *Science* **361**, 604–607 (2018).

177. K. J. Vargas, N. Schrod, T. Davis, R. Fernandez-Busnadiego, Y. V. Taguchi, U. Laugks, V. Lucic, S. S. Chandra, Synucleins have multiple effects on presynaptic architecture. *Cell Rep.* **18**, 161–173 (2017).

178. W. P. Lipiński, B. S. Visser, I. Robu, M. A. A. Fakhree, S. Lindhoud, M. M. A. E. Claessens, E. Spruijt, "Biomolecular condensates can both accelerate and suppress aggregation of α-synuclein" (preprint, Biophysics, 2022); https://doi.org/10.1101/2022.04.22.489149.

179. A. S. Sawner, S. Ray, P. Yadav, S. Mukherjee, R. Panigrahi, M. Poudyal, K. Patel, D. Ghosh, E. Kummerant, A. Kumar, R. Riek, S. K. Maji, Modulating α-Synuclein Liquid–Liquid Phase Separation: Published as part of the *Biochemistry* virtual special issue "Protein Condensates." *Biochemistry* **60**, 3676–3696 (2021).

180. K. Bhasne, S. Sebastian, N. Jain, S. Mukhopadhyay, Synergistic Amyloid Switch Triggered by Early Heterotypic Oligomerization of Intrinsically Disordered α-Synuclein and Tau. *J. Mol. Biol.* **430**, 2508–2520 (2018).

181. A. Cochard, A. Safieddine, P. Combe, M.-N. Benassy, D. Weil, Z. Gueroui, Condensate functionalization with motors directs their nucleation in space and allows manipulating RNA localization. bioRxiv [Preprint] (2022). https://doi.org/10.1101/2022.07.10.499452.

182. S. O. Rizzoli, W. J. Betz, Synaptic vesicle pools. *Nat. Rev. Neurosci.* **6**, 57–69 (2005).

183. X. Wu, Q. Cai, Z. Shen, X. Chen, M. Zeng, S. Du, M. Zhang, RIM and RIM-BP Form Presynaptic Active-Zone-like Condensates via Phase Separation. *Mol. Cell* **73**, 971-984.e5 (2019).

184. T. Yoshida, K. Takenaka, H. Sakamoto, Y. Kojima, T. Sakano, K. Shibayama, K. Nakamura, K. Hanawa-Suetsugu, Y. Mori, Y. Hirabayashi, K. Hirose, S. Takamori, Compartmentalization of soluble endocytic proteins in synaptic vesicle clusters by phase separation. *iScience* **26**, 106826 (2023).

185. X. Wu, H. Qiu, M. Zhang, Interactions between Membraneless Condensates and Membranous Organelles at the Presynapse: A Phase Separation View of Synaptic Vesicle Cycle. *J. Mol. Biol.* **435**, 167629 (2023).

186. P De Camilli, S M Harris Jr, W B Huttner, P Greengard Synapsin I (Protein I), a nerve terminal-specific phosphoprotein. II. Its specific association with synaptic vesicles demonstrated by immunocytochemistry in agarose-embedded synaptosomes. *J. Cell Biol.* **96**, 1355–1373 (1983).

187. A. Pechstein, O. Shupliakov, Taking a Back Seat: Synaptic Vesicle Clustering in Presynaptic Terminals. *Front. Synaptic Neurosci.* **2**, 143 (2010).

188. O. Bloom, E. Evergren, N. Tomilin, O. Kjaerulff, P. Löw, L. Brodin, V. A. Pieribone, P. Greengard, O. Shupliakov, Colocalization of synapsin and actin during synaptic vesicle recycling. *J. Cell Biol.* **161**, 737–747 (2003).

189. A. J. Baines, V. Bennett, Synapsin I is a microtubule-bundling protein. *Nature* **319**, 145–147 (1986).

190. F. Benfenati, F. Valtorta, J. L. Rubenstein, F. S. Gorelick, P. Greengard, A. J. Czernik, Synaptic vesicle-associated Ca2+/calmodulin-dependent protein kinase II is a binding protein for synapsin I. *Nature* **359**, 417–420 (1992).

191. A. Aguzzi, M. Altmeyer, Phase Separation: Linking Cellular Compartmentalization to Disease. *Trends Cell Biol.* **26**, 547–558 (2016).

192. W. M. Babinchak, W. K. Surewicz, Liquid–Liquid Phase Separation and Its Mechanistic Role in Pathological Protein Aggregation. *J. Mol. Biol.* **432**, 1910–1925 (2020).

193. A. Zbinden, M. Pérez-Berlanga, P. De Rossi, M. Polymenidou, Phase Separation and Neurodegenerative Diseases: A Disturbance in the Force. *Dev. Cell* **55**, 45–68 (2020).

194. J. Hochmair, C. Exner, M. Franck, A. Dominguez-Baquero, L. Diez, H. Brognaro, M. L. Kraushar, T. Mielke, H. Radbruch, S. Kaniyappan, S. Falke, E. Mandelkow, C. Betzel, S. Wegmann, Molecular crowding and RNA synergize to promote phase separation, microtubule interaction, and seeding of Tau condensates. *EMBO J.* **41**, e108882 (2022).

195. M. Atias, Y. Tevet, J. Sun, A. Stavsky, S. Tal, J. Kahn, S. Roy, D. Gitler, Synapsins regulate α-synuclein functions. *Proc. Natl. Acad. Sci.* **116**, 11116–11118 (2019).

196. W. J. Schulz-Schaeffer, The synaptic pathology of α-synuclein aggregation in dementia with Lewy bodies, Parkinson's disease and Parkinson's disease dementia. *Acta Neuropathol. (Berl.)* **120**, 131–143 (2010).

197. M. L. Kramer, W. J. Schulz-Schaeffer, Presynaptic α-Synuclein Aggregates, Not Lewy Bodies, Cause Neurodegeneration in Dementia with Lewy Bodies. *J. Neurosci.* **27**, 1405–1410 (2007).

198. A. McCormack, D. J. Keating, N. Chegeni, A. Colella, J. J. Wang, T. Chataway, Abundance of Synaptic Vesicle-Related Proteins in Alpha-Synuclein-Containing Protein Inclusions Suggests a Targeted Formation Mechanism. *Neurotox. Res.* **35**, 883–897 (2019).

RÉSUMÉ

Les maladies neurodégénératives, telles que les maladies d'Alzheimer, de Parkinson et de Huntington, sont des maladies incurables caractérisées par la dégénérescence progressive des neurones, entraînant des déficits cognitifs et moteurs chez les personnes touchées. On suppose que la formation et l'accumulation d'agrégats de protéines dans les tissus nerveux jouent un rôle essentiel dans la pathogenèse de la maladie. Des recherches récentes ont proposé que le processus d'agrégation puisse passer par une étape intermédiaire de séparation de phase (SP) - un phénomène dans lequel certaines protéines se dissocient de l'environnement cellulaire pour former des gouttelettes distinctes ayant des propriétés caractéristiques des liquides. Bien que prometteuse, l'étude du rôle de la SP dans le contexte des maladies neurodégénératives est une tâche difficile, en raison de la composition complexe des condensats cellulaires issus de la séparation de phase. Pour améliorer l'étude de la PS dans le contexte des maladies neurodégénératives, nous avons développé une méthode pour la formation et la dissolution contrôlées de condensats biomoléculaires enrichis en protéines impliquées dans l'agrégation pathologique. Tout d'abord, nous avons créé des condensats contenant de l'α-synucléine (α-Syn), le principal facteur pathologique de la maladie de Parkinson et d'autres pathologies. L'α-Syn est connue comme une protéine de type prion, ce qui signifie que ses agrégats se propagent de cellule en cellule et modèlent l'agrégation de l'α-Syn cytosolique soluble, favorisant ainsi la progression de la maladie. Cependant, ce phénomène est peu connu en ce qui concerne l'état condensé de la protéine. Pour étudier cela, nous avons exposé des cellules exprimant nos condensats d'α-Syn à des agrégats d'α-Syn préformés sous forme fibrillaire. Nous avons observé que les fibrilles déclenchaient la transition des condensats de leur état liquide à une forme agrégée fibrillaire ayant des propriétés solides et présentant des marqueurs biochimiques caractéristiques des amyloïdes. Cela nous a permis de proposer un modèle dans lequel la phase condensée de l'α-Syn accélère la propagation des agrégats pathologiques, en fournissant un pool de protéine concentrée qui peut plus facilement subir une transition amyloïde via la voie de type prion. Par la suite, nous avons construit des condensats artificiels enrichis en α-Syn et en synapsine I. Des études antérieures ont proposé que l'α-Syn et la synapsine I interagissent au niveau des terminaisons présynaptiques des neurones, où elles jouent un rôle important dans la libération des neurotransmetteurs en contrôlant le regroupement, le trafic et la libération des conteneurs de neurotransmetteurs enfermés dans la membrane, appelés vésicules synaptiques. Dans notre contexte, les condensats d'α-Syn/synapsine I étaient également soumis à une transition liquide-solide médiée par des fibrilles d'α-Syn.

ABSTRACT

Neurodegenerative diseases, such as Alzheimer's, Parkinson's, and Huntington's disease, are incurable illnesses characterized by the progressive degeneration of neurons, leading to cognitive and motor deficits in affected individuals. The formation and accumulation of protein aggregates in nervous tissues is hypothesized to play a pivotal role in disease pathogenesis. Recent studies have proposed that the aggregation process could pass through an intermediate step of phase separation (PS) - a phenomenon wherein certain proteins de-mix from the cellular environment to form distinct liquid-like droplets. Although promising, studying the role of PS in the context of neurodegenerative diseases is a challenging task, due to the intricate composition of cellular phase separated condensates. To improve the study of PS in the context of neurodegenerative diseases, we have developed a method for the controlled formation and dissolution of biomolecular condensates enriched in proteins involved in pathological aggregation. First, we created condensates containing α-synuclein (α-Syn), the main pathological factor in Parkinson’s disease and other pathologies. α-Syn is known as a prion-like protein, meaning that its aggregates spread from cell to cell and template the aggregation of soluble cytosolic α-Syn, promoting the progression of the disease. However, little is known about this phenomenon with respect to the condensed state of the protein. To investigate this, we exposed cells expressing our α-Syn condensates to preformed α-Syn aggregates in fibrillar form. We observed that fibrils triggered the transition of condensates from their liquid-like state to a fibrillar aggregated form with solid-like properties and exhibiting biochemical markers characteristic of amyloids. This allowed us to propose a model where the condensed phase of α-Syn speeds up the propagation of pathological aggregates, by providing a pool of concentrated protein that can undergo more easily an amyloid transition via the prion-like pathway. Subsequently, we have built artificial condensates enriched in α-Syn together with synapsin I. Previous studies proposed that α-Syn and synapsin I interact at the presynaptic termini of neurons, where they play an important role in the release of neurotransmitters by controlling the clustering, trafficking and release of membrane-enclosed neurotransmitter containers called synaptic vesicles. In our setting α-Syn/synapsin I condensates were also subject to a liquid-to-solid transition mediated by α-Syn fibrils.